© 2016 Rebecca A. Hortensius

BIOINSPIRED ALTERATIONS OF COLLAGEN-GLYCOSAMINOGLYCAN SCAFFOLDS FOR TISSUE REGENERATION APPLICATIONS

BY

REBECCA A. HORTENSIUS

DISSERTATION

Submitted in partial fulfillment of the requirements
for the degree of Doctor of Philosophy in Bioengineering
in the Graduate College of the
University of Illinois at Urbana-Champaign, 2016

Urbana, Illinois

Doctoral Committee:

Associate Professor Brendan Harley, Chair
Associate Professor Marni Boppart
Professor Brian Cunningham
Professor Matthew Wheeler

ABSTRACT

Following injury, adult musculoskeletal wounds undergo a process of repair, the body's way of quickly closing an area of damage. Repair is characterized by the development of granulation tissue (scar) which lacks the structural and functional properties of the native tissue's extracellular matrix (ECM). Scar formation has been linked to the presence of inflammation, as injuries in environments with little inflammation (e.g. fetal) heal via regeneration, in which the synthesized matrix physiologically mirrors that of the tissue pre-injury. The limited ability of the adult body to regenerate these tissues following injury as well as resolve excessive inflammation associated with injury or material implantation, calls for strategies to enhance and support the restoration of these tissues to their natural state. Through the use of collagen-based extracellular matrix mimics, this thesis describes bioinspired scaffold compositions aimed at providing inherent cues to direct cellular behavior towards regeneration *in vivo*. Growth factors play a significant role in the overall health, function and phenotypic fate of cells *in vivo* and *in vitro*. We used charged glycosaminoglycans (found naturally in the ECM) to electrostatically sequester growth factors within the collagen matrix, preventing biomolecule degradation and presenting relevant factors to fibroblasts and mesenchymal stem cells. We showed that these glycosaminoglycans could also influence the three-dimensional delivery of charged-based gene vectors. While necessary to prevent infection during wound healing, inflammation, especially if it is prolonged, contributes to scar formation. By incorporating the anti-inflammatory matrix of the amniotic membrane into the collagen ECM analog, we sought to provide a biomaterial that would temper this inflammatory response to allow for tissue regeneration. This fetal environment-inspired material was studied in fibroblast, stem, and immune cell populations *in vitro* and in an *in vivo* animal model. Overall, this work demonstrates the effective modification

of scaffold composition in order to address issues of transient growth factor sequestration, gene delivery capacity, or immunomodulation.

To Ruben,

For his love, support, and encouragement

ACKNOWLEDGMENTS

I would like to first acknowledge and thank those who have contributed to the work described within this thesis: Daniel Weisgerber (Chapter 4), Jacquelyn Pence (Chapter 4), and Laura Mozdzen (Chapter 4), William Grier (Chapter 5), Dr. Wheeler and the Wheeler lab group (Chapter 6). In addition, I have been fortunate to work with some amazing undergraduate students who made significant contributions to this body of work; Erica Peterson (Chapter 2), Jill Ebens (Chapters 4 & 5), and Amber Boyce (Chapter 6). You all have been a blast to work with, a joy to mentor, and have made my experience at Illinois so much richer. Thank you for all of your hard work.

I am also grateful for collaborators both at the University of Illinois at Urbana-Champaign and other institutions Dr. Mathew Wheeler, Dr. Derek Milner, Dr. Marcello Rubessa, Heather Lopez-Lake, Sammi Lotti, Kathryn Polkoff, Jacob Becraft, Dr. Dan Pack (University of Kentucky), and Kara Spiller (Drexel University).

A huge thanks is due to my advisor, Dr. Brendan Harley, for the opportunity to work in his lab and for providing an environment where I have been able to grow as a researcher. Thank you also to Dr. Matthew Wheeler, Dr. Marni Boppart and Dr. Brian Cunningham, members of my thesis committee, for providing their insight on my work.

Thank you to lab mates, past and present, for being wonderful colleagues and making each work day interesting: Steven, Sunny, Bhushan, Dan, Emily, Sara, Jackie, Laura, Bill, Emily, Aidan, and Mai.

This project would not have been possible without the support from Carle Foundation Hospital and the staff in the Biomedical Research Center. I would like to especially acknowledge Dixie

Heath, Pamela Woo, Tor Jensen, and Elida Iniguez for their advice and coordination of the tissue collections.

There are many people who provided supplies and technical expertise towards this project. Thank you Dr. Allison Stewart (Veterinary Sciences, UIUC) for the equine tenocytes, Karen Doty (Veterinary Sciences, UIUC) for sectioning for pore size analysis, Donna Epps (IGB Core Facilities, UIUC) for help with histology, Dr. Michael Insana (Bioengineering, UIUC) for use of his mechanical tester, Dr. Sandra McMasters (SCS, UIUC) for culture media preparation, Cate Wallace (Beckman Institute, UIUC) for help with SEM, Jenny Zadeh (HPCBio, IGB, UIUC) for PCA analysis and heat maps, Dr. Nathan Todd (Psychology, UIUC) for assistance with statistical analysis, and the IGB Core Facilities for assistance with real-time PCR.

I am grateful for personal funding from the NSF Graduate Research Fellowship DGE 11-44245 FLLW, the Mavis Future Faculty Fellowship, and the Graduate College's Dissertation Completion Fellowship. Additional funding from the Chemical and Biomolecular Engineering Department, the Institute for Genomic Biology, the National Science Foundation under Grant No. 1105300, the National Institute of Arthritis and Musculoskeletal and Skin Diseases of the National Institutes of Health under Award Number R03 AR062811, and the AO Foundation (S-14-54H) made this work possible. This research was carried out in part in the Frederick Seitz Materials Research Laboratory Central Facilities, University of Illinois, which are partially supported by the U.S. Department of Energy under grants DE-FG02-07ER46453 and DE-FG02-07ER46471, and the Microscopy Suite, Imaging Technology Group, Beckman Institute for Advanced Science and Technology, University of Illinois at Urbana-Champaign.

I would not have continued my graduate studies at Illinois without the amazing support and encouragement of colleagues like Ram, Surbhi, and Marina. Their friendship sustained me in the

years prior to coming to Champaign and for that I am truly grateful. I am also thankful for friends that have brought balance to my life here at UIUC; Caroline, Olivia, Nicole, Benji, and all those at UBC who have reassured me over the years.

Thank you to my parents, Brenda and Larry, for encouraging me in my education and providing the opportunities to continue my studies to this point. Thank you also to my brother, Christopher, for always being there for me. I love you all.

To my husband, Ruben – whose confidence in me is immeasurable, whose love extends through my shortcomings, whose faith brings perspective, and who is constantly reminding me not to take things so seriously – thank you for all you have done to get me to this point. I love you.

Finally, thanks to Chester for being my constant writing companion and emotional support. And for the wet-nose nudges to remind me to get outside every once in a while. Good boy.

TABLE OF CONTENTS

COMMONLY USED SYMBOLS AND ABBREVIATIONS xi

CHAPTER 1: INTRODUCTION AND BACKGROUND: TISSUE REGENERATION, MIMICRY OF THE EXTRACELLULAR MATRIX, AND NATURALLY-INSPIRED BIOMATERIALS 1

1.1 Thesis Overview 1

1.2 Motivation 1

1.3 A tissue regeneration approach 4

1.4 Extracellular matrix analogs 7

1.5 Bioactive materials to direct cellular response 11

1.6 Challenges in tissue regeneration associated with the inflammatory response 18

1.7 Naturally-derived materials for addressing inflammation 20

1.8 Conclusion 30

1.9 Tables 32

1.10 Figures 33

CHAPTER 2: USING GLYCOSAMINOGLYCANS TO ALTER GROWTH FACTOR DELIVERY AND CELLULAR RESPONSE 34

2.1 Chapter overview 34

2.2 Introduction 35

2.3 Materials and methods 37

2.4 Results 42

2.5 Discussion 46

2.6 Conclusions 51

2.7 Tables 52

2.8 Figures 54

CHAPTER 3: GENE DELIVERY INFLUENCED BY ELECTROSTATIC INTERACTIONS 59

3.1 Chapter overview 59

3.2 Introduction 60

3.3 Materials and methods 63

3.4 Results 67

3.5 Discussion 72

3.6 Conclusions 77

3.7 Figures 78

CHAPTER 4: THE INCORPORATION OF AMNIOTIC MEMBRANE MATRIX ALTERS TENOCYTE ACTIVITY IN VITRO **82**
4.1 Chapter overview 82
4.2 Introduction 83
4.3 Materials and methods 85
4.4 Results 91
4.5 Discussion 95
4.6 Conclusions 100
4.7 Figures 102
CHAPTER 5: INCORPORATION OF AMNIOTIC MEMBRANE INTO COLLAGEN SCAFFOLDS TO ADDRESS IMMUNOMODULATORY REQUIREMENTS FOR TENDON REPAIR **108**
5.1 Chapter overview 108
5.2 Introduction 109
5.3 Materials and methods 111
5.4 Results 116
5.5 Discussion 118
5.6 Conclusions 122
5.7 Tables 123
5.8 Figures 124
CHAPTER 6: MACROPHAGE RESPONSE IN VITRO AND IN VIVO TO AMNION-CONTAINING COLLAGEN-BASED SCAFFOLDS **128**
6.1 Chapter overview 128
6.2 Introduction 128
6.3 Materials and methods 131
6.4 Results 137
6.5 Discussion 140
6.6 Conclusions 143
6.7 Tables 144
6.8 Figures 146
CHAPTER 7: SUMMARY AND FUTURE DIRECTIONS **155**
7.1 Summary 155
7.2 Future Directions 158
7.3 Final Thoughts 159
APPENDIX A: SCAFFOLD FABRICATION PROTOCOLS **160**
A.1 Protocol for CG suspension preparation 160
A.2 Amniotic membrane isolation 162

A.3 Amniotic membrane drying protocol 164
A.4 C:AM suspension preparation protocol 165
A.5 Aligned CG scaffold fabrication protocol 168
A.6 Isotropic CG scaffold fabrication protocol 169
A.7 DHT crosslinking protocol 170
A.8 EDC crosslinking protocol 171
APPENDIX B: CELL CULTURE AND ASSAY PROTOCOLS 173
B.1 Tenocyte culture protocol 173
B.2 hMSC culture protocol 177
B.3 THP-1 culture protocol 181
B.4 THP-1 differentiation and polarization protocol 182
B.5 Cell seeding on CG scaffolds protocol 184
B.6 alamarBlue metabolic activity protocol 186
B.7 Hoechst DNA quantification protocol 188
B.8 RNA isolation and quantification protocol 191
B.9 RNA reverse transcription protocol 193
B.10 PCR protocol 195
REFERENCES 197

COMMONLY USED SYMBOLS AND ABBREVIATIONS

Abbreviation	Term, Definition
(h)MSC	(Human) mesenchymal stem cell or marrow stromal cell
ACL	Anterior cruciate ligament
AM	Amniotic membrane, amnion
ANOVA	Analysis of variance
Arg-1	Arginase-1
bFGF	Basic fibroblast growth factor
BSA	Bovine serum albumin
C:CS	Collagen:chondroitin sulfate scaffold
C:HA	Collagen:hyaluronic acid scaffold
C:HP	Collagen:heparin scaffold
CCL22	C-C motif chemokine 22
CD163	Cluster of differentiation 163
cDNA	Complementary DNA (deoxyribonucleic acid)
CG	Collagen-glycosaminoglycan co-precipitate
co-ECM	Decellularized colonic extracellular matrix
COL1A1	Collagen I alpha 1
COOH	Carboxyl group
COS	Chitooligosaccharides
CS	Chondroitin sulfate
DBP	Decellularized bovine pericardium
DHT	Dehydrothermal crosslinking
DMEM	Dulbecco's modified Eagle's media
DMMB	Dimethylmethylene blue
DNA	Deoxyribonucleic acid
ECM	Extracellular matrix
EDC	1-ethyl-3-(3-dimethylaminopropyl) carbodiimide hydrochloride
EDTA	Ethylenediaminetetraacetic acid
FBS	Fetal bovine serum
GAGs	Glycosaminoglycans
GAPDH	Glyceraldehyde 3-phosphate dehydrogenase; used as housekeeping gene
GDF-5	Growth/differentiation factor 5
H&E	Hematoxylin and eosin
HA	Hyaluronic acid
HGF	Hepatocyte growth factor
HP	Heparin
IDO	Indoleamine 2,3, dioxygenase
IFNγ	Interferon gamma
IGF-1	Insulin-like growth factor-1

IL-x	Interleukin; relevant variants include 1β, 2, 4, 6, 8, 10, 13
M1	Pro-inflammatory macrophage phenotype
M2a	Wound healing macrophage phenotype
M2c	Regulatory, anti-inflammatry macrophage phenotype
MMP-x	Matrix metalloproteinase; relevant variations include 1, 3, 7, 8, 13
MRC1	Mannose receptor, C type 1
NHS	N-hydroxysulfosuccinimide
OCT	Optimal cutting temperature compound
P/S	Penicillin-streptomycin
PBS	Phosphate-buffered saline
PCA	Principle components analysis
PCR	Polymerase chain reaction
PDGF-BB	Platelet-derived growth factor-BB
PDMS	Polydimethylsiloxane
PEI	Polyetylenimine
PMA	Phorbol 12-myristate-13-acetate
PTFE	Poly(tetrafluoroethylene)
RGD	Arginine-glycine-aspartic acid amino acid sequence
RLU	Relative light units
RNA	Ribonucleic acid
SCXB	Scleraxis; a transcription factor highly expressed in tendon
SEM	Scanning electron microscopy
TBJ	Tendon-bone junction
TC	Tendon cell
TCPS	Tissue Culture Polystyrene
TGF-βx	Transforming growth factor-βx; relevant isoforms include TGF-β1, TGF-β2, and TGF-β3
TIMP	Tissue inhibitor of metalloproteinases; relevant isoforms include 1, 2, 4
TNC	Tenascin-C
TNFα	Tumor necrosis factor alpha
ULA	Ultra-low attachment
VEGF	Vascular endothelial growth factor; a chemical signal produced by cells that stimulates the growth of new blood vessels (angiogenesis)

CHAPTER 1: INTRODUCTION AND BACKGROUND: TISSUE REGENERATION, MIMICRY OF THE EXTRACELLULAR MATRIX, AND NATURALLY-INSPIRED BIOMATERIALS[*]

1.1 Thesis Overview

This thesis will focus on the manipulation of collagen-glycosaminoglycan scaffolds for the use in tissue regeneration applications. As a whole, this dissertation describes the use of compositional changes to enhance the material's inherent bioactivity and ability to manipulate cellular activity. This goal can be further broken down into two different strategies: using electrostatic interactions via glycosaminoglycan charges to enhance growth factor and gene delivery (Chapters 2 & 3) and using the amniotic membrane to alter the cellular immune response within the scaffolds (Chapters 4, 5 & 6).

1.2 Motivation

1.2.1 Injuries to the tendon and tendon-bone junction

Tendons are connective tissues which act to transmit high tensile loads from muscle to bone, resulting in movement. Depending on their functional role (positional vs. energy-storing), tendons in the body can display significantly different mechanical and structural properties. Positional tendons, such as the human anterior tibialis, serve to transmit muscle-generated forces to bones to enable locomotion [1]. They are relatively inextensible under load (max. strain: 3.1%) [2] and show reduced injury levels as a result of over-use compared to energy-storing tendons [3]. Energy-storing tendons, such as the human Achilles, act like springs by stretching

[*] Portions of this chapter have been adapted from Rebecca Hortensius, Laura Mozdzen, and Brendan Harley, "Biomaterial Scaffolds for Tendon Tissue Engineering," in: M.E. Gomes, R.L. Reis and M.T. Rodrigues (Eds.), *Tendon Regeneration*, Elsevier, 2015, pp. 349-380 & Rebecca A. Hortensius and Brendan A. C. Harley. "Naturally-derived biomaterials for addressing inflammation in tissue regeneration." Experimental Biology and Medicine, 2016; 241(10):1015-24.

and recoiling under high loads [1]. While these tendons are highly extensible under load (max strain: 10.3%), they exhibit high injury rates [4].

Injury to the tendons throughout the body is common and can present in the acute or chronic state. The tendons of the hand (flexor [5], extensor [5]) are often injured, cut, or even crushed during accidents, while shoulder (rotator cuff [6, 7], biceps tendons [8, 9]) and leg injuries (Achilles [10, 11], patellar [12]) are more often injured during falls and sports accidents. Hand injuries account for approximately 10% of all emergency room visits and hand tendons are injured at an annual rate of approximately 33 in every 100,000 people [5]. The nature of hand function is to have precise and delicate control of movement to perform various tasks, and small dysfunction in ability can lead to a significant social and economic loss [5]. Similarly, the annual rate of incidence of biceps tendon rupture is approximately 1.2 in every 100,000 people, occurring more frequently in men than in women. Common complications of a biceps tendon rupture are nerve damage, re-rupture, and ossification of the tendon [9]. Currently, the vast majority of these injuries require surgical intervention.

Tears to the rotator cuff are characteristic of a separate class of tendon injury: injury at the insertion between tendon and bone. The native osteotendinous region (tendon-bone junction) is the body's solution for connecting elastic tendon to (100-fold) stiffer bone. This osteotendinous interface is 100 – 250μm wide and protects the interface from failure by minimizing stress concentrations [13] through overlapping gradients of matrix mineral content, insoluble proteins, structural alignment, and biochemical signals [13-15]. Rotator cuff tears account for more than 4.5 million physician visits and 250,000 surgeries nationally each year [16]. Surgical repair is accomplished via mechanical fixation with sutures or screws. This approach does not restore the complex structure and composition of the interface, but, rather, results in the formation of tissue

with inferior biomechanical properties (scar). Insufficient re-integration between the tendon and bone compartments is responsible for long-term joint instability and high clinical failure rates (11%-94%) [17]. Another major class of injuries that relies on successful tendon-to-bone healing is the surgical repair following an anterior cruciate ligament (ACL) tear. Commonly, a soft tissue graft (autograft or allograft, tendon or ligament) is fixed at each end into tunnels bored into the femur and tibia. Graft stabilization, mechanical strength, and eventual surgical outcomes depend on the integration of this graft with the anchoring bone [18-21].

After injury and subsequent healing (with or without surgical intervention), tendons are often unable to bear the same load as the original tissue. Scar tissue, which contains different physiochemical properties than native tendon, often replaces the complex collagen hierarchy of the tissue and limits its functionality. Its formation has been linked to the inflammatory phase of the wound healing cascade (discussed further in section 1.6). Increases in the gene expression of pro-inflammation (IL-1β, TNFα) and matrix degradation factors (MMP-3, MMP-13) as well as decreases in the expression of tendon ECM (COLI) and tendon-specific markers (SCX) have been shown in a canine flexor tendon model [22]. Studies in the healing process following acute tendon injury, in particular, show upregulation in TGF-β1 mRNA and protein expression, disruption in collagen fiber continuity and organization, and decreases in ultimate stress and modulus when compared to uninjured tendons [23, 24].

1.2.2 Chronic wounds

Chronic cutaneous wounds and their limited ability to heal represent a major problem in the field of wound care. It is estimated that more than $25 billion is spent in the US every year on the treatment of chronic wounds, which are most commonly present in the elderly and individuals

with diabetes [25, 26]. They are characterized by an extended period of inflammation, delayed angiogenesis, and the disruption in the transition to the normal proliferative and remodeling phases of wound healing (outlined in Figure 1.1A) [27].

Tendons (*e.g.*, patellar [28-30], Achilles [10, 31, 32]) also commonly display tendinopathies, characterized by pain, inflammation, and decreased functionality often as a result of overuse or deterioration due to chronic injury or disease [10, 28-32]. Approximately 50% of all sports injuries result from overuse of connective tissues such as tendons [10]. For example, Achilles tendinopathy accounts for 6-17% of all running injuries [32] and often has an unpredictable clinical outcome [31]. Patellar tendinopathy effects up to 40% of professional athletes during their career [33] but is also common in recreational [34] and adolescent athletes [35], often at a higher rate in men than in women. Many tendon injuries, such as patellar tendinopathy, are not limited to athletic endeavors, with risks also increasing with other conditions such as obesity [30].

1.3 A tissue regeneration approach

The limited ability of the body to regenerate the native structure and function of tendon following injury as well as resolve excessive inflammation associated with a range of wounds, calls for strategies to enhance and support the restoration of these tissues to their natural state. The field of tissue engineering has modeled its therapeutic approach towards this goal on a triad consisting of materials, cells, and biological factors; the three major components found in every tissue and organ. The resident cells of every tissue in the body are supported by an environment of insoluble components called the extracellular matrix (ECM) and a concert of soluble biological factors (growth factors, cytokines, hormones). The ECM, primarily composed of collagen and glycosaminoglycans, is the three-dimensional microenvironment in which cells

reside within tissues and organs of the body. It is responsible for providing instructive signals which can modulate cell bioactivity via compositional, structural, and mechanical properties. Following tissue injury, the likelihood of complete restoration of these ECM properties is low as the human body's wound healing mechanism prioritizes wound closure (repair) over tissue regeneration [36]. Therefore, even after months of ECM remodeling, natively repaired tissues exhibit disorganized matrix and decreased mechanical properties [37]. An increasingly common paradigm of tissue regeneration relies on the implantation of scaffold materials, cells, and/or soluble molecules not to replace the damaged tissue but rather to promote normal deposition of tissue with eventual material degradation for the restoration of native structure and function [38]. Tissue regeneration strategies have traditionally relied on designing biomaterials that closely mimic native traits of the ECM as a means to promote normal, site-specific cellular function. This thesis, in particular, will describe efforts to develop biomaterials that through their inherent properties can alter the activity of cells (either seeded on the scaffold or infiltrating from surrounding tissue) and biological factors.

1.3.1 Repair versus regeneration

The goal of achieving *in vivo* induced regeneration for a variety of tissues and organs following severe injury remains at the forefront of current tissue engineering investigations. Treatment options for organ injury depend significantly on the scale of the defect. Microscopic defects are often treated using a wide variety of soluble factors (*i.e.*, biomolecules, hormones, and antibiotics). However, organ-scale defects present a significantly larger wound site, requiring considerably different treatment practices. These defects, created by disease or by an acute or chronic injury can result in millimeter or centimeter scale wounds. These wounds cannot be

treated with drugs because the failure encompasses a mass of tissue which includes cells, soluble proteins, cytokines, and the extracellular matrix.

The adult mammalian response to severe injury is closure of the wound by contraction and scar tissue formation, a process termed repair. Distinct from repair, regeneration is characterized by synthesis of a physiological (normal, functional) replacement tissue in the wound site that is structurally and functionally similar to the original tissue. The contractile fibroblast phenotype, termed the myofibroblast, plays a critical role in determining the nature (repair or regeneration) of mammalian wound healing. During adult repair, myofibroblast-mediated organized wound contraction and scar tissue synthesis is observed [39]. During early fetal healing, differentiation of myofibroblasts has not yet occurred and regeneration of damaged tissue and organs occurs in the absence of contraction.

The data suggest that induced organ regeneration in the adult may be encouraged by developing techniques to mimic early fetal healing. It has been hypothesized that biomaterial ECM analogs, such as those described in section 1.4, induce regeneration by establishing an environment that selectively inhibits wound contraction by preventing the organized contractile response and blocking scar synthesis, the two processes normally responsible for closing a wound following severe injury [39]. The transforming growth factor-β (TGF-β) family of molecules has also been implicated in this ontogenetic transition between (fetal) regeneration and (adult) repair response to injury. TGF-βs are multifunctional cytokines with widespread effects on cell growth and differentiation, embryogenesis, immune regulation, inflammation, and wound healing [40]. Deficient levels of TGF-β1 and -β2 and increased levels of TGF-β3 are observed in early gestational (“fetal” regenerative healing response) compared to late gestational (“adult” repair healing response) mice. TGF-β1 and TGF-β2 are known to promote scar, while TGF-β3 may

reduce scar [41, 42]. These results suggest the use of an appropriately designed active ECM analog along with decreased TGF-β1, -β2, and increased TGF-β3 expression may play a significant role in promoting regenerative repair of tissue defects [43].

1.4 Extracellular matrix analogs

Biomaterial analogs of the extracellular matrix are a critical element of any tissue engineering product towards *in vitro* or *in vivo* clinical applications. While these scaffolds are responsible for providing the appropriate structural, mechanical, and/or biomolecular cues necessary to promote cell bioactivity and regenerative potential, it is intended that they stimulate remodeling and resultant regenerative repair of functional tissue as a temporary construct instead of as a permanent implant. Given the typical dimensions of tendon defects, such scaffolds are generally three-dimensional, exhibit high porosity to encourage cell attachment, penetration, proliferation, and nutrient/waste exchange, and contain compositional features to promote cell-matrix attachment and subsequent interactions [44].

Degradable polymeric-based biomaterials (synthetic and naturally-derived polymers) have been adopted for tendon tissue engineering applications, with their long chain molecular structure providing a backbone similar to features of the native ECM. Synthetic polymers have tailorable material properties (fine control over size, shape, and mechanical properties), scalable production, and can withstand a range of processing conditions although they lack the natural amino acids and ligands of native ECM [44, 45]. Poly(α-hydroxyacids) are a class of synthetic polymer that include poly(lactic acid) (PLA), poly(glycolic acid) (PGA), and their copolymer poly(lactic-*co*-glycolide) (PLGA), that have been widely used for a range of tissue engineering applications [44, 46]. These are FDA approved for the use as sutures, stents, and wound dressings and are widely used as ECM analogs in tissue engineering and drug delivery systems

research [47]. PLA and PGA are easily processed and their properties can be controlled through the alteration of polymer molecular weight and associated copolymers [48]. This class of polymers degrades via hydrolytic processes, releasing monomers that can be removed by natural pathways [49]. However, the heterogeneity of polymer degradation (when the inside of the material degrades faster than the outside) [49] and the acidity of the resultant byproducts [50] presents some concern.

Materials such as collagen, glycosaminoglycans (GAGs), and fibrin are derived from native components of the ECM. Such naturally-derived constructs often can provide key features of the ECM (e.g., ligand sites, MMP-degradable) to support biological recognition, cell adhesion, and subsequent cell bioactivity [44]. Collagen is a significant constituent of the natural ECM and collagen-based scaffolds have been used in a variety of applications. While offering advantages in terms of potential bioactivity, naturally-derived polymer biomaterials often have limited control over available fabrication paradigms, are mechanically weak, and can suffer from batch-to-batch variations [48]. Regardless of their limitations, collagen-based scaffolds show promise as bioactivity materials for tissue regeneration and will be the focus of the remainder of this thesis in the form of a graft copolymer of type I collagen and sulfated GAGs [39, 51].

1.4.1 Biomaterial composition

The ECM composition of tendon, largely collagen (86%), GAGs/proteoglycans (1 – 5%), and elastin (2%), provides compositional targets for the design of tissue engineering biomaterials. From the standpoint of biomaterial design, the low antigenicity and immunogenicity of collagen and the presence of ligands and peptides that aid in the formation of cell-scaffold interactions are advantageous [52]. The mechanical properties and degradation rates of collagen constructs can

also be controlled through collagen density as well as the degree of material crosslinking [52]. Glycosaminoglycans are linear polysaccharides that are a significant component of tendon ECM [52, 53] and known to play a critical role in sequestering growth factors within the ECM [54]. Bioinspired strategies for functionalizing ECM analogs with GAGs to affect growth factor availability will be discussed later in this chapter (section 1.5) and within this thesis (Chapter 2). While collagen-GAG (CG) scaffolds have been widely used for a variety of tissue engineering applications such as skin, peripheral nerve, and cartilage regeneration [52, 55-58], they have only recently been adapted for tendon applications [59-62]. Other natural polymers such as gelatin [63], chitosan [64], alginate [65], and agarose [66] have also been investigated as potential materials for ECM analogs for tendon tissue engineering applications.

1.4.2 Biomaterial structural properties

The biological activity of any ECM analog also depends significantly on its three-dimensional pore microstructure. After migrating into the scaffold, cells interact with the surrounding scaffold environment, making use of its cell surface receptors to bind to specific ligands on the scaffold surface. The first critical component of ECM analog microstructure to consider is the open or closed-cell nature of the scaffold. An open-cell pore microstructure exhibits pore interconnectivity while a closed-cell microstructure exhibits membrane-like faces between adjacent pores, effectively sealing the environment of one pore from its neighbors. Pore interconnectivity is critical for scaffold bioactivity because it allows cells to migrate through the construct and interact with other cells in a manner similar to that observed *in vivo*. In order to be used as a template for cellular growth, pores should also be large enough to allow for nutrient transport and early cellular infiltration [67], while maintaining appropriate tissue-dependent mechanical integrity. Pore size influences the specific surface area, permeability, and mechanical

properties of the material [61, 68-71]. Initial cellular attachment generally increases with an increase in specific surface area, typically inversely related to pore size. Although initial cellular attachment can be increased by reducing pore size, the ultimate disadvantages of small pores (steric hindrance, decreased permeability) provide an important design trade-off to consider [72]. A wide range of studies, across a range of biomaterial chemistries, have suggested the optimal range of pore sizes that balances these parameters, in addition to cell bioactivity, is 200-400μm [72].

Beyond pore size, the microstructural alignment of biomaterial substrates (two-dimensional) and shape and alignment of pores (three-dimensional biomaterials) is often a critical design feature to consider in biomaterial fabrication. A range of studies have suggested that successful regeneration templates for natively aligned tissues such as peripheral nerves [73], the myocardium [74], and tendon [60, 61, 75-78] must provide tissue-specific, aligned contact guidance cues that recapitulate aspects of the tissue anisotropy. In addition to altering the structural organization of ligands available to cells within the biomaterials, the degree of anisotropy can also significantly influence scaffold modulus [79]. The use of anisotropy in biomaterials has been extended from providing a bioactive platform for culturing differentiated cells from natively aligned tissues (*e.g.*, tenocytes) [60] towards a tools for inducing selective differentiation of mesenchymal stem cells (MSCs) towards a tenogenic lineage [61].

1.4.3 Passive versus instructive biomaterials

Porous, three-dimensional scaffolds have been used extensively as biomaterials in the field of tissue engineering for both *in vitro* study of cell-scaffold interactions as well as for *in vivo* investigations of tissue regeneration. These scaffolds, as analogs of the ECM, can act as a

physical support that permits resident cell activity. However, advances in the field of tissue engineering are increasingly reliant on biomaterials that instruct, rather than simply permit, a desired cellular response [80]. Tissues can be dynamic, spatially-patterned, or inhomogeneous over multiple length and time scales, thereby motivating development of approaches to engineer biomaterials at multiple structural and biomolecular levels [60, 81-83]. Such instructive biomaterials hold significant promise for clinical applications in tendon repair as well as a wide range of regenerative applications *in vivo* and mechanistic investigations in the laboratory.

1.5 Bioactive materials to direct cellular response

While material composition and structural properties are important design criteria for tendon tissue engineering, it is increasingly apparent that approaches which replicate elements of the complex biomolecular environment of the extracellular matrix are equally critical. Such biomolecular modifications can take many forms. Some efforts focus on improving the biocompatibility of synthetic polymer analogs; for instance, the incorporation of the arginine-glycine-aspartic acid (RGD) amino acid sequence to enhance cell attachment [84]. However, this section will focus on functionalization strategies for natural polymer ECM analogs.

Many biomolecular supplementation strategies are inspired by the native environment during development and fetal wound healing, tissue homeostasis, as well as the environment often found during acute or chronic wound healing processes. There are important shifts in the expression of growth factors and matrix proteins between adult and fetal tendons in the case of normal physiology as well as damage and disease. Notably, transforming growth factor beta (TGF-β) exhibits varying isoforms over the course of development, homeostasis, and wound healing. TGF-β3 is prevalent in the early timepoints during development most associated with enhanced regenerative capacity [39], but transitions to enhanced expression of TGF-β1 isoform

prior to birth (15.5 days post-conception in a mouse model of tendon development) [85]. TGF-β1 is prevalent in the wound environments of adult tendons and not in fetal tendon wounds [24]. Such transitions in growth factors between healthy and diseased tendon, as well as fetal vs. adult healing mechanisms [86], are likely to inform the selection of growth factors or TGF-β receptor inhibitors for future tendon tissue engineering materials.

1.5.1 Soluble and covalent presentation of biomolecules

Growth factors and other biomolecules play a significant role in the overall health, function and phenotypic fate of cells *in vivo* and *in vitro*. For instance, increases in tenocyte chemotaxis and proliferation are induced, dose-dependently, by insulin-like growth factor 1 (IGF-1) and platelet-derived growth factor BB (PDGF-BB) [87]. Additionally, bFGF, GDF-5, and GDF-7 have been shown to drive MSCs towards a tenogenic phenotype in anisotropic CG scaffolds [88]. Chemical signaling via soluble factor presentation depends on many variables including the concentration of the growth factor, diffusion rate within the scaffold, and metabolic activity of the cells [89]. Not surprisingly, many effective strategies require the incorporation of multiple signals to meet tissue engineering design goals: *e.g.*, incorporation of multiple factors to induce proliferation and maintain cell phenotype [87, 90]. Despite the responses seen using soluble factors, current research advances have been moving towards the design of an active, instructive biomaterial; one that endogenously contains signals to promote a desired cellular response *in vivo* or *in vitro* culture, making them attractive as 'off-the-shelf' constructs.

Covalent attachment of growth factors to an ECM analog has been proposed as a way to extend the activity and availability of a biomolecule as well as control the factor's spatial presentation. N-(3-dimethylaminopropyl)-N'-ethylcarbodiimide hydrochloride (EDC) is a commonly used

chemistry for the immobilization of factors on 2D and within 3D tissue engineering materials [87, 91, 92]. This zero length crosslinker couples carboxyl groups to primary amines. *Shen et al.* showed that VEGF could be covalently attached (not simply adsorbed) onto a porous collagen scaffold using EDC chemistry without altering the effectiveness of the growth factor; scaffolds with immobilized VEGF showed a higher degree of endothelial cells penetration into the collagen scaffold [91]. Furthermore, *Odedra et al.* showed that EDC chemistry could be used to create a gradient of VEGF within a porous collagen scaffold [92]. Previous work in the Harley lab has shown that immobilization of PDGF-BB within aligned collagen scaffolds can both extend and localize its effects and promote significant increases in tenocyte metabolic activity over long-term culture versus an equal soluble factor dose [87]. While effective, bulk covalent attachment does not allow for local growth factor presentation (*e.g.*, compartments, gradients, patterns).

Photolithography-based methods offer the potential to pattern factors within three dimensional ECM scaffolds [93, 94]. Here, biomolecules of interest can be spatially patterned within a material. Additionally, multiple factors can be attached in complementary patterns or gradients. This technique has been demonstrated on collagen scaffolds using benzophenone-based chemistry where growth factor patterns were created at a depth of 300 micrometers and the resultant pattern growth factors induced a patterned cellular response [93, 95-98]. Similarly, a number of publications highlight the generation of biomolecular patterns within three-dimensional hydrogel structures using light-based lithography methods [94, 99-101].

Growth factor loaded microparticles of various materials have also been employed in a number of tissue engineering scaffolds. This technique bypasses adding growth factors to the primary ECM analog components and uses a secondary vessel to contain the biomolecules within the

scaffold [102, 103]. Growth factor carriers have been fabricated from a range of materials: PLGA [104], gelatin [105, 106], chitosan [107], and hybrids [108, 109]. By using microspheres, control over the factor release rate can be maintained through crosslinking [110] and dual factor release can be achieved by using multiple delivery vehicles [106]. Such signals may be used to guide cell in-growth from the construct periphery while providing separate signals to aid regeneration or integration with the surrounding tissue. These approaches offer significant potential for future tissue engineering applications.

1.5.2 Sequestration of growth factors via glycosaminoglycans

While providing opportunities to augment the bioactivity of tissue engineering scaffolds, presenting biomolecules via covalent functionalization is limited to growth factors that do not need to be internalized by cells to elicit their effects. In the native ECM, growth factor sequestration and release is modulated by large polysaccharides called glycosaminoglycans (GAGs). In nature, GAGs can exist as either protein-bound proteoglycans, sulfated variants (heparan sulfate, heparin, chondroitin sulfate, dermatan sulfate, or keratan sulfate) or as a free glycosaminoglycan with no sulfate groups (hyaluronic acid) [111]. The sulfated molecules, in particular, are known to sequester growth factors electrostatically; presenting varying levels of negative charges depending on their degree of sulfation [54, 112]. These interactions are known to transiently regulate the bioavailability of growth factors, both exogenously-delivered and endogenously-produced, to cells within a tissue [81]. However, it should be noted that the degree of GAG sulfation is not solely responsible for the modulation of cellular activity and growth factor sequestration. CD44 binds the non-sulfated hyaluronic acid [111] and differences in the GAG backbone, as well as position of sulfate groups, alters the degree of protein interaction [53, 54, 113].

The knowledge of proteoglycan-protein interactions *in vivo* can be used in the design of biomaterials that rely on transient, bioinspired interactions instead of covalently-linking growth factors. Murphy et al. has demonstrated, using a two-dimensional model system, that heparin-binding peptides can enhance human mesenchymal stem cell (hMSC) bioactivity on a self-assembled monolayer via selective binding of heparin then heparin-binding growth factors to the substrate [114]. Other groups have adapted this work to fully three-dimensional materials. Incorporation of heparin-binding peptides was shown to maintain the activity and prolong the release of the heparin-binding growth factor basic fibroblast growth factor (bFGF) within PEG-based hydrogels [115]. Artificially sulfated alginate (plant-derived polysaccharide) hydrogels showed enhanced binding of heparin-binding growth factors over native alginate gels [116]. Efforts that used selectively desulfated chondroitin sulfate in a series of hydrogels resulted in a decreased ability to sequester transforming growth factor- beta 1 (TGF-β1), leading to increased MSC expression of chondrogenic cues [117].

Further, this concept has been extended to collagen-GAG biomaterials being developed explicitly for tissue engineering applications. Increasing the degree of sulfation within the GAG component of a collagen-GAG substrate induced increased dermal fibroblast adhesion and proliferation which is linked *in vivo* to the speed and quality of wound closure [118]. Similar efforts have associated increased adsorption and release of TGF-β1 within the scaffold with the degree of GAG sulfation [119]. This system of sequestration and release resulted in higher collagen synthesis by human mesenchymal stromal cells, suggesting that bioinspired GAG formulations may be used to enhance the correct presentation of growth factors to cells.

Work described in Chapter 2 of this document shows that the degree of GAG sulfation of a collagen-GAG scaffold could be used to modify the scaffold's capacity to sequester

biomolecules in order to enhance the bioactivity of scaffolds being developed explicitly for tendon tissue engineering applications [59]. The ability to mimic dose-dependent changes in cell activity in response to a single dose of growth factor highlights an intriguing avenue for future biomaterial development.

1.5.3 The use of gene delivery to alter cellular activity

The use of growth factors in tissue engineering applications is effective but not necessarily efficient, especially when growth factor half-life and cost are taken into account. The use of gene delivery vehicles takes an upstream approach to altering cellular bioactivity. Instead of providing the growth factors necessary for enhanced responses (proliferation, differentiation, etc.), this method introduces, directly to the cells, the genes that encode for the proteins of interest.

The use of viruses for gene delivery is efficient, however, non-viral gene delivery vectors are advantageous in terms of safety, design flexibility, and ease of production [120]. A range of materials has been used for these types of vectors: chitosan [121, 122], alginate [123], hydroxyapatite [124, 125], and polyethylenimine (PEI) [120, 126-129]. PEI is one of the most efficient and widely studied non-viral gene delivery vectors in literature. As a positively charged polymer, PEI complexes with the negatively charged backbone of DNA, forming a polyplex. This charge interaction allows us to capitalize further on the use of biomaterial systems with differential charges (like that of the sulfated GAG scaffold described in the previous section). Work in this area of gene activated matrices is detailed in Chapter 3 of this thesis.

1.5.4 Cellular response to biomaterials

As part of the tissue engineering triad, the cells introduced to the extracellular matrix, as either cells seeded on the matrix prior to implantation or infiltrating cells *in vivo*, play a large role in

the study of biomaterials. Three categories of cells that are of particular interest for the work described in this thesis are terminally differentiated primary cells, pluripotent adult stem cells, and immune cells.

Primary tenocytes can be isolated from tendon and approaches such as mechanical stimulation, aligned biomaterials, and growth factors have been previously applied to facilitate the maintenance of a tenocyte phenotype *in vitro* [60, 61, 87, 130]. Tenocytes are either sourced from an animal (xenograft), in which case they must be bio- and immuno-compatible with the patient, or they can be sourced from the patient (allograft), in which case there is a risk of donor site morbidity. Once obtained, the proper design of biomaterial substrate can enhance tenocyte remodeling and long-term improvements in the scaffold mechanical properties [131].

MSCs are pluripotent adult stem cells which can be readily isolated from the patient's own bone marrow and have the potential to differentiate into a variety of musculoskeletal tissues [55, 132, 133]. As many tendon injuries are composite injuries which require multi-tissue regeneration strategies (tendon-to-bone, tendon-to-muscle), the use of a multi-potent progenitor cells provides additional advantages and complexities. For these types of injuries, a biomaterial with gradation in biomechanical and biomolecular cues may eventually be able to locally direct stem cell fate down multiple tissue lineages, leading to improved multi-tissue regeneration. Additionally, MSCs have a role in modulating the immune response in wound sites. Following the initial inflammatory response, MSCs stimulate the transition to the proliferative, healing phase of the wound cascade. It has been suggested that MSCs produce biological factors that shield local fibroblasts from the negative effects of pro-inflammatory cytokines as well as promote the transition of macrophages from their pro-inflammatory to their anti-inflammatory phenotype [134-136].

While the body's immune response is a complicated concert of cells and soluble factors, it has been shown that macrophages, white blood cells initially known for their phagocytic activity, play an important role in a wound's transition from inflammation to remodeling. Recent literature has reviewed a spectrum of macrophage phenotypes; M1 (pro-inflammatory), M2a (wound healing), and M2c (regulatory) [137]. The transition from a primarily M1 population to a M2 population is indicative of better healing outcomes in diabetic foot ulcers [138]. Designing a biomaterial scaffold that facilitates this transition in vivo would be an asset to the field.

1.6 Challenges in tissue regeneration associated with the inflammatory response

Following tissue injury, the body immediately begins to work to clear the injury site of debris, close the wound, and lay down new extracellular matrix (ECM). In adult wounds this wound healing cascade can be described in three overlapping phases: inflammation, proliferation, and remodeling (Fig. 1.1). During the inflammatory phase, the chemotaxis of inflammatory cells (neutrophils, macrophages) to the wound site is stimulated by platelet release of platelet-derived growth factor (PDGF) and transforming growth factor-beta (TGF-β) [139]. Pro-inflammatory, wound macrophages secrete key inflammatory cytokines, tumor necrosis factor alpha (TNFα) and interleukin-1 (IL-1) during this phase [139]. The transition to the proliferation phase is characterized by the macrophage shift to an anti-inflammatory, tissue repair phenotype [140] and the presence of fibroblasts along with the upregulation of genes associated with matrix proteins (collagen, proteoglycans, fibronectin) [139]. The final phase of wound healing, remodeling, can continue for weeks or months as the tissue matrix is reorganized.

Inflammation, while a necessary component of wound healing, can hinder tissue regeneration in cases such as biomaterial implantation or chronic wounds. Inflammation is not only a result of the original injury; the surgical implantation and biomaterial presence can also stimulate

inflammation through the foreign body reaction (Fig. 1.1). Therefore, it should follow that the design of biomaterials for tissue regeneration, normally focused on biocompatibility and recapitulation of the composition, structure, and mechanics of native tissue, should also include features that mitigate the inflammatory response. The goal for scaffold design in the future should be two-fold: to provide instructive signals necessary for cell attachment, proliferation, and function in the context of the native tissue (bioactivity) and also to modulate the immune response.

Physical properties of scaffolds, such as composition [59, 141], mechanical properties [142], and microarchitecture [61], can all influence cell bioactivity. But these features may also explicitly regulate the immune response. Aligned, electrospun polycaprolactone fibers implanted subcutaneously in a rat model, showed increased cell infiltration and a thinner fibrous capsule as compared to fibers with random orientation [143]. Variations in pore size of polytetrafluoroethylene materials result in differential expression of pro-inflammatory cytokines in vitro and decreased fibrous capsule thickness in vivo [144].

Traditionally, materials for reducing the inflammatory response of biomaterials have relied on the incorporation of anti-inflammatory therapeutics. One technique is to use plasmids of the anti-inflammatory cytokine IL-10 in the pretreatment of cells or to incorporate them into a collagen biomaterial scaffold [145, 146]. This approach reduces inflammation and enhances MSC survival *in vitro* [145] and in an *in vivo* model for myocardial infarction, there was increased wall thickness, increased ratio of collagen III to I, and a shift to a regulatory macrophage phenotype leading to functional recovery [146]. The incorporation of anti-inflammatory drugs such as ibuprofen [147] and tetrandrine [148] into PLA-based scaffolds has also shown reduced inflammation and improved tissue regeneration in *in vivo* rat models.

The ability to leverage biologically-derived materials with intrinsic anti-inflammatory properties for tissue regeneration has the potential to generate a new class of biomaterials with the capacity to promote regeneration and alter the inflammatory response in the wound site. Coordinated efforts in biomaterial design may offer the possibility to improve regenerative potential because of the ability to alter native inflammatory responses. Pro-inflammatory signals are not inherently detrimental to healing; in fact, they are necessary for repair as long as they subside in a timely fashion [149]. It is hypothesized that biomaterials that first promote the M1 macrophage phenotype and then M2 would enhance ultimate healing [149]. These observations reinforce the idea that biomaterial design should not simply reduce or enhance inflammatory response, but that the kinetics of the inflammatory response offer intriguing targets for biomaterial design. To date, the study of a wide range of naturally-derived materials for their potential immunomodulatory/anti-inflammatory capability and their ability to support tissue regeneration has begun. From this wide variety of materials, this section focuses on three particular classes of biomaterials – chitin, decellularized extracellular matrix, and amniotic membrane – that show particularly intriguing properties in the context of biomaterial design. While many current observations described in the following sections and seen in Table 1.1 focus on solely reducing the inflammatory response, future generation tissue engineering products are likely to exhibit more nuanced control over the inflammatory cascade.

1.7 Naturally-derived materials for addressing inflammation

1.7.1 Immunomodulatory activity of chitin-derived materials

Chitin is one of the most abundant polysaccharides in nature, second only to cellulose [150]. It is an inexpensive and readily available material that is found in the exoskeletons of invertebrates, such as crabs and shrimp, as well as the cell walls of fungi and yeast [151, 152]. Chitin is a linear

polymer composed of *N*-acetyl-*D*-glucosamine subunits [151]. Since chitin is not readily dissolvable, its deacetylated derivative, chitosan, is frequently studied and used in biological applications [152, 153]. Chitosan can be further degraded and deacetylated to form chitooligosaccharides (COS) [150, 154-157].

Chitin, chitosan, and their derivatives have been extensively studied for their anti-inflammatory, anti-microbial, antioxidant, and anti-cancer effects [151, 152, 158]. The range of anti-inflammatory applications for chitin-derived materials encompasses the treatment of chronic inflammatory conditions (asthma [150], inflammatory bowel disease [157], sepsis [156], arthritis[159]), the use of chitosan composite particles for drug delivery [160], and the modulation of immune responses of implanted chitin-based biomaterials [161]. Low molecular weight chitosan oligosaccharides significantly inhibit asthma-related cytokines (IL-4, IL-13, TNFα) *in vitro* and *in vivo* [150]. Additionally, oral administration of COSs has been effective in attenuating pro-inflammatory cytokine production and reducing intestinal inflammation in models of induced colitis [157]. Bacterial-stimulated inflammation, such as that seen in acne, can also be treated with chitin-derived materials [160]. Nanoparticles of chitosan and alginate (without anti-acne mediation) were able to inhibit bacterial induction of IL-12 in macrophages in a dose-dependent manner. Further, the presence of these nanoparticles was able to also inhibit the induction of IL-6 in keratinocytes [160].

The anti-inflammatory mechanism of orally-administered chitosan, in particular, has been attributed to its release of *N*-acetyl-*β*-D-glucosamine during degradation [151, 162]. Glucosamine is a structural unit of hyaluronan, a glycosaminoglycan shown to have roles in the promotion of cell motility and accelerated wound healing. Glucosamine is also a primary component of proteoglycans of the native extracellular matrix of cartilage and connected tissue.

A decrease in the occurrence of osteoarthritis-related total joint replacements has been linked to treatment with glucosamine sulfate [159]. Further disruption of inflammation via chitin-derived materials (outside the field of tissue regeneration) has been observed through the inhibition of pro-inflammatory MMP-2 [163], the decrease in IL-1β-induced chondrocyte apoptosis [164], and the attenuation of nitric oxide and inflammatory cytokine (such as TNF-α, IL-6, IL-1β) production in *in vitro* dose-dependent culture [154, 155] as well as *in vivo* [156].

An early study of chitin as a wound healing accelerant was conducted by Prudden et al [165]. Additional study has shown that chitosan fibers stimulate early cell migration and production of granulation tissue in canine open wounds [166]. More recent work has focused on the response of specific wound healing cells to chitosan-based implants. Immune cells, particularly macrophages, have roles in inflammation and tissue regeneration. Through the production of cytokines and chemokines, macrophages attract or decrease the inflammatory cells within the injury site [161]. By modulating the macrophage response to an implant, the rate and outcome of healing can be altered and chitosan has been found to promote anti-inflammatory macrophage polarization *in vitro* without the use of exogenous growth factors/cytokines [161].

Chitosan scaffolds for use in skin, bone, cartilage, liver, nerve and blood vessel wounds have been well summarized [167, 168]. However, considering the range of anti-inflammatory uses for chitin-derivatives, the study of chitosan scaffold-based therapies for immunomodulation in tissue regeneration is limited. Chitosan fibers [166] and hydrogels [169] have been evaluated for skin regeneration. In both forms, chitosan promotes migration of inflammatory cells to the wound site and collagen matrix deposition. In the hydrogels, chitosan also promoted angiogenesis resulting in vascularization of the new tissue [169]. These findings suggest that chitin-based materials may have potential in future tissue engineering products. However, significant new efforts to link

current observations regarding immune response with functional metrics of tissue regeneration are required.

1.7.2 Decellularized matrix as scaffold for tissue regeneration

Scaffolds derived from decellularized matrix (from both allogeneic and xenogeneic sources) have been investigated as materials for regeneration in a range of tissues; heart valve [170-173], nasal cartilage [174], skeletal muscle [175], gastrointestinal tract [176, 177], ureters [178], liver [179], and flexor tendons [180]. Both segmented and whole tissues can be decellularized [177, 179]. The prevailing advantage to using decellularized matrix scaffolds is the maintenance of important properties of the native ECM. The ability to use site-specific tissue, in particular, is advantageous for tissue regeneration applications. This ensures that the distinct matrix architecture and composition are appropriate for the functional cells specific to that tissue, allowing for the enhancement of tissue-specific differentiation [181] and promoting chemotaxis and proliferation of progenitor cells [182]. Additionally, decellularized matrices have been shown to have immunomodulatory properties and the ability to influence the host response *in vivo.* Removing the cellular component of the transplanted tissue is key to this result as the cellular presence contributes to a predominantly M1 macrophage phenotype [174, 183].

Decellularized ECM scaffolds intrinsically have the chemical composition of the natural tissue; they contain ECM proteins, particularly collagen and glycosaminoglycans, that are highly conserved across species [170, 175, 183]. This conservation of biomolecules lends these materials to be biocompatible *in vivo,* exhibiting a low immune response [175, 183]. Also maintained within the scaffolds are the complex three-dimensional microstructure, important for directing cellular phenotype via geometric cues [174] and growth factors that have roles in cell

attachment, proliferation, migration, and differentiation [174]. Further, the matrix retains its mechanical properties following decellularization allowing for mimicry of the native tissue and long term function [171]. This property, in particular, negates the need for exogenous chemical crosslinking, presenting a material that is accessible to naturally occurring degradation and remodeling [176]. In contrast, manufactured collagen-based materials rely on crosslinking to increase their mechanical properties which significantly reduces the cellular degradation of the material [184]. The ability of cells to remodel their surrounding matrix is critical for regenerative success. Through the process of constructive remodeling, the degradable matrix template is gradually replaced by native tissue with the appropriate function, matrix organization, and cellular phenotype [185]. This remodeling outcome *in vivo* is dependent on a favorable response from the innate inflammation associated with both the original injury and/or the biomaterial implantation [149, 185].

While chemical crosslinking is commonly used in collagen-based ECM matrix analogs to stabilize the scaffold, it has been proposed that the inhibition of decellularized scaffold degradation, and therefore, the release of degradation products, through chemical crosslinking holds great influence over not only the regenerative capacity (noted earlier) but also the cellular immune response. Indeed, the products of enzymatically degraded porcine urinary bladder influence cell migration *in vitro* [186]. However, reports on the effects of chemically crosslinking decellularized matrices differ based on the tissue type and crosslinking agent. Porcine colonic decellularized ECM (coECM) exhibited extensive cellular infiltration and degradation *in vivo* as compared to coECM that had been chemically crosslinked with N(3-dimethylaminpropyl)-N’-ethylcarbodiimide hydrochloride [176]. Additionally, the crosslinked matrices exhibited evidence of encapsulation and disorganized connective tissue, results that are

not desired in tissue regeneration applications [176]. Conversely, carbodiimide crosslinked porcine ureteral scaffolds implanted in a subcutaneous rat model showed a macrophage phenotypic switch to the anti-inflammatory M2 phenotype [178]. Crosslinking with glutaraldehyde or genipin stimulated a pro-inflammatory M1 macrophage switch *in vivo* [178]. These data are consistent with glutaraldehyde crosslinking of decellularized bovine pericardium which resulted in limited attachment and survival of macrophage-like cells (U937) and increased release of pro-inflammatory cytokines (MMP-1) [173]. Future work should carefully consider the balance between scaffold degradation and the inflammatory wound healing response in the use of decellularized matrix for tissue regeneration applications.

Beyond the role chemical crosslinking can play in the cellular response to decellularized matrices, researchers have extensively studied how these biomaterials influence the inflammatory response *in vitro* [149, 170, 171, 173, 175, 176, 178] and *in vivo* [149, 175, 176, 178, 180]. The overwhelming observation, detailed in the following paragraphs, is that decellularized matrix can modulate the immune response by exhibiting anti-inflammatory effects and promoting a shift in macrophage phenotype from M1 to M2.

In studies of monocyte-derived macrophages cultured on decellularized bovine pericardium (DBP), researchers have observed decreased cell spreading and decreased formation of multi-nucleated cells on DBP (compared to PDMS and TCPS), indicating a low inflammatory response [170, 171]. An ex vivo culture model was used to monitor the cellular events at the interface between a fresh tissue (porcine bladder) and decellularized tissue (porcine acellular bladder matrix) [187]. There, macrophages were the first cells to move from the tissue into the decellularized matrix, where they matured to $CD163^{+}$ (M2 phenotype) cells [187].

Autologous tissue grafts have the advantage of not requiring immunosuppression but their use is limited to static organs (i.e. skin) or those that move passively (i.e. blood vessels, bladder, trachea, heart valves) [175] and by supply (like in cases of significant injury to the flexor tendons of the hand) [180]. Decellularized tissue provides a potential solution in each of these cases. Skeletal muscle was decellularized and either cultured with rat $CD3^+$ splenocytes or implanted into the tibialis anterior muscle of an immunocompetent rat [175]. Results showed decreased T cell proliferation in both experiments. Decellularized scaffolds had slower degradation times and polarized macrophages towards an M2 phenotype *in vivo* [175]. *In vitro*, the decellularized skeletal muscle led to decreased levels of pro-inflammatory TH1 cytokines (IL-2, IFN-γ) and increased levels of anti-inflammatory TH2 cytokines (IL-10) compared to fresh tissue, effectively modulating the immune response [175]. Emerging work combining decellularized bone matrices with the sequential release of growth factors/cytokines that can stimulate M1 and then M2 macrophage phenotypes has shown the ability to enhance healing and vascularization [149].

The mechanism of immunomodulatory behavior by decellularized matrices is not completely understood. It is hypothesized that the removal of MHC classes I and II during the decellularization process contributes to the anti-inflammatory effects of the matrix *in vivo*, the decreased T-cell proliferation *in vitro*, and reductions seen in IL-1 and IFN-γ expression [175]. The theory that the decellularization process exposes critical surface molecules for immunomodulation could be another explanation [175].

Like any biomaterial, there are disadvantages associated with the use of decellularized matrices. These are a result of the variations between properties on the basis of tissue source and processing (method of decellularization, crosslinking, sterilization methods) [176] along with the

potential for pathogen transfer to the host [188]. Cell-derived extracellular matrices present an exciting alternative for future study [188].

1.7.3 Fetal wound-inspired materials for regeneration and scarless healing

The wound healing process and outcome is fundamentally different in fetal as compared to adult wounds. While adult wounds exhibit inflammation and result in disorganized matrix and scar formation, healing in fetal wounds proceeds in a regenerative fashion, with neither the typical inflammatory response nor the formation of scar tissue [189-191].

The most prevalent example of fetal wound healing in literature is that of skin which has been well reviewed elsewhere [190-193]. Fetal skin has the potential to heal via complete regeneration (scarless), with normal tissue architecture and a minimal inflammatory response, but this response is dependent on gestational age and the size of the wound [194-197]. This scarless healing phenomenon does not only occur in skin tissue. Similar outcomes have been seen in tendon injury as well, where the restoration of function in adults can be hindered by the development of adhesions [24]. It should be noted that fetal scarless wound healing is not universal to all tissues. It has also been seen in heart and lung tissue but fetal wounds in the stomach, intestine, and diaphragm heal with a scar [198].

Two leading differences between adult and fetal wound healing are the cytokines/growth factors expressed following injury and the composition of the native extracellular matrix. The decreased inflammatory response in fetal wounds can be attributed to the minimal infiltration of immune cells due to lower levels of PDGF, TGF-β1 and TGF-β2 and pro-inflammatory cytokines such as IL-6 and IL-8 [190, 199-203]. Additionally, the anti-inflammatory cytokine IL-10 is significantly expressed in fetal wounds [204]. Studies have shown that treating adult wounds with IL-10

results in decreased inflammation and scarless wound repair [205, 206]. Growth factors TGF-β1 and TGF-β2 are highly expressed in adult wounds as compared to uninjured tissue but their baseline levels are maintained in fetal wounds [207]. Fetal wounds contain the third TGF-β isoform, TGF-β3, which decreases scar formation through the regulation of collagen deposition as demonstrated in fetal rat skin [208, 209]. Collagen type I is the primary ECM protein in both adult and fetal skin (normal and wounded) but fetal skin exhibits a higher ratio of collagen III to collagen I [210]. Hyaluronic acid (HA), a non-sulfated glycosaminoglycan, is also prevalent in the ECM and promotes cell proliferation and motility. Although HA is present in both adult and fetal wound fluid, it has been detected later in the healing process in fetal wound environments [211].

The results of fetal wound healing cannot be solely attributed to the sterile, intrauterine environment and the interface with the surrounding amniotic fluid. Marsupial pouch young, who develop outside of the uterus, have the ability to heal cutaneous wounds in a scarless fashion [212]. Even without the uterine environment, the wounds created on the backs of grey short-tailed opossums were able to quickly undergo re-epithelialization and dermal repair [212]. The rate and degree of regeneration is dependent on the pouch age of the animal. It has also been shown that scar formation occurs when adult tissue is placed in the fetal environment [213]. Being perfused with fetal blood and bathed in amniotic fluid is not sufficient to induce fetal-like, scarless wound healing [213]. Fetal skin can also heal without scar in an adult subcutaneous environment [214]. These observations have led researchers to focus on the role the fetal extracellular matrix has on inflammation and resultant healing.

The amniotic membrane (amnion, AM) has been investigated as a valuable biomaterial for promoting healing with low immune response and decreased scar formation [215]. The amniotic

membrane, found in the fetal environment, is the innermost layer of the placenta, surrounding the fetus *in utero*. It is composed of a single epithelial layer and a collagen-rich (collagen I as well as types III, IV, V, and VI) extracellular matrix that also contains laminin, fibronectin, elastin, and proteoglycans [215-218]. Following birth, it can be easily removed from the placenta and separated from the interfacing maternal membrane (chorion). From there it can be utilized in a range of forms: *(1)* living tissue containing cells; *(2)* decellularized matrix; or *(3)* in combination with other scaffold materials. Isolated AM matrix contains and elutes a range of biological factors (growth factors and cytokines) that are important components of the wound healing cascade [219]. The presence of anti-inflammatory cytokines such as IL-4 and IL-10 as well as inhibitors of matrix degradation (TIMPs 1, 2, 4) is of particular interest [219].

The amniotic membrane has long been recognized for its anti-inflammatory properties and wound healing capacity. The use of amnion sheets for treatment of adhesions (scar formation) between digital flexor tendons and their sheathes was reported in 1942 [220]. A 1950 report details the use of boiled amniotic membrane to treat chronic skin ulcers [221]. In it the authors describe six case studies in which patients with longstanding, unhealed leg ulcers were treated with a dressing of amnion. Each of the wounds was healed within 10 weeks of treatment and the resulting skin was thick, healthy, and elastic [221].

More recently, it has been shown that the intact amnion membrane sheet is effective in the treatment of corneal surfaces [222-224], skin wounds [219, 225], oral cavity reconstruction [226], and many other reconstruction applications summarized elsewhere [215, 227]. Amniotic membranes applied to the ocular surface in cases of surface abnormalities [222], limbal stem cell deficiency [223], and corneal ulcers [224] has led to rapid epithelialization, reduced inflammation, and surfaces that are smooth and wettable. Amniotic membranes were implanted

subcutaneously in mice and shown to enhance progenitor cell recruitment [219]. In a porcine full thickness skin defect, crosslinked collagen-amnion dermal substitutes exhibited few inflammatory cells, rapid healing, and good neovascularization [225]. Micronized, dehydrated human amnion membrane has been shown to reduce cartilage degeneration in an osteoarthritic rat model [228].

While the use of intact and injectable amniotic membrane matrix has been investigated for two-dimensional tissue regeneration applications, the potential of the AM as a bioactive component in 3D biomaterials has not been extensively studied. Three-dimensional matrices made entirely of decellularized amniotic membrane have been fabricated via lyophilization [229]. The resulting scaffold has been shown to support fetal dermal fibroblast cells *in vitro*. Recent work in our lab (described fully in Chapters 4, 5, and 6) has investigated scaffolds that combine amniotic matrix within or in combination with lyophilized collagen materials [230]. Incorporating fetal wound inspired matrix components in a collagen scaffold for tissue regeneration supports cellular health and tempers pro-inflammatory gene expression *in vitro*.

1.8 Conclusion

Emerging efforts in the field of tissue engineering seek to develop biomaterials that not only promote cell bioactivity using conventional, *tissue-specific* metrics (e.g., proliferation, differentiation, matrix synthesis), but that also begin to see the biomaterial as a vehicle that can modulate the host immune response after injury. Wound healing cascades are complex and vary tissue to tissue, but also in the context of age, disease, and the acute or chronic nature of the defect. Typical design parameters for tissue regeneration biomaterials are focused on providing the appropriate extracellular matrix analog to mimic the native tissue compositionally, structurally, and mechanically. These signals aid local cells in building new tissue as part of the

wound healing cascade. However, the process of wound healing can be hindered by the presence of an extensive inflammatory response. Recent results in the literature suggest the intriguing possibility that biomaterial design might also be considered as a tool for modulating the immune response following injury. While not specific or nuanced to date, the idea of instructive signals changing the kinetics of the wound healing cascade offers an exciting glimpse into the future of tissue engineering. The careful design of tissue regeneration biomaterials to both avoid the stimulation of an immune response and promote the resolution of any existing inflammation will be critical for efficient healing and functional outcomes, suggesting the development of immunomodulatory biomaterials as an emergent subfield of tissue engineering with significant potential for clinical success.

1.9 Tables

Table 1.1. Materials studied for the modulation of inflammation during wound healing

	Material Form	Immunomodulatory Function	Reference
CHITIN-DERIVED	Low molecular weight chitosan oligosaccharides	Significantly inhibited expression of asthma related cytokines *in vitro* and *in vivo*	[150]
	Chitosan oligosaccharides	Suppressed NF-κB activation, reduced proinflammatory cytokine production, inhibited TNF-α and oxidative stress-induced apoptosis *in vitro* and relieved intestinal inflammation *in vivo*	[157]
	Nanoparticles of chitosan and alginate	Inhibited bacterial-induced pro-inflammatory cytokine production in macrophage and keratinocyte *in vitro* culture	[160]
	Chitosan films	*In vitro* monocyte culture showed variation in pro- and anti-inflammatory cytokine production over time (corresponding to monocyte to macrophage differentiation)	[161]
	Chitosan fibers	Promoted migration of inflammatory cells to the wound site and collagen matrix deposition in open skin wounds	[166]
	Chitosan hydrogels	In treatment of third-degree burns, this chitosan material favors inflammatory cell migration and angiogenesis	[169]
DECELLULARIZED MATRIX	Bovine pericardium	Monocyte-derived macrophages seeded on the decellularized matrix in vitro exhibited decreased spreading and lower levels of pro-inflammatory interleukins	[170, 171]
	Skeletal muscle	Decreased levels of pro-inflammatory cytokines and increased levels of anti-inflammatory cytokines (*in vitro*); polarized macrophages towards M2 phenotype (*in vivo*); decreased T cell proliferation	[175]
	Porcine colon	Extensive cellular infiltration and degradation *in vivo* as compared to colonic ECM that had been chemically crosslinked	[176]
	Porcine ureter	Carbodiimide crosslinking corresponds to M2 macrophage phenotype shift in subcutaneous rat model; crosslinking with glutaraldehyde or genipin leads to M1	[178]
AMNIOTIC MEMBRANE BASED	Amniotic membrane sheet	In treatment of adhesions between digital flexor tendons and their sheathes, AM sheets exhibited no inflammation and restored function to the fingers	[220]
		Chronic ulcers treated with AM were healed within 10 weeks	[221]
		In ocular surface applications, AM leads to rapid epithelialization and reduced inflammation	[222-224]
	Collagen-amnion dermal substitute	Results in few inflammatory cells, rapid healing, and good neovascularization in porcine full thickness skin defect	[225]
	Micronized, dry amnion-chorion membrane	Injected, reduces cartilage degeneration in osteoarthritic rat model	[228]
	Collagen-amnion porous scaffolds	Decreased expression of TNF-α and MMP-3 genes, increased expression of COLI under pro-inflammatory condition *in vitro*	[230]

1.10 Figures

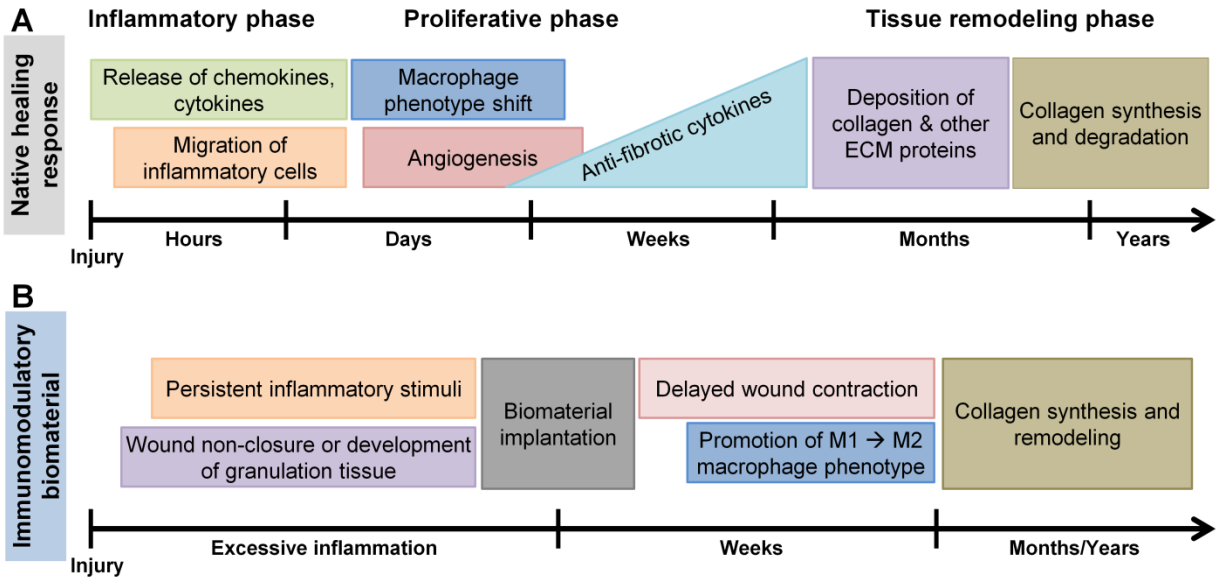

Figure 1.1. (A) Sequence of events in the body's normal response to injury (adapted from Bentzen et al. [231]). **(B)** This chain of events can change depending on the tissue type, age of the individual, disease state, and the acute/chronic nature of the defect. In some cases, wounds undergo excessive inflammation leading to chronic wounds or scar formation. Biomaterials with immunomodulatory properties have the potential to enhance healing.

CHAPTER 2: USING GLYCOSAMINOGLYCANS TO ALTER GROWTH FACTOR DELIVERY AND CELLULAR RESPONSE[†]

2.1 Chapter overview

The design of biomaterials for regenerative medicine can require biomolecular cues such as growth factors to induce a desired cell activity. Signal molecules are often incorporated into the biomaterial in either freely-diffusible or covalently bound forms. However, biomolecular environments *in vivo* are often complex and dynamic. Notably, glycosaminoglycans (GAGs) are linear polysaccharides found in the extracellular matrix involved in transient sequestration of growth factors via charge interactions. Biomaterials mimicking this phenomenon may offer the potential to amplify local biomolecular signals, both endogenously produced and exogenously added. GAGs of increasing sulfation (hyaluronic acid, chondroitin-sulfate, heparin) were incorporated into a collagen-GAG (CG) scaffold under development for tendon tissue engineering. Manipulating the degree of GAG sulfation significantly impacts sequestration of growth factors from the media. Increasing GAG sulfation improved equine tenocyte metabolic activity in normal serum (10% FBS), low serum (1% FBS), and IGF-1 supplemented media conditions. Notably, previously reported dose-dependent changes in tenocyte bioactivity to soluble IGF-1 within the CG scaffold were replicated by using a single dose of soluble IGF-1 in scaffolds containing increasingly sulfated GAGs. Collectively, these results suggest that CG scaffold GAG content can be systematically manipulated to regulate the sequestration and resultant enhanced bioactivity of growth factor signals on cell behavior within the matrix.

[†] This chapter has been adapted from the following publication: Rebecca A. Hortensius and Brendan A. C. Harley. "The use of bioinspired alterations in the glycosaminoglycan content of collagen-GAG scaffolds to regulate cell activity." Biomaterials, 2013; 34(31): 7645-7652.

2.2 Introduction

A major focus in the field of tissue engineering is the development of biomaterials able to mimic critical features of the extracellular matrix (ECM), the three-dimensional microenvironment surrounding cells in the tissues and organs of the body. Beyond the use of scaffold mechanical, structural, and compositional signals to impact cell fate, the addition of growth factors into the biomaterial is often a primary way of providing instructive signals within the matrix [81]. Methods for biochemical supplementation include providing factors free in solutions [55, 87, 232-234], covalently tethering factors in random and specific orientations to the materials [93, 235-237], and growth factor release vectors [238-240]. However, growth factor activity within the native ECM is often dictated by non-covalent interactions with ECM biomolecules such as proteins and proteoglycans that mediate transient immobilization and release.

Glycosaminoglycans (GAGs) are linear polysaccharides found in the native ECM and are known to play a critical role in sequestering growth factors within the matrix [53, 54, 112, 114, 115, 119, 241-243]. Along with structural variations in their carbohydrate backbone, GAGs can present varying levels of negative charges depending on their degree of sulfation [53, 54], making them attractive for developing growth factor sequestering biomaterials. In addition to the nonspecific, electrostatic growth factor-GAG interactions facilitated by the sulfate groups, it has also been shown that the sulfation code, the positions of the sulfate groups on the carbohydrate backbone, has an impact on growth factor binding [54]. Recently *Hudalla et al.* immobilized heparin-binding peptides on a self-assembled monolayer to demonstrate sequential binding of first heparin and then heparin-binding growth factors to the substrate in order to enhance human mesenchymal stem cell (hMSC) bioactivity [114]. Similar work has also shown that TGF-β1 can be adsorbed onto biomaterials composed of type I collagen and a sulfated hyaluronan [119].

Considering that charged moieties have been shown to sequester biomolecules [54, 114, 115, 119, 242, 243], systematic incorporation of differentially-charged GAGs within a biomaterial to selectively impact growth factor sequestration represents a promising avenue for tuning biomolecular signals. The efforts described here are therefore targeted at exploring whether the degree of GAG sulfation of a collagen-GAG scaffold could be modified to impact the scaffold's capacity to transiently sequester activity-impacting molecules within the scaffold network.

Collagen-GAG (CG) scaffolds have been used for a wide variety of applications for skin, peripheral nerve, and cartilage tissue engineering as well as 3D environments for *in vitro* studies of cell behavior [55-57, 67, 244-246]. Early development of the CG scaffold platform for skin regeneration included comparison of the effects of the type and weight percent of GAG contained in the scaffold [247], though these studies did not consider biomolecule sequestration. Based on results from *in vivo* kinetics of wound contraction and quality of regeneration studies, CG scaffolds have traditionally included a 11:1 (wt:wt) collagen:GAG ratio employing chondroitin-sulfate [248]. Recent efforts in our lab have described modification of the CG scaffold platform for tendon repair applications. As tendon is composed primarily of type I collagen arranged into aligned fibrils [77, 249, 250], we described a directional solidification method to fabricate CG scaffolds with highly anisotropic (aligned) morphology composed of longitudinally-aligned ellipsoidal pores [61]. Notably, scaffold anisotropy was found to improve equine tenocyte alignment as well as long-term maintenance of a pro-tenogenic phenotype [60, 61]. Further, incorporation of growth factor signals within the anisotropic scaffold in either freely-soluble or covalently immobilized forms have been shown to impact tenocyte bioactivity in a dose-dependent manner [87]. In particular, soluble or covalently-bound insulin-like growth factor 1 (IGF-1) was found to enhance tenocyte proliferation but at the expense of tenocyte

phenotype [61]. Similarly, soluble growth/differentiation factor 5 (GDF-5) was used to increase expression of tenogenic-specific genes within the CG scaffolds [87].

This manuscript described the manipulation of the degree of GAG sulfation within the CG scaffold to promote transient, non-covalent sequestration of growth factors for applications in tendon tissue engineering. As prior work has shown dose-dependent tenocyte responses to growth factor within the CG scaffold [61, 87], this work investigated whether alterations of GAG content within the scaffold could replicate dose-dependent effects using a single growth factor dose. Notably, it was hypothesized that scaffolds containing a highly sulfated GAG (heparin) would show an increase in transient growth factor sequestration and enhanced bioactivity of cells seeded within these scaffolds relative to less sulfated GAGs such as chondroitin-sulfate, the GAG traditionally used in CG scaffolds, or non-sulfated hyaluronic acid. The response of equine tenocytes and human mesenchymal stem cells (hMSCs) to pro-proliferation (IGF-1) and pro-tenocyte phenotype (GDF-5) factors in the culture media as well as metabolically limited culture environments (low serum) was examined to explore the impact of GAG-mediated non-covalent sequestration on cellular bioactivity [87].

2.3 Materials and methods

2.3.1 Preparation of CG suspension

A suspension of collagen and a defined glycosaminoglycan was made by homogenizing type I collagen from bovine Achilles tendon (Sigma-Aldrich, St. Louis, MO) and one of three glycosaminoglycans (GAGs): hyaluronic acid from Streptococcus equi (Sigma-Aldrich #53747, St. Louis, MO), chondroitin-sulfate from shark cartilage (Sigma-Aldrich #C4384, St. Louis, MO) or heparin from porcine intestinal mucosa (Sigma-Aldrich #H4784, St. Louis, MO) in 0.05 M

acetic acid [56]. A constant collagen concentration (1.5% w/v) and collagen:GAG ratio (11.28:1) was used for all experiments. The suspension was stored at 4°C and degassed prior to use [251].

2.3.2 Fabrication of CG scaffolds via freeze drying

CG scaffolds were fabricated as previously described [61]. Briefly, the scaffolds were produced via directional solidification using a polytetrafluoroethylene (PTFE)-copper mold. The mismatch in thermal conductivity between the mold materials promotes unidirectional heat transfer through the copper bottom when the mold is placed on a precooled freeze-dryer shelf (VirTis, Gardiner, NY). The CG suspension was added to the cylindrical wells of the mold and frozen at -10˚C for two hours prior to the sublimation of the resulting ice crystals at 0˚C and 200 mTorr. This resulted in a dry, porous scaffold 6 mm in diameter and 20 mm in length with constant pore size along its length [61].

2.3.3 Crosslinking of CG scaffold

Following lyophilization, scaffolds were sterilized and dehydrothermally crosslinked in a vacuum oven (Welch, Niles, IL) at 105˚C under vacuum for 24 hours [56]. 5 mm long sections were cut from the scaffold and used for all experiments [61]. Prior to use, these scaffolds were hydrated in 100% ethanol overnight and washed in phosphate-buffered saline (PBS) for 24 hours. Scaffolds were subsequently crosslinked using carbodiimide chemistry to make them resistant to tenocyte contraction [248, 252]. Scaffolds were immersed in 1-ethyl-3-[3-dimethylaminopropyl] carbodiimide hydrochloride (EDC) and *N*-hydroxysulfosuccinimide (NHS) at a molar ratio of 5:2:1 EDC:NHS:COOH for 2 h under shaking at room temperature. Following crosslinking, scaffolds were washed with PBS and stored in fresh PBS at 4˚C.

2.3.4 SEM analysis

Scanning electron microscopy (SEM) was used to visualize the scaffold microstructure. Dry, uncrosslinked sections from the center of the scaffold were used for analysis. Samples were sputter-coated with gold-palladium and imaged with a JEOL JSM-6060LV scanning electron microscope using secondary electron and backscattered electron detectors under high vacuum.

2.3.5 Evaluation of CG scaffold microstructure

Microstructural features (pore size, aspect ratio) of the aligned CG scaffold variants were calculated using previously described stereology approaches [61]. Briefly, serial longitudinal and transverse sections were generated from glycolmethacrylate (Polysciences, Warrington, PA) embedded scaffolds using a microtome (Leica Microsystems, Germany) and mounted on slides. Sections were then stained with aniline blue stain to facilitate the visualization of the scaffold struts on an optical microscope (Leica Microsystems, Germany). Multiple images were captured per section and then analyzed using MATLAB equipped with a linear intercept method which outputs parameters used to calculate pore diameter and aspect ratio [69]. For each GAG variant a minimum of 6 scaffold sections were analyzed (3 longitudinal, 3 transverse) with a minimum of 5 fields of view captured per section.

2.3.6 Pull down sequestration assay

The degree of growth factor sequestration by CG scaffold variants was determined via a pull down assay. Ten hydrated crosslinked scaffolds were incubated overnight at 37°C in a single well of an ultra-low attachment 6-well plate (Fisher, Waltham, MA) in 4 mL of a pH 7.4 PBS solution with 500 ng/mL IGF-1 (ProSpec, Israel) and 1% bovine serum albumin (BSA). Scaffolds fabricated from each GAG were tested separately, with wells containing the IGF-1 solution but no scaffolds used as controls. Following incubation, the amount of IGF-1 remaining

in solution was measured via an ELISA kit (R&D Systems, Minneapolis, MN). Relative pull down, the amount of IGF-1 trapped within the CG scaffolds, was calculated from the difference in IGF-1 remaining in the media of the experimental versus control wells. Pull down for each CG variant was reported as a percentage of the total IGF-1 concentration in the loading solution.

2.3.7 Tenocyte isolation and culture

Tenocytes (tendon cells) were isolated from 2-3 year old horses that were euthanized for reasons not related to tendinopathy using previously described methods [253]. Tenocytes were expanded in standard culture flasks in high glucose Dulbecco's modified Eagle's medium supplemented with 10% fetal bovine serum (Invitrogen, Carlsbad, CA), 1% Antibiotic-Antimycotic (Invitrogen, Carlsbad, CA), 1% L-glutamine (Invitrogen, Carlsbad, CA), and 50 µg/mL ascorbic acid (Wako, Richmond, VA). The tenocytes were cultured to confluence at 37˚C and 5% CO_2 and the media was changed every 3 days. Passage 4 cells were used for all culture experiments.

2.3.8 hMSC culture

Human mesenchymal stem cells (hMSC) from human bone marrow (Lonza, Switzerland) were cultured in standard culture flasks in low glucose Dulbecco's modified Eagle's medium supplemented with 10% MSC FBS (Invitrogen, Carlsbad, CA), 1% Antibiotic-Antimycotic (Invitrogen, Carlsbad, CA), 1% L-glutamine (Invitrogen, Carlsbad, CA). Media was changed every 3 days and the cells were cultured to confluence at 37˚C and 5% CO_2. Cells were used at passage 6.

2.3.9 Scaffold seeding and culture conditions

Hydrated scaffold sections (6 mm diameter, 5 mm thick) were placed in ultra-low attachment 6-well plates (Fisher, Waltham, MA). Confluent tenocytes or hMSCs were trypsinized and

resuspended at concentrations of 5 x 10^5 tenocytes or 7.5 x 10^4 hMSCs per 20 µL of media. Scaffolds were seeded with either tenocytes or hMSCs using a previously established method [61]. Briefly, 10 µL of the cell suspension was added to each scaffold and then the scaffolds were incubated for 15 minutes at 37˚C. The scaffolds were flipped over and another 10 µL of cell suspension was added for a total of 5 x 10^5 tenocytes or 7.5 x 10^4 hMSCs seeded on each scaffold. After 2 hours of incubation to facilitate initial cell attachment, additional media was added and scaffolds were incubated at 37˚C and 5% CO_2 with the media changed every 3 days for the duration of the experiment. Scaffolds were cultured in tenocyte or hMSC culture media as described above, with or without the addition of serum or soluble growth factors. While standard media contained 10% FBS, some cultures were performed at low serum levels (1%). Experiments including growth factor supplementation (50 ng/mL IGF-1, 500 ng/mL GDF-5) were performed in serum free media.

2.3.10 Quantification of cell metabolic activity

The metabolic activity of the cells contained within the CG scaffolds was measured using a non-destructive alamarBlue® assay (Invitrogen, Carlsbad, CA) [61, 251] that uses the conversion of resazurin to the fluorescent byproduct resorufin by metabolically active cells. Briefly, scaffolds were removed from culture, rinsed in PBS, then incubated in a 1x alamarBlue® solution at 37˚C for 2 hours under shaking [61]. Using a fluorescent spectrophotometer, resorufin fluorescence was measured (excitation: 540 nm, emission: 590 nm) and compared to a standard curve created from a known number of cells (tenocytes, hMSCs). While not all cells are known to attach to the scaffold during seeding [67], metabolic activity at each time point was reported as a percentage of the total number of seeded cells to provide a standard comparison metric.

2.3.11 RNA isolation and real-time PCR

RNA was isolated from cells (tenocytes or hMSCs) using an RNeasy Plant Mini kit (Qiagen, Valencia, CA). Cell seeded scaffolds were rinsed in PBS, cut longitudinally with a razor, and immersed in the kit's lysis buffer for 5 minutes on ice [87]. After lysing, RNA was isolated per the kit's instructions and total RNA quantified via spectrophotometry. The isolated RNA was reverse transcribed in a Bio-Rad S1000 thermal cycler using a QuantiTect Reverse Transcription kit (Qiagen, Valencia, CA). Real-time PCR reactions were performed in an Applied Biosystems 7900HT Fast Real-Time PCR System (Carlsbad, CA) to measure gene expression levels for collagen type I alpha 2 (*COL1A2*), scleraxis (*SCXB*), and tenascin-C (*TNC*). Glyceraldehyde 3-phosphate dehydrogenase (*GAPDH*) was used as a housekeeping gene. All primer sequences used (Table 2.1) were taken from the literature [130, 254], and were synthesized by Integrated DNA Technologies (Coralville, IA). Analysis was completed with Sequence Detection Systems software v2.4 (Applied Biosystems, Carlsbad, CA). All results were expressed as fold changes normalized to the expression levels of cells in CG scaffolds containing hyaluronic acid for the GAG constituent at the first time point unless otherwise noted.

2.3.12 Statistical analysis

One-way analysis of variance (ANOVA) was performed on all data sets followed by Tukey-HSD post-hoc test. A p-value < 0.05 was used for significance. All analyses were based on a minimum of n=3 scaffolds. In figures, error is reported as the standard error of the mean.

2.4 Results

2.4.1 Scaffold microstructure and pore size analysis

Scaffolds fabricated via freeze drying techniques showed highly porous, sponge-like features when imaged with SEM (Fig. 2.1). Analysis of scaffold microstructure suggested minimal structural differences between scaffolds. Notably, in the longitudinal direction, mean pore diameters varied between 184 and 199 μm for all three variants, with no statistically significance differences between GAG types (C:HA, C:CS, C:HP) (Table 2.2). In the transverse plane, mean pore sizes for the scaffold groups varied between 195 and 306 μm with a statistically significant difference ($p < 0.05$) observed between C:CS and C:HP scaffolds (Table 2.2). However, increasing (or decreasing) level of GAG sulfation was not correlated with a change in scaffold pore size since the transverse pore sizes of the C:HA scaffolds fall between those of the higher sulfated GAGs.

2.4.2 Growth factor sequestration within CG scaffolds

Scaffold GAG content was found to significantly impact sequestration of IGF-1 from the media to the scaffold (Fig. 2.2). Notably, sulfated C:CS and C:HP scaffolds showed significantly ($p < 0.05$) increased IGF-1 sequestration compared to non-sulfated C:HA scaffolds. Additionally, no significant increase in IGF-1 pull down was observed for non-sulfated C:HA scaffolds over control (no scaffolds) were observed (data not shown).

2.4.3 Tenocyte response to altered serum concentrations

Equine tenocyte metabolic activity was evaluated in each GAG scaffold at days 1, 4, 7 and 14 (Fig. 2.3). Cells were cultured in media with either normal (10%) or metabolically-limiting (1%) levels of fetal bovine serum (FBS). Tenocytes cultured in 10% media showed GAG-dependent trends in metabolic activity; notably C:HP scaffolds showed elevated metabolic activity over other groups at all experimental timepoints, with a significant ($p < 0.05$) increase in metabolic

activity seen compared to both C:HA and C:CS scaffolds at day 7 (Fig. 2.3A). The effect was heightened in low serum conditions, where all groups showed reduced metabolic activity compared to normal serum. However, tenocytes within the highest sulfated C:HP scaffolds showed significantly enhanced metabolic activity over the other CG scaffold variants after the first day in culture. Tenocyte metabolic activity in C:HP scaffold was significantly higher ($p < 0.05$) at days 4, 7 and 14 compared to all other scaffold groups (C:HA, C:CS; Fig.2.3B).

Prior work has linked increases in tenocyte metabolic activity with increased expression levels of the tendon-associated structural matrix gene *COL1A2* as well as decreases in the tenocyte phenotype associated gene *TNC* [87]. Expression levels of *COL1A2* and *TNC* were therefore evaluated for tenocytes cultured in normal (10% FBS) media in the three scaffold variants at days 4, 7, and 14 (Fig. 2.4). *COL1A2* gene expression was significantly upregulated in the most highly-sulfated C:HP scaffolds compared to the C:HA group at day 7 and both lower-sulfated C:HA and C:CS groups at day 14 ($p < 0.05$) (Fig. 2.4A). Separately, a trend of downregulation of *TNC* gene expression was observed with increasing GAG sulfation (Fig. 2.4B). This effect was significant ($p < 0.05$) in C:HP scaffolds compared to C:HA at days 4 and compared to both scaffold types at day 7 ($p < 0.05$) (Fig. 2.4B).

2.4.4 Tendon cell metabolic activity and gene expression with IGF-1 supplementation

Prior work has shown dose-dependent effects of IGF-1 supplementation (10, 50, 200 ng/mL) on tenocytes cultured in C:CS scaffolds [87]. These effects were reflected in both measures of growth (metabolic activity and *COL1A2* gene expression) and phenotype (gene expression of *SCXB* and *TNC*). Here, tenocytes were seeded in the three differentially-sulfated CG scaffold variants, then cultured in serum-free media supplemented with insulin-like growth factor 1 (IGF-

1) at a concentration of 50 ng/mL. Previously observed IGF-1 dose-dependent responses for tenocyte metabolic activity as well as gene expression profiles were observed for a single IGF-1 dose across scaffolds of increasing GAG-sulfation (Fig. 2.5). Tenocytes in the most highly-sulfated C:HP scaffolds showed significantly higher metabolic activity at days 4, 7, and 14 compared to cells seeded in the other GAG variants of our CG scaffolds at the same timepoints ($p < 0.01$). A trend of increasing COL1A2 expression was observed starting at day 4 in the scaffolds, with significant ($p < 0.05$) upregulation observed at days 4 and 14 in the most highly-sulfated C:HP scaffolds compared to lesser-sulfated C:HA and C:CS scaffolds (Fig. 2.5B).

Increasing levels of IGF-1 supplementation has been previously shown to decrease expression of tenocyte phenotypic markers scleraxis (*SCXB*) and tenascin-C (*TNC*) [87]. Similarly, expression of *SCXB* (Fig. 2.5C) and *TNC* (Fig. 2.5D) was significantly downregulated with increasing GAG sulfation. Notably, *SCXB* expression was significantly lower in the most highly-sulfated C:HP scaffolds than C:HA scaffolds at day 4 and significantly lower than both lesser-sulfated scaffolds variants at day 14 ($p < 0.05$). Similarly, *TNC* gene expression was significantly ($p < 0.05$) downregulated in more-highly sulfated C:CS and C:HP scaffolds compared to non-sulfated C:HA scaffolds at day 4, and significantly ($p < 0.05$) downregulated in the most highly-sulfated C:HP scaffolds versus non-sulfated C:HA scaffolds at day 14.

2.4.5 hMSC metabolic activity and gene expression with GDF-5 supplementation

Previous investigations have shown the use of sequestered heparin on chemically-defined culture substrates could impact the bioactivity of human mesenchymal stem cells (hMSCs) through transient sequestration of growth factors [114]. Separately, growth/differentiation factor 5 (GDF-5) has been identified as a pro-tenogenic morphogen [255, 256]. Here, the metabolic activity and

gene expression levels of the tenogenic gene *SCXB* were monitored in hMSCs cultured in serum-free media containing 500 ng/mL GDF-5 in the range of CG scaffolds. While hMSC metabolic activity remained low for all variants, likely a consequence of serum free conditions, hMSCs in the most highly-sulfated C:HP scaffolds were significantly ($p < 0.05$) more metabolically active than those in the C:CS scaffolds at day 4 and significantly ($p < 0.05$) more metabolically active than either of the lesser-sulfated (C:HA, C:CS) scaffolds at day 7 (Fig. 2.6A). Further, although the expression of *SCXB* was globally upregulated at day 7 compared to day 4, there was no significant difference between any of the groups (Fig. 2.6B).

2.5 Discussion

This study sought to determine whether the degree of sulfation of the GAG component of a model CG scaffold could impact growth factor sequestration and, further, whether such sequestration was sufficient to alter the bioactivity of both differentiated (equine tenocytes) and non-differentiated (hMSCs) cells. This effort was inspired by GAG-mediated sequestration of factors within the native ECM [81] and prior work showing heparin-binding peptides incorporated within a chemically-defined two-dimensional substrate were able to bind heparins from the cell culture media which in turn were able to transiently sequester growth factors on the culture surface [114, 243]. Incorporating charged moieties into a biomaterial able to replicate such sequestration of the ECM offers a route to locally amplify biomolecular signals, to either reduce required factor dose or direct autocatalytic processes. Systematic variation of sequestration capacity using bioinspired GAG design has not before been implemented in 3D collagen-based biomaterial systems.

GAGs with known differences in their degree of sulfation were integrated into a three-dimensional CG scaffold. CG scaffolds have been previously used for a range of *in vitro* and *in*

vivo applications, including prior work in our lab examining the importance of soluble growth factor supplementation schemes to enhance tenocyte bioactivity for tendon tissue engineering applications [60, 61, 251]. In particular, insulin-like growth factor 1 (IGF-1) and growth and differentiation factor 5 (GDF-5) were shown to drive dose-dependent responses in tenocyte metabolic activity and gene expression [87]. Notably, IGF-1 enhanced tenocyte proliferation but at the expense of phenotype [233, 257] while GDF-5 could be used to maintain tenogenic phenotype *in vitro* but at the expense of proliferation [255, 256]. Importantly for this application, dose-dependent increases in *COL1A2* gene expression and collagen biosynthesis as well as dose-dependent decreases in *SCXB* and *TNC* gene expression in equine tenocytes with IGF-1 supplementation have been previously described. Additionally, dose-dependent increases in expression of tenogenic markers *SCXB* and *TNC* in equine tenocytes with GDF-5 supplementation were noted [87].

The three CG scaffold variants all displayed microstructural features characteristic of low-density, open-cell foams (Fig. 2.1). All three scaffolds contained consistent pore structures in the longitudinal plane (Table 2.2), the direction previously identified as having the primary impact on tenocyte bioactivity [60, 61]. Sequestration of growth factors from the media into the scaffold structure was examined across the three CG scaffold variations using a modified pull down assay (Fig. 2.2). There was a significant increase in the amount of IGF-1 bound to the moderately (CS) and highly (HP) sulfated GAG scaffolds compared to the non-sulfated GAG (HA) scaffold. This supports the claim that the presence of charged glycosaminoglycans within the CG scaffold, even at relatively low concentration (11.28:1 collagen:GAG) can impact the sequestration of growth factors. We acknowledge that the difference in transverse pore size between C:CS and C:HP scaffolds may impact cell activity. Indeed, CG scaffold pore size has previously been observed to

impact cell attachment [67], motility [244], and even tenocyte alignment and distribution within the scaffold [61]. However, the differences in pore size between the C:CS and C:HP scaffolds in this study is outside the range of pore sizes (50 – 150 μm) previously reported to affect cell activity. Further, the difference in pore size in this study was only observed between two scaffold variants and in only a single plane, so does not explain the entirety of the reported data that showed increases and decreases in cell activity across the range of GAG types.

In order to study the effects of GAG-mediated sequestration on tenocyte bioactivity, the metabolic activity of cells cultured in the CG scaffold variants at two concentrations of FBS was examined (Fig. 2.3). The objective was to determine whether the highly sulfated GAG scaffolds could support enhanced cellular bioactivity even in metabolically limited cultures. Such observations had been previously made for hMSCs cultures on 2D, chemically-defined culture substrates presenting heparin binding peptides [114], but had not been extended to a fully-3D biomaterial composed of native ECM proteins. Since serum contains a large number of growth factors, scaffold bioactivity was evaluated at normal (10%) and restricted (1%) serum levels. At normal serum levels tenocytes proliferated in all scaffold variants and scaffold GAG sulfation impacted tenocyte metabolic activity (Fig. 2.3A) with the greatest effect observed in metabolically-limited cultures (1% serum) (Fig. 2.3B). Here, a significant effect of GAG type was seen for all culture conditions, with the most highly-sulfated C:HP scaffolds inducing significant increases in tenocyte metabolic activity at days 4, 7, and 14 in low serum conditions (Fig. 2.3B). This supports the hypothesis that the highly sulfated heparin GAG scaffolds enhance tenocyte metabolic activity even at reduced metabolic support, which may be critical for future *in vivo* studies where metabolic support is significantly reduced immediately after implantation.

Further, when examining gene expression profiles for tenocyte growth in the scaffolds under normal metabolic support, GAG sulfation-dependent increases in *COL1A2* expression was observed (Fig.2.4A) indicating an increase in the signal to produce collagen type I, a primary tendon-associated structural protein. Future investigations will employ longer culture times (4 – 8 weeks) to quantify differences in collagen production via ELISA or histology. Such studies are not included as part of this work because the current goal was to elucidate whether the initial GAG content of the scaffolds could impact cell bioactivity; longer-term experiments would involve significant scaffold remodeling, making it difficult to assess GAG-mediated influences. In addition to the effects of GAG sulfation on *COL1A2* expression, GAG-dependent downregulation of the *TNC* gene, which encodes for a glycoprotein found in developing and mature tendon, was seen (Fig. 2.4B). These results are consistent with prior work that demonstrated a tradeoff between tenocyte proliferation and maintenance of the tendon phenotype [87, 90].

Following the investigation of tenocyte bioactivity at different serum concentrations, the examination of tenocyte response to the proliferative growth factor (IGF-1) was undertaken. Prior work using the C:CS scaffold demonstrated dose-dependent increases in tenocyte proliferation with IGF-1 supplementation (10, 50, 200 ng/mL) [87]. It was hypothesized that this dose-dependent increase in tenocyte metabolic activity could be replicated with a single dose of IGF-1 (50 ng/mL) and differential levels of GAG-mediated IGF-1 sequestration within the matrix. Indeed, dose-dependent trends and significant ($p < 0.01$) increases in tenocyte metabolic activity at days 4, 7, and 14 in the CG scaffolds with the highest degree of GAG-sulfation were seen (Fig. 2.5A). In addition, GAG-dependent upregulation of *COL1A2* and downregulation of *TNC* and *SCXB* was observed (Fig. 2.5B-D). Critically, in enhanced proliferative conditions

established in scaffolds of increasing GAG-sulfation, *COL1A2* expression increased while markers of tenogenic phenotype decreased.

Finally, the use of GDF-5 to alter hMSC bioactivity within the CG scaffold variants was studied (Fig. 2.6). To specifically interrogate the addition of GDF-5, these experiments were completed in serum-free conditions, leading to a shortened experimental time (7 days) and overall reduced metabolic activity for all conditions. As seen with tenocyte cultures (Fig. 2.3), hMSC metabolic activity was enhanced in the most highly-sulfated C:HP scaffolds. These results confirm that even without serum or a pro-proliferative factor the highly sulfated GAGs can improve cellular bioactivity, likely through local amplification of biomolecule signals [243]. Examining expression of a characteristic tenogenic gene *SCXB*, global increases over time for all groups were observed with no significant differences between the GAG variants, perhaps due to the reduced metabolic support from the media or the overall GDF-5 dose.

Taken together, this work illustrates the application of bioinspired proteoglycan design within a model collagen-GAG scaffold with focus on creating a 3D biomaterial construct able to leverage concepts taken from GAG-mediated local sequestration of biomolecular signals within the native ECM. The incorporation of three distinct GAGs into a model CG scaffold was examined to determine the ability for each scaffold variant to sequester growth factors from the media. Further, scaffolds with increasing degrees of GAG sulfation were used to replicate previously observed dose-dependent effects of growth factor supplementation on cell bioactivity using single factor dosages. Notably, there was enhanced sequestration of IGF-1 within the CG scaffold structure with moderately or highly sulfated GAGs. While an increased degree of sulfation led to increased tenocyte metabolic activity in low serum and IGF-1 supplemented media conditions, this increase in metabolic activity is accompanied by a decrease in tendon

phenotypic markers. Although this effort used a single collagen:GAG ratio previously described in the literature as optimal for a range of tissue regeneration studies [56, 258], future work will include modifying the overall collagen:GAG ratio or gradually desulfating a particular GAG of interest (e.g., CS, HP [117, 259]) to investigate the impact of GAG concentration on cell bioactivity. Future endeavors may also consider more specific alteration to the carbohydrate backbone or GAG sulfation code to gain improved control over factor sequestration and release.

2.6 Conclusions

Recognizing the significance of GAGs in the native ECM for transiently sequestering and amplifying biomolecular signals, this manuscript demonstrated the use of bioinspired GAG design within a collagen-GAG scaffold to impact cell bioactivity for a tendon tissue engineering application. This study showed that increasing scaffold GAG sulfation increases equine tenocyte metabolic activity in low serum and IGF-1 supplemented media conditions, but at the expense of tendon phenotypic markers. Previously described dose-dependent effects of IGF-1 and GDF-5 supplementation on equine tenocytes and hMSCs in CG scaffolds were replicated by using a single dose of IGF-1 or GDF-5 and the series of CG scaffolds with increasing degree of GAG sulfation. These results suggest ways that scaffold chemistry may be optimized to reduce required dosages of growth factors in the cell culture media.

2.7 Tables

Table 2.1. Primer sequences used in RT-PCR.

Transcript	Sequence	Reference
COL1A2 (equine)	Forward: 5'-GCACATGCCGTGACTTGAGA-3' Reverse: 3'-CATCCATAGTGCATCCTTGATTAGG-5'	[130]
TNC (equine)	Forward: 5'-GGGCGGCCTGGAAATG-3' Reverse: 3'-CAGGCTCTAACTCCTGGATGATG-5'	[130]
SCXB (equine)	Forward: 5'-TCTGCCTCAGCAACCAGAGA-3' Reverse: 3'-TCCGAATCGCCGTCTTTC-5'	[130]
GAPDH (equine)	Forward: 5'-GCATCGTGGAGGGACTCA-3' Reverse: 3'-GCCACATCTTCCCAGAGG-5'	[130]
SCXB (human)	Qiagen QuantiTect Primer Assay Kit. Commercial product (no sequence available)	[130]
GAPDH (human)	Forward: 5'- CCATGAGAAGTATGACAACAGCC-3' Reverse: 5'- CCTTCCACGATACCAAAGTTG-3'	[254]

Table 2.2. Mean pore size (longitudinal, transverse plane) for the three aligned CG scaffold variants (GAG: Hyaluronic acid, chondroitin-sulfate, heparin). Data expressed as mean ± standard deviation, n = 3. (*) significance ($p < 0.05$) between groups in the transverse direction.

	Longitudinal pore size	**Transverse pore size**	
C:HA	184 ± 46 µm	221 ± 27 µm	
C:CS	196 ± 11 µm	195 ± 27 µm	*
C:HP	199 ± 25 µm	306 ± 31 µm	

2.8 Figures

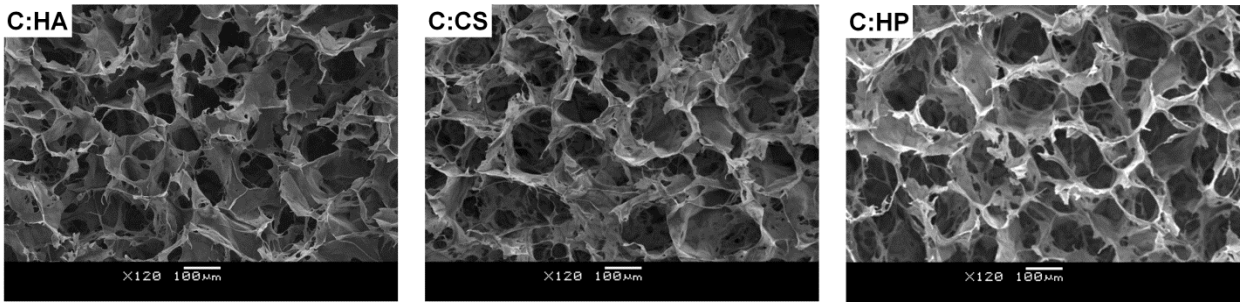

Figure 2.1. SEM images of CG scaffold pore structure for each GAG variant (*left* to *right*): collagen:hyaluronic acid (C:HA), collagen:chondroitin-sulfate (C:CS, standard), collagen:heparin (C:HP).Scale bar: 100 μm.

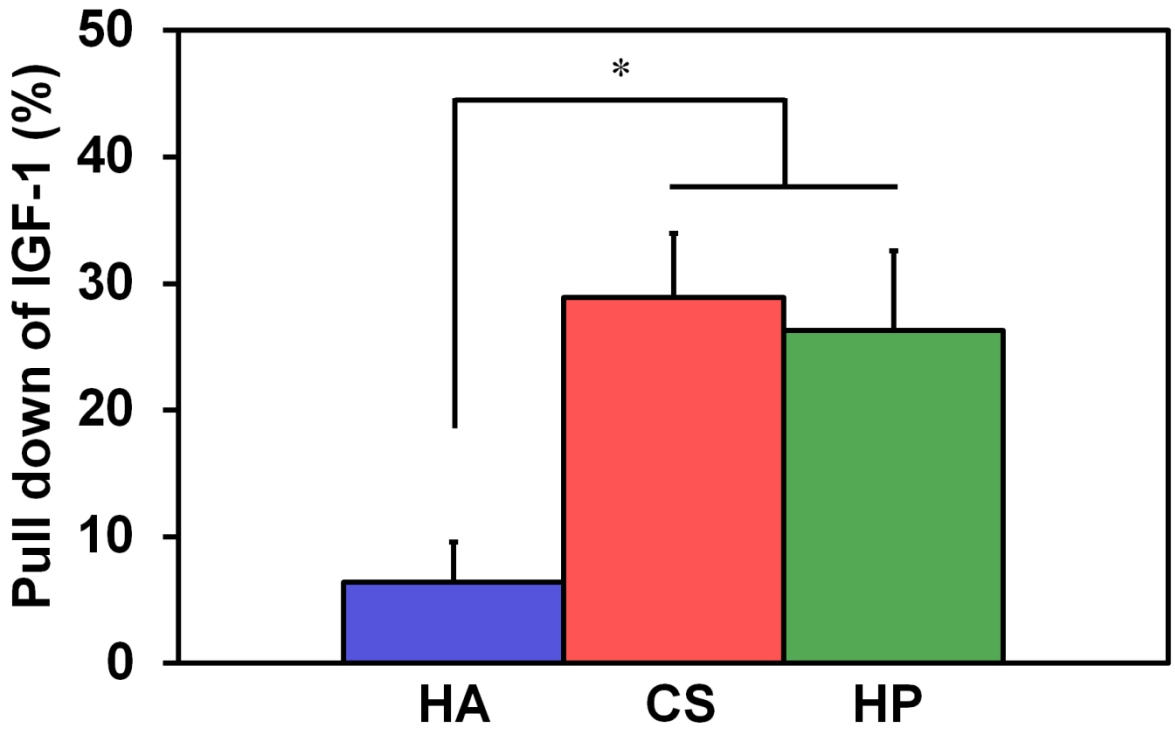

Figure 2.2. IGF-1 sequestration by CG scaffolds with varying degree of GAG sulfation. The degree of pull down is normalized to the no scaffold control. (*) significance ($p < 0.05$) between scaffold groups.

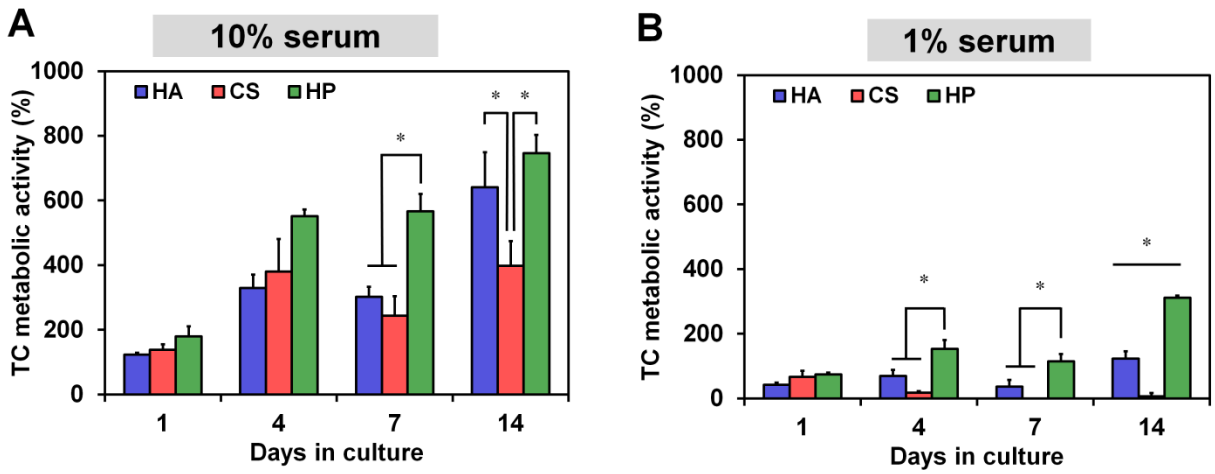

Figure 2.3. Tenocyte metabolic activity as a function of scaffold GAG sulfation as well as media serum level. **(A)** Tenocyte metabolic activity in scaffolds cultured in media containing normal (10%) FBS concentrations. (B) Tenocyte metabolic activity under reduced (1%) FBS concentrations. (*) significance ($p < 0.05$) between groups at a given time point.

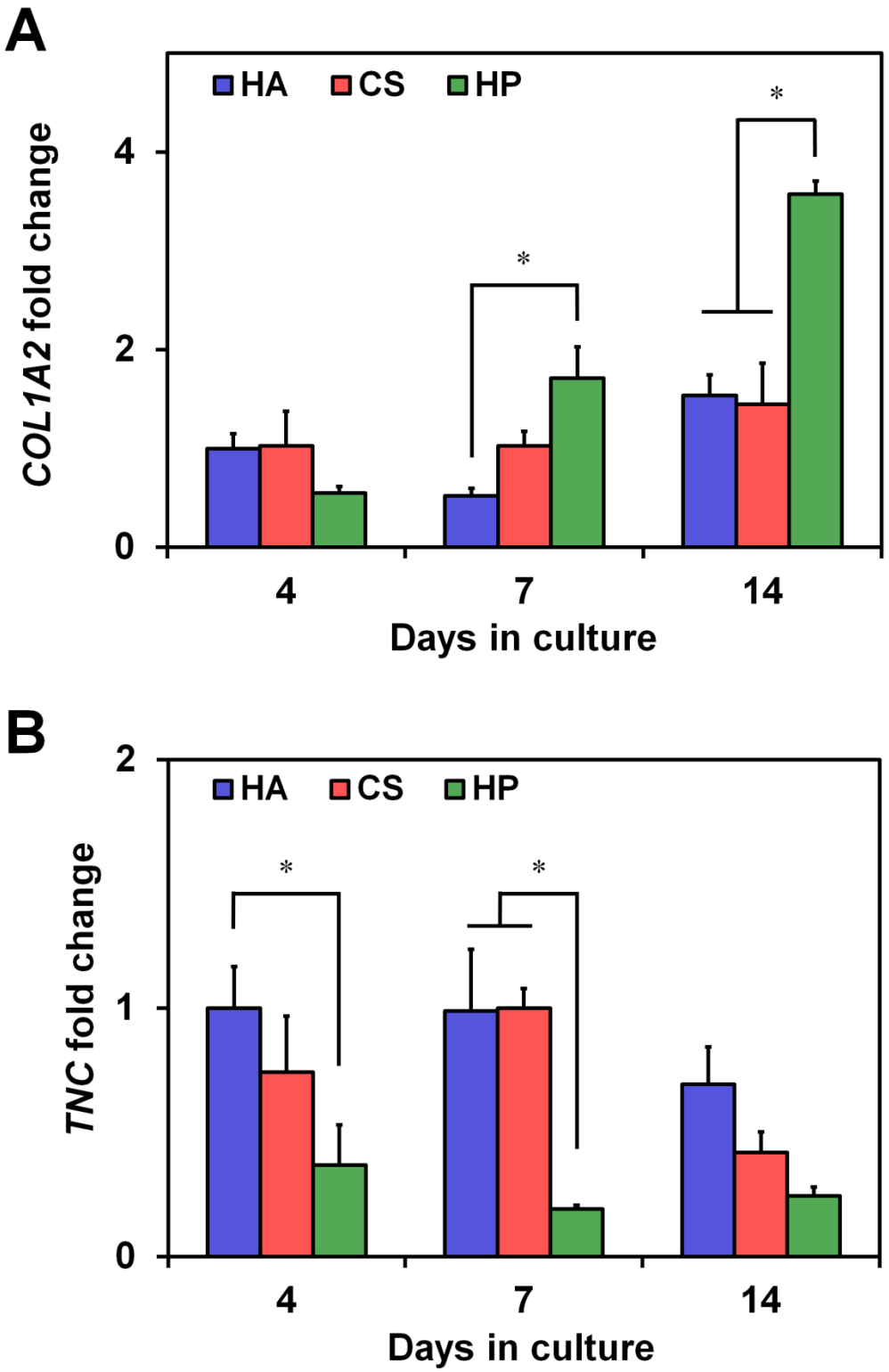

Figure 2.4. Tenocyte gene expression levels for **(A)** Collagen I (*COL1A2*) and **(B)** Tenascin C (*TNC*) as a function of scaffold GAG sulfation at days 4, 7, and 14 of culture. Gene expression was normalized to tenocytes cultured in the C:HA scaffold variant at day 4. (*) significance ($p < 0.05$) between GAG groups at a given time point.

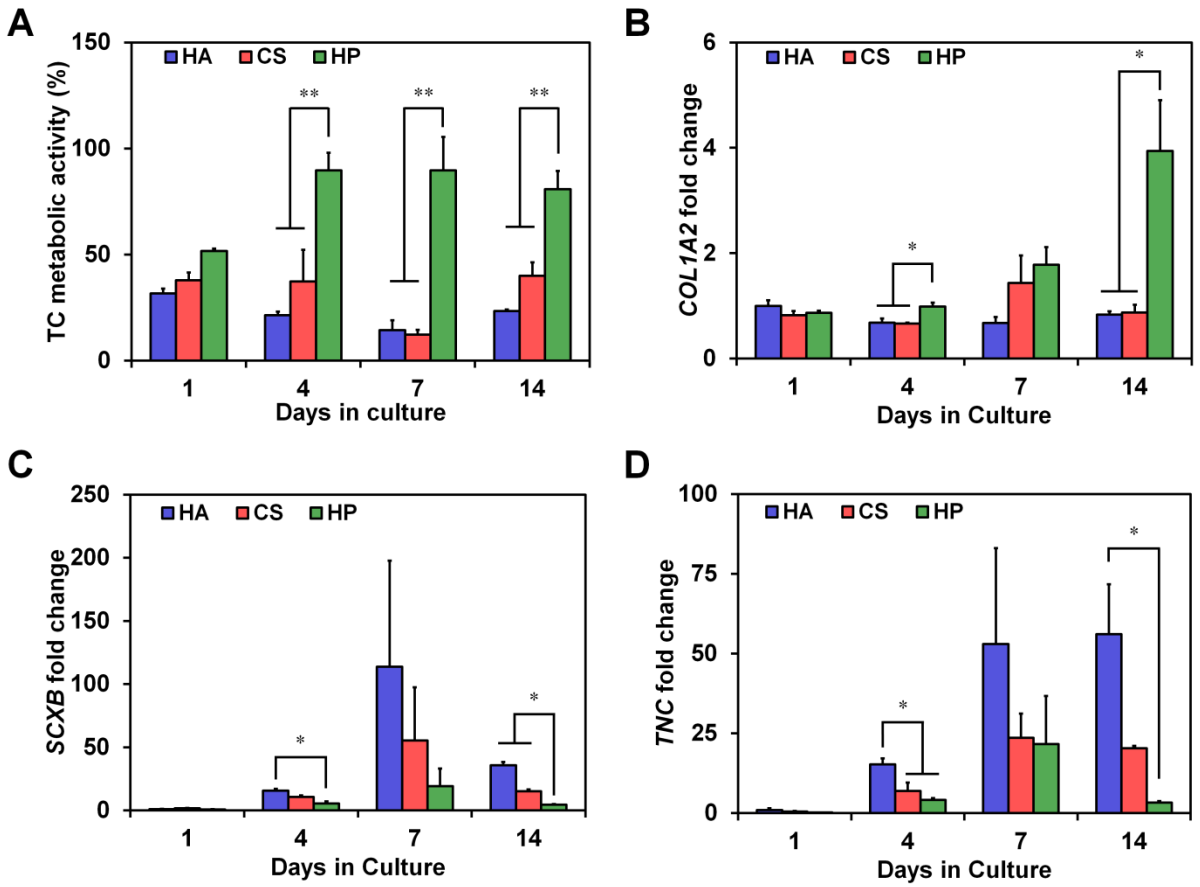

Figure 2.5. Tenocyte response to IGF-1 supplementation (50 ng/mL in serum-free media) as a function of scaffold GAG content. Tenocyte response is reported as **(A)** total metabolic activity as well as gene expression levels (normalized to C:HA scaffolds at day 1) for (**B**) collagen I (*COL1A2*), **(C)** scleraxis (*SCXB*), and **(D)** tenascin-C (*TNC*). (*) significance ($p < 0.05$) between groups at a given time point. (**) significance ($p < 0.01$) compared to all groups at a given time point.

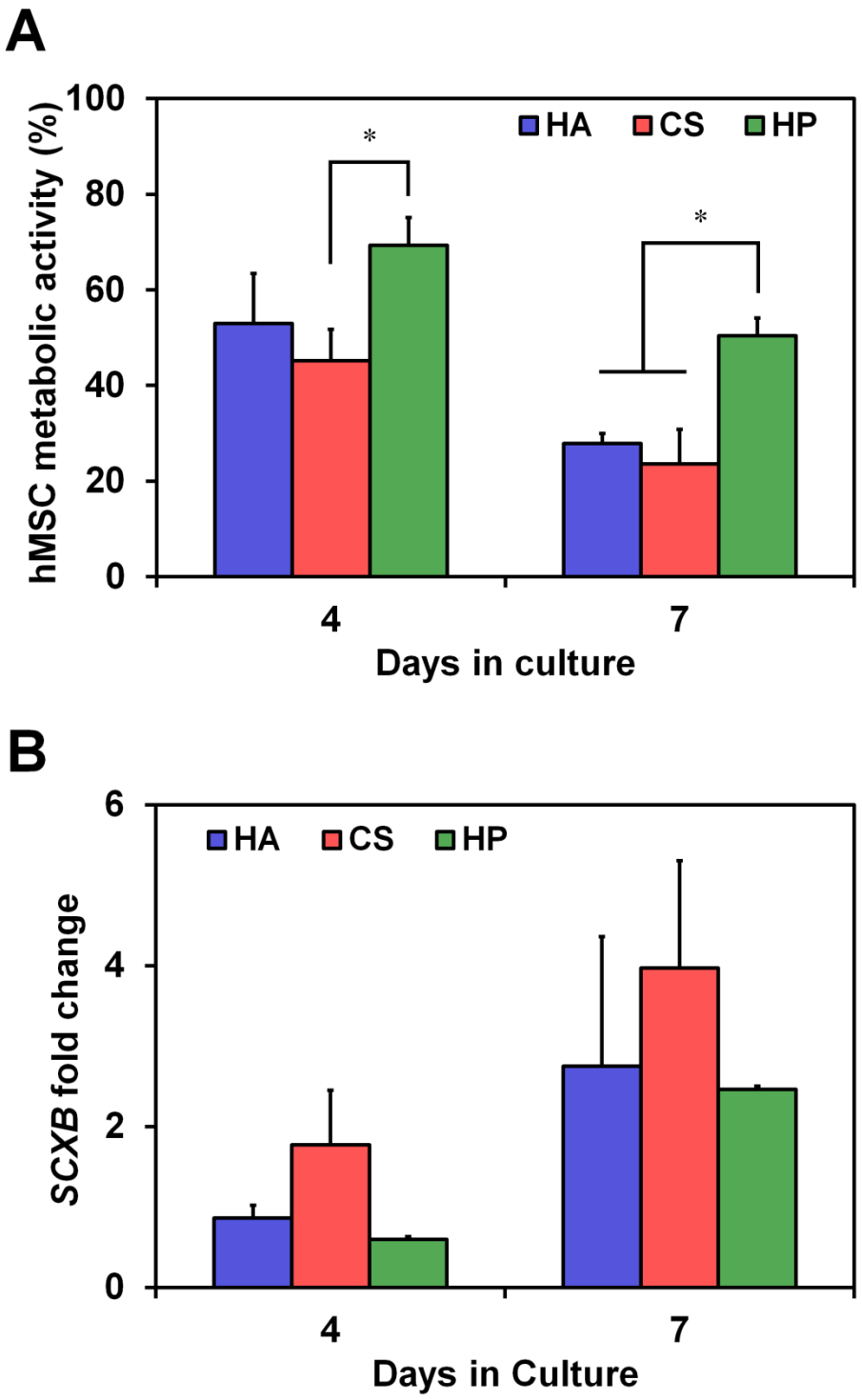

Figure 2.6. (A) Metabolic activity and **(B)** normalized (to 2D control at day 4) scleraxis gene expression of hMSCs cultured in CG scaffolds with varying GAG content in serum-free media supplemented with 500 ng/mL GDF-5. (*) significance ($p < 0.05$) between groups at a given time point.

CHAPTER 3: GENE DELIVERY INFLUENCED BY ELECTROSTATIC INTERACTIONS[‡]

3.1 Chapter overview

The design of biomaterials for increasingly complex tissue engineering applications often requires exogenous presentation of biomolecular signals. Integration of gene delivery vectors with a biomaterial scaffold offers the potential to bypass the use of expensive and relatively inefficient growth factor supplementation strategies to augment cell behavior. However, integration of cationic polymer based gene delivery vectors within three-dimensional biomaterials, particularly matrices which can carry significant surface charge, remains poorly explored. We examined the potential of polyethylenimine (PEI) as a gene delivery vector for three-dimensional collagen-glycosaminoglycan (CG) scaffolds under development for tendon repair. While acetylated versions of PEI have demonstrated improved transfection efficiency in 2D culture assays, we investigated translation of this effect to a 3D biomaterial that contains significant electrostatic charge. A reporter gene was used to examine the impact of polymer modification, polymer:DNA ratio, and the degree of sulfation of the biomaterial microenvironment on gene delivery *in vitro*. We observed highest transgene expression in acetylated and unmodified PEI at distinct polymer:DNA ratios; notably, the enhancement often seen in two-dimensional culture for acetylated PEI did not fully translate to three-dimensional scaffolds. We also found highly sulfated heparin-based CG scaffolds showed enhanced initial luciferase expression but not prolonged activity. While PEI constructs significantly reduced tenocyte metabolic health during the period of transfection, heparin-based CG scaffolds showed

[‡] This chapter has been adapted from the following publication: Rebecca A. Hortensius, Jacob R. Becraft, Daniel W. Pack, and Brendan A. C. Harley. "The effect of glycosaminoglycan content on polyethylenimine-based gene delivery within three-dimensional collagen-GAG scaffolds." Biomaterials Science, 2015; 3(4): 645-654.

the greatest recovery in tenocyte metabolic health over the full 2 week culture. These results suggest that the electrostatic environment of three-dimensional biomaterials may be an important design criterion for cationic polymer-based gene delivery.

3.2 Introduction

Traditionally, biomaterial design has focused on optimizing a range of biophysical properties such as structure, mechanics, and rate of degradation. Often, efforts have focused on artificial extracellular matrix (ECM) analogs that support cellular health and function by mimicking the native tissue's structure, mechanics, and composition. More recently, the impact of biomolecular supplementation and delivery methods has been incorporated into biomaterial design. While growth factors are still primarily introduced freely in solution as soluble media additives [87, 232-234, 260], efforts have turned to exploring approaches that could extend the time a growth factor is present within the biomaterial or that could spatially control factor localization. In these cases, designs have included strategies to release a biomolecule of interest from a degradable construct (*e.g.*, microspheres) [238-240] or to covalently bind the biomolecule to the surface of the biomaterial [93, 235, 237]. Inspired by transient immobilization of growth factors within the native ECM, recent approaches have also begun to incorporate charged moieties within the biomaterial (*e.g.*, glycosaminoglycans, heparin binding peptides) that are able to transiently sequester factors – either exogenously added or endogenously produced – to the surface of the biomaterial [114, 115, 242, 243, 261]. However, growth factors still incur a high cost, require large dosages, and suffer from relatively short half-lives as well as the potential for significant diffusive loss after *in vivo* implantation.

Gene delivery approaches offer the potential to address a number of limitations associated with conventional biomolecular supplementation. Although viral-based gene vehicles are most

efficient in achieving gene expression, concerns remain about their immunogenic safety, and hence regulatory approval [262, 263]. Non-viral gene vectors, in the form of proteins, lipids and cationic polymers, provide an alternative path for transient gene delivery [121, 129, 264-270]. One of the most efficient and well-studied off-the-shelf cationic polymers is polyethylenimine (PEI) [126, 128, 271, 272]. Through electrostatic interaction, PEI binds the negatively charged phosphates on the DNA backbone, spontaneously condensing into a polymer:DNA complex (polyplex) on the order of hundreds of nanometers [120]. The polymer:DNA weight-to-weight (w:w) ratio is a critical design parameter to control both transfection efficiency and cytotoxicity. If the w:w ratio is too low, there is minimal gene transfection. Alternatively, high polymer:DNA ratios often result in significant polymer-induced cytotoxicity [271, 273]. In the context of designing a more efficient PEI-based delivery system, recent efforts have focused on selective acetylation of the primary and secondary amines of the polymer. Acetylation decreases the density of protonated amines, decreasing the cationic charge of the polymer, and allowing for a weaker polymer:DNA interaction, leading to easier release of the nucleic acid cargo and significant improvements in gene delivery efficiency [126, 127].

Our laboratory has recently described a series of collagen-GAG (CG) scaffolds under development for tendon regenerative medicine applications. Fabricated via lyophilization, we have described approaches to create anisotropic pore architectures to improve tenocyte bioactivity as well as influence mesenchymal stem cell differentiation down a tenogenic lineage [60, 61, 274]. We have also explored the use of growth factor supplementation strategies to balance tenocyte bioactivity versus proliferation [61, 87, 275]. Recently, biomaterials such as CG scaffolds which contain charged ECM-derived matrix components have increasingly been explored in the context of bioinspired biomaterial design. For example, glycosaminoglycans

(GAGs) in the native ECM are known to play an important role in sequestering biomolecules within the matrix based on their degree of sulfation and structural variations in their carbohydrate backbone [53, 114]. Biomaterials incorporating GAGs have increasingly been explored as a means to transiently regulate growth factor availability [114, 117, 242, 243]. Recently, we demonstrated that modifying the GAG content of collagen-GAG (CG) scaffolds imparts differential capacity for non-covalent, electrostatic growth factor binding [59]. Notably, by incorporating highly sulfated heparin into the CG scaffold, we saw increased growth factor sequestration and positive impacts on cellular bioactivity compared to scaffolds containing lesser charged GAGs (hyaluronic acid, chondroitin sulfate). While modifying the degree of GAG-sulfation within three-dimensional biomaterials has been shown to impact both biomolecule sequestration and resultant cell response, its impact on the activity of cationic-polymer gene delivery vectors remains poorly understood.

The objective of this study therefore was to examine the efficiency of PEI-based gene delivery of a luciferase reporter gene to tenocytes within a collagen-GAG scaffold variant under development for tendon tissue engineering. In particular, we compared the optimal polymer:DNA ratios for transfection in two-dimensional culture and three-dimensional CG scaffolds. Further, given the known impact of scaffold GAG content on non-covalent growth factor sequestration as well as the central importance of electrostatic interactions in the context of PEI polyplexes, we explored the combined impact of polymer:DNA w:w ratio, PEI acetylation, and scaffold GAG content on polyplex efficiency. We tested the hypotheses that the electrostatic environment of the scaffold may enhance the expression or, alternatively, enhance the delivery of PEI-based gene vectors by preventing diffusion of the polyplexes out of the scaffold.

3.3 Materials and methods

3.3.1 CG suspension preparation

Type I collagen from bovine Achilles tendon (Sigma-Aldrich) was homogenized together with one of three glycosaminoglycans (GAGs): hyaluronic acid from Streptococcus equi (Sigma-Aldrich), chondroitin sulfate from shark cartilage (Sigma-Aldrich) or heparin from porcine intestinal mucosa (Sigma-Aldrich) in 0.05 M acetic acid to create a CG suspension [56]. All experiments used suspensions with a collagen concentration of 1.5% (w/v) and a collagen:GAG ratio of 11:1. The suspensions were stored at 4°C and degassed prior to use [251].

3.3.2 CG scaffold fabrication via freeze drying

CG scaffolds were fabricated using a previously described approach [61]. Briefly, the CG suspension was added to cylindrical wells (6 mm dia., 15 mm tall) in a polytetrafluoroethylene (PTFE)-copper mold then placed onto a precooled (-10^{o}C) freeze-dryer shelf (VirTis). The suspension was frozen at -10˚C for two hours prior to the sublimation of the resulting ice crystals at 0˚C and 200 mTorr [61]. Unidirectional heat transfer through the mold's copper bottom has previously been shown to induce formation of anisotropic scaffolds for tendon applications [61].

3.3.3 Crosslinking of CG scaffold

After lyophilization, scaffolds were placed in a vacuum oven (Welch) at 105˚C under vacuum for 24 hours for sterilization and dehydrothermal crosslinking [56]. Scaffolds were cut to 5 mm length (6 mm dia.) for all experiments. All CG scaffolds were hydrated in 100% ethanol overnight and washed in phosphate-buffered saline (PBS) for 24 hours. To increase their resistance to tenocyte contraction, scaffolds were crosslinked using carbodiimide chemistry [248, 252]. Scaffolds were covered with a 1-ethyl-3-[3-dimethylaminopropyl] carbodiimide

hydrochloride (EDC) and N-hydroxysulfosuccinimide (NHS) solution (molar ratio of 5:2:1 EDC:NHS:COOH) and agitated at room temperature for 2 hours. Following crosslinking, scaffolds were washed with PBS and stored in fresh PBS at 4˚C.

3.3.4 Tenocyte isolation and culture

Tenocytes (tendon cells) were isolated from 2-3 year old horses that were euthanized for reasons not related to tendinopathy using previously described methods [253]. Tenocytes were expanded in standard culture flasks in high glucose Dulbecco's modified Eagle's medium supplemented with 10% fetal bovine serum (Invitrogen), 1% Antibiotic-Antimycotic (Invitrogen), 1% L-glutamine (Invitrogen), and 50 µg/mL ascorbic acid (Wako). The media was changed every 3 days and the tenocytes were cultured to confluence at 37˚C and 5% CO_2. Passage 4 cells were used for all experiments.

3.3.5 Polyplex fabrication

The luciferase reporter vectors pGL3 (Promega) and pGLuc (New England BioLabs) were grown in DH5α E. coli (Gibco BRL) and were purified using a commercial plasmid purification kit (BioRad). Acetylation was carried out as previously described [127], with 60% acetylated PEI used throughout. Briefly, branched 25-kDa PEI (0.5 g) was transferred to a 20 mL scintillation vial in freshly distilled methanol and dissolved. Acetic anhydride was added and the reaction was carried out for 4 hours at 60°C with stirring before quenching with double distilled water, as previously described [127]. The solvent was removed under reduced pressure. The remaining solution was purified by gel filtration chromatography (PD-10 columns, Pharmacia) and eluted with double distilled water. The purified polymers were then concentrated and stored at -80°C until use.

3.3.6 Preparation of polymer-DNA polyplexes

Stock polymer solutions of unmodified or 60% acetylated PEI were thawed and diluted to 1 mg/mL. DNA (2 µg per scaffold) and PEI were combined at a range of polymer:DNA weight-to-weight ratios (1:1 to 5:1) with 20 mM PIPES and distilled water to achieve a desired final volume (30 µL) to be added per scaffold. Polyplexes were allowed to equilibrate at room temperature for 20 minutes before use.

3.3.7 Scaffold seeding and culture conditions

Hydrated and crosslinked scaffolds (6 mm in diameter, 5 mm in height) were incubated in complete media at 37˚C for at least one hour prior to seeding. Excess media was removed and the scaffolds were placed in ultra-low attachment well plates. Polyplexes were added by direct loading to the scaffolds, in a manner inspired by previous efforts by *Tierney et al* [128, 276]. Briefly, 15 µL of polyplex suspension was added to one side of the scaffold followed by 15 minute incubation at room temperature. The scaffold was then flipped over and another 15 µL of polyplex suspension was added. Following a second 15 minute incubation, tenocytes were trypsinized and resuspended at a concentration of 5 x 10^5 cells per 20 µL of media. The cells were seeded into the polyplex containing scaffolds by directly loading 10 µL of the cell suspension to each side of the scaffold using a previous described static seeding method [61]. Briefly, the scaffolds were incubated at 37˚C for 15 minutes in between each seeding and then incubated without additional media for 2 hours to allow for initial cell attachment. After two hours, serum-free growth media was gently added. Four hours post-seeding, the serum-free media was replaced with full tenocyte culture media. Media was changed every 3 days for the duration of each experiment.

3.3.8 Assay for pGL3 expression

Luciferase expression was first quantified 48 hours after cell seeding as a function of polymer:DNA w:w ratio and acetylation via a destructive assay using the Promega luciferase assay system. Scaffolds were lysed with Complete Cell Lysis Reagent and 20 µL of lysate was used for analysis. Activity was measured in relative light units (RLU) using a Lumat LB 9507 luminometer (Berthold). The results were normalized to relative light units measured from tenocyte seeded scaffolds that were treated with the pGL3 plasmid only with no PEI carrier.

3.3.9 Assay for pGLuc expression

Luciferase expression was subsequently quantified over time (through 14 days) after cell seeding using the BioLux Gaussia Luciferase Assay Kit (New England BioLabs). Aliquots of media (50 µL) were taken at regular intervals (2, 5, 7, 14 days post transfection) and stored for analysis at either 4˚C (less than 1 week storage) or -20˚C (longer than 1 week storage). Activity was again reported in relative light units (RLU) versus a DNA only, no PEI carrier control using a Lumat LB 9507 luminometer (Berthold).

3.3.10 Quantification of metabolic health

The metabolic activity of the tenocytes within the CG scaffolds was measured using the non-destructive alamarBlue® assay (Invitrogen) as previously described [61, 251]. Briefly, scaffolds were removed from culture at each timepoint, rinsed in PBS, then incubated in alamarBlue® solution at 37˚C under shaking for 2 hours [61]. Using a fluorescent spectrophotometer, resorufin fluorescence was measured (excitation: 540 nm, emission: 590 nm) and compared to a standard curve created from a known number of tenocytes. Tenocyte metabolic activity has been previously shown to be tightly correlated with overall tenocyte number within the scaffold [61,

87]. Here, metabolic activity of the tenocyte-scaffold construct was determined at each time point, then normalized to the metabolic activity of the total number of tenocytes initially seeded into the scaffold, to provide a standard comparison metric.

3.3.11 Statistical analysis

Two-way analysis of variance (ANOVA) was performed on all data sets followed by Tukey-HSD post-hoc test. Pair-wise comparisons were also completed as necessary. A p-value < 0.05 was used for significance. All analyses were based on a minimum of $n = 3$ scaffolds. In figures, error is reported as the standard error of the mean.

3.4 Results

3.4.1 The impact of polyplex polymer:DNA ratio and acetylation on gene delivery in a three dimensional CG scaffold

To screen the impact of a range of polyplex formulations on transfection efficiency within the three-dimensional CG scaffold, we quantified delivery of the pGL3 plasmid, which encodes the luciferase reporter protein, to equine tenocytes within CG scaffolds containing the conventional GAG, chondroitin sulfate (C:CS scaffold). Unmodified and acetylated PEI-containing polyplexes were tested at a range of polymer:DNA weight-to-weight ratios (1:1 to 5:1) previously validated as exhibiting high transfection activity in 2-D cultures. Luciferase expression was quantified 48 hours after seeding equine tenocytes into polyplex modified C:CS scaffolds.

Results suggested the presence of a separate optimal polymer:DNA ratio for unmodified versus acetylated PEI (Fig. 3.1). The acetylated PEI-mediated transfection efficiency of tenocytes in 2D culture, similar to previous studies [126, 127], was significantly greater at higher polymer:DNA ratios (data not shown). For three-dimensional CG scaffolds, unmodified PEI constructs showed

higher efficiency at lower polymer:DNA ratios, with a 2:1 ratio showing significantly ($p < 0.014$) increased luciferase as compared to all other polymer:DNA ratios and control in the C:CS scaffold. Also like previous 2D studies [126, 127], acetylated PEI required higher polymer:DNA ratios, with 4:1 and 5:1 polymer:DNA polyplexes showing significantly ($p < 0.05$) increased luciferase activity. However, unlike previous studies in two-dimensional culture, acetylated PEI did not significantly outperform unmodified PEI in CG scaffolds. Unmodified PEI showed significantly increased luciferase activity compared to acetylated PEI at 1:1 ($p = 0.032$), 2:1 ($p < 0.001$), and 3:1 ($p = 0.016$) polymer:DNA ratios. While luciferase activity was greater in acetylated PEI for 4:1 and 5:1 polymer:DNA ratios compared to unmodified PEI, the increases were not statistically significant.

3.4.2 The impact of acetylation on the kinetics of gene expression

We next examined the time course for luciferase expression using PEI polyplexes incorporating the pGLuc plasmid encoding the *Gaussia princeps* luciferase reporter protein. This modification allowed gene expression of tenocyte seeded C:CS scaffolds to be assessed non-destructively from aliquots taken from the culture media over 14 days (Fig. 3.2). Here, luciferase expression was normalized against a three dimensional control that contained the plasmid DNA without a delivery vector. While the naked pGLuc gene gave very low chemiluminescent background, suggesting minimal transfection efficiency (Fig. 3.1), it was not possible to track cell response over time. While the pGL3 gene allowed for tracing cell response, it had not been previously optimized for gene delivery and led to significant chemiluminescent background during analysis (Fig. 3.2).

As observed with the pGL3 plasmid, at 2 days post-transfection the 2:1, 3:1, 4:1 and 5:1 w:w ratios of the polyplexes containing unmodified PEI showed significantly ($p \leq 0.001$) higher luciferase expression compared to the control and the 1:1 w:w ratio (Fig. 3.2A). At day 5, significantly increased luciferase expression over control was still observed for 2:1, 3:1 and 5:1 polymer:DNA ratios ($p < 0.011$) for unmodified PEI constructs (Fig. 3.2A). Examining the results over time, luciferase expression in tenocytes was significantly ($p < 0.001$) greater at day 2 than at later timepoints (days 5, 7 and 14) for 2:1, 3:1, 4:1 and 5:1 unmodified PEI polyplexes. By days 7 and 14, there was no significant increase in luciferase expression over control (Fig. 3.2A).

When considering the polyplexes based on the acetylated PEI, 4:1 and 5:1 w:w ratios again led to significantly ($p < 0.001$) greater luciferase expression than the control at both days 2 and 5 (Fig. 3.2B). Luciferase expression in the 4:1 and 5:1 constructs were significantly ($p \leq 0.001$) greater than all lower polymer:DNA ratios at day 2. Examining the results with time, the 3:1, 4:1 and 5:1 PEI:DNA w:w ratio polyplexes demonstrated significantly ($p < 0.05$) increased luciferase expression at day 2 compared to all later days (Fig. 3.2B). There was no statistical significance between the polyplex groups at days 5, 7 and 14 (Fig. 3.2B).

Comparing the top performing unmodified PEI (2:1 w:w) and acetylated PEI (4:1 w:w) groups, no significant differences were observed in the performance over time between unmodified and acetylated PEI (Fig. 3.2C). Both unmodified and acetylated PEI groups significantly outperformed control (bare DNA) cultures at both day 2 ($p < 0.001$) and day 5 ($p \leq 0.02$), following similar trends seen in earlier transfection studies using these identical systems in 2D cultures [127]. Contrary to those results, acetylated PEI polyplexes again did not exhibit increased gene expression versus unmodified PEI polyplexes at any time.

3.4.3 The impact of variable GAG incorporation on polyplex efficiency

Given the observed differences in response in three-dimensional CG scaffolds versus previously reported two-dimensional cultures, we subsequently examined the impact of sulfated scaffold GAG content on gene expression. Here, a sub-set of polyplex polymer:DNA ratios were chosen for a narrow range surrounding the identified optimal unmodified (2:1) and acetylated (4:1) PEI ratios (Fig. 3.2). Unmodified PEI polyplexes were tested at polymer:DNA at ratios of 1:1, 2:1 and 3:1 while acetylated PEI polyplexes were tested at w:w ratios of 3:1, 4:1 and 5:1.

The initial impact of GAG charge on tenocyte luciferase expression was examined 2 days after tenocytes were exposed to the gene activated matrices (Fig. 3.3). For unmodified PEI polyplexes, scaffold GAG content significantly ($p < 0.05$) impacted luciferase expression. Luciferase activity was significantly ($p < 0.03$) enhanced in the CG scaffolds containing heparin (C:HP) compared to C:CS or hyaluronic acid (C:HA) CG scaffolds for a 2:1 polymer:DNA ratio (Fig. 3.3A). Luciferase activity was also significantly ($p < 0.01$) enhanced in the C:HP scaffolds compared to the C:HA scaffold for the 3:1 polymer:DNA ratio, while no difference was observed between groups at 1:1 polymer:DNA ratio (Fig. 3.3A). A similar effect was observed with acetylated PEI polyplexes (Fig. 3.3B). Here, tenocytes cultured in C:HP scaffolds show significantly ($p \leq 0.001$) enhanced luciferase expression over C:HA and C:CS scaffolds at both the 4:1 and 5:1 w:w ratios.

The expression profiles of the most effective polymer:DNA ratios (2:1 for unmodified PEI; 5:1 for acetylated PEI) were subsequently traced over 7 days in culture to determine whether scaffold GAG content was able to mediate extended DNA delivery as well (Fig. 3.4). For unmodified PEI polyplexes (2:1 w:w), a significant ($p \leq 0.001$) decrease in expression was observed across the 7 day experiment between each time point and also within each GAG

variant. The expression in the C:HP scaffolds is significantly ($p < 0.001$) higher at day 2 compared to C:HA and C:CS scaffolds (Fig. 3.4A). Results were similar for acetylated PEI polyplexes (Fig. 3.4B). Significantly ($p < 0.001$) increased luciferase expression was observed at day 2 as compared to days 5 and 7. Like with unmodified PEI, the impact of the highly charged C:HP scaffold on increased expression was limited to the first time point (day 2).

3.4.4 The impact of PEI gene delivery on tenocyte metabolic activity

PEI-based delivery vectors have been shown to have the potential for significant cytotoxicity [277]. However, we have previously shown that increasing the degree of glycosaminoglycan sulfation in the CG scaffold can enhance tenocyte metabolic health [59]. We therefore examined the long-term (14 days) consequences of PEI-based luciferase delivery on tenocyte metabolic activity as a function of scaffold GAG content for both unmodified (2:1 polymer:DNA ratio) and acetylated (5:1 polymer:DNA ratio) PEI polyplexes (Fig. 3.5). Here metabolic activity is reported as normalized against the number of initially seeded tenocytes, with data from day 2 suggesting initial cell attachment efficiencies on order of 30 – 50% as previously described for CG scaffolds by *O'Brien et al* [67]. Overall, the metabolic activity of tenocytes exposed to DNA alone was significantly ($p < 0.05$) higher than tenocytes exposed to unmodified or acetylated PEI polyplexes across all time points. However, consistent with previous observations [59], scaffold GAG content impacted cell metabolic activity. For the control group that did not receive PEI, the C:HP scaffold showed significantly ($p < 0.05$) increased metabolic activity at day 7 and 14 of culture compared to day 2. Examining the overall effect of PEI type and scaffold GAG content in more detail, while the metabolic activity of tenocytes exposed to PEI (unmodified, acetylated) is reduced compared to control for each scaffold type, the reduction is not significant at day 2 (Fig. 3.5). However, by day 4 the metabolic activity of tenocytes in scaffolds not exposed to PEI starts

to increase, with C:HA and C:HP scaffolds showing significantly ($p < 0.05$) higher metabolic activity compared to their corresponding polyplex receiving groups (Fig. 5). Identical results are also observed at day 7. By day 14 there were no significant differences in metabolic activity observed between control or either PEI groups in both the C:HA or C:CS scaffolds. Interestingly, tenocytes in the C:HP scaffolds that were exposed to PEI show significantly ($p < 0.05$) higher metabolic activity compared to all earlier time points (Fig. 3.5).

3.5 Discussion

The development of therapeutic scaffolds for tissue regeneration has largely focused on mimicking the mechanical, structural and compositional features of the extracellular matrix. Additionally, efforts are being made to increase the bioactivity of these scaffolds although much of the literature to date has focused on the presentation of recombinant proteins and growth factors [106, 278, 279]. Alternatively, gene therapy has the potential to facilitate localized, sustained delivery of beneficial growth factors by delivering therapeutic plasmids to the affected areas. Such approaches may eventually offer value in the context of wound healing [280] and for promoting lineage specification from patient-derived MSC populations [260, 281-283]. Early work in the development of gene-activated matrices demonstrated the ability to improve bone healing in a canine defect model through administration of plasmid DNA in a collagen sponge [281]. More recent studies have shown the influence PEI and nano-hydroxyapatite, individually and in combination, have on gene (reporter and therapeutic) delivery to MSCs within collagen-based scaffolds for bone regeneration [124, 128, 269, 276]. Further, studies focused on optimizing PEI chemistry for gene delivery have shown that increased efficiency of the PEI vector can be achieved through acetylation of the polymer. This was attributed to the lower electrostatic binding affinity of the polymer and DNA, as the cationic charge is reduced from

acetylation of the polymer's amine groups [127]. While this previous work suggested the electrostatic environment within the cell can impact the efficiency of gene delivery, our work here suggests that the electrostatic environment surrounding the cell can also significantly impact polyplex delivery.

The work described here examines the impact of the electrostatic environment of a three-dimensional collagen-GAG scaffold on the efficiency of PEI-based polyplexes under development for a range of gene delivery applications. Glycosaminoglycans are native to the extracellular matrix and are known for their role in sequestering growth factors *in vivo* [81]. Recent work by our group has shown that the degree of sulfation (negative charge) of the GAG component of 3D CG scaffolds could be used to impact the degree in which the scaffold was able to sequester growth factors and, furthermore, the cellular activity of equine tenocytes [59]. We sought to determine whether the presence of a three-dimensional CG scaffold impacted the efficiency of PEI-based polyplex gene delivery, and subsequently whether altering the degree of GAG sulfation in the CG scaffolds could impact polyplex activity or maintain their delivery over an extended period of time.

Initial experiments examined the response of the PEI polyplexes within CG scaffolds containing the moderately sulfated chondroitin sulfate (CS), our CG scaffold standard. It was found that the unmodified PEI polyplexes led to significantly higher luciferase expression at lower PEI:DNA w:w ratios when compared to acetylated PEI polyplexes 2 days after transfection (Fig. 3.1). While the acetylated polyplexes seemed to have higher expression at higher w:w ratios, it was not statistically significant. This is in contrast to transfection results seen in 2D [126, 127]. In order to examine the time course of transfection and expression, luciferase expression was subsequently monitored over an extended 14 day period (Fig. 3.2A). The active time of

luciferase expression in the polyplex seeded C:CS scaffolds (compared to bare DNA alone) was found to be limited to 2-5 days (Fig. 3.2). Unmodified PEI polyplexes showed significantly improved luciferase expression at 2:1, 3:1, 4:1 and 5:1 w:w ratios at day 2 and 2:1, 3:1 and 5:1 at day 5. Consistent with initial results and those in the literature, acetylated PEI polyplexes at higher w:w ratios (4:1, 5:1) were the only variants to show significantly higher luciferase expression, again at both day 2 and 5 post-transfection (Fig. 3.2B). Interestingly, acetylation did not significantly improve luciferase expression, with the top performing unmodified (2:1) and acetylated (4:1) PEI showing nearly identical performance over time (Fig. 3.2C).

In order to determine the effect of the electrostatic environment on gene delivery efficiency, polyplex delivery efficiency was subsequently tested across three CG scaffold variants, each with a differentially sulfated glycosaminoglycan: hyaluronic acid (HA), chondroitin sulfate (CS), or heparin (HP). A non-sulfated GAG, hyaluronic acid was not expected to have a positive impact on gene delivery efficiency or duration. Chondroitin sulfate (CS), a moderately sulfated GAG, was tested as the conventional CG scaffold formulation reported in the literature [56]. As a highly-sulfated, negatively charged glycosaminoglycan, we hypothesized the C:HP scaffolds would more strongly interact with the positively charged PEI polyplexes, retaining more of the polyplex within the scaffold and enhancing either the efficiency or duration of gene expression.

Indeed, increasing the degree of sulfation of the CG scaffolds, through incorporating highly sulfated heparin, led to significantly improved gene delivery efficiencies in both unmodified and acetylated PEI polyplexes two days after tenocytes were exposed to the gene activated matrices (Fig. 3.3). The effects were observed at higher w:w ratios of the range tested for unmodified and acetylated PEI, suggesting at low cationic polymer densities the effect of scaffold GAG content was lost. Notably, significant increases in luciferase expression were noted for tenocytes in the

C:HP scaffolds versus both C:HA and C:CS scaffolds for a 2:1 w:w polymer:DNA ratio using unmodified PEI (Fig. 3.3A). Similar results were observed at 4:1 or 5:1 w:w ratios using acetylated PEI (Fig. 3.3B). These results suggest that the electrostatic scaffold environment can significantly impact the short term efficiency of gene delivery. Considering recent approaches describing fabrication of CG scaffolds with regional control over composition [284], these results also suggest a path for developing biomaterials able to spatially-enhance the efficiency of a ubiquitously added gene delivery vector. However, when examining the impact of scaffold GAG content over the course of 7 days (Fig. 3.4), it was apparent that scaffold GAG content may not be sufficient to enhance the duration of functional gene delivery. Here, the significant increase in luciferase expression between scaffolds only appears at day 2 (2:1 unmodified, 5:1 acetylated polyplexes), with no significant differences seen between groups at days 5 or 7 (Fig. 3.4).

The mechanism by which scaffold GAG content impacts PEI delivery remains undetermined. The presence of increasingly anionic GAGs within the CG scaffolds may promote the maintenance of the cationic polyplex in the scaffold, decreasing the rate of diffusive loss. Alternatively, scaffold GAG content may enhance partial dissociation of the DNA from the polymer, potentially allowing for effective transcription within the cells. As unmodified PEI constructs exhibit higher charge [127], they may be sequestered in the charged C:CS and C:HP scaffolds more readily than the acetylated PEI. Further, interactions with the charged GAG, especially in the case of the more weakly associated acetylated PEI polyplexes, may also facilitate the release of the DNA from the polyplex, with acetylated PEI showing highest transfection efficiency in the C:HP scaffolds (Fig. 3.4). While future efforts will need to examine mechanisms by which the scaffold GAG content impacts polyplex stability or retention, it is

clear that the biophysical properties of a tissue engineering scaffold can significantly impact polyplex-based gene delivery. Further, these results highlight that polyplexes optimized in conventional two-dimensional cultures may show significantly different behavior when translated to biomaterial systems.

Moving forward, it would be important to extend these studies to examine the transfection efficiency on a per-cell basis. Experiments such as those were not performed as part of this study because established methods (e.g., normalizing to protein or DNA content) could not be performed in the presence of the collagen scaffold or the charged PEI polymer, respectively. In the future, the use of a GFP reporter and flow cytometry would be a viable way to obtain the percent of transfected cells present as a function of culture time. Further, while here we examined delivery of a reporter gene, delivery of a therapeutic gene to direct mesenchymal stem cell differentiation towards a tenogenic lineage would be an important step in the development of a functional gene delivery matrix for tendon repair. Recent efforts understanding conserved processes of tendon development and repair offer a number of therapeutic targets for incorporation into a gene activated matrix in the future [15, 285-287].

Finally, a well-documented drawback of PEI-based gene delivery systems is the significant potential for PEI-induced cytotoxicity [277]. At first glance, results from this study suggest that appropriate design of the correct biomaterial platform may offer an orthogonal design parameter for enhancing the activity of a given gene delivery vector. However, here we also explored the potential for the scaffold GAG content to enhance tenocyte long-term metabolic activity as a potential strategy to help cells recover more rapidly after the cytotoxic insult associated the PEI polyplex exposure. Tenocyte metabolic activity was monitored over 2 weeks in the GAG scaffolds variants as they were exposed to different gene delivery vehicles: DNA only control,

2:1 unmodified PEI polyplexes, and 5:1 acetylated PEI polyplexes (Fig. 3.5). There are significant, but temporary, decreases in the metabolic activity at early time points (4, 7 days) for cells exposed to the DNA polyplexes, corresponding to the active period of time for polyplex transfection. Notably, we observed significantly enhanced recovery of the metabolic health of tenocytes cultures in the heparin-based CG scaffolds by day 14. These results are encouraging as they suggest no long term damage may have been done to the cells as a result of the transfection. Further, these results mimic previous findings showing that C:HP scaffolds can enhance cell activity in metabolically taxing environments.

3.6 Conclusions

It has been previously shown that the GAG content of CG scaffolds can impact the transient sequestration of growth factors and subsequent cellular responses. Here we described the effect that sulfated GAG content of CG scaffolds has on gene delivery via cationic polymeric polyplexes. Using the cationic polymer polyethylenimine (PEI) to condense DNA into polyplexes, we were able to also examine the impact of polymer acetylation and polymer:DNA weight-to-weight ratio on delivery of a luciferase reporter gene within a three-dimensional biomaterial. We found that increasing the weight-to-weight ratio and employing the highly sulfated heparin glycosaminoglycan in the scaffold design increased the initial luciferase expression in tenocytes treated for acetylated PEI polyplexes. Notably, heparin-based CG scaffolds also enhanced metabolic activity over 14 days. These results suggest that the electrostatic environment of a gene activated scaffold may prove to be an important design parameter to consider in order to enhance the efficiency and perhaps to moderate cytotoxic side-effects of cationic polymer based gene therapy for tissue engineering applications.

3.7 Figures

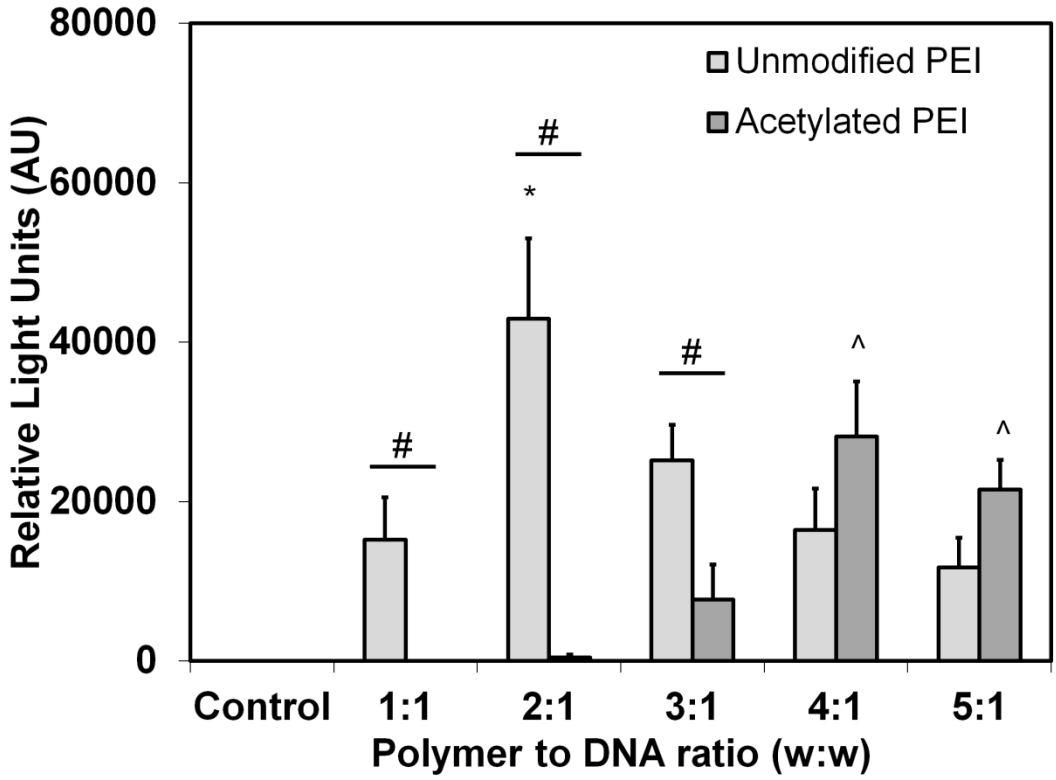

Figure 3.1. Luciferase expression (pGL3 vector) 48 hours post-transfection from tenocytes cultured in 3D C:CS scaffolds. (*) significant ($p < 0.05$) up-regulation compared to all other unmodified PEI groups. (^) significant ($p < 0.05$) up-regulation compared to control, 1:1, and 2:1 acetylated PEI groups. (#) significant ($p < 0.05$) up-regulation between unmodified and acetylated PEI groups at given polymer:DNA ratio.

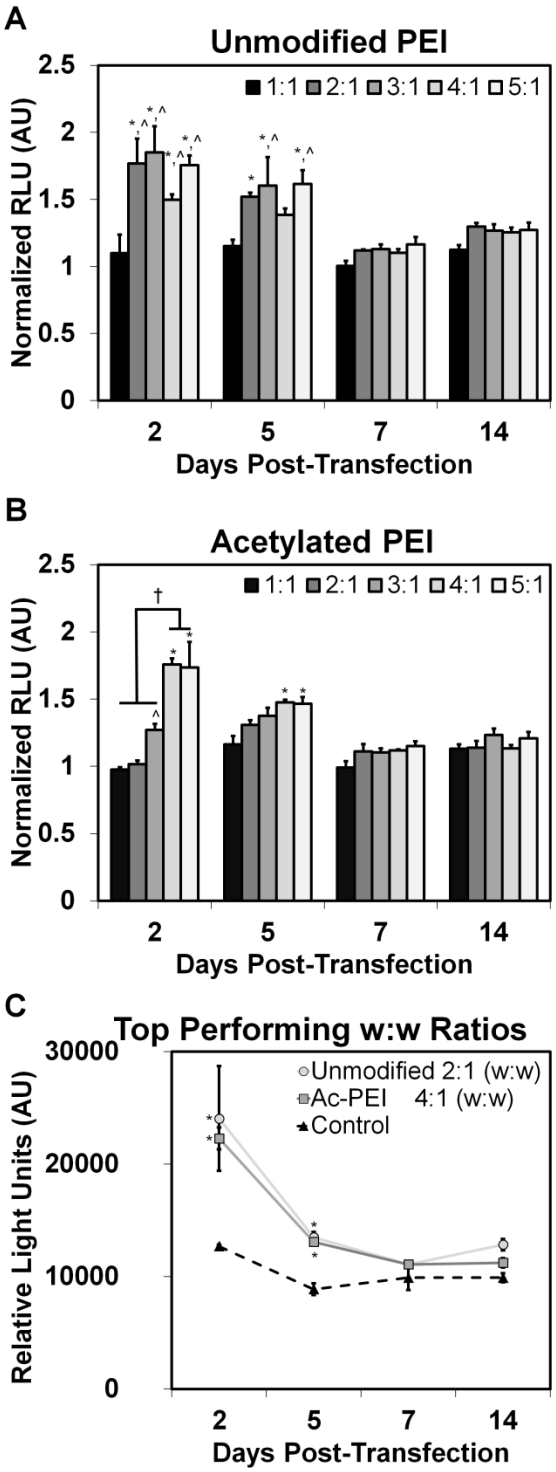

Figure 3.2. Luciferase expression (pGLuc vector) in tenocytes over two weeks of culture in C:CS scaffolds. Expression of polyplex variant with unmodified PEI (**A**) or acetylated PEI (**B**) over the full range of weight-to-weight ratios. Relative light units (RLUs) are normalized to a 3D control of DNA without a polymer vector. (**C**) Top performing ratios (w:w) for unmodified and acetylated PEI over 14 days. (*) significance ($p < 0.05$) when compared to control. (^) significance ($p < 0.05$) between 1:1 ratio at same day. (†) significance ($p < 0.05$) between groups.

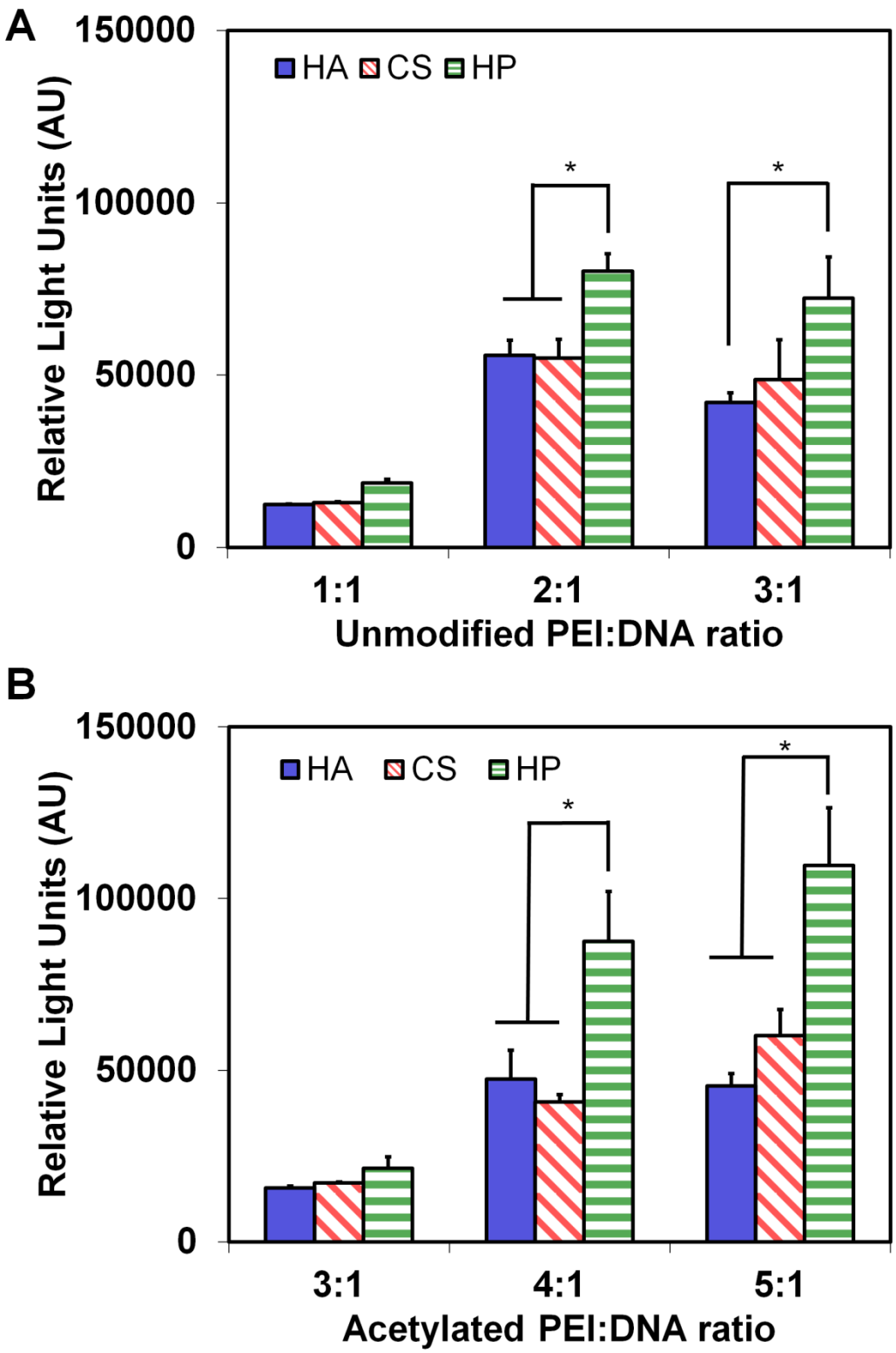

Figure 3.3. Day 2 luciferase expression (pGLuc) of a focused range of weight-to-weight ratios for each type of PEI within scaffolds of varying charge. (*) significance ($p < 0.05$) between groups.

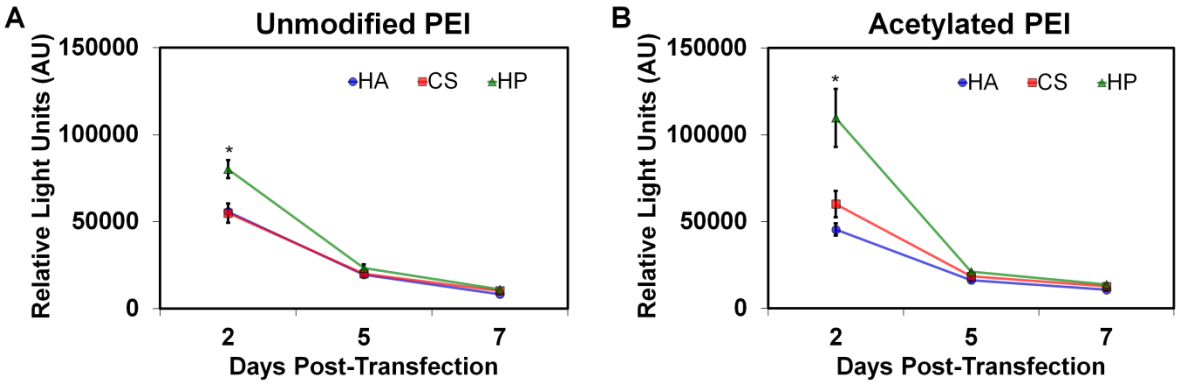

Figure 3.4. Luciferase expression (pGLuc) from the most effective weight-to-weight ratios in scaffolds with variant glycosaminoglycan content over 7 days. (*) significant ($p < 0.05$) increase relative to other timepoints within the same scaffold group.

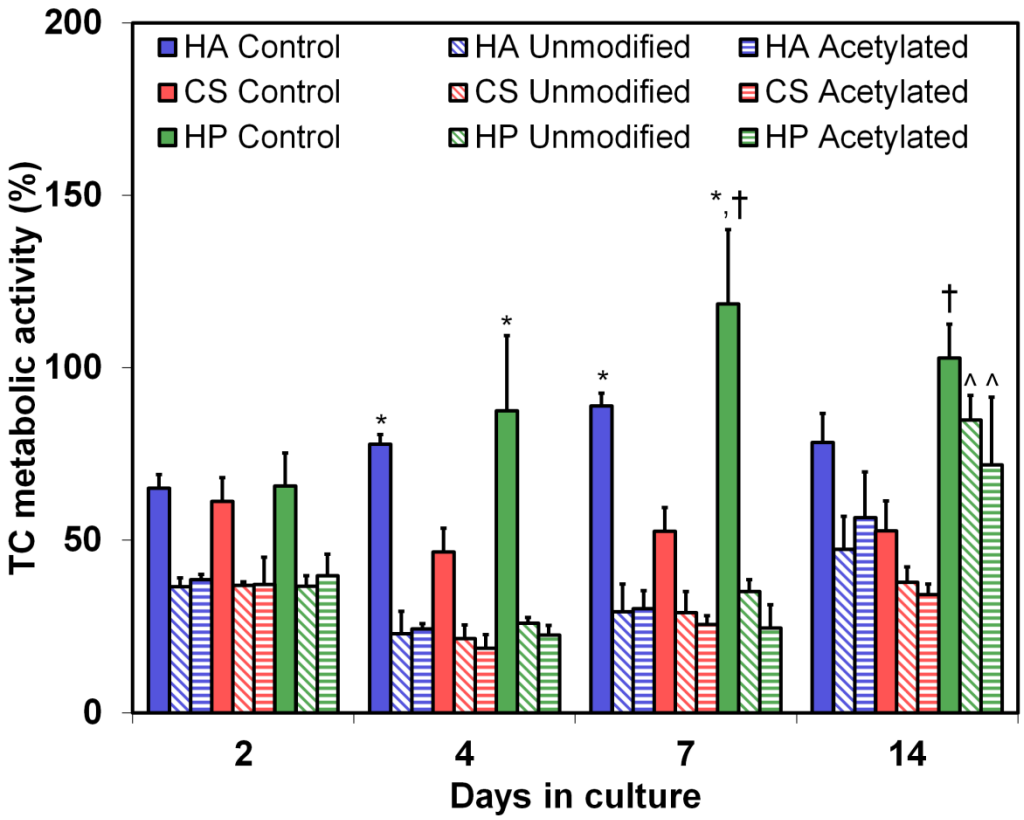

Figure 3.5. Tenocyte metabolic activity as a function of scaffold GAG content as well as polyplex group. (*) significance ($p < 0.05$) over corresponding experimental groups at same timepoint. (^) significance ($p < 0.05$) between earlier timepoints. (†) significance ($p < 0.05$) to day 2 groups.

CHAPTER 4: THE INCORPORATION OF AMNIOTIC MEMBRANE MATRIX ALTERS TENOCYTE ACTIVITY IN VITRO[§]

4.1 Chapter overview

Adult tendon wound repair is characterized by the formation of disorganized collagen matrix which leads to decreases in mechanical properties and scar formation. Studies have linked this scar formation to the inflammatory phase of wound healing. Instructive biomaterials designed for tendon regeneration are often designed to provide both structural and cellular support. In order to facilitate regeneration, success may be found by tempering the body's inflammatory response. This work combines collagen-glycosaminoglycan scaffolds, previously developed for tissue regeneration, with matrix materials (hyaluronic acid and amniotic membrane) that have been shown to promote healing and decreased scar formation in skin studies. The results presented show that scaffolds containing amniotic membrane matrix have significantly increased mechanical properties and that tendon cells within these scaffolds have increased metabolic activity even when the media is supplemented with the pro-inflammatory cytokine interleukin-1 beta. Collagen scaffolds containing hyaluronic acid or amniotic membrane also temper the expression of genes associated with the inflammatory response in normal tendon healing (TNF-α, COLI, MMP-3). These results suggest that alterations to scaffold composition, to include matrix known to decrease scar formation *in vivo*, can modify the inflammatory response in tenocytes.

[§] This chapter has been adapted from the following publication: Rebecca A. Hortensius, Jill H. Ebens, Brendan A. C. Harley. "Immunomodulatory effects of amniotic membrane matrix incorporated into collagen scaffolds." Journal of Biomedical Materials Research: Part A, 2016; 104(6): 1332-1342.

4.2 Introduction

Tendon healing following injury, even when surgically repaired, results in fibrocartilagenous scar formation which in turn leads to decreased ultimate tendon strength and disorganized collagen fibers. Adult wound repair occurs in the three overlapping phases: inflammation, proliferation, and remodeling [249, 288]. The inflammatory phase in adult wound healing is characterized by the recruitment of cells to the site of injury [139, 249]. Platelets release platelet-derived growth factor (PDGF) and transforming growth factor-beta (TGF-β) in order to initiate the chemotaxis of fibroblasts and inflammatory cells (neutrophils, macrophages) to the wound [139]. Additionally, TGF-β stimulates macrophages to secrete the key inflammatory cytokines, tumor necrosis factor alpha (TNFα) and interleukin-1 (IL-1) during this phase [139]. Scar formation is the ultimate end point of adult wound repair and studies have shown that the inflammatory response is an essential prerequisite for scarring [189]. The limited healing of tendons calls for new techniques and materials that will promote tendon regeneration *in vivo*.

In contrast to adult wounds, healing in fetal cutaneous wounds proceeds in a regenerative fashion, with neither the typical inflammatory response nor the formation of scar tissue [189-191]. Extensive studies have shown that differences between adult and fetal wound healing are found at many levels of the wound healing cascade; cells, cytokines, growth factors, and the ECM [190]. Fetal wounds exhibit lower levels of PDGF, TGF-β1 and TGF-β2 [201]; leading to reduced numbers of immune cells in fetal skin and lower inflammatory reaction [190, 199, 200]. Pro-inflammatory cytokines (e.g. TGF-β1) are also less prevalent in fetal wounds [202, 203]. *Beredjiklian et al* examined differences between adult and fetal tendon wound healing via partial mid-substance tenotomies of the lateral extensor tendon in pregnant ewes and their fetal lambs [24]. Maternal and fetal tendons were harvested for histological and mechanical testing 7 days

post-surgery. Testing showed that fetal tendons exhibited highly aligned and organized collagen fibers, no macroscopic abnormalities or adhesions, and no increases in TGF-β1 expression; all in direct contrast to the corresponding adult tendons.

We hypothesize the composition of biomaterials that mimic the extracellular matrix found in low inflammatory environments (such as the fetal wound environment) may be particularly relevant for modifying adult immune responses. The non-sulfated glycosaminoglycan hyaluronic acid (HA) is found in both adult and fetal wounds [211] and assists in rapid cell proliferation and motility. HA is a significant component of the fetal, scarless wound healing cascade [289] and has been extensively studied in the context of burns and chronic wounds [290] as well as reducing adhesion [291]. Separately, the amniotic membrane (AM), known for its anti-inflammatory and anti-microbial properties as well as scarless wound healing capacity, is the innermost layer of the placenta. Clinicians and scientists have shown that the intact AM sheet is valuable in the treatment of corneal surfaces [222-224], skin wounds [219, 225], oral cavity reconstruction [226] and many other reconstruction applications [215, 227]. In addition, the use of dry, micronized human amnion membrane has been shown to reduce cartilage degeneration in an osteoarthritic rat model [228]. While the AM has been implemented successfully in these wound healing applications and studied as an anti-inflammatory therapeutic for degenerative disease, its potential as a bioactive component in 3D biomaterials has not been extensively investigated.

Collagen-glycosaminoglycan (CG) scaffolds have been used in a wide variety of applications for skin, peripheral nerve, and cartilage tissue engineering as well as 3D environments for *in vitro* studies of cell behavior [55-58, 67, 244, 292]. It has been shown that in severe skin wounds the application of these scaffolds decreases the population of myofibroblasts at the wound site [293].

By delaying these contraction processes, collagen-based scaffolds have induced regeneration and decreased scar formation in skin and nerve defects [36]. Our lab has recently developed scaffold variants to mimic the anisotropic microstructure of native tendons [61]. While typically fabricated with chondroitin sulfate, modifications to the scaffolds' glycosaminoglycan (GAG) content were subsequently used to modulate growth factor sequestration, much like the native tendon ECM [59]. The capacity to alter the biomolecular environment and cellular response via scaffold composition may be a way to address needs for immunomodulatory biomaterials for tissue regeneration. The work described here combines CG scaffolds with fetal wound healing-inspired matrix (HA, AM) in order to study their ability to temper pro-inflammatory conditions *in vitro*.

4.3 Materials and methods

4.3.1 Amnion membrane isolation

In collaboration with Carle Foundation Hospital Tissue Repository (Urbana, IL), human placentas were obtained following uncomplicated vaginal births. The amniotic membrane (AM) matrix components have been isolated from these placentas as described [294]. Briefly, excess blood was washed from the fetal membrane and the AM was mechanically separated from the placenta [294]. The AM was cut into sections, washed, and then decellularized via incubation in thermolysin (125 μg/mL) [295]. Decellularized AM were then rinsed with shaking in PBS to remove cellular debris and stored in PBS at 4°C. Following 24-48h of storage, in which the spongy layer of the AM was allowed to swell, decellularized AM pieces were scraped (spatula) in order to fully separate the AM matrix of the compact layer from the underlying spongy layer. The remaining matrix (basement membrane, compact layer) was lyophilized and stored in a dessicator until further use.

4.3.2 Amnion membrane characterization

Biopsies of placental tissue were fixed in 10% formalin and embedded in paraffin in a cross-sectional orientation. Serial slices of 5 μm thickness were cut and mounted on slides. Slides were deparaffinized and stained with either hematoxylin and eosin (H&E) or Masson's Trichrome stain. All slides were mounted with Permount and a coverslip prior to imaging on an optical microscope (Leica Microsystems, Germany). The isolated decellularized and dried amniotic membrane was analyzed for its collagen and GAG content via a hydroxyproline [296] and a 1,9-dimethylmethylene blue (DMMB) [297] assay, respectively.

4.3.3 Preparation of collagen suspension

A suspension of collagen and one of three components was made by homogenizing type I collagen from microfibrillar collagen (Collagen Matrix, Oakland, NJ) in 0.5 M acetic acid with either ***(1)*** chondroitin sulfate from shark cartilage (Sigma Aldrich, St Louis, MO), ***(2)*** hyaluronic acid from Streptococcus equi (Sigma-Aldrich, St. Louis, MO), or ***(3)*** ground (mortar and pestle) and, further, homogenized amniotic membrane as collected above [56]. Scaffolds containing CS and HA components were made with a 11:1 collagen:component ratio while C:AM were made at a 5:1 w:w ratio due to the high AM collagen content. All scaffolds were made with a target total density of 0.5% w/v [251]. The suspensions were stored at 4°C and degassed prior to use [251].

4.3.4 Fabrication of collagen-based scaffolds via freeze drying

Isotropic CG scaffolds were fabricated as previously described [61, 69]. The collagen suspension was transferred to an aluminum tray mold and placed into the freeze-dryer with a shelf temperature of 4°C. The suspension was frozen to a final freezing temperature of -40°C. To form a porous, sponge-like scaffold, ice crystals were sublimated under vacuum (200 mTorr) at 0°C.

4.3.5 Crosslinking of CG scaffold

In order to sterilize and dehydrothermally crosslink the scaffolds, the lyophilized sheets were placed in a vacuum oven (Welch, Niles, IL) at 105˚C under vacuum for 24 hours [56]. A biopsy punch was used to cut 6mm diameter cylinders from the 4mm thick scaffold sheet for use in all experiments. Scaffolds were hydrated by soaking in 100% ethanol overnight and washing in PBS for 24 hours. Scaffolds were then crosslinked via carbodiimide chemistry by immersing in 1-ethyl-3-[3-dimethylaminopropyl] carbodiimide hydrochloride (EDC) and *N*-hydroxysulfosuccinimide (NHS) at a molar ratio of 5:2:1 EDC:NHS:COOH for 1.5 h under shaking at room temperature [248, 298]. Prior to use, scaffolds were washed with and stored in PBS at 4˚C.

4.3.6 SEM analysis

Scanning electron microscopy (SEM) was used to visualize the cross-sectional interior microstructure of dry, uncrosslinked scaffolds. Samples were imaged with a JEOL JSM-6060LV scanning electron microscope using secondary electron and backscattered electron detectors under low vacuum.

4.3.7 Mechanical testing

Compression testing was carried out on crosslinked, hydrated samples. Scaffolds from each group (CS, HA, AM) were cut from the scaffold sheet (approx. 4 mm thick) with 12mm biopsy punches before being hydrated and crosslinked as described above. Using a TA.XTplus Texture Analyzer (StableMicro Systems Ltd., Surrey, UK) equipped with a 1 kg load cell, the stress-strain behavior of each scaffold variant was measured. Samples were loaded in unconfined

compression to approximately 75% strain at a rate of 0.01 mm/min. The elastic moduli were determined from the linear elastic region (approx.. 1-10% strain) of each stress-strain plot [248].

4.3.8 Pull down sequestration assay

The degree of cytokine sequestration in each CG scaffold variant was determined via a pull down assay [59]. Three hydrated, crosslinked scaffolds were placed in a single well of an ultra-low attachment 24-well plate (Fisher, Waltham, MA) with 1 mL of a pH 7.4 PBS solution supplemented with 1 ng/mL interleukin-1 beta (IL-1β) (ProSpec, Israel) and 1% bovine serum albumin (BSA). Control wells containing the IL-1β solution and no scaffolds were used. The scaffolds and controls were incubated under gentle shaking at 37˚C for 1 hour. Immediately following incubation, an ELISA kit (R&D Systems, Minneapolis, MN) was used to measure the amount of IL-1β remaining in solution. The difference between the concentration of IL-1β remaining in the solutions containing scaffolds and the solutions that did not have scaffolds (controls) was regarded to be the amount of cytokine in the scaffolds. IL-1β pull down for each CG variant was reported as a percentage of the total IL-1β concentration in the loading solution.

4.3.9 Tenocyte isolation and culture

Tenocytes (tendon cells) were isolated from 2-3 year old horses and expanded in growth media: high glucose Dulbecco's modified Eagle's medium supplemented with 10% fetal bovine serum (Invitrogen, Carlsbad, CA), 1% Antibiotic-Antimycotic (Invitrogen, Carlsbad, CA), 1% L-glutamine (Invitrogen, Carlsbad, CA), and 50 µg/mL ascorbic acid (Wako, Richmond, VA) in standard culture flasks [253]. The cells were cultured at 37˚C and 5% CO_2 and the media was changed every 3 days until the tenocytes reached confluence. Passage 5 cells were used for all experiments.

4.3.10 Scaffold seeding and culture conditions

Hydrated, crosslinked scaffolds were soaked in growth media for one hour at 37°C before being placed in ultra-low attachment 6-well plates (Fisher, Waltham, MA). Confluent tenocytes were trypsinized and resuspended in growth media at a concentration of 2.5 x 10^5 tenocytes per 20 µL. Scaffold variants were seeded with tenocytes using a previously established static seeding method [61]. The scaffolds were incubated for 15 minutes at 37˚C following the addition of 10 µL of the cell suspension to one side of the scaffold. The scaffolds were then flipped over and another 10 µL of cell suspension was added for a total of 2.5 x 10^5 tenocytes seeded on each scaffold. To allow for initial cell attachment, scaffolds were placed in the incubator for 2 hours. After this period, additional media was added and scaffolds were incubated at 37˚C and 5% CO_2 for 24h before the media was changed for one of three inflammatory media variants. These variants included: ***(1)*** growth media (control), ***(2)*** media supplemented with 0.1 ng/mL of the pro-inflammatory factor interleukin-1 beta (IL-1β) (inflammatory), and ***(3)*** media supplemented with 1 ng/mL of IL-1β (high inflammatory). Scaffolds were cultured in culture media as described above, with or without the addition of serum, for the duration of the experiment. Media changes occurred every 3 days.

4.3.11 Histological analysis of cell-seeded scaffolds

Following 7 days of culture, tenocyte-seeded scaffolds were fixed in 10% formalin overnight and then washed and stored in PBS. Fixed scaffolds were blocked with PBS containing 2% bovine serum albumin and 0.1% Tween 20 for one hour under shaking at room temperature. Then scaffolds were incubated overnight in vimentin antibody (Cell Signaling Technology, 1:800 dilution), washed and stored in 0.1% Tween 20 PBS. Prior to embedding at -80°C, scaffolds were soaked in 20% sucrose for 1 hour followed by Optimal cutting temperature compound

(OCT) for 1 hour. Sections of 25 micro thickness were obtained using a Leica CM3050 S cryostat and imaged via fluorescence microscopy (Leica DMI4000B fluorescence microscope, Qimaging camera). Fluorescent and brightfield channels were merged using ImageJ.

4.3.12 Quantification of TGF-β1 protein release

Tenocyte-seeded scaffolds were cultured in serum-free media variants for 24h. Following this culture period, the amount of TGF-β1released into the media was measured via an ELISA kit (R&D Systems, Minneapolis, MN). Concentrations were determined using a standard curve and a four parameter logistic (4-PL) curve-fit. Results were normalized to acellular scaffold variants cultured in control media.

4.3.13 Quantification of cell metabolic activity

Metabolic activity of the tenocytes within the collagen scaffolds was measured using a non-destructive alamarBlue® assay (Invitrogen, Carlsbad, CA) [61, 251]. Briefly, scaffolds were removed from culture, rinsed in PBS, and incubated under gentle shaking at 37˚C for 2 hours in a 1x alamarBlue® solution containing the media variant of the primary culture. Using a fluorescent spectrophotometer, resorufin fluorescence was measured (excitation: 540 nm, emission: 590 nm) and compared to a standard curve created from a known number of cells from the start of the experiment. The standard curve was run on well-plated cells, with known numbers of cells in each well, ranging from 25% to 300% of the number of cells seeded per scaffold. Metabolic activity was tracked over a 7 day period and, at each time point, was interpolated to the standard curve and reported as a percentage of the total number of seeded cells.

4.3.14 Gene expression analysis through RNA isolation and real-time PCR

An RNeasy Plant Mini kit (Qiagen, Valencia, CA) was used to isolate RNA from cell-seeded scaffolds. The scaffolds were rinsed in PBS, cut in half with a razor, and immersed in the kit's lysis buffer for 5 minutes on ice [87]. Following the kit's instructions, RNA was isolated and total RNA was quantified via spectrophotometry. The QuantiTect Reverse Transcription kit (Qiagen, Valencia, CA) was used to reverse transcribe the isolated RNA in a Bio-Rad S1000 thermal cycler. Real-time PCR reactions were performed in an Applied Biosystems 7900HT Fast Real-Time PCR System (Carlsbad, CA) to measure gene expression levels for collagen I (COL1A2), matrix metalloproteinase-3 (MMP-3), scleraxis (SCXB), and tumor necrosis factor-alpha (TNF-α). Glyceraldehyde 3-phosphate dehydrogenase (GAPDH) was used as a housekeeping gene (differences in GAPDH expression between groups were compared and found to be statistically insignificant: $p > 0.05$). Sequence Detection Systems software v2.4 (Applied Biosystems, Carlsbad, CA) was used to complete analysis. All results were expressed as fold changes relative to expression levels of cells in scaffolds of the same type and at the same time point but cultured in the control media.

4.3.15 Statistical analysis

One-way analysis of variance (ANOVA) followed by Tukey-HSD post-hoc test was performed on all data sets except for metabolic activity. The metabolic activity was analyzed using a two-way, repeated measures ANOVA followed by Tukey-HSD post-hoc test. A p-value < 0.05 was used for significance. All analyses were based on a minimum of n=4 scaffolds. Error is reported as the standard error of the mean in the figures.

4.4 Results

4.4.1 Placental structure and amnion composition

Histological staining of placental biopsies shows the structure of the amniotic membrane in relation to the rest of the placenta (Fig.4.1A,B). H&E staining (Fig. 4.1A) shows a single layer of epithelial cells on the surface of the amniotic membrane. Masson's Trichrome staining (Fig. 4.1B) indicates that the amniotic membrane is rich in collagen. Quantitative analysis determined AM collagen content (40.83±0.04 wt%) and sulfated GAG content (0.22±0.11 wt%).

4.4.2 Scaffold microstructure, mechanics, and histological analysis

The elastic modulus of each of the CG scaffold variants varied between 0.1 and 1 kPa showing a significant effect of the included matrix (Fig. 4.1C). Scaffolds containing chondroitin sulfate (CS) had an average elastic modulus of 0.169±0.010 kPa. Substituting hyaluronic acid (HA) for CS resulted in a significant increase in modulus to 0.511±0.052 kPa while adding amniotic membrane (AM) showed a further significant increase (1.065±0.083 kPa). The scaffold variants all showed an open porous network via SEM with pores on the order of 100 μm (Fig. 4.1D) and by day 7 of culture the tenocytes were well distributed throughout the scaffolds with no obvious differences in cell aggregation or distribution (Fig. 4.1E).

4.4.3 Tendon cell metabolic activity under pro-inflammatory media conditions

The metabolic activity of equine tenocytes cultured within the CG scaffold variants was evaluated prior to the pro-inflammatory challenge (day 0) and subsequently at days 1, 4, and 7 (Fig. 4.2). Each scaffold variant supported metabolic health over time. However, scaffolds containing HA or AM showed a greater increase in metabolic activity. Cells within C:AM scaffolds cultured in control media showed increased metabolic activity compared to C:CS (standard, control) scaffolds at all time points (Fig. 4.2A). The same was seen in cells cultured in C:AM scaffolds with media supplemented with the pro-inflammatory cytokine IL-β at

inflammatory (Fig. 4.2B) and high inflammatory levels (Fig. 4.2C). Additionally, scaffolds containing hyaluronic acid also promoted significantly increased tenocyte metabolic activity over the C:CS scaffolds, especially in high inflammatory media, as seen at all time points (Fig. 4.2C).

Reorganizing the data to display cell metabolic activity across all media conditions for each scaffold type (Fig. 4.2D-F), we find that, following the introduction of variant medias, there was no significant difference in cell metabolic activity between C:CS scaffolds across all media conditions (Fig. 4.2D). Interestingly, while cell metabolic activity trended to increase throughout the 7 days experiment, cells in amniotic membrane matrix scaffolds showed significantly enhanced ($p < 0.05$, day 4) cell metabolic activity in response to inflammatory or high inflammatory media formulations (Fig. 4.2F).

4.4.4 Gene expression of tenocytes cultured in CG scaffolds under IL-1β challenge

PCR was used to examine the relative expression of inflammatory and tenocyte phenotypic genes over the course of 7 days of culture in pro-inflammatory media conditions. The reported fold changes are compared to cells cultured in the same scaffold type but in control media. Tenocyte expression of tumor necrosis factor-alpha (TNF-α), a pro-inflammatory cytokine, is significantly downregulated ($p < 0.05$) in AM containing scaffolds compared to C:HA scaffolds cultured in inflammatory media at day 7 (Fig. 4.3A). Further, although not statistically significant, AM scaffolds also showed TNF-α downregulation compared to CS scaffolds ($p = 0.0814$). When the cell-seeded scaffolds were cultured in high inflammatory media, both HA and AM scaffolds induced lower TNF-α expression compared to the standard C:CS scaffolds (Fig. 4.3B).

Further gene expression analysis focused on markers of tendon phenotype (Fig. 4.4). Collagen I (COLI) is the primary ECM protein in tendon and is secreted by tenocytes. COLI gene expression was significantly downregulated in CS scaffolds following 1 day of inflammatory challenge by IL-1β when compared to C:HA scaffolds (Fig. 4.4A). Following 4 days of culture in inflammatory media, tenocytes in C:CS scaffolds were expressing COLI at significantly lower levels than those in parallel HA or AM scaffolds and in the C:CS scaffolds in control media. Across all timepoints cells in both AM and HA scaffolds were maintaining COLI expression comparable to their respective controls. Scaffolds cultured in high inflammatory media showed no significant differences in COLI gene expression at day 1 (Fig. 4.4B). Analysis of subsequent days shows significant downregulation of tenocyte COLI expression in all scaffolds (except HA at day 4) as compared to corresponding scaffolds in control media.

Matrix metalloproteinase-3 (MMP-3) is involved in matrix breakdown in normal tendon remodeling and in early wound healing. Under the *in vitro* inflammatory conditions presented here, there was no significant difference in the MMP-3 gene expression between scaffolds or when compared to control media (Fig. 4.4C). When considering the cells cultured in scaffolds exposed to high inflammatory media, MMP-3 expression is expectantly high in all groups at day 1 (Fig. 4.4D). By day 4, tenocytes in AM scaffolds had significantly lower MMP-3 expression, no different from their respective control, as compared to cells cultured in CS or HA scaffolds.

The expression level of the pro-tenogenic transcription factor scleraxis (*SCXB*) was subsequently analyzed. While the scaffold variants used here did not contain aligned microstructural elements known to promote tenogenic expression profiles, results show little difference between groups due to scaffold type or media condition (Fig. 4.4E, F). Cells in HA scaffolds show downregulation of *SCXB* expression compared to CS scaffolds (day1) and control media (day 7)

in inflammatory media conditions (Fig. 4.4E). *SCXB* expression is also downregulated in high inflammatory media compared to control media in HA scaffolds (day 1) and all scaffolds at day 7 (Fig. 4.4F).

4.4.5 Short term protein release from pro-inflammatory tenocyte culture

In the absence of a pro-inflammatory signal (control media), cells seeded in CS scaffolds release significantly more TGF-β1 than those seeded in HA or AM scaffolds (Fig. 4.5A). When the cell-seeded scaffolds are exposed to IL-1β in the inflammatory media, there was a significantly higher concentration of TGF-β1 in the media surrounding the collagen scaffolds containing CS as compared to the HA scaffolds (Fig. 4.5B). In the high inflammatory media, there was no statistically significant difference between the amount of TGF-β1 released from each of the scaffold groups (Fig. 4.5C).

4.4.6 Cytokine sequestration within scaffold variants

A pull down assay was employed to determine whether the three scaffold types were differentially sequestering or trapping the pro-inflammatory cytokine (IL-1β) and, thus, influencing the cellular response. While the results suggest increased pull down when moving from CS to HA to AM scaffolds, there is no statistically significant difference between the entrapment of IL-1β in the three scaffold variants (Fig. 4.6).

4.5 Discussion

The inflammatory phase of adult wound healing is important for inducing the rapid closure of wounds but, as a result, leads to disorganized matrix and scar formation [189]. Studies in the healing process following acute tendon injury, in particular, show upregulation in TGF-β1 mRNA and protein expression, disruption in collagen fiber continuity and organization, and

decreases in ultimate stress and modulus when compared to uninjured tendons [23, 24]. Increases in the gene expression of pro-inflammation (*IL-1β, TNFα*) and matrix degradation factors (*MMP-3*, *MMP-13*) as well as decreases in the expression of tendon ECM (*COLI*) and tendon-specific markers (*SCX*) have also been shown in a canine flexor tendon model [22]. In designing a biomaterial to drive tendon regeneration *in vivo*, the presence of an inflammatory environment should be considered.

It has been previously shown that fetal wounds have the capacity to facilitate scarless wound healing with a limited inflammatory response. Interestingly, this phenomenon is not solely defined by the sterile, intrauterine environment. Fetal marsupials such as the gray short-tailed opossum, which develop outside of the uterus, heal cutaneous wounds in a scarless fashion [212]. Research has also shown that scar formation occurs in adult sheep skin transplanted onto fetal lambs, but not in adjacent fetal skin wounds [213]. Due to the unique nature of these results, efforts have begun to focus on the ECM and the role it plays in wound healing [191]. Hyaluronic acid (HA), shown to have a dominant presence in fetal wounds both in the wound ECM [299] and surrounding fluid [211], has been used in three-dimensional skin grafts to reduce scar formation [300]. Amniotic membrane has also been used in the treatment of skin wounds [219, 225]. As a result, our effort here investigated whether CG scaffolds containing hyaluronic acid or amniotic membrane matrix could reduce the immune response associated with interleukin-1beta (IL-1β) in tenocytes.

Collagen-based scaffold content was altered by incorporating HA or AM in the collagen-glycosaminoglycan suspension instead of the standard chondroitin sulfate (CS). Prior to incorporation into the scaffold, the AM matrix was partially characterized for collagen and sulfated GAG content. The complete makeup of the amniotic membrane is not known; however,

other studies have reported that in addition to these two matrix components, the AM also contains HA [215], elastin and denatured collagen [217]. Following scaffold lyophilization, SEM analysis revealed that all scaffold variants had an open porous microstructure (Fig. 4.1D). Mechanical testing on hydrated, crosslinked samples revealed significant increases in modulus when moving from CS to HA to AM scaffolds. Each scaffold contained the same overall material density and exhibited similar pore structure indicating that the matrix content affects scaffold modulus. While statistically significant, the relative differences in the moduli are still small compared to native tendon. However, these differences may alter local cellular behavior and warrant further investigation in the future. While the scaffolds tested here have insufficient mechanical strength for direct tendon application, separate efforts in our group have shown reinforcement strategies sufficient to boost the tensile modulus of the scaffold to greater than 1 MPa [251, 301]. When examining the distribution of cells following the 7 days of culture, the representative images in Figure 1E do not show any evidence of cellular clumping in any of the collagen-based scaffolds, including C:AM.

Interleukin-1β is a pro-inflammatory cytokine secreted by macrophages during the inflammatory phase of wound healing and was used in this study as the pro-inflammatory challenge. We first examined metabolic activity of tenocytes seeded within these scaffolds over a 7 day period (Fig. 4.2). Not only do the amnion scaffolds support tenocyte metabolic health in control media, cells are significantly more active in AM scaffolds than CS scaffolds (Fig. 4.2A). Further, tenocytes in AM scaffolds show increased metabolic activity in response to the pro-inflammatory challenge of IL-1β (Fig. 4.2B,C). Since metabolic health is dependent on the number of cells present as well as the metabolic activity on a per cell basis, the increase of these in the AM scaffolds is a critical finding.

Genes associated with the early inflammatory response in tendon healing (*TNF-α, COL1A2, MMP-3*) were differentially regulated in tenocytes in each of the three different scaffold environments. Each of these has been studied within the context of the normal tendon healing cascade [22]. The pro-inflammatory factor TNF-α, which works alongside IL-1β, is normally upregulated in adult tendon healing [22]. The results seen here show an upregulation of TNF-α expression in CS scaffolds while there is downregulation of this pro-inflammatory marker in HA and AM scaffolds after 7 days of culture (Fig. 4.3A). Especially in the high inflammatory media conditions (Fig. 4.3B), cells in HA and AM scaffolds show significant downregulation of TNF-α suggesting that these fetal ECM components may maintain their native anti-inflammatory properties within the CG scaffold platform.

When considering genes associated with matrix deposition and remodeling, altering the CG scaffold composition also resulted in differences in expression (Fig. 4.4). Collagen I (*COL1A2*) is the primary ECM protein in tendon and is secreted by tenocytes but is downregulated in the first days following tendon injury compared to healthy tendons [22]. In this experiment, *COL1A2* gene expression of scaffolds cultured in the inflammatory media is only significantly downregulated in the CS scaffolds when compared to the control media (day 4) (Fig. 4.4A). HA and AM scaffolds show no significant differences in expression when compared to their respective controls. Our results show higher *COL1A2* expression in the cells cultured in the inflammatory media in HA scaffolds compared to CS (day 1) and both scaffold types (day 4) (Fig. 4.4A). Cell-constructs cultured in the high inflammatory media exhibited *COL1A2* downregulation compared to the control in all groups (at days 4 and 7) except for HA at day 4 (Fig. 4.4B). Typically upregulated in adult tendon injury [22], MMP-3 expression was no different from the control media in the groups exposed to inflammatory media (Fig. 4.4C).

However, in high inflammatory media conditions, cells in AM scaffolds (day 4) showed significantly lower expression of MMP-3 that was no different from the control media (Fig. 4.4D). These results together suggest that fetal wound inspired matrices alter the pro-inflammatory effects usually seen in tendon wound sites. Implementing scaffolds such as these in tendon regeneration applications may reduce inflammation-induced scar formation.

Tendon is a highly anisotropic tissue with tenocytes longitudinally aligned within its microstructure. Geometric cues such as this have been shown to play a role in the maintenance of the tenocyte phenotype *in vitro* [60, 61]. However, due to ease of bulk fabrication, the current study used isotropic CG scaffolds, eliminating any geometric cues that would maintain the tenocyte phenotype. Gene expression of the tendon-specific gene scleraxis (*SCXB*) was monitored over the 7 day culture period (Fig. 4.4 E,F). Results give no indication that the addition of HA or AM into the scaffold either promotes or hinders expression of *SCXB*. Future work will employ anisotropic scaffolds that allow for tenocyte alignment and phenotypic preservation [60].

Important questions remain: why do scaffolds containing HA or AM alter the cell response to inflammatory signals? And what is the means of mechanism? Transforming growth factor-beta 1 (TGF-β1) is a protein that is highly expressed in adult wound healing but found at very low levels in fetal wounds. We hypothesized that AM-matrix decorated scaffolds may promote lower TGF-β1expression. An alternative hypothesis was that AM scaffolds may sequester the IL-1β from the media, preventing it from interacting with the cells within the scaffold.

With regards to the presence of TGF-β1, we report significantly less TGF-β1 released from the HA and AM containing scaffolds compared to the CS scaffolds (Fig. 4.5A). Once IL-1β was

introduced to the media, AM scaffolds were not significantly different from the other scaffold variants (Fig. 4.5B,C). However, scaffolds containing HA showed significantly lower (versus CS scaffolds) TGF-β1 release in the inflammatory media groups (Fig. 4.5B). These results were normalized versus acellular scaffolds to reveal cell-specific secretions; given the potential for AM-matrix to be processed in a manner to facilitate release of large doses of growth factors [219], ongoing efforts are examining how these endogenous factors may also affect cell activity. To examine the interaction between IL-1β and the different scaffold variants, a pull down assay was employed. While no significant difference in sequestration of IL-1β was observed between scaffold groups, the overall trend suggests that AM scaffolds have the potential to be optimized to sequester more IL-1β than CS scaffolds (Fig. 4.6). Together these observations suggest that while material composition may be important in modifying the inflammatory response *in vitro*, the complete mechanism is not yet understood. Additional studies will seek to differentiate further, and over longer time periods, the impact of scaffold composition on growth factor production, sequestration, and release. Future studies will explore the mechanism behind the results seen here, including how cell-matrix interactions are directly influencing cellular response to a pro-inflammatory environment.

A limitation of this current work is that supplementing media with a single pro-inflammatory factor is not adequate to replicate the complex inflammatory environment seen *in vivo*. Ongoing work is evaluating cell response to more complex inflammatory signals (e.g. TNF-α in combination with IL-1β) and *in vitro* macrophage phenotype in response to scaffold composition as well as inflammatory response and healing in an *in vivo* porcine defect model.

4.6 Conclusions

In an attempt to replicate the scarless, fetal wound healing properties in scaffolds for tendon regeneration, this study incorporated hyaluronic acid and amniotic membrane matrix into collagen-based scaffolds. In vitro experiments used interleukin-1 beta to create a pro-inflammatory environment. Bioactivity of the tenocytes cultured within these scaffold variants was assessed over a 7 day period. Following the pro-inflammatory challenge, equine tenocytes in amniotic membrane scaffold variants showed increased metabolic activity. These fetal wound inspired components also contributed to decreased tumor necrosis factor-alpha and matrix metalloproteinase-3 gene expression as well as increased expression of collagen I. Together, these results propose a biomaterial for modifying the inflammatory response associated with scar formation.

4.7 Figures

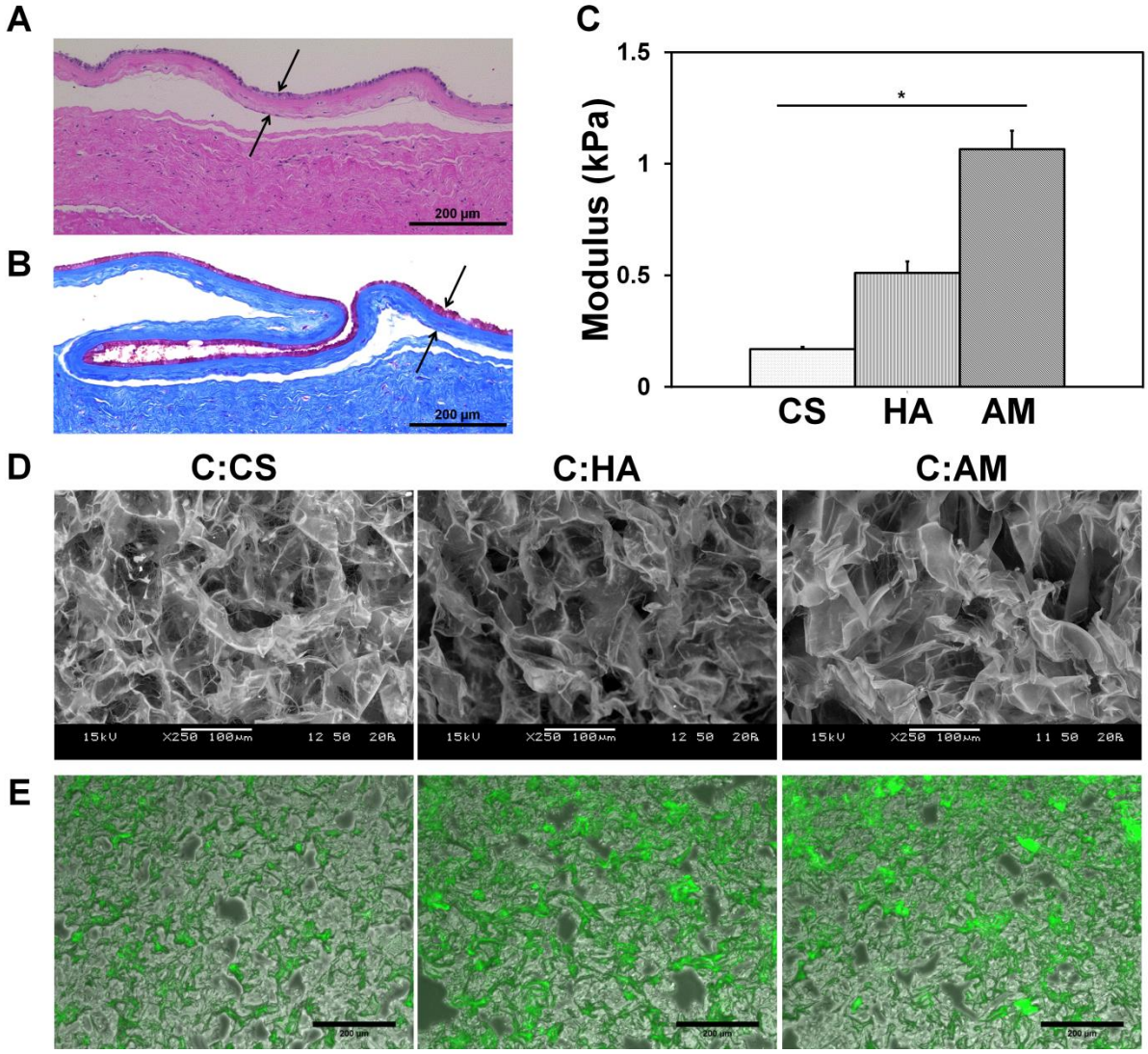

Figure 4.1. Amniotic membrane histological analysis, scaffold mechanical and microstructural analysis. **(A)** Placental section stained with H&E. Arrows indicate amniotic membrane. Scale bar: 200 µm. **(B)** Masson's Trichrome staining of placental section. Arrows indicate amniotic membrane. Scale bar: 200 µm. **(C)** Elastic modulus of scaffold variants under compression. (*) significance ($p < 0.05$) between scaffold groups. **(D)** SEM images of scaffold variants; collagen:chondroitin sulfate (C:CS), collagen:hyaluronic acid (C:HA), collagen: amniotic membrane (C:AM) (left to right). Scale bar: 100 µm. (**E**) Histological staining of vimentin in cell-seeded scaffolds with varying composition at day 7. Left to right: collagen:chondroitin sulfate (C:CS), collagen:hyaluronic acid (C:HA), collagen: amniotic membrane (C:AM). Scale bar: 200 µm.

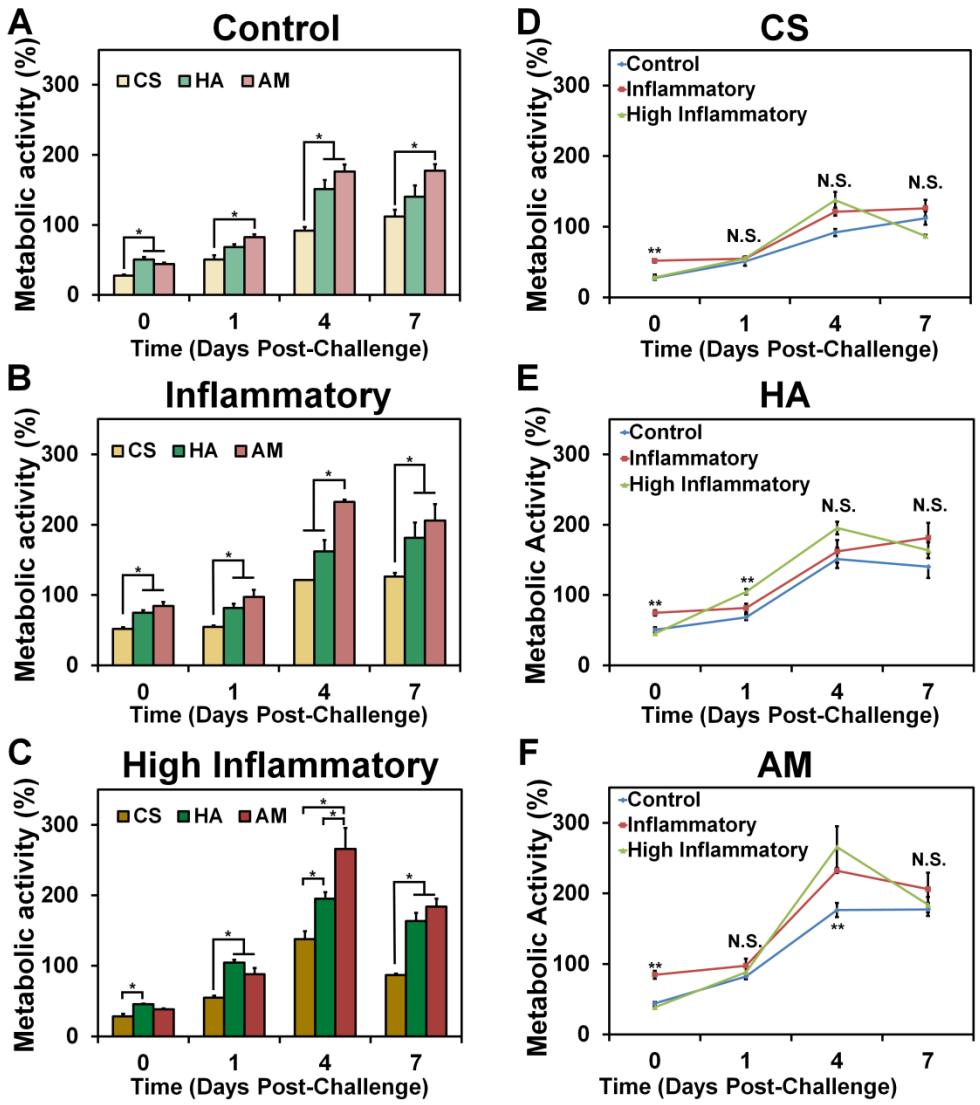

Figure 4.2. Tenocyte metabolic activity in scaffolds cultured in (**A**) control media, (**B**) inflammatory media containing 0.1 ng/mL IL-1β, and (**C**) high inflammatory media supplemented with 1 ng/mL IL-1β. (*) significance between groups indicated ($p < 0.05$). The same data has been grouped by scaffold type and plotted in (**D**) collagen:chondroitin sulfate, (**E**) collagen:hyaluronic acid, and (**F**) collagen:amniotic membrane. (**) significance compared to all groups at given time point ($p < 0.05$). (N.S.) no significant differences between groups at a given timepoint ($p > 0.05$).

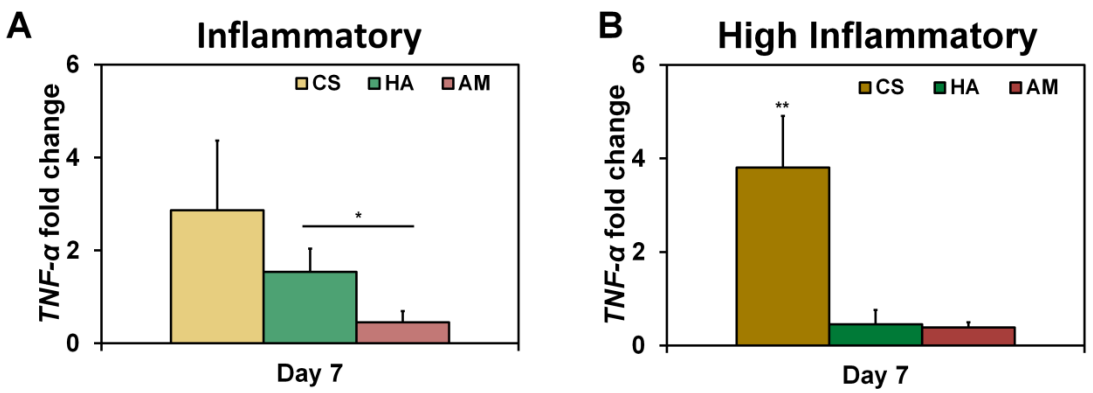

Figure 4.3. Gene expression of tumor necrosis factor-alpha (TNF-α) in tenocytes cultured in three scaffold variants in (**A**) inflammatory (0.1 ng/mL IL-1β) and (**B**) high inflammatory (1 ng/mL IL-1β) media conditions. Gene expression was normalized to tenocytes cultured in respective scaffold in control (no inflammatory factors) media. (*) significance between groups indicated ($p < 0.05$). (**) significance compared to all groups at given time point ($p < 0.05$).

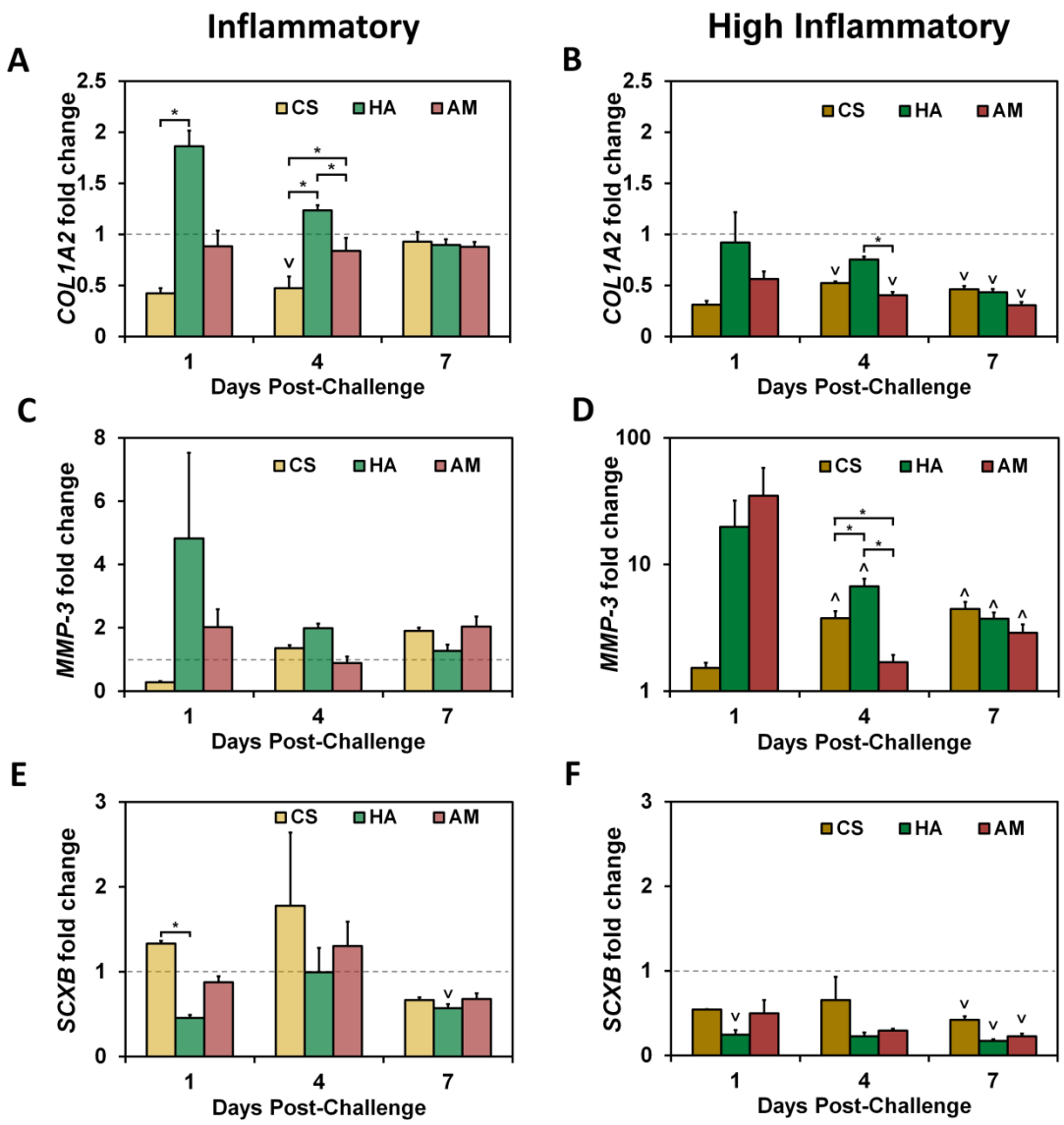

Figure 4.4. Tenocyte gene expression levels of collagen I (*COL1A2*; **A, B**), matrix metalloproteinase-3 (*MMP-3*; **C, D**), and scleraxis (*SCXB*; **E, F**) as a function of scaffold content at days 1, 4, and 7 of culture in inflammatory (0.1 ng/mL IL-1β) (**A, C, E**) and high inflammatory (1 ng/mL IL-1β) (**B, D, F**) media. Gene expression was normalized to tenocytes cultured in respective scaffold in control (no inflammatory factors) media. (*) significance between groups indicated ($p < 0.05$). (∧,∨) significant increase, decrease (respectively) compared to corresponding control (same scaffold type, same time point) ($p < 0.05$).

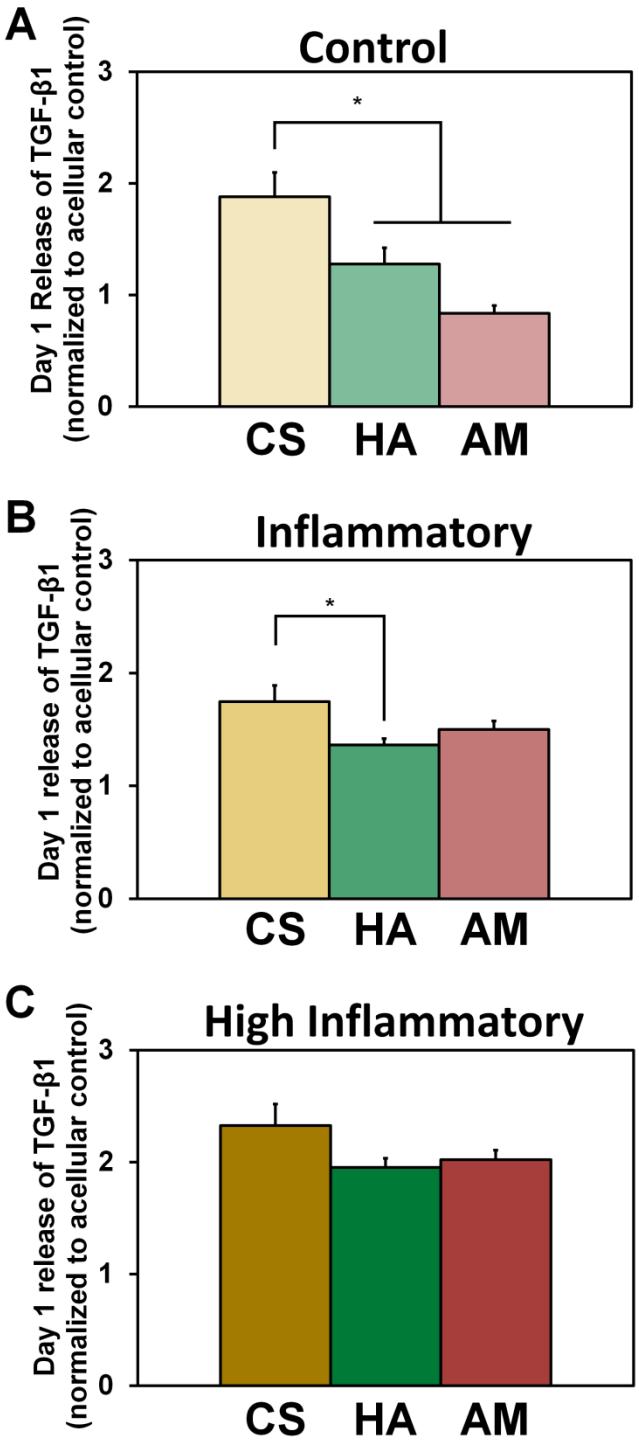

Figure 4.5. Transforming growth factor-beta 1 (TGF-β1) release from tenocyte-seeded scaffolds of varying compositions. Measurements were made after 24 hours of culture in serum-free medias: (**A**) inflammatory (0.1 ng/mL IL-1β) and (**B**) high inflammatory (1 ng/mL IL-1β). (*) significance between groups indicated ($p < 0.05$).

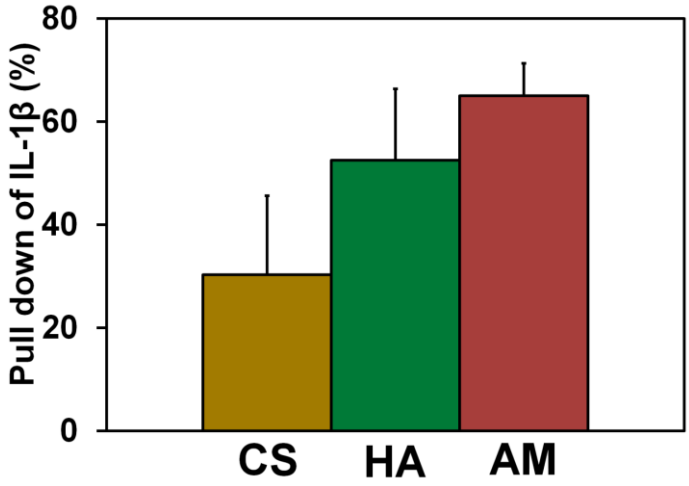

Figure 4.6. Pull down of IL-1β by scaffolds with varying compositions. The degree of pull down was normalized to the concentration of IL-1β in a solution without scaffolds.

CHAPTER 5: INCORPORATION OF AMNIOTIC MEMBRANE INTO COLLAGEN SCAFFOLDS TO ADDRESS IMMUNOMODULATORY REQUIREMENTS FOR TENDON REPAIR[**]

5.1 Chapter overview

Tendon tears often require surgical intervention and even then result in poor outcomes due to scar formation and re-failure. Biomaterial implants offer the potential to address multiple underlying concerns preventing improved tendon repair. Wrapping repaired tendons with commercially available collagen membranes is a technique used in rotator cuff and Achilles tendon surgeries to improve the mechanical strength of the repair. Modifications to the composition of a biomaterial implant have shown potential to alter the inflammatory response and establish conditions for improved regenerative repair. Here, we describe integrating these concepts into a three dimensional extracellular matrix analog that combines anti-inflammatory amniotic membrane (AM) matrix with an anisotropic collagen-glycosaminoglycan (CG) scaffold. AM-derived matrix was incorporated directly within the scaffold microstructure during fabrication to form a C:AM composite. Alternatively, native amniotic matrix was wrapped around the CG scaffold in a manner similar to current collagen membrane wraps. Human mesenchymal stem cells (MSCs) cultured within these materials were evaluated for metabolic health and immunomodulatory gene expression in response to inflammatory media challenge of interleukin 1 beta (IL-1β) and tumor necrosis factor alpha (TNF-α). The scaffolds were able to maintain MSC metabolic activity in all media conditions over the course of a 7 day culture.

[**] This chapter has been adapted from the following publication: Rebecca A. Hortensius, Jill H. Ebens, and Brendan A.C. Harley, "Incorporation of amniotic membrane into collagen scaffolds to address immunomodulatory requirements for tendon repair." *In preparation.*

Expression of genes encoding for pro-inflammatory cytokines was downregulated in AM containing scaffolds. Further work needs to be done to elucidate the origins of these effects.

5.2 Introduction

While the human body is capable of repairing minor tendon injuries, native repair processes often result in a loss of structural integrity and mechanical strength due to the formation of poorly organized granulation tissue (scar) [302]. In the cases of massive tissue tears or degeneration due to chronic conditions, surgical strategies are frequently required. A range of suturing techniques have been developed to facilitate tendon-to-tendon reattachment or tendon graft insertion [303]; however, despite surgical improvements these large injuries too result in diminished tendon functionality and have a high incidence of re-tear. The implantation of biomaterial scaffolds offers a promising avenue for the promotion of tendon repair and regeneration *in vivo*. At the most basic level, biomaterial implants can be used to mechanically stabilize the surgical reconnection. Products such as the GraftJacket Regenerative Tissue Matrix (Wright Medical Technology), Restore Orthobiologic Implant (DePuy Orthopaedics), TissueMend Soft Tissue Repair Matrix (Stryker Orthopaedics), and CuffPatch Bioengineered Tissue Reinforcement (Arthrotek) are currently being studied [304] and used in the clinic for rotator cuff [305-307] and Achilles tendon tears [308, 309]. Through their use as wraps around tendon repairs, they provide mechanical support to the injured area, promote retention of surgically placed sutures, and provide a matrix for cellular and vascular ingrowth [310]. However, they only provide a two dimensional shell around the existing tendon and do not contain internal support of the tendon body. An inherently three-dimensional scaffold may be better suited for this application.

The inflammatory response following injury plays a significant role in the ultimate healing of a tissue [189]. Pro-inflammatory cytokines (such as IL-1β) have been shown to induce the expression of inflammatory enzymes and matrix degradation factors in tendon cells which leads to tendon destruction and loss of biomechanical integrity [311]. Additionally, by blocking the activity of pro-inflammatory cytokine tumor necrosis factor alpha (TNFα), increased biomechanical strength in a rat rotator cuff model has been observed [11]. It is hypothesized that modulating this early phase of wound healing through tissue engineering strategies (materials, cells, and/or soluble factors) could lead to decreased scar formation and, ultimately, better healing outcomes. The anti-inflammatory properties of the amniotic membrane (AM), the innermost layer of a placenta, have contributed to its success as a wound matrix in the treatment of a range of tissues (cornea [222-224], skin [219, 225], oral mucosa [226], and others [215, 227]). In ocular applications, the use of amniotic membranes tempered inflammation and increased the rate of re-epithelialization when used for surface abnormalities [222], limbal stem cell deficiency [223], and corneal ulcers [224]. Additionally, amniotic membranes have shown the ability to enhance progenitor cell recruitment in a mouse model [219]. Similar to the current clinical products listed above, a 1942 report detailed the use of amniotic membrane sheets in the treatment of scar formation in digital flexor tendons following injury and subsequent repair [220].

Collagen-glycosaminoglycan (CG) scaffolds are three-dimensional extracellular matrix mimics that have been applied to a range of tissue engineering applications [55-58, 67, 244, 292]. Their mechanism of regeneration is based on their ability to inhibit myofibroblast recruitment to the wound site [293] and therefore the contraction/scar formation that follows [312]. To mimic the tendon's native structural alignment, recently a new class of anisotropic CG scaffolds have been

developed [61]. Separately, to introduce anti-inflammatory properties into these CG scaffolds, AM derived matrix components have been incorporated into the chemical composition of the scaffold during fabrications [230]. Their addition to the CG scaffold promoted fibroblast metabolic activity and tempered pro-inflammatory gene expression *in vitro* [230]. However, the mode of the AM's anti-inflammatory activity is still unknown, suggesting new studies to examine the effects of its unique matrix composition [215, 218], soluble factors that it contains [219, 313], or a combination of the two.

Considering the need for tendon regeneration platforms and the role inflammation plays in wound healing, the work described in this manuscript combines a three-dimensional, microstructurally aligned CG scaffold with a two-dimensional anti-inflammatory allograft shell for *in vitro* evaluation of this core-shell composite. In this work, we examine what dictates the cellular response to amnion materials; direct contact with the matrix or altering the kinetics of growth factor availability. We examine whether the amniotic membrane matrix needs to be directly incorporated into the bulk of the CG scaffold analog to induce an anti-inflammatory effect on cells under inflammatory culture conditions or if the incorporation of the AM membrane as a membrane shell surrounding a conventional CG scaffold core can provide anti-inflammatory capabilities as well.

5.3 Materials and methods

5.3.1 Amnion membrane isolation

Human placentas were obtained following uncomplicated vaginal births. The amniotic membrane (AM) matrix components were isolated from these placentas as previously described [230, 294]. Briefly, the AM was mechanically separated from the placenta, washed, and

decellularized via incubation in thermolysin (125 μg/mL) [295]. Following decellularization, AM were rinsed in PBS with shaking to remove cellular debris and then stored in PBS at 4°C. The spongy layer of the AM was allowed to swell for 24-48 hours before it was separated from the AM and discarded. The matrix was lyophilized in a sheet and stored in a dessicator until further use.

5.3.2 Preparation of collagen suspension

Type I collagen from microfibrillar collagen (Collagen Matrix, Oakland, NJ) was homogenized in 0.5 M acetic acid with either chondroitin sulfate from shark cartilage (Sigma Aldrich, St Louis, MO) or homogenized amniotic membrane as collected above. A collagen:chondroitin sulfate (C:CS) ratio of 11:1 was used while C:AM suspensions were made at a 5:1 w:w ratio due to the high AM collagen content. Each suspension was made with a total density of 0.5% w/v, stored at 4°C, and degassed prior to use [251].

5.3.3 Fabrication of anisotropic scaffolds via freeze drying

Collagen scaffolds were fabricated as previously described [61]. Briefly, collagen suspensions were added to cylindrical molds made of polytetrafluoroethylene (PTFE) sides and a copper bottom. When placed on a precooled (-10˚C) freeze-dryer shelf (VirTis, Gardiner, NY), unidirectional heat transfer through the copper bottom promotes the growth of elongated ice crystals. The suspensions were frozen at -10˚C for two hours prior to the sublimation of the resulting ice crystals at 0˚C and 200 mTorr. Molds of 8 mm diameter and 20 mm in height were used for cell culture experiments.

5.3.4 Fabrication of wrapped, anisotropic collagen-based scaffolds via freeze drying

Similar to previous work [251], scaffold-amniotic membrane core-shell constructs were created by cutting a dry sheet of AM to size and placing it along the circumferential surface of the cylindrical, PTFE-copper mold (8 mm diameter, 20 mm height). The C:CS suspension was then pipetted into the center of the mold. The freeze drying cycle used for these core-shell scaffolds was identical to the C:CS and C:AM anisotropic scaffolds.

5.3.5 Crosslinking of CG and CG-AM core-shell scaffolds

Scaffolds were sterilized and dehydrothermally crosslinked under vacuum in a vacuum oven (Welch, Niles, IL) at 105˚C for 24 hours [56]. 5 mm long sections were cut from the scaffold and used for all *in vitro* culture experiments [61]. Scaffolds were hydrated in 100% ethanol overnight and washed in two changes of phosphate-buffered saline (PBS) over 36 hours. Chemical crosslinking was applied to strengthen the scaffolds against contraction by seeded cells [248, 252]. Scaffolds were immersed in a solution of 1-ethyl-3-[3-dimethylaminopropyl] carbodiimide hydrochloride (EDC) and *N*-hydroxysulfosuccinimide (NHS) at a molar ratio of 5:2:1 EDC:NHS:COOH. Scaffolds were crosslinked for 1.5h under shaking at room temperature. Scaffolds were washed with PBS before being stored in fresh PBS at 4˚C.

5.3.6 SEM analysis

The cross-sectional microstructure of dry, uncrosslinked scaffolds was visualized using scanning electron microscopy (SEM). Samples were imaged with a Philips XL30 ESEM-FEG scanning electron microscope under high vacuum.

5.3.7 Human mesenchymal stem cell culture

Bone marrow-derived human mesenchymal stem cells (Lonza, Switzerland) were cultured in standard culture flasks in low glucose Dulbecco's modified Eagle's medium supplemented with

10% MSC FBS (Invitrogen, Carlsbad, CA), 1% L-glutamine (Invitrogen, Carlsbad, CA), and 1% Antibiotic-Antimycotic (Invitrogen, Carlsbad, CA). Media was changed every 3 days and the cells were cultured to confluence at 37˚C and 5% CO_2. Cells were used at passage 6.

5.3.8 Scaffold seeding and culture conditions

Hydrated, crosslinked CG scaffolds were soaked in growth media for overnight at 37°C before being tapped dry on a Kimwipe and placed in ultra-low attachment 6-well plates (Fisher, Waltham, MA). Confluent hMSCs were trypsinized and resuspended in growth media at a concentration of approximately 78,000 cells per 20 µL in preparation for static seeding [61]. Ten microliters of the cell suspension were added to one side of the scaffolds. Then the scaffolds were incubated for 15 minutes at 37˚C, flipped over and another 10 µL of cell suspension was added. To allow for initial cell attachment, scaffolds were placed in the incubator for 2 hours before additional growth media was added. Scaffolds were incubated at 37˚C and 5% CO_2 for 24h before the media was exchanged for one of three inflammatory challenge media with media being replaced every 3 days:

(1) Control: growth media

(2) Inflammatory: media supplemented with 0.1 ng/mL of the pro-inflammatory factor interleukin-1 beta (IL-1β) and 1 ng/mL tumor necrosis factor alpha (TNFα)

(3) High inflammatory: media supplemented with 1 ng/mL of IL-1β and 10 ng/mL tumor necrosis factor alpha (TNFα).

5.3.9 Metabolic activity quantification

A non-destructive alamarBlue® assay (Invitrogen, Carlsbad, CA) was used to measure the metabolic activity of the MSCs within the collagen scaffolds [61, 251]. At the start of the experiment, a metabolic activity standard curve was created by culturing a known number of cells (ranging from 25-300% of the total cells seeded) for 2 hours in a 1x alamarBlue® solution supplemented with cytokines from each of the three media variants. At each experimental timepoint (days 1, 4, 7), scaffolds were removed from culture, rinsed in PBS, and incubated under gentle shaking at 37˚C for 2 hours in a 1x alamarBlue® solution containing the media variant of the primary culture. Using a fluorescent spectrophotometer, resorufin fluorescence was measured (excitation: 540 nm, emission: 590 nm). Metabolic activity was interpolated to the standard curve and reported as a percentage of the total number of seeded cells.

5.3.10 Gene expression analysis through RNA isolation and real-time PCR

RNA was isolated from scaffolds at each timepoint with an RNeasy Plant Mini kit (Qiagen, Valencia, CA). The scaffolds were rinsed in PBS to remove any dead/unattached cells, cut in half with a razor, and immersed in the kit's lysis buffer for 5 minutes on ice [87]. RNA was isolated following the kit's instructions and total RNA was quantified using a Nanodrop. The RNA was reverse transcribed using a QuantiTect Reverse Transcription kit (Qiagen, Valencia, CA) and a Bio-Rad S1000 thermal cycler. Real-time PCR was performed with an Applied Biosystems 7900HT Fast Real-Time PCR System (Carlsbad, CA) to measure gene expression levels for hepatocyte growth factor (*HGF*), interleukin 6 (IL-6, *IL6*), interleukin 8 (IL-8, *CXCL8*), indoleamine 2,3, dioxygenase (*IDO1*) and transforming growth factor beta 1 (*TGFB1*). Glyceraldehyde 3-phosphate dehydrogenase (*GAPDH*) was used as a housekeeping gene. All results were expressed as fold changes relative to expression levels of cells cultured in scaffolds

of the same type and at the same time point but in control media. Primer sequences are located in Table 5.1.

5.3.11 Statistical analysis

One-way analysis of variance (ANOVA) followed by Tukey-HSD post-hoc test was performed on gene expression data at each timepoint. The metabolic activity was analyzed using a two-way, repeated measures ANOVA followed by Tukey-HSD post-hoc test. A p-value < 0.05 was used for significance. All analyses were based on a minimum of n=4 scaffolds. Error is reported as the standard error of the mean in the figures.

5.4 Results

5.4.1 Scaffold microstructure

SEM images taken of transverse planes through each scaffold variant showed an open pore structure with rounded pores on the order of 200 micrometers in size, with longitudinal cross-sections showing more elongated pores (Fig. 5.1). The core-shell C:CS-AM scaffolds show consistent union between the scaffold core and the AM shell without evidence of delamination, confirming that the membrane is well integrated with the bulk of the material (Fig. 5.1C).

5.4.2 Cell metabolic activity under pro-inflammatory media conditions

The human mesenchymal stem cells (MSCs) that were cultured within each CG scaffold variant were evaluated for metabolic health prior to the pro-inflammatory challenge (day 0) and at subsequent timepoints (days 1, 4, and 7) (Fig. 5.2). There were no statistically significant differences between the metabolic activity of cells within these scaffold groups over the course of the entire 7 day experiment, regardless of whether the scaffolds were in control media (Fig. 5.2A), inflammatory media (Fig. 5.2B), or high inflammatory media (Fig. 5.2C).

5.4.3 Expression of immunomodulatory genes in MSCs cultured in 3D scaffolds under pro-inflammatory conditions

The expression of MSC immunomodulatory genes such as hepatocyte growth factor (HGF), indoleamine 2,3, dioxygenase (IDO) and transforming growth factor beta 1 (TGF-β1) were evaluated via PCR. Fold changes were normalized to GAPDH (housekeeping gene) and the expression from cells cultured in the same scaffold variant in control media.

Cellular HGF expression in inflammatory (Fig. 5.3A) and high inflammatory (Fig. 5.3B) media resulted in no significant differences between groups or compared to the control, except for the C:AM group in high inflammatory media at day 4. This sample group showed significantly lower expression compared to the corresponding scaffolds in control media. Similarly, there was no significant difference in IDO expression (Fig. 5.3C, Fig. 5.3D) with respect to either of the variables (scaffold type, media condition). The final immunomodulatory gene evaluated was TGF-β1. In both the inflammatory (Fig. 5.3E) and high inflammatory (Fig. 5.3F) media, the TGF-β1 expression in the C:CS scaffolds starts low, trends up at day 4 before dropping again by day 7. In the inflammatory media, the peak in C:CS expression at day 4 is significantly different from the C:AM group at that timepoint (Fig. 5.3E). In the high inflammatory media, expression of TGF- β1 in the C:AM and wrap scaffolds shows a downward trend overtime, resulting in expression in the wrapped scaffold significantly different from the control at day 7 (Fig. 5.3F).

5.4.4 Expression of pro-inflammatory genes MSCs cultured in 3D scaffolds under pro-inflammatory conditions

Additionally, the relative expression of genes encoding for pro-inflammatory cytokines interleukin 6 (IL-6) and interleukin 8 (IL-8) were analyzed via PCR (Fig. 5.4). In both inflammatory media (Fig. 5.4A) and high inflammatory media (Fig. 5.4B), the expression of IL-6

is significantly lower ($p < 0.05$) in C:AM scaffolds compared to C:CS scaffolds following 1 day of pro-inflammatory media challenge (Fig. 5.4A). In the following days in inflammatory media culture, IL-6 expression is higher in C:CS scaffolds compared to C:AM and the AM wrapped scaffolds, although this trend is not significant (Fig. 5.4A). However, at day 4 of culture in high inflammatory media, MSCs in C:CS scaffolds show a statistically significant ($p < 0.05$) increase in the expression of pro-inflammatory IL-6 compared to the control and the scaffolds that contain AM (C:AM and AM wrapped scaffolds) (Fig. 5.4B).

When evaluating the expression of IL-8 in 3D MSC culture in inflammatory media, an increase in expression in C:CS scaffolds is observed at days 1 and 4 along with lower levels of expression in the AM-containing scaffolds (Fig. 5.4C). Although these trends are not significant in the inflammatory condition, statistically significant observations can be made regarding IL-8 expression in the high inflammatory condition. At all timepoints (days 1, 4, 7), the AM wrap scaffolds are expressing IL-8 at levels no different from the control ($p > 0.05$) (Fig. 5.4D). Further, at days 4 and 7 the AM wrap scaffolds are exhibiting significant downregulation ($p < 0.05$) of this pro-inflammatory gene when compared to C:CS scaffolds (Fig. 5.4D).

5.5 Discussion

In the treatment of massive tendon tears, biomaterials provide an alternative to the reliance on native healing cascades or use of surgical techniques, both with outcomes compromised by scar formation, decreased mechanical properties, and high re-failure rates. In designing bioactive materials for this application, the *in vivo* ECM architecture and local growth factor/cytokine environment must be kept in mind. Especially important is the understanding that the material implant is likely to experience the body's native inflammatory response; in response to the injury, the implant, or both. Extended inflammation can have detrimental effects on healing

outcomes. Facilitating the transition from the inflammatory phase of healing to one of proliferation and remodeling is a strategy to prevent the occurrence of scar formation.

Collagen-glycosaminoglycan (CG) scaffolds are degradable, bioactive, three-dimensional materials that mimic the composition and microstructure of the extracellular matrix. Studied for an array of applications [55-58, 67, 244, 292], they promote regeneration by preventing fibroblast initiated contraction [293, 312]. The amniotic membrane also promotes regeneration, typically in two-dimensional applications, by tempering the inflammatory response at the injury site.

This work demonstrates the incorporation of amniotic membrane matrix into both the bulk of a collagen-based, open pore scaffold and in wrap form in a scaffold core-membrane shell configuration. Each of these scaffold variants, along with a collagen-chondroitin sulfate control, exhibit rounded pores in the transverse cross-section and elongated pores in the longitudinal direction (Fig. 5.1). This anisotropy is produced using freeze drying and a mold of mismatched thermal conductivity. It has been previously shown that this aligned microstructure, mimicking the anisotropic characteristics of native tendon, maintains tenocyte phenotype within the material [60] and enhances MSC differentiation towards a tenogenic phenotype [88]. Further, the core-shell wrap design is inspired by current surgical techniques that implement the use of commercially available tendon wraps [304] and *in vitro* work that has attribute increased mechanical competence in the CG scaffolds to a core-shell configuration [251]. An added feature of the AM wrap is that ability to incorporate more membrane matrix per scaffold (3.4 times in mass) than in the traditional C:AM scaffold.

Mesenchymal stem/stromal cells (MSCs) are multipotent progenitor cells [314] found in many tissues throughout the body [315], but primarily harvested from bone marrow and adipose tissue for tissue engineering applications [316]. MSCs are capable of self-renewal [314] and differentiation into specialized cells found in tendon, bone, cartilage, ligament, and fat [317]. MSCs are also present in sites of injury. Due to these properties, MSC culture within biomaterials is often studied. As multipotent cells, MSCs are a likely cell source to be co-implanted with bioactive substrates intent on providing guided differentiation towards a tissue of choice. Additionally, one global objective is to evaluate *in vitro* the cytocompatibility, bioactivity, and differentiation capacity of the designed materials on an element of the native cellular environment. For this reason, the bioactivity of the MSCs seeded within the scaffold variants presented here was evaluated, using an alamarBlue metabolic activity assay (Fig. 5.2). The cells respond consistently to each scaffold variant (C:CS, C:AM, and C:CS-AM wrap) under each media condition (growth media control (Fig. 5.2A), inflammatory media (Fig. 5.2B), and high inflammatory media (Fig. 5.2C)). Metabolic activity is initially low, as not all cells attach to the scaffold, but increased overtime showing that the scaffolds support the cellular activity of the MSCs. Even though high levels of IL-1β have led to decreased MSC proliferation [318], there are no significant differences here associated with inflammatory media challenge in any of the scaffold types.

In the body, MSCs home to sites of injury and inflammation as part of the tissue repair/regeneration process. Their complex immunomodulatory role in wound healing has been studied extensively and, while it is not completely clear how MSCs regulate the body's immune response, several MSC secreted factors have been identified as key immunomodulators [319]. Hepatocyte growth factor (HGF) and indoleamine 2,3, dioxygenase (IDO) [315, 317] as well as

transforming growth factor beta 1 (TGF-β1) [314, 315, 317] are used by MSCs to elicit immunosuppressive effects. The increased secretion of each of these factors following interferon-gamma (IFN-γ) led to reduced proliferation in allogenic mixed lymphocyte reactions [317]. In addition to IFN-γ, IL-1β and TNFα are major pro-inflammatory cytokines that contribute to the inflammatory environment in the early stages of wound healing [318, 320, 321]. In the current study, the changes in the gene expression of these three factors was minimal (Fig. 5.3). Cells in each scaffold exposed to IL-1β and TNFα media challenges exhibited expression no different from the control media (with the exception of the downregulation of TGF-β1 in AM wrap scaffolds in high inflammatory media at day 7 (Fig. 5.3F)). However, when the expression of pro-inflammatory genes (IL-6, IL-8) is evaluated, expression is downregulated in AM-containing scaffolds, especially in high inflammatory conditions (Fig. 5.4 B,D).

It is suggested, although still unclear, from these data that the MSCs seeded within each of these scaffold variants are not displaying their typical immunosuppressive function (increased levels of HGF, IDO, TGF-β1) following a pro-inflammatory challenge. Counter to this observation, the AM-containing scaffolds show significant downregulation of pro-inflammatory genes (IL-6, IL-8) in MSCs. It would be interesting to investigate whether the scaffolds are preventing the inflammatory cytokines (IL-1β and TNFα) from acting on the MSCs. Ongoing work is focused on quantifying cytokine secretion in this experiment. Future work should evaluate bone marrow-derived MSC immunomodulatory response to IL-1β and TNFα in two dimensions. Priming the MSCs with pro-inflammatory factors prior to seeding in each CG scaffold, as in Aktas et al [321], will allow for more incremental analysis of MSC response to inflammatory cytokines and collagen-based scaffold materials. Also, MSC culture in conjunction with an immune cell type

(e.g. macrophages, T cells) will allow for investigation of downstream effects of scaffold-led immunomodulation.

5.6 Conclusions

The amniotic membrane serves as a powerful source of anti-inflammatory material. While it has been used in two-dimensional tissue regeneration applications, the potential benefits in translating it to three-dimensional biomaterials is yet unknown. In this manuscript, AM matrix was incorporated into 3D collagen-based materials via two means; bulk incorporation or as a membrane wrap surrounding a collagen-glycosaminoglycan core. The fabrication of these scaffolds allowed for microstructural anisotropy to mimic the aligned ECM of the tendon. Human mesenchymal stromal cells, known for their immunomodulatory properties, were cultured in these scaffolds under pro-inflammatory media conditions. The results surrounding the maintenance of these immunomodulatory properties within these AM-containing scaffolds are inconclusive. Further work needs to be done to elucidate the origin of these effects.

5.7 Tables

Table 1.1. Primer sequences used in RT-PCR.

Transcript	Sequence	Reference
HGF	Forward: ATGCATCCAAGGTCAAGGAG Reverse: TTCCATGTTCTTGTCCCACA	[317]
IL6	Forward: CAATATTAGAGTCTCAACCCCCA Reverse: TTCTCTTTCGTTCCCGGTGG	NCBI Primer BLAST search
CXCL8	Forward: ACTGAGAGTGATTGAGAGTGGAC Reverse: AACCTCTGCACCCAGTTTTC	[322]
IDO1	Forward: CGCTGTTGGAAATAGCTTC Reverse: CAGGACGTCAAAGCACTGAA	[317]
TGFB1	Forward: CAGATCCTGTCCAAGCTG Reverse: TCGGAGCTCTGATGTGTT	[317]
GAPDH	Forward: AAGGTGAAGGTCGGAGTCAAC Reverse: GGGGTCATTGATGGCAACAATA	[322]

5.8 Figures

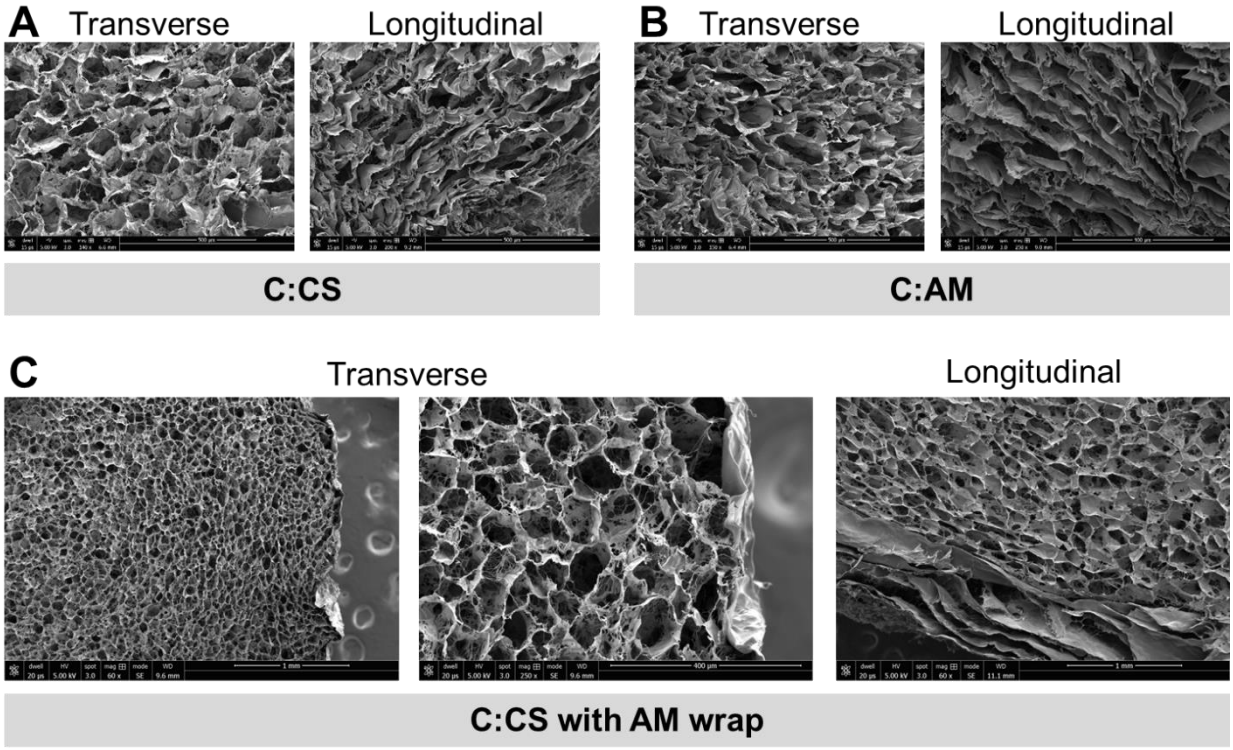

Figure 5.1. Scanning electron microscopy of (**A)** collagen-chondroitin sulfate scaffolds, (**B**) collagen-amniotic membrane scaffolds, and (**C**) core shell scaffolds with collagen-chondroitin sulfate core and amniotic membrane shell. Each scaffold was fabricated via unidirectional freeze drying to produce the anisotropic pores seen in the longitudinal sections. Scale bars are indicated in each image.

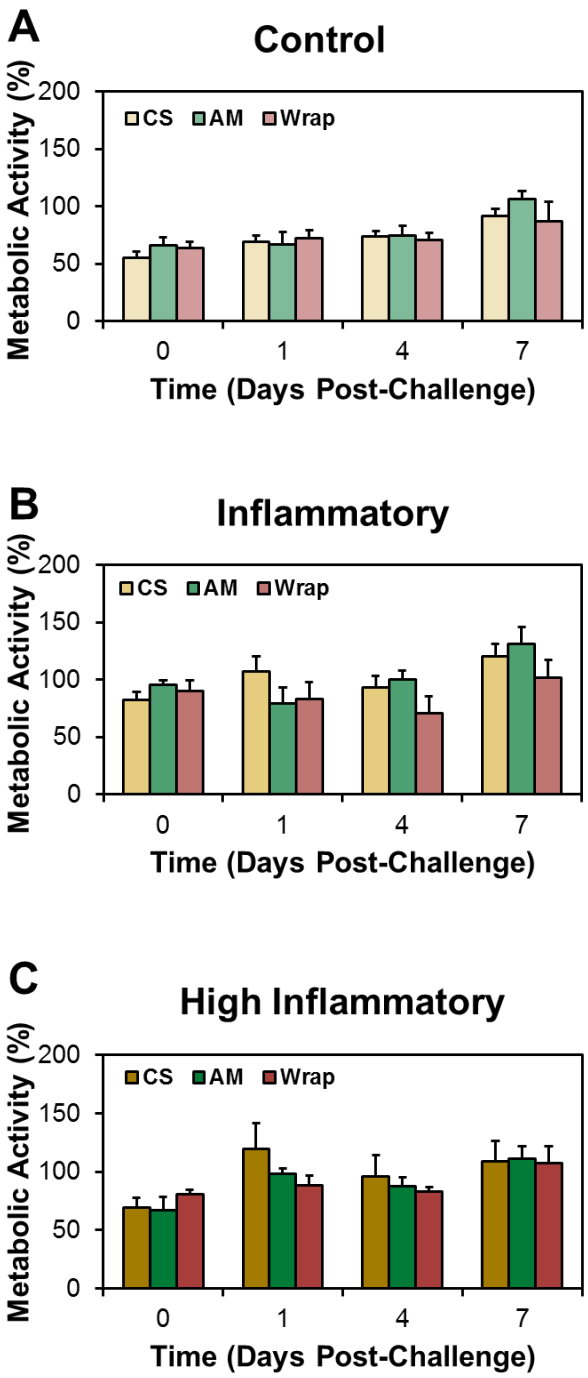

Figure 5.2. Human mesenchymal stem cell metabolic activity in each scaffold variant was completed using alamarBlue. CS = collagen-chondroitin sulfate scaffolds, AM = collagen-amniotic membrane scaffolds, and Wrap = core shell scaffolds with collagen-chondroitin sulfate core and amniotic membrane shell (**A**) Culture in growth media (control). (**B**) Culture in media supplemented with 0.1 ng/mL of the pro-inflammatory factor interleukin-1 beta (IL-1β) and 1 ng/mL tumor necrosis factor alpha (TNFα) (inflammatory). **(C)** Culture in media supplemented with 1 ng/mL of IL-1β and 10 ng/mL tumor necrosis factor alpha (TNFα) (high inflammatory).

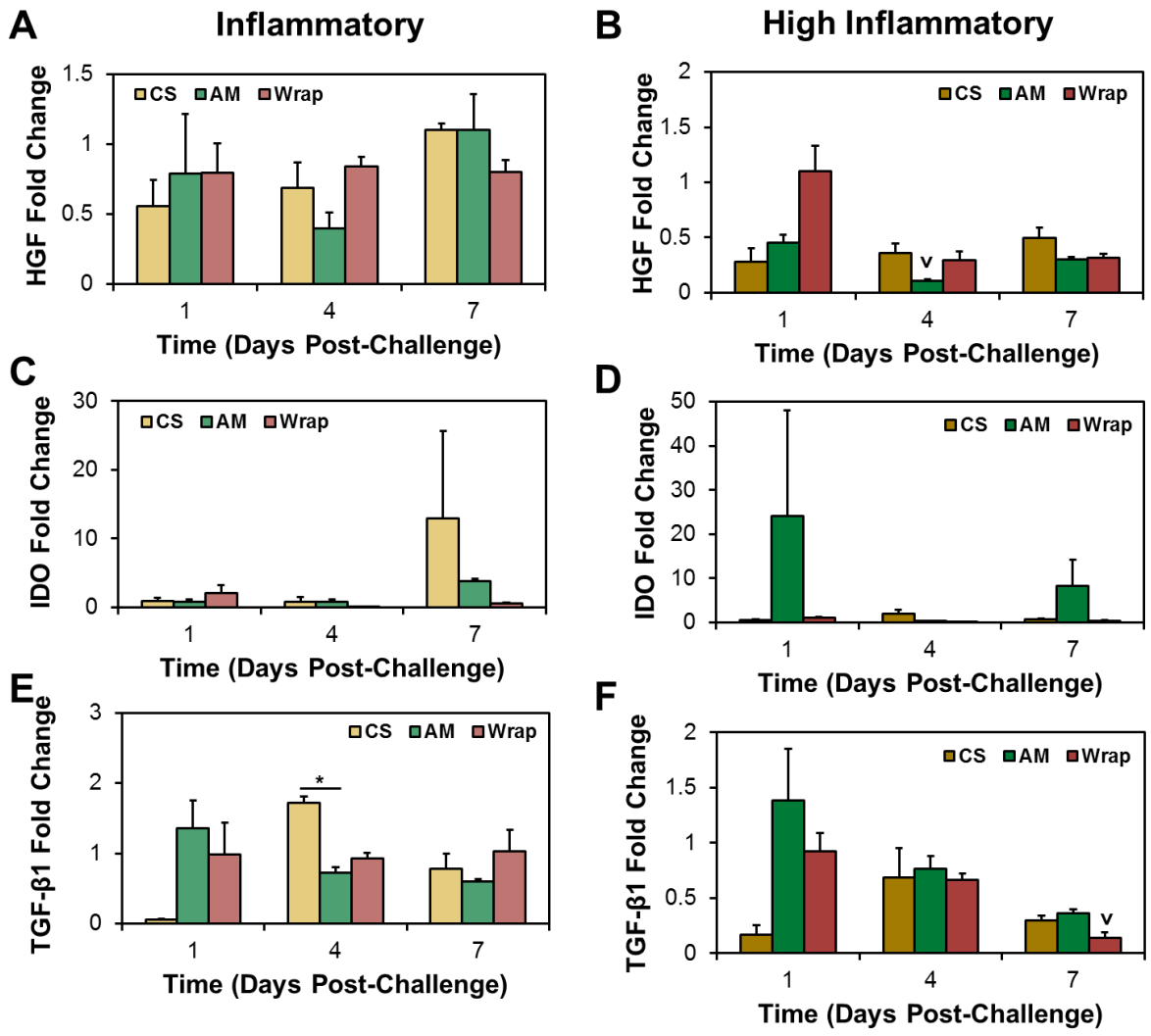

Figure 5.3. Expression of MSC immunomodulatory genes, HGF (**A, B**), IDO (**C, D**), and TGF-β1 (**E, F**) in scaffolds cultured in media supplemented with 0.1 ng/mL of the pro-inflammatory factor interleukin-1 beta (IL-1β) and 1 ng/mL tumor necrosis factor alpha (TNFα) (inflammatory) **(A, C, E)** or media supplemented with 1 ng/mL of IL-1β and 10 ng/mL tumor necrosis factor alpha (TNFα) (high inflammatory) **(B, D, F)**. Expressed as fold change internally normalized to GAPDH and externally normalized to the expression of cells in the same scaffold, at the same timepoint, in control media.

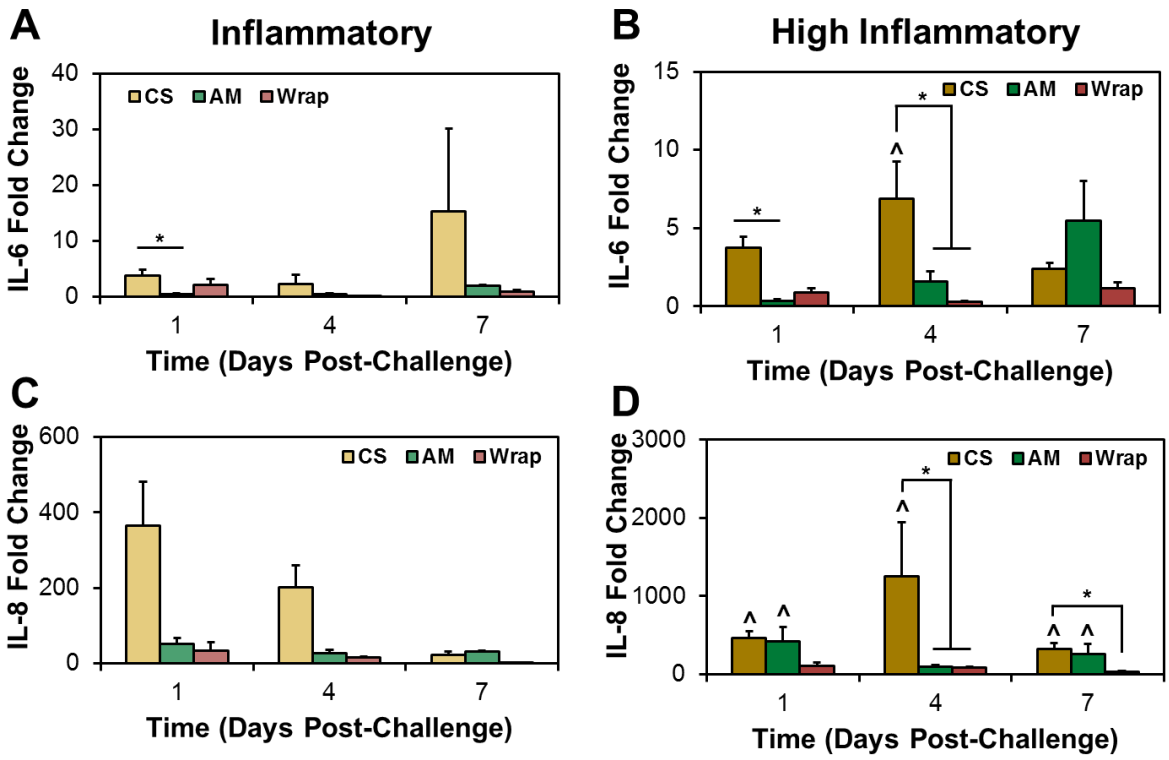

Figure 5.4. Expression of pro-inflammatory genes, IL-6 (**A, B**) and IL-8 (**C, D**) in scaffolds cultured in media supplemented with 0.1 ng/mL of the pro-inflammatory factor interleukin-1 beta (IL-1β) and 1 ng/mL tumor necrosis factor alpha (TNFα) (inflammatory) **(A, C)** or media supplemented with 1 ng/mL of IL-1β and 10 ng/mL tumor necrosis factor alpha (TNFα) (high inflammatory) **(B, D)**. Expressed as fold change internally normalized to GAPDH and externally normalized to the expression of cells in the same scaffold, at the same timepoint, in control media.

CHAPTER 6: MACROPHAGE RESPONSE IN VITRO AND IN VIVO TO AMNION-CONTAINING COLLAGEN-BASED SCAFFOLDS[††]

6.1 Chapter overview

Prolonged inflammation following injury is detrimental to healing. Macrophages have a large influence on the transition between the phases of the wound healing cascade (inflammation, proliferation, remodeling) through their plasticity and ability to display a spectrum of phenotypes. A biomaterial design that facilitates this transition would be advantageous in tissue regeneration applications. Collagen-glycosaminoglycan porous scaffolds, in combination with the matrix of the anti-inflammatory amniotic membrane, were studied for their ability to facilitate the macrophage phenotypic shift necessary for improved wound healing *in vitro* and in an *in vivo* porcine mandibular defect. The results indicate that while the scaffolds do not support a M1 (pro-inflammatory) phenotype *in vitro*, there is some upregulation of M1 associated genes at early time points *in vivo*. The presence of a M2 (pro-healing, anti-inflammatory) associated macrophage phenotype is much more dominant *in vitro* culture. Future work will focus on studying macrophage response in an inflammatory environment *in vitro* and expanding the use of histological staining and larger sample numbers *in vivo*.

6.2 Introduction

General wound healing occurs in what can be described as three consecutive, overlapping phases: inflammation, proliferation, and remodeling. During inflammation, inflammatory cells (such as neutrophils, macrophages) are recruited to the wound site [139]. In the proliferation

[††] This chapter has been adapted from the following publication: Rebecca A. Hortensius, Amber Boyce, Matthew Wheeler, and Brendan A.C. Harley, "Macrophage response in vitro and in vivo to amnion-containing collagen-based scaffolds." *In preparation.*

phase, fibroblasts express genes associated with matrix proteins (collagen, proteoglycans, fibronectin) and begin to lay down new matrix [139]. This transition from the inflammatory to the proliferative phase of healing is critical [323]. Extended inflammation hinders injury resolution and has been associated with scar formation [189]. For weeks and months following new matrix deposition, remodeling and reorganization of the matrix occurs as part of the final phase of the healing cascade.

While the interactions between the extensive population of cells (local and immune) and signaling molecules in the wound healing cascade is complex, macrophages have been identified not only as the initial immune cells at a site of injury but key for ultimate tissue regeneration [324, 325]. Macrophages are classically known for their roles in endocytotic removal of cellular and matrix debris following injury. However, macrophages have a larger influence on the entire time course of the wound healing cascade through their plasticity and ability to display a spectrum of phenotypes [137]. Although macrophage phenotype exists on a continuum, literature has established a number of phenotypes based on the mode of macrophage activation and resultant factor secretion [137]. Macrophages can display a set of attributes that align them with a classically activated (M1) phenotype, wound healing (M2a) phenotype, and regulatory/anti-inflammatory (M2c) phenotype. Recent work by Spiller et al has started to examine how the balance of these macrophages can influence healing in vivo, finding that in patients with diabetic foot ulcers, the phenotypic shift of the macrophage population from M1 to M2 is indicative of better healing outcomes [138].

In the field of tissue regeneration, where implanted materials must both overcome the body's potential inflammatory response to the material as well as the inflammation associated with an established injury site, it would be advantageous to consider the stimulation of a M1-M2

phenotype shift in material design. Scaffolds of decellularized matrix have shown the inherent ability to promote an anti-inflammatory environment and a M1-M2 macrophage phenotype shift *in vitro* [149, 170, 171, 173, 175, 176, 178] and *in vivo* [149, 175, 176, 178, 180]. Additionally, by combining decellularized bone matrices with the sequential release of biomolecules that stimulate a M1 and then M2 macrophage phenotype, researchers have shown the ability to enhance bone healing and vascularization [149]. Further, studies have shown that macrophage behavior is different amongst commercially available dermal wound matrices (Integra, PriMatrix, AlloMend, Oasis) [326]. Together, this work shows that biomaterials that alter macrophage phenotype may be beneficial in stimulating tissue regeneration *in vivo*.

Extracellular matrix mimics, like the Integra Dermal Regeneration Template, composed of collagen and glycosaminoglycans (GAGs) have been studied for a range of tissue engineering applications such as skin, peripheral nerve, cartilage, and tendon regeneration [52, 55-62]. By altering the composition of these collagen-based scaffolds, their ability to sequester growth factors [59] and temper inflammatory effects in fibroblast populations has been enhanced [230]. The incorporation of the amniotic membrane matrix, an anti-inflammatory, anti-scarring allograft material used in two dimensional wound healing applications [215, 219, 222-227], has led to decreased expression of pro-inflammatory genes in scaffold-seeded tenocytes under inflammatory culture conditions *in vitro* [230]. However, the use of the amniotic membrane to alter macrophage phenotype in collagen scaffolds for tissue regeneration has not been previously studied. Here, we study the effects of collagen scaffolds with and without the incorporation of the amniotic membrane on macrophages *in vitro*. Additionally, due to the clinical importance of translating lab-tested materials to animal models, we also implanted these same scaffold variants in a porcine model to study the early inflammatory response *in vivo*.

6.3 Materials and methods

6.3.1 Amnion membrane isolation

Human placentas from uncomplicated vaginal births were collected as medical waste by Carle Foundation Hospital (Urbana, IL). The amniotic membrane (AM) was isolated as previously described [230, 294]. With forceps, the AM was separated from the placenta, washed, and decellularized via incubation in thermolysin (125 μg/mL) [295]. Then the AM was rinsed by shaking in phosphate buffered saline (PBS) to remove cellular debris and stored in PBS at 4°C. Following 24-48 hours in storage, the spongy layer of the AM was removed and discarded. The matrix was lyophilized as a sheet and stored in a dessicator until further use.

6.3.2 Preparation of collagen suspension

A suspension of microfibrillar collagen (C) type I (Collagen Matrix, Oakland, NJ) in 0.5 M acetic acid was homogenized with either chondroitin sulfate (CS) from shark cartilage (Sigma Aldrich, St Louis, MO) or dry, ground amniotic membrane (AM) as collected above [56]. Scaffolds containing CS were made with a 11:1 C:CS ratio and the C:AM suspension was made at a 5:1 w:w ratio due to the high collagen content of AM. All scaffolds were made with a total density of 0.5% w/v [251]. The suspensions were degassed prior to use and stored at 4°C [251].

6.3.3 Fabrication of collagen-based scaffolds via freeze drying

Isotropic CG scaffolds were fabricated as previously described [61, 69]. For *in vitro* culture, scaffold sheets were made by transferring each collagen suspension to a separate aluminum, rectangular tray mold. A Genesis freeze-dryer (VisTis, Gardener, NY) was used to freeze the suspension to a final freezing temperature of -40°C. Scaffolds for *in vivo* culture were made in 6 well (10 mm diameter, 10 mm height) custom polysulfone array molds. Here, suspensions were

frozen to a final freezing temperature of -10°C. In each condition, ice crystals were sublimated under vacuum (200 mTorr) at 0°C.

6.3.4 Preparation of CG scaffolds for use

In order to sterilize and dehydrothermally (DHT) crosslink the scaffolds, the lyophilized sheets for *in vitro* culture and the cylindrical scaffolds for in vivo used were placed in a vacuum oven (Welch, Niles, IL) at 105˚C under vacuum for 24 hours [56]. Following DHT treatment, a biopsy punch was used to cut 6mm diameter cylinders from the 4mm thick scaffold sheet for use in all *in vitro* experiments. All scaffolds were hydrated by soaking in 100% ethanol overnight and washing in sterile PBS for 24 hours. To increase mechanics, all scaffolds were crosslinked via carbodiimide chemistry by immersing in 1-ethyl-3-[3-dimethylaminopropyl] carbodiimide hydrochloride (EDC) and *N*-hydroxysulfosuccinimide (NHS) at a molar ratio of 5:2:1 EDC:NHS:COOH (relative to moles of carboxylic acid (COOH) groups present in collagen) for 1.5 hours under shaking at room temperature [248, 298]. Prior to use, scaffolds were washed with and stored at 4˚C in sterile PBS.

6.3.5 Monocyte culture and differentiation

A human monocytic cell line (THP1 cells; ATCC, Manassas, VA), derived from an infant with leukemia, was cultured per the supplier's instructions. Briefly, THP1s were cultured in suspension in standard tissue culture flasks in RPMI-1640 media, 10% heat-inactivated fetal bovine serum (FBS), and 1% penicillin–streptomycin (P/S). Cultures were started at a concentration of approximately $3x10^5$ cells and subcultured when the concentration reached approximately $8x10^5$ cells. THP1 cells were differentiated into M0 macrophages in ultra-low attachment flasks by exposure to media supplemented with 320 nM phorbol 12-myristate-13-

acetate (PMA) for 3 days. Following washes with fresh media and lifting via cell scraping, these cells could then be used for scaffold seeding or polarization in 2D, as described below.

6.3.6 Macrophage seeding and culture conditions

Hydrated, crosslinked CG scaffolds were soaked in culture media overnight at 37°C before being tapped dry on a Kimwipe and placed in ultra-low attachment 24-well plates (Fisher, Waltham, MA). M0 macrophages were suspended in culture media at a concentration of approximately $5.5x10^5$ cells per 20 µL in preparation for static seeding [61]. Ten microliters of the cell suspension were added to one side of the scaffolds. Then the scaffolds were incubated for 15 minutes at 37˚C, flipped over and another 10 µL of cell suspension was added. To allow for initial cell attachment, scaffolds were placed in the incubator for 2 hours before additional growth media was added. Scaffolds were incubated at 37˚C and 5% CO_2. Scaffolds from each composition (n=6) and M0 in 2D culture (n=3) were collected at days 1, 4, 7 for RNA isolation. Media was changed on days 3 and 6.

6.3.7 Macrophage polarization in two dimensions

Two dimensional controls of polarized macrophages were implemented as follows. Equal to the number of cells seeded per scaffold, $5.5x10^5$ cells were plated in each well of an ultra-low attachment 6 well plate. Polarization to a M1 phenotype (n=3) was completed using 100 ng/mL interferon-gamma (IFN-γ, ProSpec) and 100 ng/mL LPS (Sigma-Aldrich). For a M2a phenotype (n=3), 40 ng/mL of interleukin 4 (IL-4, ProSpec) and 20 ng/mL interleukin 13 (IL-13) were added to each well. Interleukin 10 (IL-10, ProSpec) was added at 40 ng/mL to induce a M2c phenotype (n=3). A M0 control was used as well (n=3). Each group was allowed to polarize for 2 days before the cells were collected for RNA isolation.

6.3.8 Surgical implantation in porcine mandibular defect

C:CS and C:AM scaffolds were implanted in male Yorkshire pigs (n=6) approximately 6 months of age and weighing between 197 and 247 lbs. Each animal was subjected to three 8mm diameter bilateral surgical ramus defects on each side of the mandible (Fig. 6.1). The treatment group was randomized for each pig but, cautious of global effects on the inflammatory response, each pig only received one type of scaffold for all six of its mandibular defects.

The described surgical procedures and associated protocols and facilities were approved by the University of Illinois at Urbana-Champaign Institutional Animal Care and Use committee. All pigs received a sedative cocktail (TARK) consisting of Telazol (tiletamine and zolazepam; Pfizer, New York, NY), Atropine (Neogen Corporation, Lexington, KY), Rompun (xylaazine; Lloyd Laboratories, Shenandoah, IA) and Ketamine (Ketaset®, Fort Dodge Animal Health, Fort Dodge, IA) intramuscularly prior to surgery and intravenously via the ear vein canula, as necessary. During surgery, an endotracheal administration of 3-5% isoflurane was administered in oxygen as anesthesia.

Surgery proceeded using a previously described protocol [327], Briefly, a single submandibular and retromandibular incision tracing the exterior contour of the mandible was made. The underlying fat and muscle were incised and elevated. The periosteum was incised and prised to expose the posterior region of the underlying hemimandible. A right-angle surgical drill with an 8 mm (outer diameter) trephine (Stryker, Portage, MI) was used to create three bicortical (full thickness), 8 mm diameter cylindrical defects on the exposed region of the hemimandible (ramus) (Fig. 6.2 A, B). The excised bone was cut into three pieces and immersed in RNA*later* solution for future RNA isolation. Irrigation with 0.9% physiological saline was used during

drilling to prevent heat damage to the surrounding tissue. Each scaffold was fit into the 8 mm defect, rehydrated using 0.9% physiological saline, and anchored at one point to the surrounding mandible using Vetbond (3-M, Minneapolis, MN) (Fig. 6.2 C, D).

The wound site was closed by suturing, with 3-0 Vicryl (Ethicon, Inc, San Angelo, TX), the previously described incisions in the periosteum, masseter muscle, superficial fat, and skin. A three layer continuous stitch was used; Vetbond was applied to the skin layer incision. Both during and after surgery, vital signs were taken every 15 min until the pig became sternally recumbent. Physical and social behavior was evaluated twice daily for up to 2 weeks post-surgery.

6.3.9 Explant collection and processing

One pig from each treatment group was sedated and euthanized at days 3, 7 and 14 post-surgery. The mandible was explanted and, from each pig, three random samples were taken for RNA isolation and the three remaining samples were collected for histological analysis. For RNA isolation, scaffolds were isolated from the bone and stored in RNA*later* solution at 4°C until RNA isolation and PCR could be performed. For histological analysis, scaffolds and the surrounding bone were isolated using a bone saw. The samples were immediately fixed in formalin overnight, washed with PBS, decalcified using Calci-clear Rapid (National Diagnostics) overnight, embedded in OCT, and stored at -80°C until use.

6.3.10 Analysis of gene expression profiles for scaffolds cultured in vitro

RNA from cells in polarized 2D culture conditions was isolated at day 2 while scaffolds from each composition (n=6) were collected at days 1, 4, 7 (Fig. 6.3). The plates/scaffolds were rinsed in PBS and then scaffolds were cut in half with a razor blade while cells were scraped off the

plates. The resultant scaffolds/cells were immersed in the lysis buffer of the RNeasy Plant Mini kit (Qiagen, Valencia, CA) for 5 minutes on ice [87]. Following the kit's instructions, RNA was isolated and total RNA was quantified using a NanoDrop Lite. RNA reverse transcription was carried out using the QuantiTect Reverse Transcription kit (Qiagen, Valencia, CA) in a Bio-Rad S1000 thermal cycler. Real-time PCR reactions were performed in an Applied Biosystems 7900HT Fast Real-Time PCR System (Carlsbad, CA). Glyceraldehyde 3-phosphate dehydrogenase (*GAPDH*) was used as a housekeeping gene for the genes listed in Table 6.1. Sequence Detection Systems software v2.4 (Applied Biosystems, Carlsbad, CA) was used to complete analysis. The expression levels from the 2D polarization experiment (normalized to M0 cells at day 0) were used to show the strength of each phenotypic marker (Fig. 6.4).

6.3.11 Analysis of gene expression profiles for scaffolds implanted in vivo

RNA was isolated from scaffold explants by first removing the RNA*later* solution following centrifugation and then proceeding in the same manner described above. RNA was isolated from day 0 bone explants using a bead beater (Mini-BeadBeater-16, BioSpec Products) during the lysis step prior to continuing with the RNeasy Plant Mini kit's instructions. Reverse transcription and PCR analysis was carried out as described above. Results are presented as fold change relative to expression in all bone explants isolated on the day of surgery. The genes analyzed are listed in Table 6.2.

6.3.12 Clustering analysis in R

R software was used to conduct further analysis on the *in vitro* macrophage gene expression. Principle component analysis was completed in addition to heat map generation, which displays

the expression of genes across all samples as a gradient based on the standard deviation from the mean expression across all samples.

6.3.13 Statistical analysis

Two-way analysis of variance (ANOVA) followed by Tukey-HSD post-hoc test was performed on all data sets. A p-value < 0.05 was used for significance. All analyses were based on a minimum of n=3 scaffolds, higher n values were used as noted. In the figures, error is reported as the standard error of the mean.

6.4 Results

6.4.1 Expression of pro-inflammatory genes in macrophage in vitro culture

Following 1, 4, and 7 days of culture, the expression of pro-inflammatory genes: interleukin 1 beta (IL-1β), tumor necrosis factor alpha (TNFα), and vascular endothelial growth factor (VEGF) was evaluated via PCR from macrophages (initially seeded as M0 phenotype) cultured in C:CS and C:AM scaffolds and 2D M0 controls (Fig. 6.5). Expression was normalized to gene levels of 2D M0 macrophages at day 0. All three genes showed expression levels less than one (1), indicating low expression of pro-inflammatory genes as compared to this day 0 control. Expression of genes encoding for the pro-inflammatory cytokine IL-1β (Fig. 6.5A) were highest at day 1 in all groups ($p < 0.05$) and, at the day 1 time point, all groups were statistically different from each other with AM scaffolds having the highest IL-1β expression. Expression of TNFα was also higher at day 1 in all groups over the timepoints at days 4, 7 ($p < 0.05$) (Fig. 6.5B). Both scaffold groups showed higher expression of VEGF compared to the 2D control at day 1 while expression only in AM was higher at day 4, CS at day 7 ($p < 0.05$) (Fig. 6.5C).

6.4.2 Expression of M2a and M2c macrophage markers in 3D in vitro culture

Expression of genes associated with wound-healing (M2a; Fig. 6.6) and regulatory (M2c; Fig. 6.7) macrophages were evaluated over the 7 day experiment in M0-seeded 2D and 3D culture. Of particular interest are the statistically significant ($p < 0.05$) increases in expression level of CCL22 and PDGF in the macrophage-seeded scaffold groups overtime (Fig. 6.6A, D). By day 7, CS scaffolds are supporting higher CCL22 expression compared to all groups at day 7 and to the CS groups at days 1 and 4. The AM group is showing significantly higher CCL22 expression at day 7 compared to day 1 (Fig. 6.6A). Additionally, the PDGF data (Fig. 6.6D) show significant increases in gene expression in cells in AM scaffolds at day 7 compared to all other time points as well as in CS scaffolds between day 1 and 7. This scaffold data is, surprisingly, significantly lower than the PDGF expression in the 2D control at day 7 (Fig. 6.6D). When considering expression of genes associated with the macrophage M2c phenotype (Fig. 6.7), the scaffolds support the expression of MMP-7 in AM (day 1, 4) and CS (day 4) scaffolds as compared to the M0 control ($p < 0.05$) (Fig. 6.7B). These trends dissipate by day 7. MMP-8 expression is also significantly increased in both scaffolds groups at day 1 but not so at the later time points (Fig. 6.7C).

6.4.3 Results of gene clustering analysis

The M1/M2 macrophage ratio for each scaffold group was calculated but summing the GAPDH normalized genes associated with M1 phenotypes and dividing by the sum of the same values for M2 associated genes. There was no statistically significant difference between the macrophage ratio in CS vs AM scaffolds. However, both groups supported a M2 phenotype with all ratios being below one (1) (Fig. 6.8A). Principle components analysis (PCA) (Fig. 6.8B) shows that the scaffold groups cluster together at days 1 and 4 but do not strongly associate with the 2D polarized controls (M1, M2a, M2c). By day 7, the clusters for CS and AM scaffolds are further

apart. Observations from the heat map generated (Fig. 6.8C) include the clustering of M1 macrophage-associated genes (IL-1β, TNFα, VEGF) towards the top of the map, where higher expression is seen in the scaffolds at the earlier time points, and clustering of M2-associated genes (MRC1, CD163, PDGF, CCL22) at the bottom of the map, where higher expression is dominated by the later time points.

6.4.4 Gene expression of pro- and anti-inflammatory genes following implantation in vivo

Scaffolds implanted into a porcine mandibular defect were removed 3, 7, or 14 days following surgery and PCR was used to characterize gene expression levels relative to the expression in the bone explanted to create the wound at day 0 (Fig. 6.9). The expression of the gene for IL-1β (pro-inflammatory cytokine) was significantly ($p < 0.05$) increased in AM scaffolds at day 3, compared to the CS scaffolds and control (Fig. 6.9A). IL-1β expression in AM scaffolds significantly drops over time ($p < 0.05$). Conversely, the expression of pro-inflammatory TNFα is increased in CS scaffolds at day 3, although this trend is not significant (Fig. 6.9B) and the expression level is well below 1 (bone control at day 0). When considering the expression of M2 markers, the expression of arginase-1 (Arg-1) is significantly higher ($p < 0.05$) in bone scaffold groups at day 3, compared to the bone control (Fig. 6.9C). In the AM scaffolds, this expression significantly drops overtime. While the expression of IL-10 is higher in AM scaffolds compared to CS scaffolds at day 3 (Fig. 6.9D), this observation is not significant and there are no statistically significant differences in this gene's expression across groups or time. Finally, when considering the M1/M2 ratio (Fig. 6.10A) of all genes analyzed (Table 6.2), all the ratios are under one (indicating a dominant M2 phenotype) but there is no significant difference between the scaffold groups.

6.5 Discussion

In the study of biomaterials for tissue regeneration, it is important to consider the role the implanted material will play as part of native wound healing. Will it withstand the cascade of cellular activity? Will it contribute to the already present inflammatory response? Will it assist in the transition from inflammation to proliferation? It is in this last question that the role of macrophages, myeloid derivatives that span a spectrum of phenotypes, becomes increasingly important. While inflammation is essential for cellular recruitment, defense against pathogens, and removal of debris, prolonged inflammation is detrimental to long term healing outcomes [323]. Macrophages are a key player in the transition across each phase of wound healing through population shifts from classically activated (M1, pro-inflammatory) to wound-healing (M2a) to regulatory (M2c, anti-inflammatory) phenotypes.

Macrophages exist locally in tissues and have the ability to self-maintain throughout adulthood. However, during inflammation, macrophages are derived and replenished from blood circulating monocytes [328]. In vitro this differentiation can be stimulated by 12-myristate-13-acetate (PMA) which results in inactive macrophages (M0). From this inactive state, macrophages can take on the three phenotypes outlined above. M1 macrophages are activated by IFNγ and TNFα (produced in the body by natural killer cells and T helper 1 cells), act in defense of intracellular pathogens, and produce pro-inflammatory cytokines such as IL-1, IL-6, and IL-23 [137]. The secretion of IL-4 by basophils and mast cells is responsible for the macrophage polarization into a wound healing phenotype (M2a) and this phenotype is maintained by the secretion of IL-4 and IL-13 by T helper 2 cells [137]. M2a macrophages secrete components of the extracellular matrix [329] and are less efficient in presenting antigens to T cells, producing pro-inflammatory cytokines, and destroying intracellular pathogens [330]. Regulatory (M2c) macrophages usually

arise during the later stages of wound healing where their anti-inflammatory role is largely based on their secretion of IL-10, a cytokine that can inhibit the production and activity of pro-inflammatory cytokines [331].

In the studies described here, we explore how biomaterial composition can alter macrophage response *in vitro* and *in vivo*. By using collagen-based scaffolds already studied for tissue regeneration applications, we explored the incorporation of the anti-inflammatory matrix of the amniotic membrane (AM) and its effects on macrophage phenotype. We hypothesized that the use of the AM would result in a diminished M1 (pro-inflammatory) macrophage population and an enhanced M2a/M2c population both *in vitro* and *in vivo*.

M0 macrophages were cultured in 3D collagen:chondroitin sulfate (CS) and collagen:amniotic membrane (AM) scaffolds as well as in 2D, as a control. All genes were normalized to expression in the 2D M0 control at day 0 of the experiment. In the genes associated with a M1 macrophage phenotype (IL-1β, TNFα, VEGF), expression was lower than the day 0 control (< 1) (Fig. 6.5). Expression in all groups was at its highest at day 1 and was significantly lower at days 4 and 7 in IL-1β and TNFα (Fig. 6.5A, B). The overall gene expression is low and the scaffolds are tracking with the M0 control over time; through this, the scaffolds show no support for the pro-inflammatory M1 phenotype. When considering the genes associated with the wound healing, M2a macrophages (Fig. 6.6), an increase in expression of CCL22 (Fig. 6.6A) and PDGF (Fig. 6.6D) in CS and AM scaffolds occurs overtime (by day 7) although this trend is not supported in other M2a genes (MRC1 and TIMP3). Finally, higher CD163 expression (M2c macrophage marker) is seen in AM scaffolds by day 7 and while both CS and AM scaffolds support MMP-7 and MMP-8 expression at earlier time points, this trend is diminished by day 7 (Fig. 6.7). Higher level analysis confirms these findings (Fig. 6.8). Low M1/M2 ratios (Fig.

6.8A) show a predominant M2 macrophage phenotype over time and heat map visualization (Fig. 6.8C) appears to show a switch from high expression of M1 genes at early time points to higher expression of M2 associated genes at day 7. Together these data suggest that both CS and AM scaffolds do more to support an M2a/M2c phenotype than an M1 phenotype. However, more work is needed to determine how and whether there are benefits to including AM in tissue regeneration scaffolds.

There are several options to expand this work *in vitro*. While the amniotic membrane has been well characterized by others [219], it would be interesting to evaluate the growth factor and cytokine release from the matrix post-processing and following incorporation into the CG scaffold. It is likely that the biomolecules in the material are responsible for the effects we have seen in Chapters 4 and 5 of this thesis. If the cytokines necessary for macrophage polarization (IFNγ, TNFα, IL-4, IL-13, and IL-10) are present in the amnion at high levels, future experiments should be run in serum free media to try to elucidate this effect. Further, this *in vitro* study was completed by seeding M0 (inactive) macrophages into each scaffold variant. It would be interesting to stimulate an M1 phenotype prior to scaffold seeding or culture cell-seeded scaffolds in a pro-inflammatory environment and then monitor the kinetics of macrophage phenotype.

The results of the *in vivo* subcritical porcine mandibular model remain inconclusive. AM scaffolds show early upregulation of both M1 and M2 markers in some cases (IL-1β and Arg-1, respectively) (Fig. 6.9A, C) but no or little change in similar markers over all time points (TNFα, IL-10) (Fig. 6.7B, D). Preliminary H&E staining shows the scaffold integrates into the defect at the day 7 time point (Fig. 6.10B); ongoing work is evaluating, histologically, the presence of M1 and M2 macrophage populations over time. In vivo experiments should be repeated with a higher

sample number to increase the probability of finding significant differences between groups. Additionally, optimizing the procedure for collecting RNA from the bone explants will improve the RNA normalization procedure. If RNA could be isolated from each sample, the scaffold explants could be matched to their corresponding bone core for analysis instead of being normalized to an average expression across all animals (eliminating any baseline differences between pigs).

6.6 Conclusions

The amniotic membrane has been used as an anti-inflammatory matrix in 2D and shown, in 3D collagen-based scaffolds, to have inflammation-tempering effects on fibroblast (Chapter 4) and mesenchymal cell populations (Chapter 5). Due to the importance of the macrophage in the wound healing cascade, this work sought to evaluate macrophage response to these 3D materials for tissue regeneration. Both scaffolds (with and without amniotic membrane) promoted an M2 (pro-healing, anti-inflammatory) macrophage phenotype *in vitro*. In order to fully realize the potential of three dimensional materials that incorporate an anti-inflammatory allograft (like the amniotic membrane) in the field of tissue regeneration, more work needs to be done to study this effect *in vitro* and *in vivo*.

6.7 Tables

Table 6.1. Gene primers used for *in vitro* human macrophage experiments.

Description	Gene	Forward Sequence Reverse Sequence	Citation
M1 Markers	TNFα	CCTCTCTCTAATCAGCCCTCTG GAGGACCTGGGAGTAGATGAG	[322]
	IL-1β	ATGATGGCTTATTACAGTGGCAA GTCGGAGATTCGTAGCTGGA	[138]
	VEGF	AGGGCAGAATCATCACGAAGT AGGGTCTCGATTGGATGGCA	[138]
M2a Markers	CCL22	GCGTGGTGTTGCTAACCTTCA AAGGCCACGGTCATCAGAGT	[326]
	MRC1	AAGGCGGTGACCTCACAAG AAAGTCCAATTCCTCGATGGTG	[138]
	TIMP3	ACCGAGGCTTCACCAAGATG CATCATAGACGCGACCTGTCA	[138]
	PDGF	CTCGATCCGCTCCTTTGATGA CGTTGGTGCGGTCTATGAG	[138]
M2c Markers	CD163	TTTGTCAACTTGAGTCCCTTCAC TCCCGCTACACTTGTTTTCAC	[326]
	MMP7	CCCCCTGCATTTCAGGAA TCCTGGCCCATCAAATGG	[332]
	MMP8	CCAAGTGGGAACGCACTAACTTGA TGGAGAATTGTCACCGTGATCTCTT	[333]
Reference	GAPDH	AAGGTGAAGGTCGGAGTCAAC GGGGTCATTGATGGCAACAATA	[138]

Table 6.2. Gene primers used for *in vivo* porcine mandibular defect RT-PCR.

Description	Gene	Forward Sequence Reverse Sequence	Citation
Pro-inflammatory	IL-1β	CCAATTCAGGGACCCTACC CATGGCTGCTTCAGAAACCT	[334]
	IL-8	TTCTTCTTTATCCCCAAACTGG CCACATGTCCTCAAGGTAGGA	[334]
	TNFα	TTGTCGCTACATCGCTGAAC CCAGTAGGGCGGTTACAGAC	[334]
	TGF-β1	CGGCCCTTCCTGCTCCTCAT TTCCAGCCCAGGTCCTTCC	[335]
Macrophage marker	CD163	CTTGGGGCAGCGTTGGCAGGAATAG ATGCAGGGCTGATGTCCCCTCTGTC	[336]
	Arg-1	CCAGTCCATGGAGGTCTGTCTTAT TGCTACTGCCGTGTTCACCG	[335]
	CCR-2	GCGGGGTCACCTGGGTGGTA AGTGGCAGGACCAGCCCCAA	[335]
Anti-inflammatory	IL-10	TGAAGAGTGCCTTTAGCAAGCTC CTCATCTTCATCGTCATGTAGGC	[336]
Reference	GAPDH	CGTCCCTGAGACACGATGGT CCCGATGCGGCCAAAT	[337]

6.8 Figures

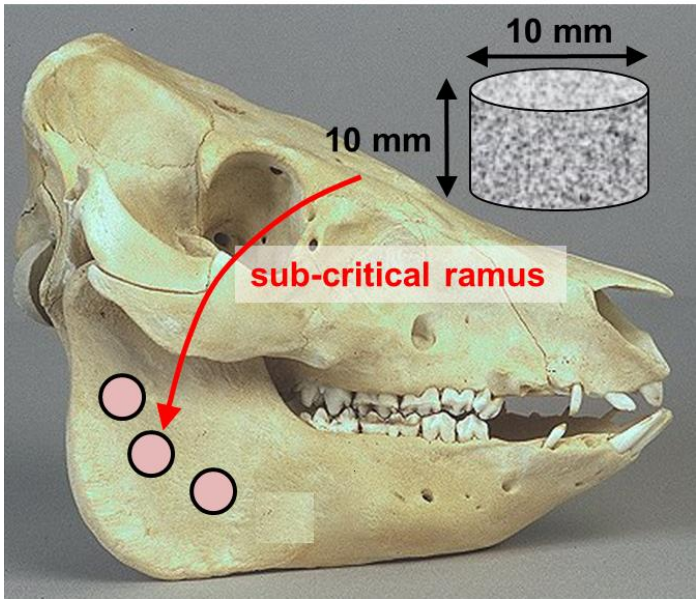

Figure 6.1. Schematic of subcritical porcine mandibular ramus defect. Three 8 mm holes were drilled in each side of the pig jaw.

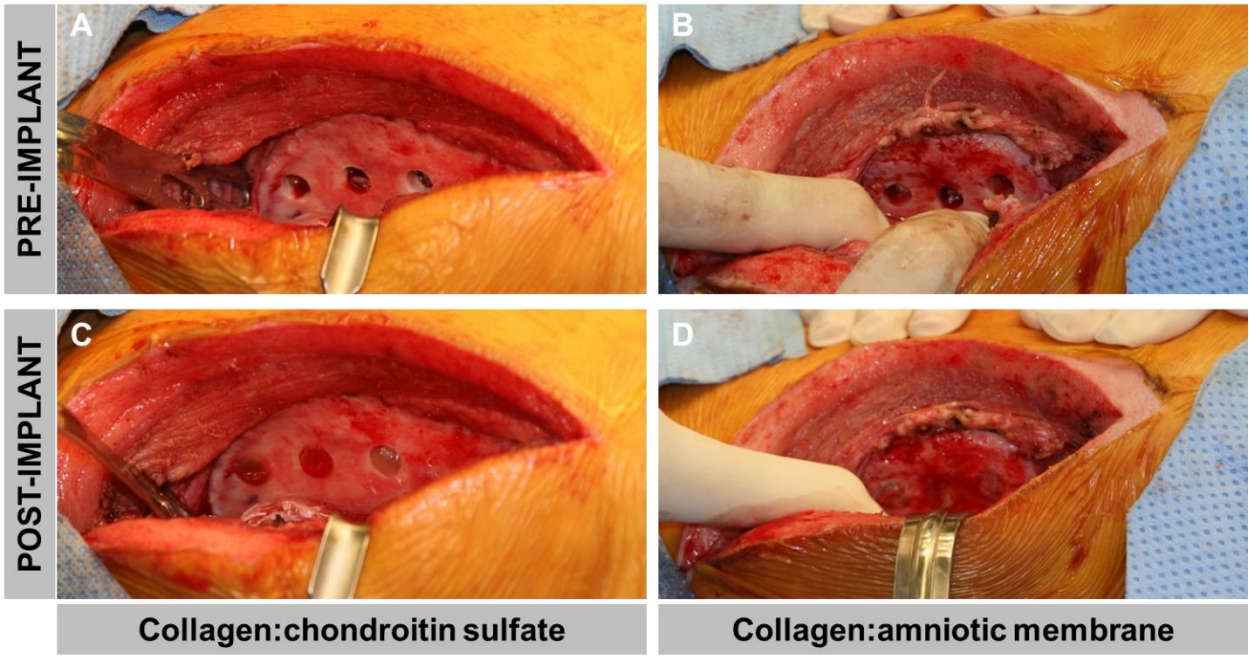

Figure 6.2. Photographs from pig surgeries showing holes pre-implant (**A, B**) and post-implant with collagen:chondroitin sulfate (**C**) and collagen:amniotic membrane (**D**) scaffolds.

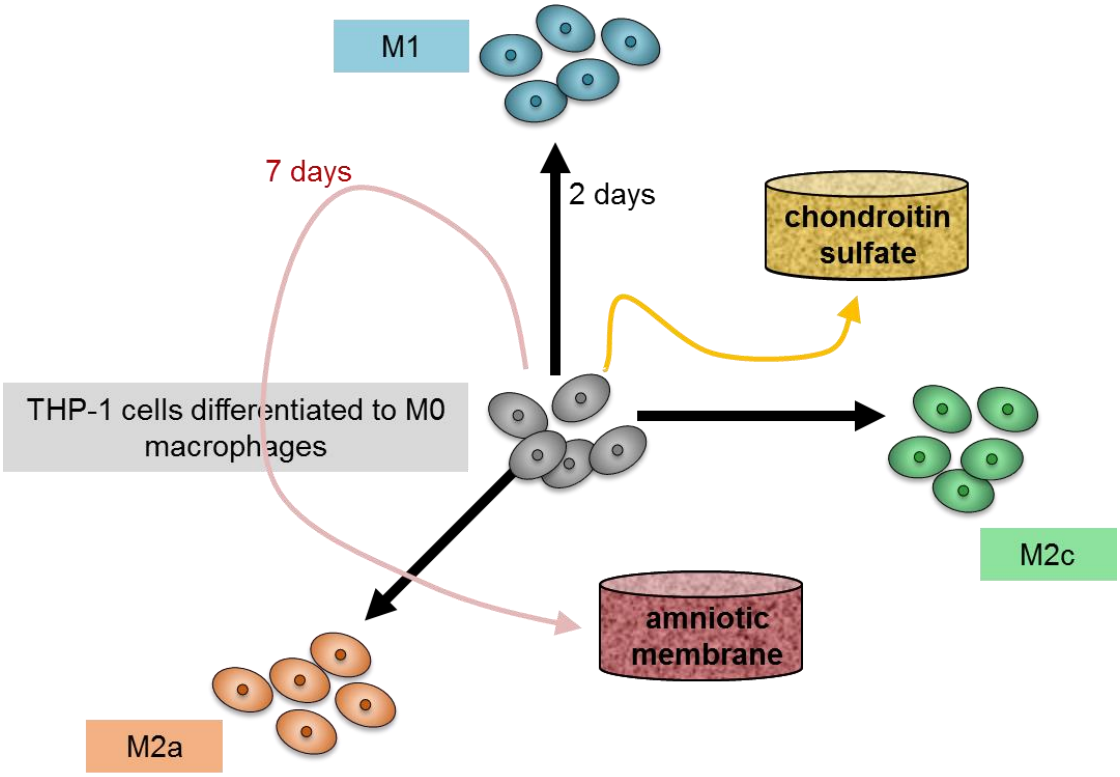

Figure 6.3. Schematic of *in vitro* macrophage experiment.

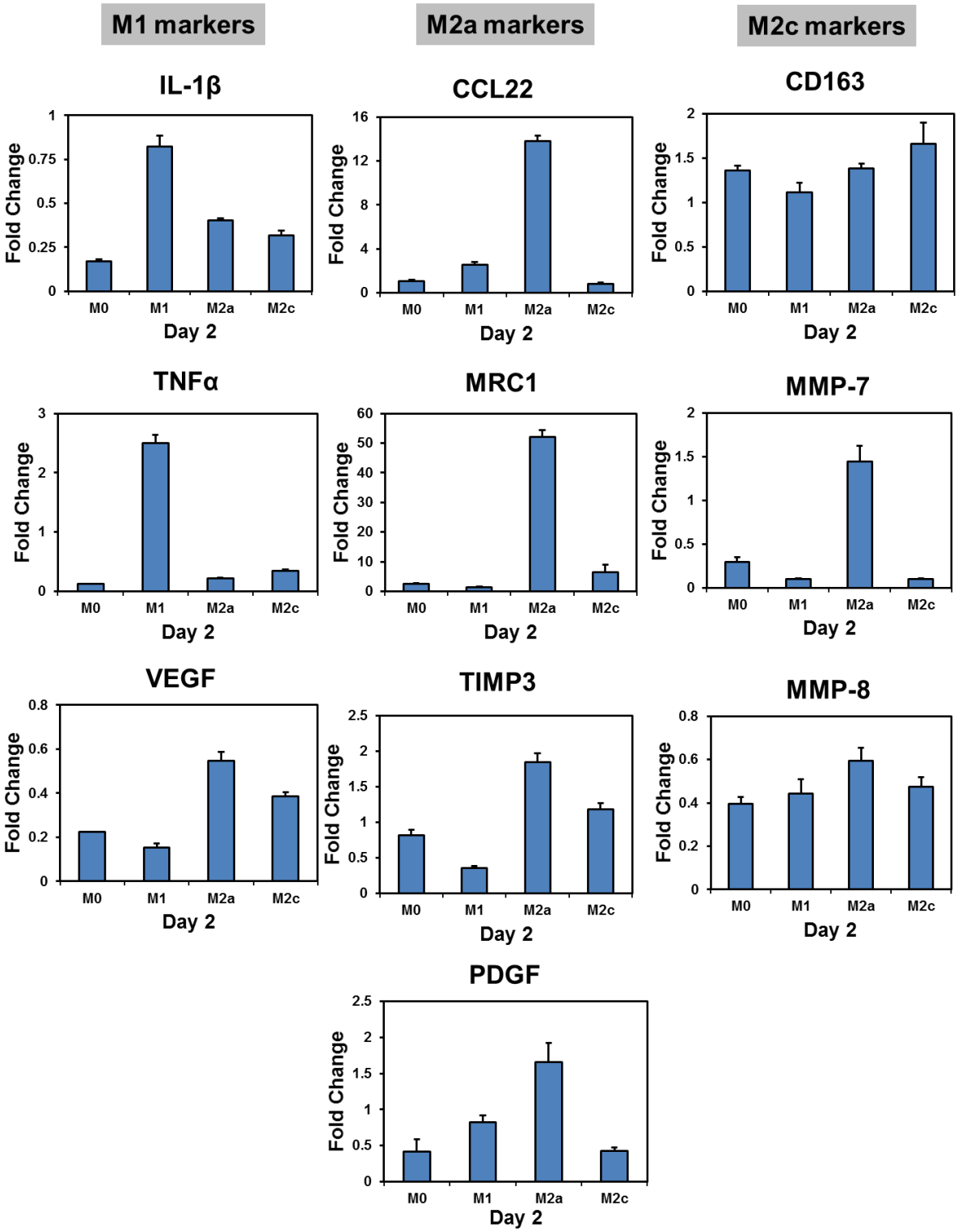

Figure 6.4. Results of 2D macrophage polarization experiments.

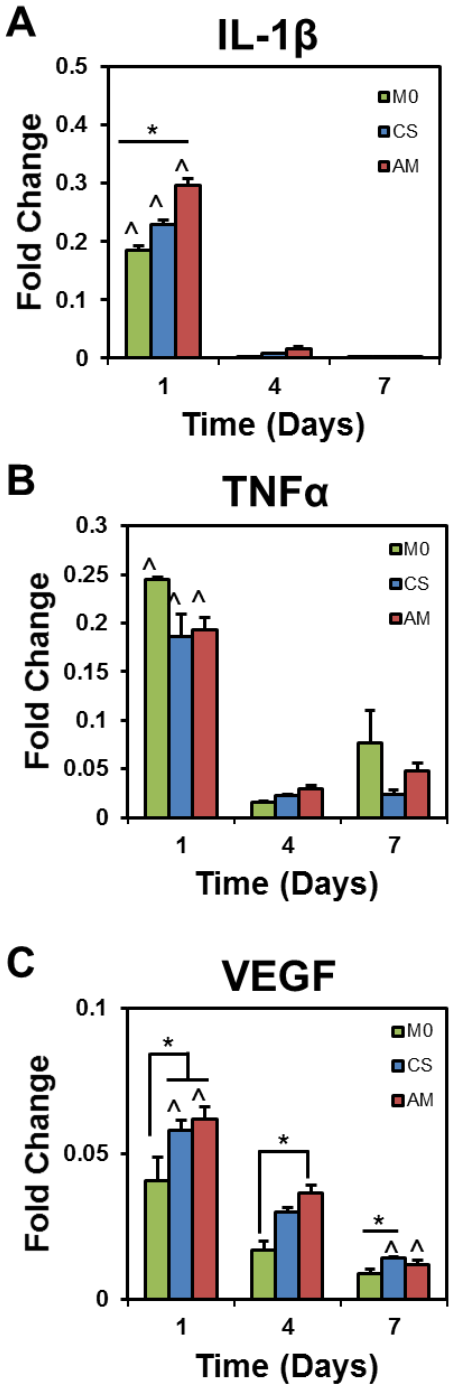

Figure 6.5. Expression of pro-inflammatory, M1-related genes in M0 macrophages seeded in collagen:chondroitin sulfate (CS) and collagen:amniotic membrane (AM) scaffolds and 2D controls (M0) over 7 days of culture. (**A**) interleukin 1 beta (IL-1β); (**B**) tumor necrosis factor alpha (TNFα); (**C**) vascular endothelial growth factor (VEGF). Expression is normalized to M0 macrophages from day 0 of the experiment. * significant difference between expression of groups indicated, ^ significant difference between group indicated and corresponding group at other time points ($p < 0.05$).

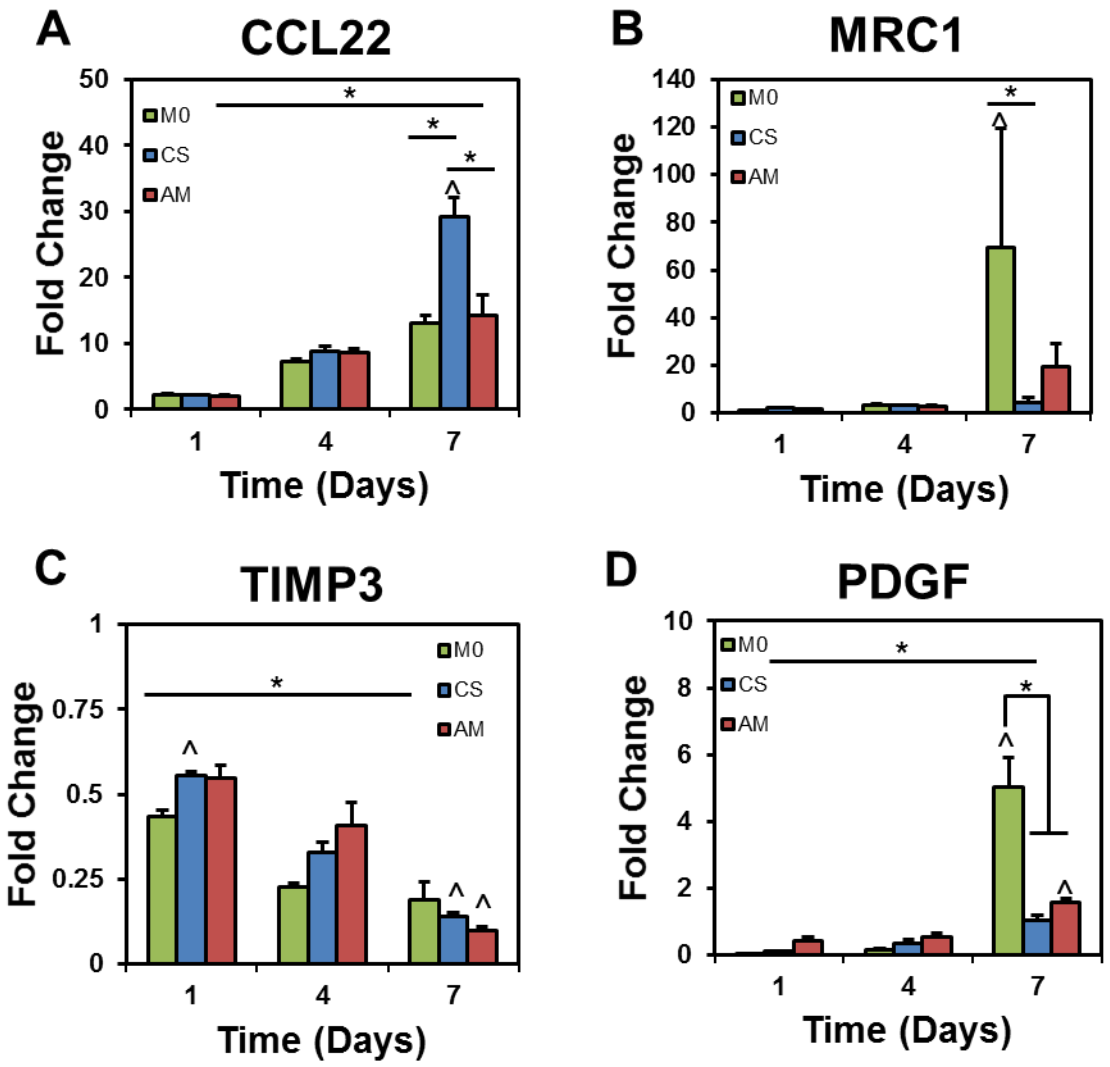

Figure 6.6. Expression of M2a macrophage markers: (**A**) C-C motif chemokine 22 (CCL22), (**B**) mannose receptor, C type 1 (MRC1), (**C**) tissue inhibitor of metalloproteinase 3 (TIMP3), (**D**) platelet-derived growth factor (PDGF) in M0 macrophages seeded in collagen:chondroitin sulfate (CS) and collagen:amniotic membrane (AM) scaffolds and 2D controls (M0) over 7 days of culture. Expression is normalized to M0 macrophages from day 0 of the experiment. * significant difference between expression of groups indicated, ^ significant difference between group indicated and corresponding group at other time points ($p < 0.05$).

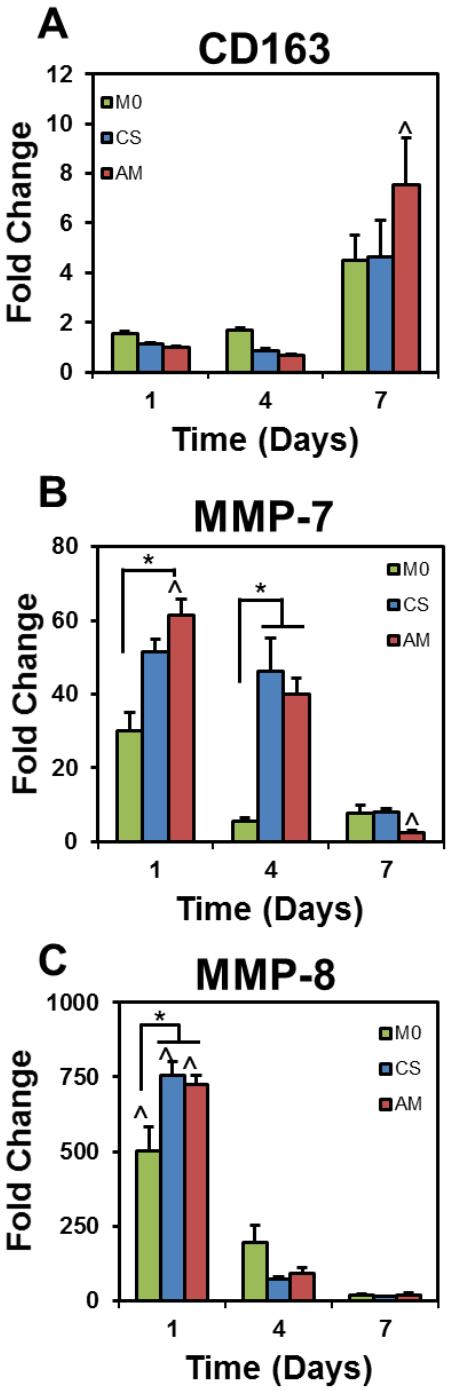

Figure 6.7. Genes associated with M2c macrophage phenotype were monitored for expression over 7 days of culture in 2D controls (M0) and in M0 macrophage-seeded scaffolds - collagen:chondroitin sulfate (CS) and collagen:amniotic membrane (AM). (**A**) Cluster of differentiation 163 (CD163), (**B**) Matrix metalloproteinase 7 (MMP-7), (**C**) Matrix metalloproteinase 8 (MMP-8). Expression is normalized to M0 macrophages from day 0 of the experiment. * significant difference between expression of groups indicated, ^ significant difference between group indicated and corresponding group at other time points ($p < 0.05$).

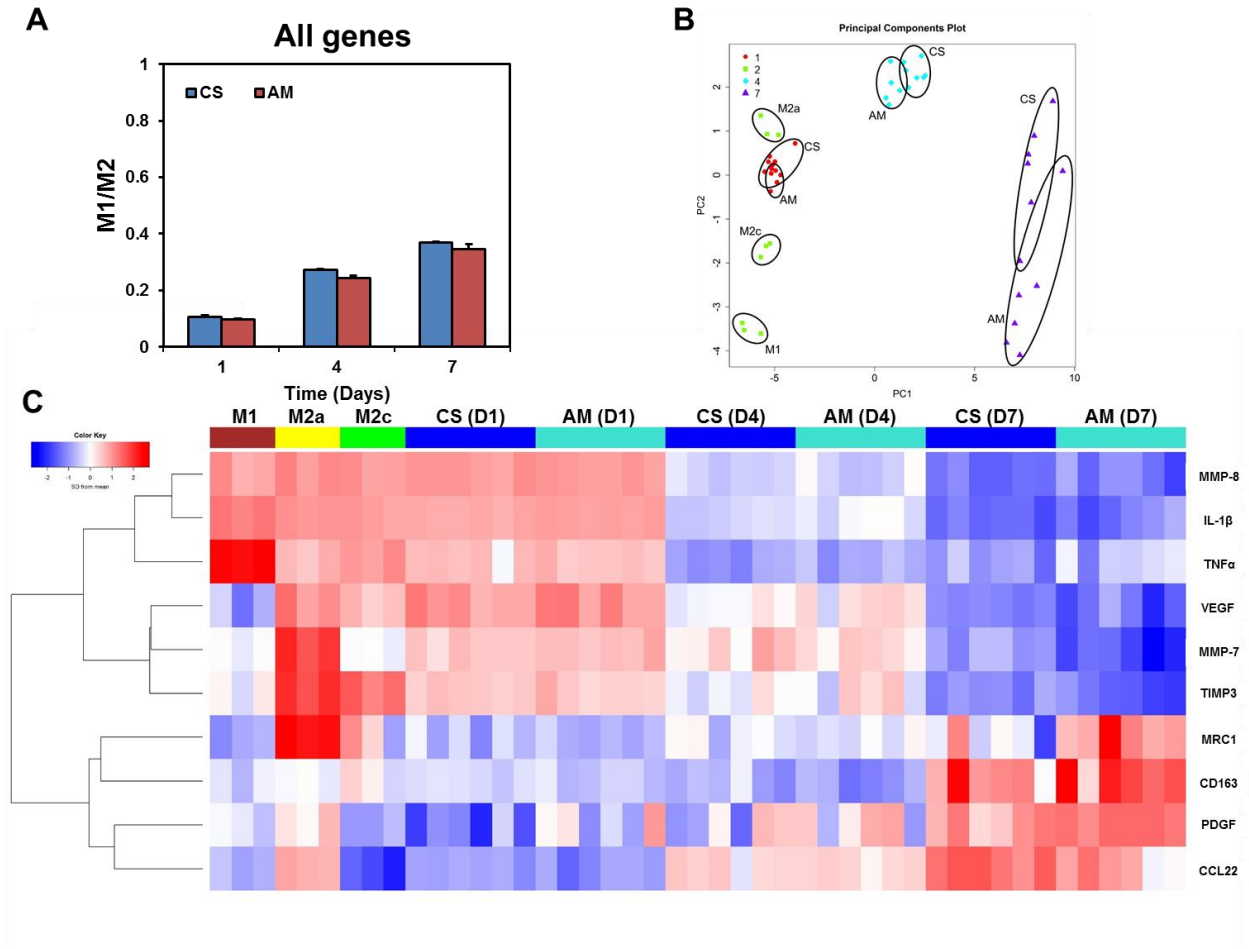

Figure 6.8. Alternative displays of macrophage gene expression data. (**A**) Collection of M1-M2 ratio across all genes probed in the macrophage seeded scaffolds (collagen:chondroitin sulfate (CS) and collagen:amniotic membrane (AM)). (**B**) Principle components plot of scaffolds overtime with the inclusion of macrophage polarization controls carried out in 2D (day 2). (**C**) Heat map displaying array of expression levels for each gene (rows) across macrophages polarized in 2D and each of the scaffold groups over time (columns).

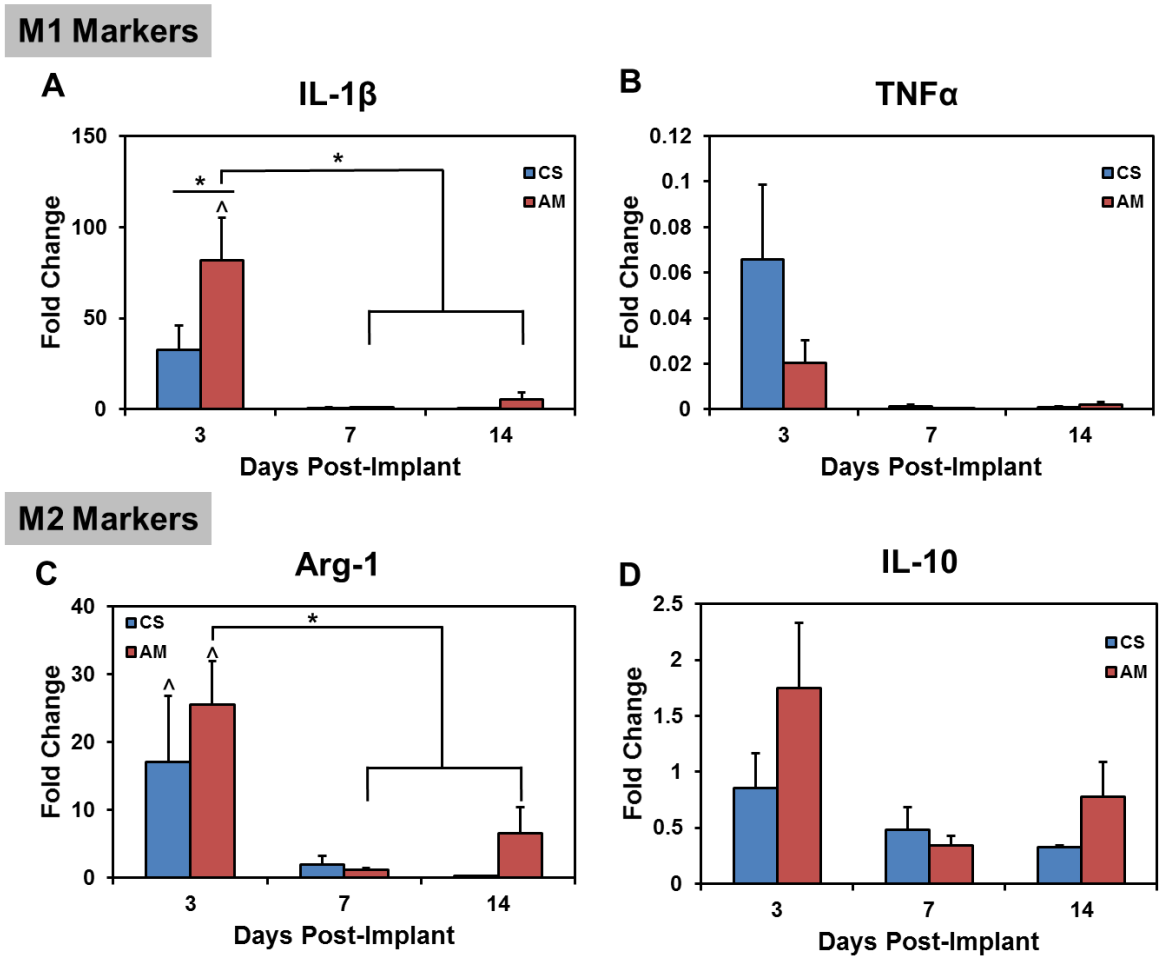

Figure 6.9. Expression of markers for M1 (**A, B**) and M2 (**C, D**) macrophages in scaffolds (collagen:chondroitin sulfate (CS) and collagen:amniotic membrane (AM)) implanted in subcritical porcine mandibular defects. Expression is normalized to levels from day 0 bone explants. * significant difference ($p < 0.05$) between expression of groups indicated. ^ significant difference between group indicated and bone control ($p < 0.05$).

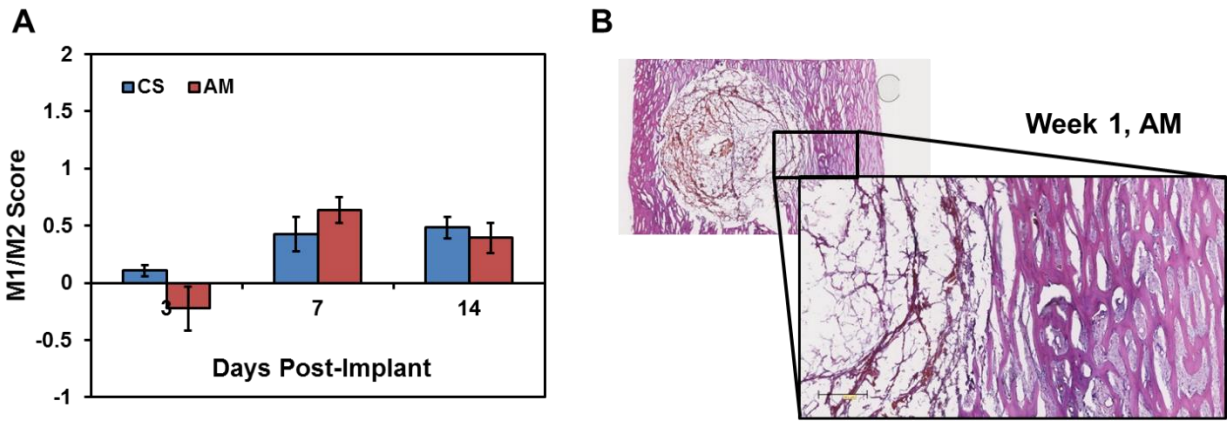

Figure 6.10. (**A**) M1/M2 macrophage healing score of all porcine genes analyzed. (**B**) Preliminary H&E staining of explant from AM experimental group, day 7 time point.

CHAPTER 7: SUMMARY AND FUTURE DIRECTIONS

7.1 Summary

Wound healing across many tissue types results in subpar outcomes and could benefit from material-based interventions devised to promote restoration of native tissue through the process of regeneration. Through this work, we have sought to develop strategies for altering the composition of collagen-based biomaterials in order to enhance their inherent tissue regeneration capacity. Mimicry of the extracellular matrix is a common strategy for biomaterials for tissue engineering applications so, in addition to using porous, collagen materials, each of our approaches was based on naturally occurring phenomena. This work demonstrates the effective modification of scaffold composition in order to address issues of transient (not covalent) growth factor sequestration, gene delivery capacity, or immunomodulation. As a result, this thesis demonstrates that changing the material composition alone can have marked control over soluble factor and cellular responses.

Chapter 2 of this thesis demonstrated the ability to mimic the *in vivo* sequestration of growth factors by the selective inclusion of glycosaminoglycans (GAGs) within the collagen-GAG scaffold. The degree of GAG sulfation is one of the main factors that dictates electrostatic binding of positively-charged growth factors in the body. In this study, GAGs with a range of sulfation degrees were incorporated into the collagen suspension used to form open foam collagen-glycosaminoglyacn (CG) scaffolds. Increasing scaffold GAG sulfation led to increased tenocyte metabolic activity in low serum and IGF-1 supplemented media conditions. This followed the significantly increased pulldown of IGF-1 in scaffolds with sulfated GAGs compared to scaffolds with non-sulfated GAGs. These data demonstrate that scaffold chemistry is important for growth factor presentation, providing inspiration for a number of ongoing

research efforts looking to more precisely tailor the local biomolecular environment for cells within the scaffold.

Continuing with the use of GAG-based electrostatic interactions, the work in Chapter 3 investigated how the differences in GAG charge can also be leveraged to influence the delivery of non-viral gene vectors called polyplexes to cells within the scaffold. Polyplexes are formed by combining cationic polymer with the gene of interest; these spontaneously condense into a nanoparticle as the polymer interacts with the negative DNA backbone. Interested to see how the electrostatic scaffold environment would alter the 3D delivery of a reporter gene, polyplexes (with varying polymer acetylation and polymer:DNA weight-to-weight ratios) were introduced into the scaffolds and cultured with tenocytes. Increasing the weight-to-weight ratio and using a highly sulfated glycosaminoglycan in the CG scaffold resulted in increased the reporter gene expression in tenocytes treated with acetylated PEI polyplexes. Findings from this work suggest that the electrostatic environment of a gene activated scaffold may prove to be an important design parameter to consider in order to enhance the efficiency of cationic polymer based gene therapy for tissue engineering applications.

Shifting from a focus on materials for addressing cell behavior critical for later stages of wound healing such as proliferation and cell-mediated matrix remodeling, Chapter 4 describes a new class of collagen biomaterial that uses bioinspired changes in composition to alter the inflammatory phase of wound repair. Influenced by the scarless wound healing seen in fetal tissues, this study incorporated materials from the fetal wound environment (hyaluronic acid and amniotic membrane matrix) into the established collagen-based scaffolds. These fetal wound inspired components, particularly the collagen-amniotic membrane scaffold composite, induced increased metabolic activity in equine tenocytes even after a pro-inflammatory challenge with

interleukin 1 beta. These scaffolds also supported downregulated pro-inflammatory gene expression profiles in these cells in response to inflammatory challenge.

Following the promise seen in the ability of collagen-amniotic membrane (AM) scaffolds to temper the inflammatory response in a fibroblast cell population, Chapter 5 outlines work that examined the mode of AM incorporation into the scaffold and resultant cellular response in mesenchymal stem cells that are a key element of immunomodulatory responses seen in vivo. AM matrix was either directly incorporated into the collagen scaffold during fabrication to form a C:AM composite scaffold, or the intact AM membrane was introduced as a membrane-based wrap around a conventional CG scaffold to create a core-shell composite biomaterial. The fabrication of these scaffolds allowed for microstructural anisotropy to mimic the aligned ECM of the tendon. After culturing the MSC-seeded scaffolds in pro-inflammatory conditions, the genes associated with MSC immunomodulation remained unchanged across all scaffold groups (including the control) although pro-inflammatory genes were downregulated in the AM scaffolds. Additional work needs to be done to further understand the role of AM scaffolds in influencing progenitor cell behavior *in vitro*, but these findings suggest the effects of AM within the collagen biomaterial may be realized via modulation of the biochemical (not structural) microenvironment of the scaffold.

Macrophages are critical components in the transition between each phase of the wound healing cascade (inflammation, proliferation, remodeling) due to their phenotypic plasticity. The work of Chapter 6 probes the effect of anti-inflammatory matrix (AM) containing scaffolds *in vitro* and *in vivo* by monitoring macrophage phenotype. The results indicate that while the scaffolds do not support a M1 (pro-inflammatory) phenotype *in vitro*, there is some upregulation of M1 associated genes at early time points *in vivo*. The presence of a M2 (pro-healing, anti-

inflammatory) associated macrophage phenotype is much more dominant in *in vitro* culture. Ongoing work will address questions of macrophage response under inflammatory conditions and more extensive characterization of macrophage phenotype *in vivo*.

7.2 Future Directions

By limiting the need for covalent chemistries or delivery vehicles and reducing the required dosage of growth factors necessary in cell culture media or for diffusive pre-loading, the use of charged-based growth factor sequestration has the potential to enhance the *in vitro* study and *in vivo* application of biomaterials. This work demonstrated the effects of GAG sequestration with just one growth factor, in just one type of scaffold. Future work could apply this technique to other scaffolds for other tissues, such as a mineralized collagen scaffold for bone, and evaluate its effectiveness in sequestering different growth factors, singly or in combination.

The potential for future work in the area of 3D, anti-inflammatory biomaterials that use the amniotic membrane is vast. Work going forward would benefit from a detailed characterization of the amniotic membrane outside of the CG scaffold platform. This could include verification of processing (decellularization, in particular), a full analysis of its composition (matrix and growth factors/cytokines), and evaluation of the cellular response to the amnion as a 2D substrate (in the form of a control in *in vitro* experiments). As mentioned previously, further work in monitoring macrophage response in the CG scaffolds should include some sort of inflammatory challenge (by using M1 macrophages or applying inflammatory cytokines to the media) to study the influence of the scaffolds on the kinetics of the phenotypic switch to M2 macrophages. Additionally, due to the complex nature of the native immune response and importance of cellular signaling as part of wound resolution, characterizing the effect of the CG scaffold in a co-culture environment (MSCs and macrophages, macrophages and fibroblasts) would advance

the understanding of the role it could play in tissue regeneration. Of course, as this work is intended for clinical applications, further study in in vivo animal models should be carried out.

7.3 Final Thoughts

The compositional changes implemented here offer a path forward in the development of bioactive, three-dimensional, collagen-based scaffolds for tissue regeneration. By addressing concerns at multiple levels of the wound healing cascade, this thesis provides a unique look at material design for reducing inflammation or enhancing growth factor activity for a range of functions. The idea of instructive signals changing the kinetics of the wound healing cascade offers an exciting glimpse into the future of tissue engineering where this emerging subfield presents significant potential for clinical success.

APPENDIX A: SCAFFOLD FABRICATION PROTOCOLS

A.1 Protocol for CG suspension preparation

Reference: [51, 69]

Reagents

- Purified fibrillar collagen (Collagen Matrix) or collagen from bovine tendon (Sigma-Aldrich C9879); stored at 4ºC
- Chondroitin sulfate sodium salt from shark cartilage (Sigma-Aldrich C4384); stored at 4ºC
- Heparin sodium salt from porcine intestinal mucosa (Sigma-Aldrich H4784 or H3149); stored at 4ºC
- Hyaluronic acid from Streptococcus equi (Sigma-Aldrich 53747); stored at -20ºC
- Glacial acetic acid (Sigma-Aldrich 71251)
- Ethylene glycol (VWR BDH1125-4LP)
- Deionized water

Equipment and Supplies

- Recirculating chiller (Fisher Isotemp Model 900)
- Rotor-stator (IKA 0593400) with large head attachment
- Disperser (IKA 3565001)
- Jacketed beaker (Ace Glass 5340-110)
- Freeze-dryer (VirTis Genesis)
- Dual range balance (Mettler Toledo XS105)
- Beakers
- Parafilm
- Spatula

Procedure

*This procedure describes how to make 300 mL of 0.5% CG suspension at an 11:1 collagen:glycosaminoglycan ratio. Scale collagen and GAG content appropriately to create different volumes and ratios of suspension.

1. Fill recirculating chiller with a 50/50 mix of ethylene glycol and deionized water, making sure that the cooling coils are completely immersed in the liquid. Set the recirculating chiller to 4ºC.

2. Attach recirculating chiller to jacketed beaker so that the coolant enters at the jacketed beaker's base and exits at the beaker's top. Allow for the temperature to equilibrate to 4ºC, about 30 minutes. Maintaining this temperature is important, as it will prevent the collagen from denaturing during the blending process.

3. Prepare a 0.05 M solution of acetic acid by adding 0.87 mL of glacial acetic acid to 300 mL of deionized water.

4. Weigh 1.5 g of collagen and add to the jacketed beaker.

5. Pour 250 mL of the 0.05 M acetic acid into the jacketed beaker.

6. Assemble the rotor-stator and attach it to the disperser. Lower the rotor-stator into the suspension. The rotor-stator should be vertical and off-centered in the beaker for optimal blending.

7. Blend the suspension at 10,000 rpm at 4ºC until smooth, approximately 5 minutes. The height of the rotor-stator may need to be adjusted during the blending process: If the rotor-stator is positioned too high, the holes on its side will be visible; if it is too low, the suspension will bubble excessively. Periodically check to see if the rotor-stator is clogged with collagen; remove clogs with a spatula as needed.

8. Add 50 mL of 0.05 M acetic acid to a 50 mL centrifuge tube. Weigh out 0.133 g of chondroitin sulfate, heparin, or hyaluronic acid (GAG) and add to a 50 mL centrifuge tube. Vortex until the GAG is fully dissolved. Let the GAG solution rest in the refrigerator (4ºC) for at least 10 minutes.

9. Add the GAG solution drop-wise to the collagen suspension while it is being mixed at 10,000 rpm at 4ºC. Periodically manually stir in any GAG that remains on the surface of the suspension using a spatula. It may be necessary to stop and unclog the rotor-stator with a spatula during this process.

10. Once all of the GAG solution has been added, blend at 10,000 rpm at 4ºC until smooth, approximately 10 minutes. Periodically check to ensure the rotor-stator is lowered to the correct depth, as the suspension will gradually become less viscous and creep up the sides of the jacketed beaker. Periodically check to see if the rotor-stator is clogged; remove clogs with a spatula as needed.

11. Store the suspension overnight at 4ºC.

12. Degas the suspension to remove any air bubbles prior to use. It is recommended to degas approximately 20 mL at a time, until the solution starts to boil. To minimize suspension loss during the degassing process, cover the beaker with slit Parafilm.

13. Store the suspension at 4ºC. Periodically check the CG suspension; if not homogenous, re-blend at 4ºC.

A.2 Amniotic membrane isolation

Reference: [294, 295]
Reagents

- Calcium and Magnesium Free Hank's Balanced Salt Solution (CMF-HBSS) (Fisher Scientific SH3003103)
- Penicillin, Streptomycin, Amphotericin B (Anti-anti) (ThermoFisher 15140122)
- Phosphate buffered solution (PBS) (Fisher Scientific BW17516F12)
- Thermolysin (Sigma-Aldrich T7902)
- 70% ethanol solution
- 10% bleach solution
- Dish soap

Equipment and Supplies

- Disposable-Blade Dissection Handles (Size 3, 4.87 inches) (Fisher Scientific 08-913-5)
- Disposable blades (Blade size: 15; Length: 1.375 in. (3.5cm)) (Fisher Scientific 08-916-5D)
- Scissors (Fisher Scientific 8681)
- Forceps (Fisher Scientific 08-875)
- Spatula (Fisher Scientific 14-373)
- Sterilization pouches (3.5" x 9") (Fisher Scientific 01-812-51)
- 6 Beakers (VWR 13912-240)
- Petri dishes (Fisher Scientific 08-757-14)
- Stainless-Steel Utility Tray (Fisher Scientific 13-361 C)
- Nalgene Jars (250 mL) (Sigma-Aldrich Z380245-1PAK)
- Nalgene Jars (1000 mL) (Sigma-Aldrich Z380261-1PAK)
- Transport container (e.g. small cooler) with biohazard stickers
- Aluminum foil
- Autoclave tape
- Kimwipes

Procedure

➢ Prior to a collection, prepare the following and store in the Biomedical Research Center (BRC) at Carle Foundation Hospital:

1. Put knife handles, scissors, forceps, and spatulas in individual sterilization pouches. Cover glass beakers with foil and secure with autoclave tape. Loosen lids of Nalgene jars (disengage threads to prevent melting them closed) and secure lids with autoclave tape. Autoclave all these materials in a secondary container on a gravity cycle that reaches a temperature of 121°C for at least 30 minutes.

2. Prepare at least 2 bottles of CMF-HBSS solution with 10% Anti-anti solution. Store in cold room at Carle so collection coordinator can use it to keep placenta wet while in storage.

➢ Once a placenta is being stored in the Carle Biomedical Research Center cold room:

1. Make a fresh solution of thermolysin (125 μg/mL) in PBS (approximately 100 mL). Sterile filter.

2. Do all isolation procedures in a biosafety cabinet. Spray metal utility tray with 70% ethanol, dry with Kimwipe. Move placenta from collection container to tray.

3. With scissors, remove the umbilical cord from the placenta. Place cord in collection container. Wash blood off surface of placenta with HBSS.

4. Pull amniotic membrane (AM) free from placenta with forceps. Scrape with spatula, if necessary. Place AM in beaker with ~250 mL of HBSS.

5. Wash AM in a total of three (3) rounds of fresh HBSS (using 3 separate beakers works well). Depending on the size and state of the matrix, cutting the membrane into smaller pieces and manually scraping blood and the spongy layer away may be required for appropriate cleaning.

6. If the membrane hasn't been cut yet, cut now into pieces that will each fit into a large petri dish. This usually results in ~4 pieces.

7. Transfer all placenta waste and liquids back into collection container. Place container in biohazard waste bin. Add 10% bleach solution to tray and let soak during next steps.

8. Cover AM with ~25 mL of thermolysin solution. Shake petri dishes occasionally over this 20 minute decellularization step.

9. Setup three (3) beakers with ~250 mL of PBS. After decellularization, vigorously rinse AM pieces, moving to a fresh beaker of PBS for a total of three (3) washes.

10. Store AM pieces in PBS in small Nalgene jars. Label with AM collection details and biohazard stickers. Place small Nalgene jars into larger Nalgene jars for secondary containment. Label as biohazard and as "exempted biological material."

11. Wash already bleached metal tray. Bleach all beakers and instruments and then wash with soap and water. Bleach hood for 10 minutes with 10% bleach. Wipe then spray with 70% ethanol. Transport AM to RAL lab using DRS approved procedures (https://www.drs.illinois.edu/Programs/BiologicalMaterialTransport). Store at 4°C.

A.3 Amniotic membrane drying protocol

Reference: [230]

Reagents

- Cell Grade Sterile Water

Equipment and Supplies

- Forceps (Fisher Scientific 08-875)
- Spatula (Fisher Scientific 14-373)
- T-75 cell culture flasks (ThermoFisher Scientific 12-565-349)
- Petri dishes (Fisher Scientific 08-757-14)
- 5 x 5 inch aluminum pans for freeze drying
- Parafilm

Procedure

1. Following AM isolation (described in A.2.) store AM in PBS at 4°C for 24-48 hours. In this time the spongy layer will swell.

2. Remove AM from storage container and place in a large Petri dish. Using a spatula, scrape the spongy layer from surface of the membrane.

3. Place AM with ~35 mL of sterile cell grade water in a T-75 culture flask. Wash under shaking for 30 minutes.

4. Repeat steps 2-3 twice more to thoroughly remove the spongy layer and wash the PBS salts from the membrane.

5. Transfer AM piece(s) to metal pans for freeze drying. Add ~20 mL of sterile cell grade water and spread the membrane out into a single layer. Cover pan with slit Parafilm.

6. Freeze dry the membrane using the "-40°C amnion protocol."

7. Store dried amnion in foil pouch in desiccator.

A.4 C:AM suspension preparation protocol

Reference: [230]

Reagents

- Purified fibrillar collagen (Collagen Matrix); stored at 4ºC
- Dried amniotic membrane sheet (prepared as described in A.2. and A.3.)
- Glacial acetic acid (Sigma-Aldrich 71251)
- Ethylene glycol (VWR BDH1125-4LP)
- Deionized water

Equipment and Supplies

- Recirculating chiller (Fisher Isotemp Model 900)
- Rotor-stator (IKA 0593400) with large head attachment
- Small dispersing element (IKA)
- Disperser (IKA 3565001)
- Jacketed beaker (Ace Glass 5340-105)
- 100 mL Nalgene jar
- 50 mL conical tube
- Freeze-dryer (VirTis Genesis)
- Dual range balance (Mettler Toledo XS105)
- Beakers
- Parafilm
- Spatula

Procedure

*This procedure describes how to make 150 mL of 0.5% C:AM suspension at an 5:1 collagen:amniotic membrane ratio. It accounts for the collagen mass of the AM membrane and makes the total dry mass equivalent to CG suspensions outlined in A.1. This has been the most successful concentration and ratio throughout this project. Batch sizes of 50 mL have also been used by putting a small Nalgene in the jacketed beaker and surrounding it with Kimwipes and water.

1. Fill recirculating chiller with a 50/50 mix of ethylene glycol and deionized water, making sure that the cooling coils are completely immersed in the liquid. Set the recirculating chiller to 4ºC.

2. Attach recirculating chiller to jacketed beaker so that the coolant enters at the jacketed beaker's base and exits at the beaker's top. Allow for the temperature to equilibrate to 4ºC, about 30 minutes. Maintaining this temperature is important, as it will prevent the collagen from denaturing during the blending process.

3. Prepare a 0.05 M solution of acetic acid by adding 0.435mL of glacial acetic acid to 150 mL of deionized water.

4. Weigh out 0.136 g of dry amniotic membrane. Using a mortar and pestle, grind into smaller pieces. Add up to 5 mL of acetic acid solution while grinding.

5. Transfer amniotic membrane to 50 mL conical tube. Bring final volume to 25 mL with acetic acid solution. Use small dispersing element to homogenize amniotic membrane further. Store solution at 4°C until needed.

6. Weigh 0.68 g of collagen and add to the jacketed beaker.

7. Pour remaining 0.05 M acetic acid into the jacketed beaker.

8. Assemble the rotor-stator and attach it to the disperser. Lower the rotor-stator into the suspension. The rotor-stator should be vertical and off-centered in the beaker for optimal blending.

9. Blend the suspension at 10,000 rpm at 4ºC until smooth, approximately 5 minutes. The height of the rotor-stator may need to be adjusted during the blending process: If the rotor-stator is positioned too high, the holes on its side will be visible; if it is too low, the suspension will bubble excessively. Periodically check to see if the rotor-stator is clogged with collagen; remove clogs with a spatula as needed.

10. Add the AM solution drop-wise to the collagen suspension while it is being mixed at 10,000 rpm at 4ºC. Periodically manually stir in any GAG that remains on the surface of the suspension using a spatula. It may be necessary to stop and unclog the rotor-stator with a spatula during this process.

11. Once all of the GAG solution has been added, blend at 10,000 rpm at 4ºC until smooth, approximately 10 minutes. Periodically check to ensure the rotor-stator is lowered to the correct depth, as the suspension will gradually become less viscous and creep up the sides of the jacketed beaker. Periodically check to see if the rotor-stator is clogged; remove clogs with a spatula as needed.

12. Store the suspension overnight at 4ºC.

13. Degas the suspension to remove any air bubbles prior to use. It is recommended to degas approximately 20 mL at a time, until the solution starts to boil. To minimize suspension loss during the degassing process, cover the beaker with slit Parafilm.

14. Store the suspension at 4ºC. Periodically check the CG suspension; if not homogenous, re-blend at 4ºC.

A.5 Aligned CG scaffold fabrication protocol

Reference: [61, 251]

Reagents

- CG suspension; store at 4°C
- Welch DirecTorr Gold synthetic pump oil (Fisher 01-184-105)

Supplies and equipment

- Freeze-dryer (VirTis Genesis)
- PTFE-copper freeze-drying mold
- Beakers
- Parafilm
- Aluminum foil

Procedure

*This procedure describes the fabrication of aligned scaffolds (with and without amniotic membrane shells). Check that oil is clean (not yellow) before and after each freeze-dryer run, replacing when necessary.

1. Degas CG suspension in Parafilm-covered beaker by pulling vacuum inside freeze-dryer to remove all air bubbles. Make sure the condenser is at least -50°C or cooler before degassing.

2. Begin to cool freeze-dryer shelves by running 'Tf = xx C shelf cool' program where xx is the desired freezing temperature (-10, -40, or -60°C).

3. If making scaffold-membrane composites, cut amniotic membranes to size, roll, and place in PTFE-copper freeze-drying mold holes.

4. Pipette ~ 1 mL (8 mm diameter holes) or ~550 μL (6 mm diameter holes) of suspension into each hole in PTFE-copper freeze-drying mold.

5. Cancel shelf cool program and place freeze-dryer mold on the pre-cooled shelf. Shut the freeze-dryer door and run program 'Aligned Tf = xx' where xx is the desired freezing temperature (-10, -40, or -60°C).

A.6 Isotropic CG scaffold fabrication protocol

Reference: [69]

Reagents

- CG suspension; store at 4°C
- Welch DirecTorr Gold synthetic pump oil (Fisher 01-184-105)

Supplies and equipment

- Freeze-dryer (VirTis Genesis)
- Aluminum, polysulfone tray molds (3x3" or 5x5")
- Polysulfone cylindrical molds (10 mm diameter x 10 mm height)
- Beakers
- Parafilm
- Aluminum foil

Procedure

*This procedure describes the fabrication of 4 mm tall scaffold sheets and 10 mm diameter isotropic scaffolds. Check that oil is clean (clear, not yellowed) before and after each freeze-dryer run, replacing when necessary. It is easiest to replace the oil just after a run, when the oil is still warm.

1. Degas the CG suspension in a beaker (covered in Parafilm with small slits) by pulling vacuum inside freeze-dryer. Degas just to the boiling point to remove all air bubbles. Make sure the condenser is at least -50°C or cooler before degassing.

2. Add 24.2 mL of CG suspension to a 3x3" tray mold or 67.2 mL to a 5x5" mold. Ensure that the suspension reaches the corners and push any bubbles or unblended collagen to the edge using tweezers. To make cylindrical scaffolds, pipette ~800 μL of CG suspension into each mold.

3. Place molds in freeze dryer and run program at desired freezing temperature.

A.7 DHT crosslinking protocol

Reference: [51, 248]

Supplies and equipment

- Sterile air filter (Millipore SLGP033RS)
- Vacuum oven (Welch Vacuum, Fisher 13-262-52)
- Welch DirecTorr Gold synthetic pump oil (Fisher 01-184-105)

Procedure

*Note: Periodically check vacuum pump oil levels. Change oil at least once every 6-12 months. Change sterile air filter on 'Purge' line regularly.

1. Turn on vacuum oven and set the temperature to 105ºC.

2. Once vacuum oven has reached temperature set point, place scaffolds in opened aluminum pouches carefully inside the oven. Close the oven door.

3. Close the 'Purge' valve, located on the lower right face of the vacuum oven. Completely open the 'Vacuum' valve.

4. Turn on the vacuum pump and make sure vacuum is pulled to a sufficiently low level (<1 in Hg). Allow scaffolds to crosslink for 24 hours.

5. After crosslinking is complete, turn off the vacuum pump, close the 'Vacuum' valve, open the 'Purge' valve, then carefully remove scaffolds from the oven. Quickly seal the aluminum pouches, taking care to ensure that the aluminum pouches are sufficiently "puffed" so that the scaffolds will not be crushed during storage. Store sealed pouches with scaffolds (now sterile) in desiccator until time of use.

A.8 EDC crosslinking protocol

Reference: [248, 251]

Reagents

- 1-ethyl-3-[3-dimethylaminopropyl]carbodiimide hydrochloride (EDAC, Sigma-Aldrich E7750); Store at -20oC
- N-hydroxysulfosuccinimide (NHS, Sigma-Aldrich H7377); Store in desiccator
- Sterile phosphate-buffered saline (PBS)
- Sterile water
- 100% ethanol

Supplies and equipment

- 6-well plates (Fisher 08-772-1B)
- 50 mL centrifuge tubes
- Razor blades
- Biopsy punches (6 mm)
- Syringe and syringe filter
- MTS 2/4 digital microtiter shaker (IKA 3208001)
- Dual range balance (Mettler Toledo XS105)

Procedure

* Note: all steps should be performed in the laminar flow hood unless otherwise noted.

1. Cut scaffolds to be crosslinked to size using a razor blade or biopsy punch.

2. Transfer scaffold pieces to sterile centrifuge tube, remove from laminar flow hood, and weigh pieces on dual range balance.

3. Hydrate pieces in 100% ethanol overnight.

4. Rinse pieces several times in PBS and then let soak in PBS for 24 h before crosslinking.

5. Determine the EDAC and NHS concentrations to be used in crosslinking solution. The sample calculations in this protocol are done with a 5:2:1 EDAC:NHS:COOH molar ratio where COOH is carboxylic acid groups in CG material based on a conversion factor of 1.2 mmol COOH per gram of collagen [338]. The mass of EDAC and NHS required can be calculated as follows:

$$M_{EDAC} = M_{scaffold}\left(0.0012\frac{mol_{COOH}}{g_{collagen}}\right)\left(\frac{5mol_{EDAC}}{1mol_{COOH}}\right)\left(\frac{191.7g_{EDAC}}{1mol_{EDAC}}\right) \quad \textbf{(Equation A.1)}$$

$$M_{NHS} = M_{scaffold}\left(0.0012\frac{mol_{COOH}}{g_{collagen}}\right)\left(\frac{2mol_{NHS}}{1mol_{COOH}}\right)\left(\frac{116.0g_{NHS}}{1mol_{NHS}}\right) \quad \textbf{(Equation A.2)}$$

6. Mix the EDAC and NHS in sterile water. Approximately 0.75 mL of solution will be needed per scaffold piece (6-8 mm diameter, 3-5 mm thick).

7. In the laminar flow hood, sterile filter the solution and add to 6-well plates.

8. Add scaffolds in crosslinking solution and place well plate on digital microtiter shaker in incubator at 37^{o}C. Allow scaffolds to crosslink under moderate shaking for 30-120 min. Crosslinking time should be increased for less permeable constructs such as membranes and high solids content scaffolds.

9. Remove EDAC/NHS solution and rinse scaffolds in sterile PBS under moderate shaking for 10-15 min.

10. Remove first PBS wash solution and rinse scaffolds in fresh PBS under moderate shaking for an additional 30-45 min. Store in fresh sterile PBS at 4°C until use.

APPENDIX B: CELL CULTURE AND ASSAY PROTOCOLS

B.1 Tenocyte culture protocol

Reference: [61, 251, 253]

Reagents

- Complete tendon cell media (500 mL); Store at 4^{o}C

435 mL high glucose DMEM (Fisher SH30022.FS)

50 mL fetal bovine serum (Invitrogen 16140-071)

5 mL pen-strep (Invitrogen 15140-122)

5 mL L-glutamine (Invitrogen 25030-081)

5 mL amphotericin B solution (MP Biomedical 091672348)

25 mg ascorbic acid (Wako 014-04801)

Sterile filter before use

- DMSO (Fisher D128-500)
- Sterile phosphate-buffered saline without Ca2+ or Mg2+ (PBS)
- Trypsin-EDTA (Invitrogen 25300-062)
- Trypan blue (Sigma-Aldrich T8154)

Supplies and equipment

- Sterile filter
- Sterile pipettes (5, 10, 25 mL)
- T75 tissue culture flasks
- Hausser phase contrast hemocytometer
- Tabletop centrifuge
- Optical microscope
- Water bath (37oC)

*Note: all steps should be performed in the laminar flow hood unless otherwise noted.

➢ *Tendon cell thawing procedure*

1. Place complete tendon cell media in water bath and warm to 37ºC.

2. Thaw frozen cell vials in 37ºC water bath for about 2 min.

3. Transfer the thawed cells and freezing media to a 15 mL centrifuge tube. Add complete tendon cell media until the cerulean effect has dissipated, then bring the volume up to 10 mL.

4. Gently re-suspend the cells in the diluted media and pellet the cells at 1000 rpm for 7 min.

5. Aspirate off the media supernatant and add a total of 5-10 mL of media to the conical tubes depending on desired dilution for counting.

6. Mix the 10 μL cell suspension aliquot with 10 μL of Trypan blue. Pipette several times to mix the stain and cell suspension.

7. Place a cover slip on the hemocytometer and pipette 10 μL of the stain/cell suspension into the hemocytometer.

8. Cell counts are performed in as many of the nine separate regions of the hemocytometer as is feasible. Average number of cells per region is used to calculate the total cell population. For this calculation, the dilution factor is typically 2 (1:1 ratio of cell suspension to Trypan blue).

*Total Cell Population = (Mean Cells per Region) * Dilution * 10,000 * (Cell Suspension Volume)*

9. Seed the cells at the required density (usually 10,000-50,000 cells/cm^2). Use around 10-12 mL media for a 100 mm dish, 12-14 mL for a T75, or 7-8 mL for a T25.

10. Place the flask(s) into the incubator. Check the confluence every 24 h and feed cells every 72 h.

➢ *Tendon cell feeding procedure*

1. Warm complete tendon cell media and sterile PBS in water bath to 37ºC.

2. When the media and PBS are warm, wipe them dry with paper towel and spray with 70% ethanol before placing in the sterile hood.

3. Remove all old media from each flask, taking care not to scrape the cells with the pipette tip.

4. Add 12-14 mL of complete tendon cell media. Return the flasks to the incubator and repeat every 72 h.

➢ *Tendon cell passaging procedure*

1. Warm complete tendon cell media, sterile PBS, and 3 mL trypsin-EDTA per T75 flask to be passaged in water bath to 37ºC.

2. When the media, PBS and trypsin are warm, wipe them dry with paper towel and spray with 70% ethanol before placing in the sterile hood.

3. Remove all old media from each flask, taking care not to scrape the cells with the pipette tip.

4. Add 10 mL of PBS per flask and leave the PBS in the flask to rinse the cells for 30 s. Swirl gently to remove any excess media from the cells.

5. Remove the PBS and add 3 mL of trypsin per flask. Return the flasks to the incubator for 6 min to allow for the cells to detach from the tissue culture plastic (allow the cells to sit for 3-4 additional min in the incubator if they do not detach after 6 min). Slap flasks a few times to detach cells.

6. Add 6 mL of complete tendon cell media to each flask to neutralize the trypsin and to flush cells off of the tissue culture plastic.

7. Remove the trypsin, additional media, and cells from the flask and put into a conical tube. Remove a 10 μL cell suspension aliquot for counting. Centrifuge the cells at 1000 rpm for 7 min.

8. While cells are spinning down, mix the 10 μL cell suspension aliquot with 10 μL of Trypan blue. Pipette several times to mix the stain and cell suspension.

9. Place a cover slip on the hemocytometer and pipette 10 □L of the stain/cell suspension into the hemocytometer.

10. Cell counts are performed in as many of the nine separate regions of the hemocytometer as is feasible. Average number of cells per region is used to calculate the total cell population. For this calculation, the dilution factor is typically 2 (1:1 ratio of cell suspension to Trypan blue).

*Total Cell Population = (Mean Cells per Region) * Dilution * 10,000 * (Cell Suspension Volume)*

11. Aspirate off the media supernatant and add new media to dilute cells to desired concentration.

12. Seed the cells at the required density (usually 10,000-50,000 cells/cm^2). Use around 10-12 mL media for a 100 mm dish, 12-14 mL for a T75, or 7-8 mL for a T25.

13. Place the flask(s) into the incubator. Check the confluence every 24 h and feed cells every 72 h.

➢ *Tendon cell freezing procedure*

1. Grow cells to confluence and replace media the day before freezing.

2. Warm complete tendon cell media, sterile PBS, and 3 mL trypsin-EDTA per T75 flask to be passaged in water bath to 37^{o}C.

3. When the media, PBS and trypsin are warm, wipe them dry with paper towel and spray with 70% ethanol before placing in the sterile hood.

4. Remove all old media from each flask, taking care not to scrape the cells with the pipette tip.

5. Add 10 mL of PBS per flask and leave the PBS in the flask to rinse the cells for 30 s. Swirl gently to remove any excess media from the cells.

6. Remove the PBS and add 3 mL of trypsin per flask. Return the flasks to the incubator for 6 min to allow for the cells to detach from the tissue culture plastic (allow the cells to sit for 3-4 additional min in the incubator if they do not detach after 6 min). Slap flasks a few times to detach cells.

7. Add 6 mL of complete tendon cell media to each flask to neutralize the trypsin and to flush cells off of the tissue culture plastic.

8. Remove the trypsin, additional media, and cells from the flask and put into a conical tube. Remove a 10 μL cell suspension aliquot for counting. Centrifuge the cells at 1000 rpm for 7 min.

9. While cells are spinning down, mix the 10 μL cell suspension aliquot with 10 μL of Trypan blue. Pipette several times to mix the stain and cell suspension.

10. Place a cover slip on the hemocytometer and pipette 10 μL of the stain/cell suspension into the hemocytometer.

11. Cell counts are performed in as many of the nine separate regions of the hemocytometer as is feasible. Average number of cells per region is used to calculate the total cell population. For this calculation, the dilution factor is typically 2 (1:1 ratio of cell suspension to Trypan blue).

*Total Cell Population = (Mean Cells per Region) * Dilution * 10,000 * (Cell Suspension Volume)*

12. Aspirate off the media supernatant and calculate volume of freezing media needed to re-suspend 1-3 x 10^6 cells per mL (freezing media: 50% DMEM, 40% FBS, 10% DMSO).

13. Aliquot cells into 1 mL cryogenic tubes and place in -20°C freezer for 1 h.

14. Place cryogenic tubes in -80°C freezer. Cells can be stored here for up to 6 months. For longer-term storage, keep cells at -80°C for at least 24 h and then carefully move to liquid nitrogen storage in IGB.

B.2 hMSC culture protocol

Reference: [88]

Reagents

- Complete hMSC media (500 mL); store at 4°C

445 mL low glucose DMEM (SCS Media Facility); store at 4°C

50 mL MSC-validated fetal bovine serum (Invitrogen 12662-029); store at -20°C

5 mL antibiotic-antimyotic (Invitrogen 15140-122); store at -20°C

- Trypsin-EDTA (Invitrogen 25300-062); store at -20°C
- Trypan blue (Sigma-Aldrich T8154)
- DMSO (Fisher D128-500)
- Sterile phosphate-buffered saline without Ca^{2+} or Mg^{2+} (PBS)

Supplies and equipment

- Hausser phase contrast hemacytometer (Fisher 02-671-5)
- Tabletop centrifuge (VWR 53513-812)
- Optical microscope (Leica Microsystems DMIL LED)
- Water bath (37°C, Fisher 15-474-35)
- Sterile filters
- Sterile pipettes (5, 10, 25 mL)
- T75 tissue culture flasks

*Note: all steps should be performed in the laminar flow hood unless otherwise noted.

➢ *MSC thawing procedure*

1. Place complete MSC media in water bath and warm to 37°C.

2. Thaw frozen cell vials in 37°C water bath for about 2 min.

3. Transfer the thawed cells and freezing media to a 15 mL centrifuge tube. Add complete MSC media until the cerulean effect has dissipated, then bring the volume up to 9 mL.

4. Remove a 10 μL cell suspension aliquot for counting. Gently re-suspend the cells in the diluted media and pellet the cells at 600 g for 5 min.

5. While cells are spinning down, mix the 10 μL cell suspension aliquot with 10 μL of Trypan blue. Pipette several times to mix the stain and cell suspension.

6. Place a cover slip on the hemacytometer and pipette 10 μL of the stain/cell suspension into the hemacytometer.

7. Cell counts are performed in as many of the nine separate regions of the hemacytometer as is feasible. Average number of cells per region is used to calculate the total cell population. For this calculation, the dilution factor is typically 2 (1:1 ratio of cell suspension to Trypan blue).

*Total Cell Population = (Mean Cells per Region) * Dilution * 10,000 * (Cell Suspension Volume)*

8. Seed the cells at the required density (usually 5,000-6,000 cells/cm2). Use around 10-12 mL media for a 100 mm dish, 12-14 mL for a T75, or 7-8 mL for a T25.

9. Place the flask(s) into the incubator. Check the confluence every 24 h and feed every 3 days. Cells are usually confluent after 7-9 days. Do not use past passage 6.

- *MSC feeding procedure*

1. Warm complete MSC or lineage-specific induction media in water bath to 37°C.

2. When the media is warm, wipe dry with paper towel and spray with 70% ethanol before placing in the sterile hood.

3. Remove all old media from each flask or well plate, taking care not to scrape the cells with the pipette tip.

4. Add appropriate volume of media. Return the flasks or well plates to the incubator and feed every 3 days. Adjust volume of media accordingly for different sized containers.

- *MSC passaging procedure*

1. Warm complete MSC media, sterile PBS, and 3 mL trypsin-EDTA per T75 flask to be passaged in water bath to 37°C.

2. When the media, PBS and trypsin are warm, wipe them dry with paper towel and spray with 70% ethanol before placing in the sterile hood.

3. Remove all old media from each T75 flask, taking care not to scrape the cells with the pipette tip.

4. Add 10 mL of PBS per T75 flask and leave the PBS in the flask to rinse the cells for 30 s. Swirl gently to remove any excess media from the cells. Adjust volumes of PBS, media, and trypsin accordingly for different sized flasks.

5. Remove the PBS and add 3 mL of trypsin per T75 flask. Return the flasks to the incubator for 6 min to allow for the cells to detach from the tissue culture plastic (allow the cells to sit for 3-4 additional min in the incubator if they do not detach after 6 min). Slap flasks a few times to detach cells.

6. Add 6 mL of complete MSC media to each flask to neutralize the trypsin and to flush cells off of the tissue culture plastic.

7. Remove the trypsin, additional media, and cells from the flask and put into a conical tube. Remove a 10 μL cell suspension aliquot for counting. Centrifuge the cells at 600 g for 5 min.

8. While cells are spinning down, mix the 10 μL cell suspension aliquot with 10 μL of Trypan blue. Pipette several times to mix the stain and cell suspension.

9. Place a cover slip on the hemacytometer and pipette 10 μL of the stain/cell suspension into the hemacytometer.

10. Cell counts are performed in as many of the nine separate regions of the hemacytometer as is feasible. Average number of cells per region is used to calculate the total cell population. For this calculation, the dilution factor is typically 2 (1:1 ratio of cell suspension to Trypan blue).

*Total Cell Population = (Mean Cells per Region) * Dilution * 10,000 * (Cell Suspension Volume)*

11. Aspirate off the media supernatant and add new media to dilute cells to desired concentration.

12. Seed the cells at the required density (usually 5,000-6,000 cells/cm2). Use around 10-12 mL media for a 100 mm dish, 12-14 mL for a T75, or 7-8 mL for a T25.

13. Place the flask(s) into the incubator. Check the confluence every 24 h and feed cells every 3 days.

➢ *MSC freezing procedure*

1. Grow cells to confluence and replace media the day before freezing.

2. Warm complete MSC media, sterile PBS, and 3 mL trypsin-EDTA per T75 flask to be passaged in water bath to 37°C.

3. When the media, PBS and trypsin are warm, wipe them dry with paper towel and spray with 70% ethanol before placing in the sterile hood.

4. Remove all old media from each flask, taking care not to scrape the cells with the pipette tip.

5. Add 10 mL of PBS per T75 flask and leave the PBS in the flask to rinse the cells for 30 s. Swirl gently to remove any excess media from the cells. Adjust volumes of PBS, media, and trypsin accordingly for different sized flasks.

6. Remove the PBS and add 3 mL of trypsin per T75 flask. Return the flasks to the incubator for 6 min to allow for the cells to detach from the tissue culture plastic (allow the cells to sit for 3-4 additional min in the incubator if they do not detach after 6 min). Slap flasks a few times to detach cells.

7. Add 6 mL of complete tenocyte media to each flask to neutralize the trypsin and to flush cells off of the tissue culture plastic.

8. Remove the trypsin, additional media, and cells from the flask and put into a conical tube. Remove a 10 μL cell suspension aliquot for counting. Centrifuge the cells at 600 g for 5 min.

9. While cells are spinning down, mix the 10 μL cell suspension aliquot with 10 μL of Trypan blue. Pipette several times to mix the stain and cell suspension. Place a cover slip on the hemacytometer and pipette 10 μL of the stain/cell suspension into the hemacytometer.

10. Cell counts are performed in as many of the nine separate regions of the hemacytometer as is feasible. Average number of cells per region is used to calculate the total cell population. For this calculation, the dilution factor is typically 2 (1:1 ratio of cell suspension to Trypan blue).

*Total Cell Population = (Mean Cells per Region) * Dilution * 10,000 * (Cell Suspension Volume)*

11. Aspirate off the media supernatant and calculate volume of freezing media needed to re-suspend 1-10 x 106 cells per mL (freezing media: 50% complete MSC media, 40% FBS, 10% DMSO).

12. Aliquot cells into 1 mL cryogenic tubes and place in -20°C freezer for 1 h.

13. Place cryogenic tubes in -80°C freezer. Cells can be stored here for up to 6 months. For longer-term storage, keep cells at -80°C for at least 24 h and then carefully move to liquid nitrogen storage in IGB.

B.3 THP-1 culture protocol

Reference: [326, 339]; Discussions with Kara Spiller (Drexel)

Reagents

- THP-1 cells (ATCC TIB-202)
- Complete growth medium:

Heat Inactivated RPMI-1640 (ATCC 30-2001)

10% Heat Inactivated Fetal Bovine Serum (FBS) (ATCC 30-2020)

1% Penicillin-Streptomycin (P/S) (Invitrogen 15140-122)

(New 500ml bottle of media + 50ml FBS + 5ml P/S)

Supplies and equipment

- Hausser phase contrast hemacytometer (Fisher 02-671-5)
- Tabletop centrifuge (VWR 53513-812)
- Optical microscope (Leica Microsystems DMIL LED)
- Water bath (37°C, Fisher 15-474-35)
- T25 tissue culture flasks
- T75 tissue culture flasks

Procedure

*Note: all steps should be performed in the laminar flow hood unless otherwise noted.

1. Thaw frozen cells in 37°C water bath by swirling gently. Transfer cells to a 15 ml tube, add 9 mL of media, spin at ~130 rcf for 5 min.

2. Remove supernatant and resuspend in 5 mL of HI-RPMI.

3. Count cells using a hemacytometer (as described in B.1. and B.2.)

4. Bring cell suspension to a concentration of $3x10^5$ cell/mL. Add 2.5 mL of cell suspension in T25 cell culture flasks. Check daily to ensure cells are not adhering and to do a maintenance cell count. Renew media every 2-3 days.

5. Subculture when cells reach a concentration of $8x10^5$ cell/mL by adding fresh media or replacing media. Cultures can be established by centrifugation and subsequent resuspension at of $3x10^5$ cell/mL. Eventually, it will be necessary to culture in larger (T75) culture flasks. Do not allow the cell concentration to exceed of $1x10^6$ cell/mL.

B.4 THP-1 differentiation and polarization protocol

Reference: [326, 339]; Discussions with Kara Spiller (Drexel)

Reagents

- THP-1 cells (ATCC TIB-202)
- Cytokines: LPS (Sigma L4391); IFN-γ, IL-4, IL-13, IL-10 (ProSpec; human recombinant)
- Complete growth medium:

Heat Inactivated RPMI-1640 (ATCC 30-2001)

10% Heat Inactivated Fetal Bovine Serum (FBS) (ATCC 30-2020)

1% Penicillin-Streptomycin (P/S) (Invitrogen 15140-122)

(New 500ml bottle of media + 50ml FBS + 5ml P/S)

- Phorbol 12-myristate-13-acetate (PMA) (Sigma P1585)
- Accutase solution (Sigma A6964)

Supplies and equipment

- Hausser phase contrast hemacytometer (Fisher 02-671-5)
- Tabletop centrifuge (VWR 53513-812)
- Optical microscope (Leica Microsystems DMIL LED)
- Water bath (37°C, Fisher 15-474-35)
- Ultra-low attachment 6-well plates (Fisher 07-200-601)
- Ultra-low attachment T-75 tissue culture flasks (ThermoFisher Scientific 12-565-349)

1. Prepare PMA by creating a 1mg/mL solution in 100% ethanol. Divide into 50 µL aliquots and freeze at -20°C for future use.
*Warning: PMA is a carcinogen. Handle and dispose of appropriately. Protect from light.

2. To differentiate cells into macrophages, add 2 µL of PMA stock solution (100 µg/ml) for every 1 ml of media. This step can be performed after transferring the cells to the well or by mixing the cells and the PMA in a 50 mL centrifuge tube and then transferring to the appropriate culture flask.

3. Resuspend cells at concentration of 1x106 cell/mL (assume 25% differentiation efficiency) and plate in ULA culture containers (2 mL per 6 well plate or 10 mL per T75 flask). Label the plates with “Caution contains PMA – Carcinogen”.

4. Incubate the plates under standard cell culture conditions (37˚C and 5% CO_2) for 3 days.

5. Collect media/cells in a 50ml centrifuge tube through a combination of treatment with accutase and cell scraping. Centrifuge and resuspend in fresh media to wash the PMA from the cells. Now the cells are M0 and can be used for 2D (concentration guidelines below) or 3D culture.
*Dispose of PMA-contaminated media through DRS waste management.

Well Plate	**Surface area**	**Cells/well**	**V_{final}/well**	**Stock (Cellls/ml)**
T25Flask	25 cm^2	2.5 $x10^6$	2.5 ml	1.0 $x10^6$ cells/ml
6	9.8 cm^2	$1.0x10^6$	2 ml	$0.5x10^6$ cells/ml
12	3.8 cm^2	$0.4x10^6$	1 ml	$0.4x10^6$ cells/ml
24	2.0 cm^2	$0.2x10^6$	0.5 ml	$0.4x10^6$ cells/ml
96	0.32 cm^2	$0.3x10^5$	200 µl	$0.1x10^6$ cells/ml

6. To polarize M0 macrophages to different phenotypes, add complete growth medium and add cytokines as follows. Incubate under standard conditions for 48 hours.
*Note: Always include a control where no cytokines are added and cells are cultured under similar conditions.

M0	***M1***	***M2a***	***M2c***
Just media	100ng/ml IFNy 100ng/ml LPS	40ng/ml IL-4 20ng/ml IL-13	40ng/ml IL-10

- NOTE: No MSCF is needed for these cells since the PMA is what differentiates the THP-1 monocytes into macrophages.

B.5 Cell seeding on CG scaffolds protocol

Reference: [61, 251]

Reagents

- Complete media for specific cell type; store at 4ºC
- Trypsin-EDTA (Invitrogen 25300-062); store at -20ºC
- Trypan blue (Sigma-Aldrich T8154)
- Sterile phosphate-buffered saline without Ca2+ or Mg2+ (PBS)

Supplies and equipment

- Ultra-low attachment 6-well plates (Fisher 07-200-601)
- Hausser phase contrast hemacytometer (Fisher 02-671-5)
- Tabletop centrifuge (VWR 53513-812)
- Optical microscope (Leica Microsystems DMIL LED)
- Water bath (37ºC, Fisher 15-474-35)
- Sterile pipettes (5, 10, 25 mL)
- Kimwipes

Procedure

*Note: all steps should be performed in the laminar flow hood unless otherwise noted.

1. Soak scaffolds overnight in the media to be used for seeding (0.5 mL per scaffold).
2. Warm complete media, sterile PBS, and 3 mL trypsin-EDTA per T75 flask in water bath to 37ºC.
3. When the media, PBS and trypsin are warm, wipe them dry with paper towel and spray with 70% ethanol before placing in the sterile hood.
4. Remove all old media from each flask, taking care not to scrape the cells with the pipette tip.
5. Add 10 mL of PBS per T75 flask and leave the PBS in the flask to rinse the cells for 30 s. Swirl gently to remove any excess media from the cells. Adjust volumes of PBS, media, and trypsin accordingly for different sized flasks.
6. Remove the PBS and add 3 mL of trypsin per flask. Return the flasks to the incubator for 6 min to allow for the cells to detach from the tissue culture plastic. Tap flasks until cells detach.
7. Add 6 mL of complete cell media to each flask to neutralize the trypsin and to flush cells off of the tissue culture plastic.

8. Remove the trypsinized cell solution from the flask and put into a conical tube. Centrifuge the cells at 1000 rpm for 7 min (tenocytes), 600 g for 5 min (hMSC), or 130 g for 5 min (macrophages; follow B.4. protocol prior to this step).

9. Resuspend the cell pellet in a small volume of media.

10. Mix the 10 μL cell suspension aliquot with 10 μL of Trypan blue (90 μL for macrophages). Pipette several times to mix the stain and cell suspension.

11. Place a cover slip on the hemacytometer and pipette 10 μL of the stain/cell suspension into the hemacytometer.

12. Cell counts are performed in as many of the nine separate regions per side of the hemacytometer as is feasible (Typically four corners and center). Average number of cells per region is used to calculate the total cell population. For this calculation, the dilution factor is 2 (for tenocytes and hMSCs) or 10 (for macrophages).

13. Total Cell Population = (Mean Cells per Region) * Dilution * 10,000 * (Cell Suspension Volume)

14. Add additional media to dilute cells to desired concentration (usually 5×10^5 for tenocytes, 1×10^5 for hMSCs, and ~8×10^5 for macrophages) per 20 μL.

15. Carefully remove excess media from scaffolds with a Kimwipe and place 3-4 scaffold pieces in each well of Ultra-low attachment 6-well plates. Do not overdry scaffolds as this will lead to reduced viability.

16. Add 10 μL of cell suspension to each scaffold piece. Place scaffolds in incubator for 15 mins. Remove scaffolds from incubator, flip over, add additional 10 μL of cell suspension to the other side of each scaffold, and return to incubator for 2 h to allow for cell attachment.

17. Carefully add 5-6 mL complete media per well to each well. Change media every 3 days over the course of the experiment.

B.6 alamarBlue metabolic activity protocol

Reference: [61, 251, 340]

Reagents

- Complete cell media for cell type of interest (described in B.1.-B.3.); Store at 4°C
- Sterile phosphate-buffered saline without Ca2+ or Mg2+ (PBS)
- alamarBlue (Invitrogen DAL1100)

Supplies and equipment

- 24-well plates (Fisher 08-772-1)
- 96-well plates
- MTS 2/4 digital microtiter shaker (IKA 3208001)
- Water bath (37°C)
- Fluorescent spectrophotometer (Varian)

*Note: all steps should be performed in the laminar flow hood unless otherwise noted. The volumes of reagents used are correct for 8 mm diameter, 5 mm thick scaffold pieces.

Procedure

1. Warm media, sterile PBS, and alamarBlue in water bath to 37°C.

2. Before starting an experiment, generate a standard curve with a known number of cells. Do at least eight sample points: one well with just media, one well with media and alamarBlue, and then six wells with media, alamarBlue, and a different number of cells (usually ranging 25-300% of the number of cells seeded in the scaffolds).

3. Add media and cell suspension in different ratios to each well so that the total volume is 900 μL. Two wells should not have any cells.

4. Add 100 μL alamarBlue to each well except for one without cells. Incubate at 37°C under gentle (~50 rpm) shaking for 2-4 h. During this time, healthy cells convert the active ingredient in alamarBlue (resazurin) to the highly fluorescent resorufin. Make sure not to incubate cells too long or all of the resazurin will be reduced to resorufin.

5. After incubation, pipette 100 μL in triplicate from each sample well into a 96-well plate.

6. Measure fluorescence (excitation: 570 nm, emission: 585 nm) on the spectrophotometer. Use the 'Kinetics' program in the Cary Eclipse software to read plate '96 well clear.'

7. For measuring cell metabolic activity on scaffolds, pipette 900 μL media into each well (one well for each scaffold piece plus two control wells). Add 100 μL alamarBlue to each well except for one control well.

8. Remove scaffolds to be assayed and rinse in warm, sterile PBS to remove excess media and unattached/dead cells. Add scaffolds to experimental wells and incubate at 37^{o}C under gentle (~50 rpm) shaking for 2-4 h. The incubation time should be identical to the time used to make the standard curve.

9. After incubation, pipette 100 μL L in triplicate from each sample well into a 96-well plate.

10. Measure fluorescence (excitation: 570 nm, emission: 585 nm) on the spectrophotometer. Use the 'Kinetics' program in the Cary Eclipse software to read plate '96 well clear.' Fluorescent intensity can be extrapolated on standard curve to give metabolic activity.

11. This assay is non-destructive so scaffolds can continue to be cultured for longer times.

B.7 Hoechst DNA quantification protocol

Reference: [61, 251, 341]

Reagents

- Hoechst dye buffer (500 mL); store at 4ºC for up to 3 months

400 mL deionized water

58.44 g sodium chloride (RAL storeroom)

0.605 g Tris base (RAL storeroom)

0.185 g disodium EDTA (Sigma-Aldrich E5134)

Adjust pH to 7.4, bring total volume to 500 mL, sterile filter before use

- Papain buffer (100 mL); store at 4ºC

100 mLsterile phosphate-buffered saline without Ca2+ or Mg2+ PBS

1 mL 0.5 M EDTA (pH = 8.0, Sigma-Aldrich EDS); store at 4ºC

79 mg cysteine-HCl (Sigma-Aldrich 00320)

- Hoechst 33258 dye solution (1 mL); store at 4ºC for up to 6 months

1 mL sterile water

1 mg Hoechst 33258 dye (Invitrogen H1398); store at 4ºC

- Papain from Carica papaya (Sigma-Aldrich 76218); store at -20ºC
- Sterile phosphate-buffered saline without Ca2+ or Mg2+ (PBS)

Supplies and equipment

- 96-well plates (Fisher 12-565-369)
- Vortex (Fisher 02-215-365)
- Water bath (60ºC, Fisher 15-460-2SQ)
- Fluorescence spectrophotometer (Tecan, Room 104 RAL)
- Microcentrifuge tubes (1.5 mL)

Procedure

*Note: steps 1-2 should be performed in the laminar flow hood.

➢ *Standard Curve Procedure*

1. At the beginning of each experiment, a standard curve should be generated with a known number of cells. Make up active papain enzyme solution by dissolving 2.4 mg papain in 1mL papain buffer in the 60ºC water bath.

2. In 1.5 mL microcentrifuge tube, spin down 100 μL of cell solution (5 times cell seeding volume) for 3 min at 12000 rpm.

3. Remove supernatant and add 300 μL papain enzyme solution to tube. Pipette to resuspend cells. Allow to digest for 24 h in the 60ºC water bath.

4. After 24 h, vortex cell lysate thoroughly.

5. Prepare 1 mL of digest by dissolving 2.4 mg papain in 1 mL papain buffer in the 60ºC water bath.

6. Perform half dilutions to prepare standard (5x, 2.5x, 1.25x, 0.625x, 0.3125x cells seeded plus control). Label tubes for 2.5-.3125x points and add 150 μL of papain enzyme solution to each tube. Starting with the 2.5x sample, add 150 μL from the next higher concentration tube to the tube and vortex (150 μL from 5x into 2.5x, then 150 μL from x into 1.25x, etc.).

7. Prepare Hoechst working dye solution by adding 0.5 μL dye solution to 5 mL Hoechst dye buffer. Vortex thoroughly. Prepare a second set of microcentrifuge tubes. To each tube add 600 μL of dye solution and 30 μL of corresponding cell lysate for a total volume of 630 μL. Vortex thoroughly. The Hoechst dye fluorescently binds to double-stranded DNA from the lysed cells, allowing quantification of DNA and thus cell number.

8. Pipette 190 μL from each tube in triplicate into a black 96-well plate.

9. Measure fluorescence (excitation: 360 nm, emission: 465 nm) on the spectrophotometer in RAL 104. Use the ‘DNA F200’ program and remember to reserve the F200 machine on the Google Calendar prior to use. For each data point, adjust the fluorescence reading by subtracting the reading from the blank control. The standard curve is created by plotting cell number as a function of adjusted fluorescent intensity.

➢ *Cell Quantification Procedure*

*Note: step 2 should be performed in the laminar flow hood.

1. For measuring cell number on scaffolds, pipette 300 μL of papain enzyme solution into microcentrifuge tubes (one for each scaffold plus controls: one tube containing a blank scaffold with no seeded cells as a background control).

2. Remove scaffolds to be assayed and rinse in warm, sterile PBS to remove excess media and unattached/dead cells. Add scaffolds to microcentrifuge tubes and incubate in 60ºC water bath for 24 h. Vortex occasionally to facilitate digestion of scaffold.

3. After incubation, pipette 600 μL Hoechst working dye solution into new set of microcentrifuge tubes.

4. Remove samples from water bath and vortex thoroughly. Add 30 μL from each tube to its corresponding tube containing working dye solution. Vortex thoroughly.

5. Pipette 190 μL from each tube in triplicate from each sample well into a 96-well plate.

6. Measure fluorescence (excitation: 360 nm, emission: 465 nm) on the spectrophotometer in RAL 104. Use the 'DNA F200' program and remember to reserve the F200 machine on the Google Calendar prior to use. For each data point, adjust the fluorescence reading by subtracting the reading from the background control. Adjusted fluorescent intensity can be extrapolated on the standard curve to give a cell number.

B.8 RNA isolation and quantification protocol

Reference: [60, 342]

Reagents

- RNeasy Plant Mini Kit (Qiagen 74904)
- β-mercaptoethanol (Sigma M7522-100ML)
- 70% ethanol (use RNase free water when making solution)
- Sterile phosphate-buffered saline without Ca2+ or Mg2+ (PBS)
- RNase-free water
- Ice

Supplies and equipment

- 2 mL RNase free non-graduated microcentrifuge tubes
- RNase free pipette tips
- Ice bucket
- Kimwipes
- Microcentrifuge

Procedure

➢ *Reagent prep (before starting)*

1. Lysis buffer: Add 10 μL β-mercaptoethanol (14.3 M) per 1 mL of Buffer RLT supplied with Qiagen kit. This solution can be stored at room temperature for 1 month.

2. Buffer RPE: Add 4 volumes of 100% ethanol to the bottle of Buffer RPE supplied with Qiagen kit.

➢ *RNA Extraction*

*Note: All steps are performed at room temperature. Work quickly; limit the number of samples for RNA extraction to 18-24 in each sitting. RNase free tips should be used throughout.

1. Label one microcentrifuge tube for each sample.

2. Put some ice (2nd floor RAL) in an ice bucket.

3. Wash scaffolds in PBS three times, cut in half with razor blade, and then place in labeled tubes.

4. Add ~ 500 µL of ice-cold lysis buffer to each tube and keep on ice for ~ 5 min, shaking tubes periodically to help the buffer infiltrate the scaffolds. Scale amount of lysis buffer appropriately.

5. Pipette lysate into a labeled QIAShredder column. Place scaffold pieces in column as well. Spin at 14,000 rpm for 2.5 min.

6. Add equal volume of 70% ethanol to each sample and mix by pipetting up and down.

7. Add half of the lysate + ethanol to labeled RNeasy column (with 2-mL collection tube).

8. Centrifuge at 12,000 rpm for 30 s. Discard flow-through and replace column.

9. Add the remaining lysate + ethanol to the column.

10. Centrifuge at 12,000 rpm for 30 s. Discard flow-through and replace column.

11. Add 700 µL Buffer RW1 to the column.

12. Centrifuge at 12,000 rpm for 30 s. Discard flow-through and replace column.

13. Pipet 500 µL Buffer RPE into the column.

14. Centrifuge at 12,000 rpm for 30 s. Discard flow-through and replace column.

15. Add another 500 µL Buffer RPE into the column.

16. Centrifuge at 12,000 rpm for 2.5 min. Discard flow-through and place the column in a new 2 mL collection tube (supplied with kit).

17. Centrifuge at 12,000 rpm for 2.0 min.

18. Transfer the column to a new labeled, 1.5-mL collection tube.

19. Pipet 30 µL RNase-free water into the column and wait 5 min.

20. Centrifuge the RNeasy column at 12,000 rpm for 1.5 min.

21. Store RNA at -80°C for later use or put on ice if directly proceeding to quantification, reverse transcription, and RT-PCR.

22. If quantifying RNA, use 2 µL water to blank the NanoDrop Lite (set to the RNA menu). Quantify RNA by pipetting 2 µL of each sample onto pedestal and pushing the ‘sample’ button. Clean platform with a Kimwipe between each sample.

B.9 RNA reverse transcription protocol

Reference: [60, 342]

Reagents:

- QuantiTect Reverse Transcription Kit (Qiagen 205313)
- RNA samples
- Ice

Supplies and equipment

- BIO-RAD S1000 ThermoCycler
- Ice bucket
- 200 µL microcentrifuge tubes

Procedure

1. Label PCR tubes for number of reactions needed and defrost reverse transcription kit components on ice if needed. Keep kit components and RNA samples on ice. Turn on thermocycler so it can warm up.

2. Label 200 µL conical tubes with sample identifiers (1 per sample).

3. Calculate the volume of RNA sample required for a 10 µL reaction (typically 10 ng of cDNA will be desired per well for subsequent RT-PCR experiment):

$$Vol\ of\ RNA = \frac{10\ ng * \#\ of\ primer\ sets * \#\ of\ repeats * 1.10}{[RNA]}$$

*Note: 1.10 is for 10% excess.

4. Calculate the amount of water needed for each reaction (RNA+water = 6uL total volume)

Note: If the total RNA volume necessary is above 6 µL, use only 6 µL.

5. Pipette the required amount of water into each 200 µL conical tube.

6. Add 1 µL of gDNA wipeout and mix (vortex or pipette) each conical tube.

7. Add required RNA volumes to each tube, mix, and close lids.

8. Load samples into thermocycler. Close lid with extra quarter turn of tightness.

9. Run the 'CAV1' program. Change volume to 10 µL. This will begin by incubating the samples at 42°C for 2 min.

10. While the first step is running, prepare reaction buffer. Note that the RT buffer (green tubes) and the Primer Mix (purple tubes) can be combined in one tube. If you do this, place a check

mark on the lid of the green tube. Combine 2.5 µL of RT buffer/primer mix with 0.5 µL reverse transcriptase (red tubes) per sample (make enough for at least n+2 reactions) into a single tube and vortex well.

11. Pipet 3 µL of reaction buffer mix into each PCR tube once the 2 min initial incubation is complete. Close tubes, lid, and then press enter to skip to the next step, which is a 15 min incubation at 42°C followed by 95°C incubation for 3 min.

12. When cycle is complete, remove samples and store at -20°C.

B.10 PCR protocol

Reference: [60, 342]

Reagents

- QuantiTect SYBR Green Kit (Qiagen 204145); store at -20°C although individual kit aliquots may be stored at 4°C once opened.
- Primers (Integrated DNA Technologies)

Dilute to 30 μM in TE buffer (pH = 8.0)

Aliquot and store at -20°C or keep at 4°C

- Ice
- DNase removal buffer

Supplies and equipment

- Rainier multi-pipettes
- 384-well plates (Invitrogen 4309849)
- Plate covers (Invitrogen 4311971)
- Sealing tool
- Rainier pipette tips (VWR)
- RNase-free PCR tubes (500 μL, CLSL stockroom)
- Ice bucket
- Vortex (Fisher 02-215-365)
- Applied Biosystems 7900HT Fast Real-Time PCR system (Applied Biosystems)
- Sequence Detection Systems software v2.4 (Applied Biosystems)

Procedure

*Note: keep PCR area as clean as possible and remember to wipe down area with DNase removal buffer following each plate prep. Remember to reserve time on the PCR system on the IGB website (each plate takes 1 h 55 min to run).

1. Diagram plate layout and determine the amount of water, SYBR green, and primers you will need. Master mix 1 consists of SYBR green and primers and is added at 5.2 μL per well for 10

μL reactions. Master mix 2 is RNase-free water and cDNA and is added at 4.8 μL per well for 10 μL reactions. Make up 10% excess reagent for each mix.

2. Make up master mix 1 (V = 5.2μL * # of cDNA samples * # of replicates*110%;) for each primer set. Each replicate for a 10 μL reaction requires 5 μL of SYBR green, 0.1 μL forward primer, 0.1 μL of reverse primer. Mix primers before pipetting.

3. Make up master mix 2 (V = 4.8μL*# of genes * # of replicates * 110%) for each sample.

4. Vortex each tube of master mix 1 thoroughly and pipet into wells.

5. Vortex each tube of master mix 2 thoroughly and pipet into wells.

6. Place cover on plate. Make sure the plate is sealed tightly on all edges with the sealing tool.

7. Keep plate protected from light at 4°C until ready to analyze.

8. Transport to IGB 124A and set up plate on PCR machine. Follow instructions obtained during training on machine, making sure to add extra stage to determining product melting point. SYBR green dye non-specifically binds to all DNA, so the melting curve must be obtained to confirm the presence of a single product.

9. Analyze results using the Sequence Detection Systems software to obtain Ct values. For multiple plates, make sure the threshold is set at the same number for each primer pair. Calculate fold changes in expression using the delta-delta Ct method.

REFERENCES

[1] Birch HL. Tendon matrix composition and turnover in relation to functional requirements. Blackwell Publishing; 2007. p. 241-8.

[2] Maganaris CN, Paul JP. In vivo human tendinous tissue stretch upon maximum muscle force generation. J Biomech. 2000;33:1453-9.

[3] Batson EL, Paramour RJ, Smith TJ, Birch HL, Patterson-Kane JC, Goodship AE. Are the material properties and matrix composition of equine flexor and extensor tendons determined by their functions? Equine Vet J. 2003;35:314-8.

[4] Lichtwark GA, Wilson AM. In vivo mechanical properties of the human Achilles tendon during one-legged hopping. J Exp Biol. 2005;208:4715-25.

[5] de Jong JP, Nguyen JT, Sonnema AJM, Nguyen EC, Amadio PC, Moran SL. The Incidence of Acute Traumatic Tendon Injuries in the Hand and Wrist: A 10-Year Population-based Study. Clin Orthop Surg. 2014;6:196-202.

[6] Kim HM, Galatz LM, Lim C, Havlioglu N, Thomopoulos S. The effect of tear size and nerve injury on rotator cuff muscle fatty degeneration in a rodent animal model. Journal of Shoulder and Elbow Surgery. 2012;21:847-58.

[7] Plate JF, Brown PJ, Walters J, Clark JA, Smith TL, Freehill MT, et al. Advanced Age Diminishes Tendon-to-Bone Healing in a Rat Model of Rotator Cuff Repair. Am J Sports Med. 2014.

[8] Reuther KE, Thomas SJ, Sarver JJ, Tucker JJ, Lee C-S, Gray CF, et al. Effect of return to overuse activity following an isolated supraspinatus tendon tear on adjacent intact tendons and glenoid cartilage in a rat model. Journal of Orthopaedic Research. 2012:n/a-n/a.

[9] Hinchey JW, Aronowitz JG, Sanchez-Sotelo J, Morrey BF. Re-rupture rate of primarily repaired distal biceps tendon injuries. Journal of Shoulder and Elbow Surgery. 2014;23:850-4.

[10] Kvist DM. Achilles Tendon Injuries in Athletes. Sports Medicine. 2012;18:173-201.

[11] Gulotta LV, Kovacevic D, Cordasco F, Rodeo SA. Evaluation of tumor necrosis factor alpha blockade on early tendon-to-bone healing in a rat rotator cuff repair model. Arthroscopy. 2011;27:1351-7.

[12] Leys T, Salmon L, Waller A, Linklater J, Pinczewski L. Clinical Results and Risk Factors for Reinjury 15 Years After Anterior Cruciate Ligament Reconstruction A Prospective Study of Hamstring and Patellar Tendon Grafts. Am J Sports Med. 2012;40:595-605.

[13] Wopenka B, Kent A, Pasteris JD, Yoon Y, Thomopoulos S. The tendon-to-bone transition of the rotator cuff: a preliminary Raman spectroscopic study documenting the gradual mineralization across the insertion in rat tissue samples. Appl Spectrosc. 2008;62:1285-94.

[14] Genin GM, Kent A, Birman V, Wopenka B, Pasteris JD, Marquez PJ, et al. Functional grading of mineral and collagen in the attachment of tendon to bone. Biophys J. 2009;97:976-85.

[15] Thomopoulos S, Genin GM, Galatz LM. The development and morphogenesis of the tendon-to-bone insertion - what development can teach us about healing. J Musculoskelet Neuronal Interact. 2010;10:35-45.

[16] Yamaguchi K, Ditsios K, Middleton WD, Hildebolt CF, Galatz LM, Teefey SA. The Demographic and Morphological Features of Rotator Cuff DiseaseA Comparison of Asymptomatic and Symptomatic Shoulders. J Bone Joint Surg Am. 2006;88:1699-704.

[17] Genin GM, Kent A, Birman V, Wopenka B, Pasteris JD, Marquez PJ, et al. Functional Grading of Mineral and Collagen in the Attachment of Tendon to Bone. Biophysical Journal. 2009;97:976-85.

[18] Matsumoto T, Kubo S, Sasaki K, Kawakami Y, Oka S, Sasaki H, et al. Acceleration of tendon-bone healing of anterior cruciate ligament graft using autologous ruptured tissue. Am J Sports Med. 2012;40:1296-302.
[19] Ekdahl M, Wang JH, Ronga M, Fu FH. Graft healing in anterior cruciate ligament reconstruction. Knee Surg Sports Traumatol Arthrosc. 2008;16:935-47.
[20] Sasaki K, Kuroda R, Ishida K, Kubo S, Matsumoto T, Mifune Y, et al. Enhancement of tendon-bone osteointegration of anterior cruciate ligament graft using granulocyte colony-stimulating factor. Am J Sports Med. 2008;36:1519-27.
[21] Carbone A, Carballo C, Ma R, Wang H, Deng X, Dahia C, et al. Indian hedgehog signaling and the role of graft tension in tendon-to-bone healing: Evaluation in a rat ACL reconstruction model. J Orthop Res. 2016;34:641-9.
[22] Manning CN, Havlioglu N, Knutsen E, Sakiyama-Elbert SE, Silva MJ, Thomopoulos S, et al. The early inflammatory response after flexor tendon healing: a gene expression and histological analysis. J Orthop Res. 2014;32:645-52.
[23] Galatz LM, Sandell LJ, Rothermich SY, Das R, Mastny A, Havlioglu N, et al. Characteristics of the rat supraspinatus tendon during tendon-to-bone healing after acute injury. J Orthop Res. 2006;24:541-50.
[24] Beredjiklian PK, Favata M, Cartmell JS, Flanagan CL, Crombleholme TM, Soslowsky LJ. Regenerative versus reparative healing in tendon: a study of biomechanical and histological properties in fetal sheep. Ann Biomed Eng. 2003;31:1143-52.
[25] Malhotra S, Hu MS, Marshall CD, Leavitt T, Cheung AT, Gonzalez JG, et al. Mesenchymal Stromal Cells as Cell-Based Therapeutics for Wound Healing. Stem Cells Int. 2016;2016:4157934.
[26] Sen CK, Gordillo GM, Roy S, Kirsner R, Lambert L, Hunt TK, et al. Human skin wounds: a major and snowballing threat to public health and the economy. Wound Repair Regen. 2009;17:763-71.
[27] Swift ME, Kleinman HK, DiPietro LA. Impaired wound repair and delayed angiogenesis in aged mice. Lab Invest. 1999;79:1479-87.
[28] Dragoo JL, Wasterlain AS, Braun HJ, Nead KT. Platelet-Rich Plasma as a Treatment for Patellar Tendinopathy A Double-Blind, Randomized Controlled Trial. Am J Sports Med. 2014;42:610-8.
[29] Charousset C, Zaoui A, Bellaiche L, Bouyer B. Are Multiple Platelet-Rich Plasma Injections Useful for Treatment of Chronic Patellar Tendinopathy in Athletes? A Prospective Study. Am J Sports Med. 2014;42:906-11.
[30] Fairley J, Toppi J, Cicuttini FM, Wluka AE, Giles GG, Cook J, et al. Association between obesity and magnetic resonance imaging defined patellar tendinopathy in community-based adults: a cross-sectional study. BMC Musculoskelet Disord. 2014;15.
[31] Maffulli N, Spiezia F, Longo UG, Denaro V, Maffulli GD. High volume image guided injections for the management of chronic tendinopathy of the main body of the Achilles tendon. Physical Therapy in Sport. 2013;14:163-7.
[32] Longo UG, Rittweger J, Garau G, Radonic B, Gutwasser C, Gilliver SF, et al. No Influence of Age, Gender, Weight, Height, and Impact Profile in Achilles Tendinopathy in Masters Track and Field Athletes. Am J Sports Med. 2009;37:1400-5.
[33] Ferretti A. Epidemiology of jumper's knee. Sports Med. 1986;3:289-95.

[34] Zwerver J, Bredeweg SW, Akker-Scheek Ivd. Prevalence of Jumper's Knee Among Nonelite Athletes From Different Sports A Cross-Sectional Survey. Am J Sports Med. 2011;39:1984-8.
[35] Cook JL, Khan KM, Kiss ZS, Griffiths L. Patellar tendinopathy in junior basketball players: a controlled clinical and ultrasonographic study of 268 patellar tendons in players aged 14–18 years. Scandinavian Journal of Medicine & Science in Sports. 2000;10:216-20.
[36] Yannas IV. Tissue and organ regeneration in adults. New York: Springer; 2001.
[37] Rhett JM, Ghatnekar GS, Palatinus JA, O'Quinn M, Yost MJ, Gourdie RG. Novel therapies for scar reduction and regenerative healing of skin wounds. Trends Biotechnol. 2008;26:173-80.
[38] Murphy WL, Peters MC, Kohn DH, Mooney DJ. Sustained release of vascular endothelial growth factor from mineralized poly(lactide-co-glycolide) scaffolds for tissue engineering. Biomaterials. 2000;21:2521-7.
[39] Yannas IV. Tissue and Organ Regeneration in Adults. New York: Springer; 2001.
[40] Border WA, Noble NA, Ketteler M. TGF-B: a cytokine mediator of glomerulosclerosis and a target for therapeutic intervention. Kidney Int Suppl. 1995;49:S59-S61.
[41] Lin RY, Sullivan KM, Argenta PA, Meuli M, Lorenz HP, Adzick NS. Exogenous transforming growth factor-B amplifies its own expression and induces scar formation in a model of human fetal skin repair. Ann Surg. 1995;222:146-54.
[42] Shah M, Foreman DM, Ferguson MW. Neutralisation of TGF-B1 and TGF-B2 or exogenous addition of TGF-B3 to cutaneous rat wounds reduces scarring. J Cell Sci. 1995;108:985-1002.
[43] Soo C, Beanes SR, Hu F-Y, Zhang X, Catherine Dang C, Chang G, et al. Ontogenetic Transition in Fetal Wound Transforming Growth Factor-B Regulation Correlates with Collagen Organization. Am J Pathol. 2003;163:2459-76.
[44] Liu X, Holzwarth JM, Ma PX. Functionalized synthetic biodegradable polymer scaffolds for tissue engineering. Macromol Biosci. 2012;12:911-9.
[45] Fisher OZ, Khademhosseini A, Langer R, Peppas NA. Bioinspired materials for controlling stem cell fate. Acc Chem Res. 2010;43:419-28.
[46] Amass W, Amass A, Tighe B. A review of biodegradable polymers: Uses, current developments in the synthesis and characterization of biodegradable polyesters, blends of biodegradable polymers and recent advances in biodegradation studies. Polym Int. 1998;47:89-144.
[47] Place ES, George JH, Williams CK, Stevens MM. Synthetic polymer scaffolds for tissue engineering. Chem Soc Rev. 2009;38:1139-51.
[48] Liu X, Ma PX. Polymeric scaffolds for bone tissue engineering. Ann Biomed Eng. 2004;32:477-86.
[49] Rezwan K, Chen QZ, Blaker JJ, Boccaccini AR. Biodegradable and bioactive porous polymer/inorganic composite scaffolds for bone tissue engineering. Biomaterials. 2006;27:3413-31.
[50] Naderi H, Matin MM, Bahrami AR. Review paper: critical issues in tissue engineering: biomaterials, cell sources, angiogenesis, and drug delivery systems. J Biomater Appl. 2011;26:383-417.
[51] Yannas IV, Lee E, Orgill DP, Skrabut EM, Murphy GF. Synthesis and characterization of a model extracellular matrix that induces partial regeneration of adult mammalian skin. Proc Natl Acad Sci USA. 1989;86:933-7.

[52] Harley BAC, Gibson LJ. In vivo and in vitro applications of collagen-GAG scaffolds. Chemical Engineering Journal. 2008;137:102-21.
[53] Raman R, Sasisekharan V, Sasisekharan R. Structural insights into biological roles of protein-glycosaminoglycan interactions. Chem Biol. 2005;12:267-77.
[54] Gama CI, Tully SE, Sotogaku N, Clark PM, Rawat M, Vaidehi N, et al. Sulfation patterns of glycosaminoglycans encode molecular recognition and activity. Nat Chem Biol. 2006;2:467-73.
[55] Farrell E, O'Brien FJ, Doyle P, Fischer J, Yannas I, Harley BA, et al. A collagen-glycosaminoglycan scaffold supports adult rat mesenchymal stem cell differentiation along osteogenic and chondrogenic routes. Tissue Engineering. 2006;12:459-68.
[56] Yannas IV, Lee E, Orgill DP, Skrabut EM, Murphy GF. Synthesis and characterization of a model extracellular matrix that induces partial regeneration of adult mammalian skin. Proc Natl Acad Sci USA. 1989;86:933-7.
[57] Harley BA, Freyman TM, Wong MQ, Gibson LJ. A new technique for calculating individual dermal fibroblast contractile forces generated within collagen-GAG scaffolds. Biophys J. 2007;93:2911-22.
[58] Harley BA, Spilker MH, Wu JW, Asano K, Hsu HP, Spector M, et al. Optimal degradation rate for collagen chambers used for regeneration of peripheral nerves over long gaps. Cells Tissues Organs. 2004;176.
[59] Hortensius RA, Harley BA. The use of bioinspired alterations in the glycosaminoglycan content of collagen-GAG scaffolds to regulate cell activity. Biomaterials. 2013;34:7645-52.
[60] Caliari SR, Weisgerber DW, Ramirez MA, Kelkhoff DO, Harley BAC. The influence of collagen-glycosaminoglycan scaffold relative density and microstructural anisotropy on tenocyte bioactivity and transcriptomic stability. J Mech Behav Biomed Mater. 2012;11:27-40.
[61] Caliari SR, Harley BAC. The effect of anisotropic collagen-GAG scaffolds and growth factor supplementation on tendon cell recruitment, alignment, and metabolic activity. Biomaterials. 2011;32:5330-40.
[62] Shen W, Chen X, Chen J, Yin Z, Heng BC, Chen W, et al. The effect of incorporation of exogenous stromal cell-derived factor-1 alpha within a knitted silk-collagen sponge scaffold on tendon regeneration. Biomaterials. 2010;31:7239-49.
[63] Wissemann KW, Jacobson BS. Pure gelatin microcarriers: synthesis and use in cell attachment and growth of fibroblast and endothelial cells. In Vitro Cell Dev Biol. 1985;21:391-401.
[64] Bagnaninchi PO, Yang Y, Zghoul N, Maffulli N, Wang RK, Haj AJ. Chitosan microchannel scaffolds for tendon tissue engineering characterized using optical coherence tomography. Tissue Eng. 2007;13:323-31.
[65] Lee KY, Mooney DJ. Alginate: properties and biomedical applications. Prog Polym Sci. 2012;37:106-26.
[66] Mauck RL, Soltz MA, Wang CC, Wong DD, Chao PH, Valhmu WB, et al. Functional tissue engineering of articular cartilage through dynamic loading of chondrocyte-seeded agarose gels. J Biomech Eng. 2000;122:252-60.
[67] O'Brien FJ, Harley BA, Yannas IV, Gibson LJ. The effect of pore size on cell adhesion in collagen-GAG scaffolds. Biomaterials. 2005;26:433-41.
[68] Greiner A, Wendorff JH. Electrospinning: A Fascinating Method for the Preparation of Ultrathin Fibers. Angewandte Chemie International Edition. 2007;46:5670-703.
[69] O'Brien FJ, Harley BA, Yannas IV, Gibson L. Influence of freezing rate on pore structure in freeze-dried collagen-GAG scaffolds. Biomaterials. 2004;25:1077-86.

[70] O'Brien FJ, Harley BA, Waller MA, Yannas IV, Gibson LJ, Prendergast PJ. The effect of pore size on permeability and cell attachment in collagen scaffolds for tissue engineering. Technology and Health Care. 2007;15:3-17.
[71] Zeltinger J, Sherwood JK, Graham DA, M\"ueller R, Griffith LG. Effect of pore size and void fraction on cellular adhesion, proliferation, and matrix deposition. Tissue Engineering. 2001;7:557-72.
[72] Murphy CM, Haugh MG, O'Brien FJ. The effect of mean pore size on cell attachment, proliferation and migration in collagen–glycosaminoglycan scaffolds for bone tissue engineering. Biomaterials. 2010;31:461-6.
[73] Kim YT, Haftel VK, Kumar S, Bellamkonda RV. The role of aligned polymer fiber-based constructs in the bridging of long peripheral nerve gaps. Biomaterials. 2008;29:3117-27.
[74] Engelmayr GC, Jr., Cheng M, Bettinger CJ, Borenstein JT, Langer R, Freed LE. Accordion-like honeycombs for tissue engineering of cardiac anisotropy. Nat Mater. 2008;7:1003-10.
[75] Moffat KL, Kwei AS, Spalazzi JP, Doty SB, Levine WN, Lu HH. Novel Nanofiber-Based Scaffold for Rotator Cuff Repair and Augmentation. Tissue Eng Part A. 2009;15:115-26.
[76] Xie J, Li X, Lipner J, Manning CN, Schwartz AG, Thomopoulos S, et al. "Aligned-to-random" nanofiber scaffolds for mimicking the structure of the tendon-to-bone insertion site. Nanoscale. 2010;2:923-6.
[77] Liu Y, Ramanath HS, Wang DA. Tendon tissue engineering using scaffold enhancing strategies. Trends Biotechnol. 2008;26:201-9.
[78] Yin Z, Chen X, Chen JL, Shen WL, Hieu Nguyen TM, Gao L, et al. The regulation of tendon stem cell differentiation by the alignment of nanofibers. Biomaterials. 2010;31:2163-75.
[79] Gibson LJ, Ashby MF. Cellular solids: structure and properties. 2nd ed. Cambridge, U.K.: Cambridge University Press; 1997.
[80] Kloxin AM, Tibbitt MW, Kasko AM, Fairbairn JA, Anseth KS. Tunable hydrogels for external manipulation of cellular microenvironments through controlled photodegradation. Adv Mater. 2010;22:61-6.
[81] Place ES, Evans ND, Stevens MM. Complexity in biomaterials for tissue engineering. Nat Mater. 2009;8:457-70.
[82] Hudalla GA, Murphy WL. Biomaterials that regulate growth factor activity via bioinspired interactions. Adv Funct Mater. 2011;21:1754-68.
[83] Caliari SR, Grier WK, Weisgerber DW, Mahmassani Z, Boppart MD, Harley BAC. Collagen scaffolds incorporating coincident patterns of instructive structural and biochemical cues for osteotendinous junction engineering. Adv Healthc Mater. 2015.
[84] Brandley BK, Schnaar RL. Covalent attachment of an Arg-Gly-Asp sequence peptide to derivatizable polyacrylamide surfaces: support of fibroblast adhesion and long-term growth. Anal Biochem. 1988;172:270-8.
[85] Galatz L, Rothermich S, VanderPloeg K, Petersen B, Sandell L, Thomopoulos S. Development of the supraspinatus tendon-to-bone insertion: localized expression of extracellular matrix and growth factor genes. J Orthop Res. 2007;25:1621-8.
[86] Soo C, Beanes SR, Hu F-Y, Zhang X, Catherine Dang C, Chang G, et al. Ontogenetic transition in fetal wound transforming growth factor-B regulation correlates with collagen organization. Am J Pathol. 2003;163:2459-76.
[87] Caliari SR, Harley BA. Composite growth factor supplementation strategies to enhance tenocyte bioactivity in aligned collagen-GAG scaffolds. Tissue Eng Part A. 2013;19:1100-12.

[88] Caliari SR, Harley BA. Structural and biochemical modification of a collagen scaffold to selectively enhance MSC tenogenic, chondrogenic, and osteogenic differentiation. Adv Healthc Mater. 2014;3:1086-96.
[89] Santos E, Hernández RM, Pedraz JL, Orive G. Novel advances in the design of three-dimensional bio-scaffolds to control cell fate: translation from 2D to 3D. Trends Biotechnol. 2012;30:331-41.
[90] Thomopoulos S, Harwood FL, Silva MJ, Amiel D, Gelberman RH. Effect of several growth factors on canine flexor tendon fibroblast proliferation and collagen synthesis in vitro. J Hand Surg Am. 2005;30:441-7.
[91] Shen YH, Shoichet MS, Radisic M. Vascular endothelial growth factor immobilized in collagen scaffold promotes penetration and proliferation of endothelial cells. Acta Biomater. 2008;4:477-89.
[92] Odedra D, Chiu LL, Shoichet M, Radisic M. Endothelial cells guided by immobilized gradients of vascular endothelial growth factor on porous collagen scaffolds. Acta Biomater. 2011;7:3027-35.
[93] Martin TA, Caliari SR, Williford PD, Harley BA, Bailey RC. The generation of biomolecular patterns in highly porous collagen-GAG scaffolds using direct photolithography. Biomaterials. 2011;32:3949-57.
[94] Culver JC, Hoffmann JC, Poché RA, Slater JH, West JL, Dickinson ME. Three-dimensional biomimetic patterning in hydrogels to guide cellular organization. Adv Mater. 2012;24:2344-8.
[95] Caliari SR, Gonnerman EA, Grier WK, Weisgerber DW, Banks JM, Alsop AJ, et al. Collagen scaffold arrays for combinatorial screening of biophysical and biochemical regulators of cell behavior. Adv Healthc Mater. 2015;4:58-64.
[96] Alsop AT, Pence JC, Weisgerber DW, Harley BAC, Bailey RC. Photopatterning of VEGF within collagen-GAG scaffolds can induce a spatially confined response in human umbilical vein endothelial cells. Acta Biomater. 2014;10:4715-22.
[97] Banks JM, Mozdzen LC, Harley BAC, Bailey RC. The combined effects of matrix stiffness and growth factor immobilization on the bioactivity and differentiation capabilities of adipose-derived stem cells. Biomaterials. 2014;35:8951-9.
[98] Pence JC, Gonnerman EA, Bailey RC, Harley BAC. Strategies to balance covalent and non-covalent biomolecule attachment within collagen-GAG biomaterials. Biomater Sci. 2014;2:1296-304.
[99] Kapur TA, Shoichet MS. Immobilized concentration gradients of nerve growth factor guide neurite outgrowth. J Biomed Mater Res A. 2004;68:235-43.
[100] DeForest CA, Polizzotti BD, Anseth KS. Sequential click reactions for synthesizing and patterning three-dimensional cell microenvironments. Nat Mater. 2009;8:659-64.
[101] Polizzotti BD, Fairbanks BD, Anseth KS. Three-dimensional biochemical patterning of click-based composite hydrogels via thiolene photopolymerization. Biomacromolecules. 2008;9:1084-7.
[102] Habraken WJ, Boerman OC, Wolke JG, Mikos AG, Jansen JA. In vitro growth factor release from injectable calcium phosphate cements containing gelatin microspheres. J Biomed Mater Res A. 2009;91:614-22.
[103] Kawai K, Suzuki S, Tabata Y, Ikada Y, Nishimura Y. Accelerated tissue regeneration through incorporation of basic fibroblast growth factor-impregnated gelatin microspheres into artificial dermis. Biomaterials. 2000;21:489-99.

[104] Cohen S, Yoshioka T, Lucarelli M, Hwang LH, Langer R. Controlled delivery systems for proteins based on poly(lactic/glycolic acid) microspheres. Pharm Res. 1991;8:713-20.
[105] Solorio L, Zwolinski C, Lund AW, Farrell MJ, Stegemann JP. Gelatin microspheres crosslinked with genipin for local delivery of growth factors. J Tissue Eng Regen Med. 2010;4:514-23.
[106] Patel ZS, Young S, Tabata Y, Jansen JA, Wong ME, Mikos AG. Dual delivery of an angiogenic and an osteogenic growth factor for bone regeneration in a critical size defect model. Bone. 2008;43:931-40.
[107] Gan Q, Wang T. Chitosan nanoparticle as protein delivery carrier--systematic examination of fabrication conditions for efficient loading and release. Colloids Surf B Biointerfaces. 2007;59:24-34.
[108] Lee M, Li W, Siu RK, Whang J, Zhang X, Soo C, et al. Biomimetic apatite-coated alginate/chitosan microparticles as osteogenic protein carriers. Biomaterials. 2009;30:6094-101.
[109] Wang J, Chen J-S, Zong J-Y, Zhao D, Li F, Zhuo R-X, et al. Calcium Carbonate/Carboxymethyl Chitosan Hybrid Microspheres and Nanospheres for Drug Delivery. J Phys Chem C. 2010;114:18940-5.
[110] Thote AJ, Chappell JT, Jr., Gupta RB, Kumar R. Reduction in the initial-burst release by surface crosslinking of PLGA microparticles containing hydrophilic or hydrophobic drugs. Drug Dev Ind Pharm. 2005;31:43-57.
[111] Ruoslahti E, Yamaguchi Y. Proteoglycans as modulators of growth factor activities. Cell. 1991;64:867-9.
[112] Rawat M, Gama CI, Matson JB, Hsieh-Wilson LC. Neuroactive chondroitin sulfate glycomimetics. J Am Chem Soc. 2008;130:2959-61.
[113] Robinson DE, Buttle DJ, Short RD, McArthur SL, Steele DA, Whittle JD. Glycosaminoglycan (GAG) binding surfaces for characterizing GAG-protein interactions. Biomaterials. 2012;33:1007-16.
[114] Hudalla GA, Kouris NA, Koepsel JT, Ogle BM, Murphy WL. Harnessing endogenous growth factor activity modulates stem cell behavior. Integr Biol (Camb). 2011;3:832-42.
[115] Zhang L, Furst EM, Kiick KL. Manipulation of hydrogel assembly and growth factor delivery via the use of peptide-polysaccharide interactions. J Control Release. 2006;114:130-42.
[116] Freeman I, Kedem A, Cohen S. The effect of sulfation of alginate hydrogels on the specific binding and controlled release of heparin-binding proteins. Biomaterials. 2008;29:3260-8.
[117] Lim JJ, Temenoff JS. The effect of desulfation of chondroitin sulfate on interactions with positively charged growth factors and upregulation of cartilaginous markers in encapsulated MSCs. Biomaterials. 2013;34:5007-18.
[118] van der Smissen A, Hintze V, Scharnweber D, Moeller S, Schnabelrauch M, Majok A, et al. Growth promoting substrates for human dermal fibroblasts provided by artificial extracellular matrices composed of collagen I and sulfated glycosaminoglycans. Biomaterials. 2011;32:8938-46.
[119] Hempel U, Hintze V, Moller S, Schnabelrauch M, Scharnweber D, Dieter P. Artificial extracellular matrices composed of collagen I and sulfated hyaluronan with adsorbed transforming growth factor beta 1 promote collagen synthesis of human mesenchymal stromal cells. Acta Biomater. 2012;8:659-66.
[120] Forrest ML, Koerber JT, Pack DW. A degradable polyethylenimine derivative with low toxicity for highly efficient gene delivery. Bioconjug Chem. 2003;14:934-40.

[121] Amaduzzi F, Bomboi F, Bonincontro A, Bordi F, Casciardi S, Chronopoulou L, et al. Chitosan-DNA complexes: charge inversion and DNA condensation. Colloids Surf B Biointerfaces. 2014;114:1-10.
[122] Carrillo C, Sune JM, Perez-Lozano P, Garcia-Montoya E, Sarrate R, Fabregas A, et al. Chitosan nanoparticles as non-viral gene delivery systems: determination of loading efficiency. Biomed Pharmacother. 2014;68:775-83.
[123] Wegman F, Geuze RE, van der Helm YJ, Cumhur Oner F, Dhert WJ, Alblas J. Gene delivery of bone morphogenetic protein-2 plasmid DNA promotes bone formation in a large animal model. J Tissue Eng Regen Med. 2014;8:763-70.
[124] Curtin CM, Cunniffe GM, Lyons FG, Bessho K, Dickson GR, Duffy GP, et al. Innovative collagen nano-hydroxyapatite scaffolds offer a highly efficient non-viral gene delivery platform for stem cell-mediated bone formation. Adv Mater. 2012;24:749-54.
[125] Curtin CM, Tierney EG, McSorley K, Cryan SA, Duffy GP, O'Brien FJ. Combinatorial gene therapy accelerates bone regeneration: non-viral dual delivery of VEGF and BMP2 in a collagen-nanohydroxyapatite scaffold. Adv Healthc Mater. 2015;4:223-7.
[126] Forrest ML, Meister GE, Koerber JT, Pack DW. Partial acetylation of polyethylenimine enhances in vitro gene delivery. Pharm Res. 2004;21:365-71.
[127] Gabrielson NP, Pack DW. Acetylation of polyethylenimine enhances gene delivery via weakened polymer/DNA interactions. Biomacromolecules. 2006;7:2427-35.
[128] Tierney EG, Duffy GP, Hibbitts AJ, Cryan SA, O'Brien FJ. The development of non-viral gene-activated matrices for bone regeneration using polyethyleneimine (PEI) and collagen-based scaffolds. J Control Release. 2012;158:304-11.
[129] Elangovan S, D'Mello SR, Hong L, Ross RD, Allamargot C, Dawson DV, et al. The enhancement of bone regeneration by gene activated matrix encoding for platelet derived growth factor. Biomaterials. 2014;35:737-47.
[130] Taylor SE, Vaughan-Thomas A, Clements DN, Pinchbeck G, Macrory LC, Smith RK, et al. Gene expression markers of tendon fibroblasts in normal and diseased tissue compared to monolayer and three dimensional culture systems. BMC Musculoskelet Disord. 2009;10:27.
[131] Tilley JMR, Chaudhury S, Hakimi O, Carr AJ, Czernuszka JT. Tenocyte proliferation on collagen scaffolds protects against degradation and improves scaffold properties. J Mater Sci: Mater Med. 2012;23:823-33.
[132] Kilian KA, Bugarija B, Lahn BT, Mrksich M. Geometric cues for directing the differentiation of mesenchymal stem cells. PNAS. 2010;107:4872-7.
[133] Caliari SR, Weisgerber DW, Grier WK, Mahmassani Z, Boppart MD, Harley BAC. Collagen Scaffolds Incorporating Coincident Gradations of Instructive Structural and Biochemical Cues for Osteotendinous Junction Engineering. Adv Healthcare Mater. 2015:n/a-n/a.
[134] Kim J, Hematti P. Mesenchymal stem cell-educated macrophages: a novel type of alternatively activated macrophages. Exp Hematol. 2009;37:1445-53.
[135] Nakajima H, Uchida K, Guerrero AR, Watanabe S, Sugita D, Takeura N, et al. Transplantation of mesenchymal stem cells promotes an alternative pathway of macrophage activation and functional recovery after spinal cord injury. J Neurotrauma. 2012;29:1614-25.
[136] Manning CN, Martel C, Sakiyama-Elbert SE, Silva MJ, Shah S, Gelberman RH, et al. Adipose-derived mesenchymal stromal cells modulate tendon fibroblast responses to macrophage-induced inflammation in vitro. Stem Cell Res Ther. 2015;6:74.

[137] Mosser DM, Edwards JP. Exploring the full spectrum of macrophage activation. Nat Rev Immunol. 2008;8:958-69.
[138] Nassiri S, Zakeri I, Weingarten MS, Spiller KL. Relative Expression of Proinflammatory and Antiinflammatory Genes Reveals Differences between Healing and Nonhealing Human Chronic Diabetic Foot Ulcers. J Invest Dermatol. 2015;135:1700-3.
[139] Diegelmann RF, Evans MC. Wound healing: an overview of acute, fibrotic and delayed healing. Front Biosci. 2004;9:283-9.
[140] Novak ML, Koh TJ. Phenotypic transitions of macrophages orchestrate tissue repair. Am J Pathol. 2013;183:1352-63.
[141] Weisgerber DW, Caliari SR, Harley BA. Mineralized collagen scaffolds induce hMSC osteogenesis and matrix remodeling. Biomater Sci. 2015;3:533-42.
[142] Haugh MG, Murphy CM, McKiernan RC, Altenbuchner C, O'Brien FJ. Crosslinking and mechanical properties significantly influence cell attachment, proliferation, and migration within collagen glycosaminoglycan scaffolds. Tissue Eng Pt A. 2011;17:1201-8.
[143] Cao H, McHugh K, Chew SY, Anderson JM. The topographical effect of electrospun nanofibrous scaffolds on the in vivo and in vitro foreign body reaction. J Biomed Mater Res A. 2010;93:1151-9.
[144] Bota PC, Collie AM, Puolakkainen P, Vernon RB, Sage EH, Ratner BD, et al. Biomaterial topography alters healing in vivo and monocyte/macrophage activation in vitro. J Biomed Mater Res A. 2010;95:649-57.
[145] Holladay C, Power K, Sefton M, O'Brien T, Gallagher WM, Pandit A. Functionalized scaffold-mediated interleukin 10 gene delivery significantly improves survival rates of stem cells in vivo. Mol Ther. 2011;19:969-78.
[146] Holladay CA, Duffy AM, Chen X, Sefton MV, O'Brien TD, Pandit AS. Recovery of cardiac function mediated by MSC and interleukin-10 plasmid functionalised scaffold. Biomaterials. 2012;33:1303-14.
[147] Yuan ZM, Zhao JW, Zhu WK, Yang ZL, Li B, Yang HL, et al. Ibuprofen-loaded electrospun fibrous scaffold doped with sodium bicarbonate for responsively inhibiting inflammation and promoting muscle wound healing in vivo. Biomater Sci-Uk. 2014;2:502-11.
[148] Wang QS, Cui YL, Gao LN, Guo Y, Li RX, Zhang XZ. Reduction of the pro-inflammatory response by tetrandrine-loading poly(L-lactic acid) films in vitro and in vivo. J Biomed Mater Res A. 2014;102:4098-107.
[149] Spiller KL, Nassiri S, Witherel CE, Anfang RR, Ng J, Nakazawa KR, et al. Sequential delivery of immunomodulatory cytokines to facilitate the M1-to-M2 transition of macrophages and enhance vascularization of bone scaffolds. Biomaterials. 2015;37:194-207.
[150] Chung MJ, Park JK, Park YI. Anti-inflammatory effects of low-molecular weight chitosan oligosaccharides in IgE-antigen complex-stimulated RBL-2H3 cells and asthma model mice. Int Immunopharmacol. 2012;12:453-9.
[151] Jayakumar R, Prabaharan M, Sudheesh Kumar PT, Nair SV, Tamura H. Biomaterials based on chitin and chitosan in wound dressing applications. Biotechnol Adv. 2011;29:322-37.
[152] Azuma K, Osaki T, Minami S, Okamoto Y. Anticancer and anti-inflammatory properties of chitin and chitosan oligosaccharides. J Funct Biomater. 2015;6:33-49.
[153] Shukla SK, Mishra AK, Arotiba OA, Mamba BB. Chitosan-based nanomaterials: a state-of-the-art review. Int J Biol Macromol. 2013;59:46-58.

[154] Pangestuti R, Bak SS, Kim SK. Attenuation of pro-inflammatory mediators in LPS-stimulated BV2 microglia by chitooligosaccharides via the MAPK signaling pathway. Int J Biol Macromol. 2011;49:599-606.
[155] Lee SH, Senevirathne M, Ahn CB, Kim SK, Je JY. Factors affecting anti-inflammatory effect of chitooligosaccharides in lipopolysaccharides-induced RAW264.7 macrophage cells. Bioorg Med Chem Lett. 2009;19:6655-8.
[156] Qiao Y, Bai XF, Du YG. Chitosan oligosaccharides protect mice from LPS challenge by attenuation of inflammation and oxidative stress. Int Immunopharmacol. 2011;11:121-7.
[157] Yousef M, Pichyangkura R, Soodvilai S, Chatsudthipong V, Muanprasat C. Chitosan oligosaccharide as potential therapy of inflammatory bowel disease: therapeutic efficacy and possible mechanisms of action. Pharmacol Res. 2012;66:66-79.
[158] Ngo DH, Kim SK. Antioxidant effects of chitin, chitosan, and their derivatives. Adv Food Nutr Res. 2014;73:15-31.
[159] Bruyere O, Pavelka K, Rovati LC, Gatterova J, Giacovelli G, Olejarova M, et al. Total joint replacement after glucosamine sulphate treatment in knee osteoarthritis: results of a mean 8-year observation of patients from two previous 3-year, randomised, placebo-controlled trials. Osteoarthr Cartilage. 2008;16:254-60.
[160] Friedman AJ, Phan J, Schairer DO, Champer J, Qin M, Pirouz A, et al. Antimicrobial and anti-inflammatory activity of chitosan-alginate nanoparticles: a targeted therapy for cutaneous pathogens. J Invest Dermatol. 2013;133:1231-9.
[161] Oliveira MI, Santos SG, Oliveira MJ, Torres AL, Barbosa MA. Chitosan drives anti-inflammatory macrophage polarisation and pro-inflammatory dendritic cell stimulation. Eur Cells Mater. 2012;24:136-52; discussion 52-3.
[162] Xia WS, Liu P, Zhang JL, Chen J. Biological activities of chitosan and chitooligosaccharides. Food Hydrocolloid. 2011;25:170-9.
[163] Kim MM, Kim SK. Chitooligosaccharides inhibit activation and expression of matrix metalloproteinase-2 in human dermal fibroblasts. FEBS Lett. 2006;580:2661-6.
[164] Chen Q, Liu SQ, Du YM, Peng H, Sun LP. Carboxymethyl-chitosan protects rabbit chondrocytes from interleukin-1beta-induced apoptosis. Eur J Pharmacol. 2006;541:1-8.
[165] Prudden JF, Migel P, Hanson P, Friedrich L, Balassa L. The discovery of a potent pure chemical wound-healing accelerator. Am J Surg. 1970;119:560-4.
[166] Ueno H, Yamada H, Tanaka I, Kaba N, Matsuura M, Okumura M, et al. Accelerating effects of chitosan for healing at early phase of experimental open wound in dogs. Biomaterials. 1999;20:1407-14.
[167] Kim IY, Seo SJ, Moon HS, Yoo MK, Park IY, Kim BC, et al. Chitosan and its derivatives for tissue engineering applications. Biotechnol Adv. 2008;26:1-21.
[168] Muzzarelli RAA. Chitins and chitosans for the repair of wounded skin, nerve, cartilage and bone. Carbohyd Polym. 2009;76:167-82.
[169] Boucard N, Viton C, Agay D, Mari E, Roger T, Chancerelle Y, et al. The use of physical hydrogels of chitosan for skin regeneration following third-degree burns. Biomaterials. 2007;28:3478-88.
[170] Ariganello MB, Simionescu DT, Labow RS, Lee JM. Macrophage differentiation and polarization on a decellularized pericardial biomaterial. Biomaterials. 2011;32:439-49.
[171] Ariganello MB, Labow RS, Lee JM. In vitro response of monocyte-derived macrophages to a decellularized pericardial biomaterial. J Biomed Mater Res A. 2010;93:280-8.

[172] Umashankar PR, Arun T, Kumary TV. Effect of chronic inflammation and immune response on regeneration induced by decellularized bovine pericardium. J Biomed Mater Res A. 2013;101:2202-9.
[173] McDade JK, Brennan-Pierce EP, Ariganello MB, Labow RS, Michael Lee J. Interactions of U937 macrophage-like cells with decellularized pericardial matrix materials: influence of crosslinking treatment. Acta Biomater. 2013;9:7191-9.
[174] Elsaesser AF, Bermueller C, Schwarz S, Koerber L, Breiter R, Rotter N. In vitro cytotoxicity and in vivo effects of a decellularized xenogeneic collagen scaffold in nasal cartilage repair. Tissue Eng Part A. 2014;20:1668-78.
[175] Fishman JM, Lowdell MW, Urbani L, Ansari T, Burns AJ, Turmaine M, et al. Immunomodulatory effect of a decellularized skeletal muscle scaffold in a discordant xenotransplantation model. Proc Natl Acad Sci U S A. 2013;110:14360-5.
[176] Keane TJ, Dziki J, Castelton A, Faulk DM, Messerschmidt V, Londono R, et al. Preparation and characterization of a biologic scaffold and hydrogel derived from colonic mucosa. J Biomed Mater Res B Appl Biomater. 2015.
[177] Nowocin AK, Southgate A, Gabe SM, Ansari T. Biocompatibility and potential of decellularized porcine small intestine to support cellular attachment and growth. J Tissue Eng Regen Med. 2013.
[178] Koch H, Hammer N, Ossmann S, Schierle K, Sack U, Hofmann J, et al. Tissue engineering of ureteral grafts: preparation of biocompatible crosslinked ureteral scaffolds of porcine origin. Front Bioeng Biotechnol. 2015;3.
[179] Mazza G, Rombouts K, Rennie Hall A, Urbani L, Vinh Luong T, Al-Akkad W, et al. Decellularized human liver as a natural 3D-scaffold for liver bioengineering and transplantation. Sci Rep. 2015;5.
[180] Raghavan SS, Woon CY, Kraus A, Megerle K, Choi MS, Pridgen BC, et al. Human flexor tendon tissue engineering: decellularization of human flexor tendons reduces immunogenicity in vivo. Tissue Eng Part A. 2012;18:796-805.
[181] Medberry CJ, Crapo PM, Siu BF, Carruthers CA, Wolf MT, Nagarkar SP, et al. Hydrogels derived from central nervous system extracellular matrix. Biomaterials. 2013;34:1033-40.
[182] French KM, Boopathy AV, DeQuach JA, Chingozha L, Lu H, Christman KL, et al. A naturally derived cardiac extracellular matrix enhances cardiac progenitor cell behavior in vitro. Acta Biomater. 2012;8:4357-64.
[183] Brown BN, Valentin JE, Stewart-Akers AM, McCabe GP, Badylak SF. Macrophage phenotype and remodeling outcomes in response to biologic scaffolds with and without a cellular component. Biomaterials. 2009;30:1482-91.
[184] Zilla P, Human P, Bezuidenhout D. Bioprosthetic heart valves: the need for a quantum leap. Biotechnol Appl Biochem. 2004;40:57-66.
[185] Badylak SF. Decellularized allogeneic and xenogeneic tissue as a bioscaffold for regenerative medicine: factors that influence the host response. Ann Biomed Eng. 2014;42:1517-27.
[186] Reing JE, Zhang L, Myers-Irvin J, Cordero KE, Freytes DO, Heber-Katz E, et al. Degradation products of extracellular matrix affect cell migration and proliferation. Tissue Eng Part A. 2009;15:605-14.
[187] Bullers SJ, Baker SC, Ingham E, Southgate J. The human tissue-biomaterial interface: a role for PPARgamma-dependent glucocorticoid receptor activation in regulating the CD163+ M2 macrophage phenotype. Tissue Eng Part A. 2014;20:2390-401.

[188] Xing Q, Yates K, Tahtinen M, Shearier E, Qian Z, Zhao F. Decellularization of fibroblast cell sheets for natural extracellular matrix scaffold preparation. Tissue Eng Part C Methods. 2015;21:77-87.
[189] Eming SA, Krieg T, Davidson JM. Inflammation in wound repair: molecular and cellular mechanisms. J Invest Dermatol. 2007;127:514-25.
[190] Zgheib C, Xu J, Liechty KW. Targeting inflammatory cytokines and extracellular matrix composition to promote wound regeneration. Adv Wound Care (New Rochelle). 2014;3:344-55.
[191] Larson BJ, Longaker MT, Lorenz HP. Scarless fetal wound healing: a basic science review. Plast Reconstr Surg. 2010;126:1172-80.
[192] Adzick NS, Lorenz HP. Cells, matrix, growth factors, and the surgeon. The biology of scarless fetal wound repair. Ann Surg. 1994;220:10-8.
[193] Bullard KM, Longaker MT, Lorenz HP. Fetal wound healing: Current biology. World J Surg. 2003;27:54-61.
[194] Colwell AS, Krummel TM, Longaker MT, Lorenz HP. An in vivo mouse excisional wound model of scarless healing. Plast Reconstr Surg. 2006;117:2292-6.
[195] Lorenz HP, Whitby DJ, Longaker MT, Adzick NS. Fetal wound healing. The ontogeny of scar formation in the non-human primate. Ann Surg. 1993;217:391-6.
[196] Somasundaram K, Prathap K. Intra-uterine healing of skin wounds in rabbit foetuses. J Pathol. 1970;100:81-6.
[197] Cass DL, Bullard KM, Sylvester KG, Yang EY, Longaker MT, Adzick NS. Wound size and gestational age modulate scar formation in fetal wound repair. J Pediatr Surg. 1997;32:411-5.
[198] Colwell AS, Longaker MT, Lorenz HP. Mammalian fetal organ regeneration. Adv Biochem Eng Biotechnol. 2005;93:83-100.
[199] Olutoye OO, Zhu X, Cass DL, Smith CW. Neutrophil recruitment by fetal porcine endothelial cells: implications in scarless fetal wound healing. Pediatr Res. 2005;58:1290-4.
[200] Naik-Mathuria B, Gay AN, Zhu X, Yu L, Cass DL, Olutoye OO. Age-dependent recruitment of neutrophils by fetal endothelial cells: implications in scarless wound healing. J Pediatr Surg. 2007;42:166-71.
[201] Olutoye OO, Yager DR, Cohen IK, Diegelmann RF. Lower cytokine release by fetal porcine platelets: a possible explanation for reduced inflammation after fetal wounding. J Pediatr Surg. 1996;31:91-5.
[202] Liechty KW, Adzick NS, Crombleholme TM. Diminished interleukin 6 (IL-6) production during scarless human fetal wound repair. Cytokine. 2000;12:671-6.
[203] Liechty KW, Crombleholme TM, Cass DL, Martin B, Adzick NS. Diminished interleukin-8 (IL-8) production in the fetal wound healing response. J Surg Res. 1998;77:80-4.
[204] Liechty KW, Kim HB, Adzick NS, Crombleholme TM. Fetal wound repair results in scar formation in interleukin-10-deficient mice in a syngeneic murine model of scarless fetal wound repair. J Pediatr Surg. 2000;35:866-72; discussion 72-3.
[205] Peranteau WH, Zhang L, Muvarak N, Badillo AT, Radu A, Zoltick PW, et al. IL-10 overexpression decreases inflammatory mediators and promotes regenerative healing in an adult model of scar formation. J Invest Dermatol. 2008;128:1852-60.
[206] Gordon A, Kozin ED, Keswani SG, Vaikunth SS, Katz AB, Zoltick PW, et al. Permissive environment in postnatal wounds induced by adenoviral-mediated overexpression of the anti-inflammatory cytokine interleukin-10 prevents scar formation. Wound Repair Regen. 2008;16:70-9.

[207] Shah M, Foreman DM, Ferguson MW. Neutralising antibody to TGF-beta 1,2 reduces cutaneous scarring in adult rodents. J Cell Sci. 1994;107 (Pt 5):1137-57.
[208] Hsu M, Peled ZM, Chin GS, Liu W, Longaker MT. Ontogeny of expression of transforming growth factor-beta 1 (TGF-beta 1), TGF-beta 3, and TGF-beta receptors I and II in fetal rat fibroblasts and skin. Plastic and reconstructive surgery. 2001;107:1787-94; discussion 95-6.
[209] Soo C, Beanes SR, Hu FY, Zhang X, Dang C, Chang G, et al. Ontogenetic transition in fetal wound transforming growth factor-beta regulation correlates with collagen organization. Am J Pathol. 2003;163:2459-76.
[210] Merkel JR, DiPaolo BR, Hallock GG, Rice DC. Type I and type III collagen content of healing wounds in fetal and adult rats. Proc Soc Exp Biol Med. 1988;187:493-7.
[211] Longaker MT, Chiu ES, Adzick NS, Stern M, Harrison MR, Stern R. Studies in fetal wound healing. V. A prolonged presence of hyaluronic acid characterizes fetal wound fluid. Ann Surg. 1991;213:292-6.
[212] Armstrong JR, Ferguson MW. Ontogeny of the skin and the transition from scar-free to scarring phenotype during wound healing in the pouch young of a marsupial, Monodelphis domestica. Dev Biol. 1995;169:242-60.
[213] Longaker MT, Whitby DJ, Ferguson MW, Lorenz HP, Harrison MR, Adzick NS. Adult skin wounds in the fetal environment heal with scar formation. Ann Surg. 1994;219:65-72.
[214] Lorenz HP, Longaker MT, Perkocha LA, Jennings RW, Harrison MR, Adzick NS. Scarless wound repair: a human fetal skin model. Development. 1992;114:253-9.
[215] Niknejad H, Peirovi H, Jorjani M, Ahmadiani A, Ghanavi J, Seifalian AM. Properties of the amniotic membrane for potential use in tissue engineering. Eur Cells Mater. 2008;15:88-99.
[216] Malak TM, Ockleford CD, Bell SC, Dalgleish R, Bright N, Macvicar J. Confocal Immunofluorescence Localization of Collagen Type-I, Type-III, Type-IV, Type-V and Type-VI and Their Ultrastructural Organization in Term Human Fetal Membranes. Placenta. 1993;14:385-406.
[217] Wilshaw SP, Kearney JN, Fisher J, Ingham E. Production of an acellular amniotic membrane matrix for use in tissue engineering. Tissue Eng. 2006;12:2117-29.
[218] Cooper LJ, Kinoshita S, German M, Koizumi N, Nakamura T, Fullwood NJ. An investigation into the composition of amniotic membrane used for ocular surface reconstruction. Cornea. 2005;24:722-9.
[219] Koob TJ, Rennert R, Zabek N, Massee M, Lim JJ, Temenoff JS, et al. Biological properties of dehydrated human amnion/chorion composite graft: implications for chronic wound healing. Int Wound J. 2013;10:493-500.
[220] Pinkerton MC. Amnioplastin for adherent digital flexor tendons. Lancet. 1942;1:70-2.
[221] Troensegaard-Hansen E. Amniotic grafts in chronic skin ulceration. Lancet. 1950;1:859-60.
[222] Azuara-Blanco A, Pillai CT, Dua HS. Amniotic membrane transplantation for ocular surface reconstruction. Br J Ophthalmol. 1999;83:399-402.
[223] Tseng SC, Prabhasawat P, Barton K, Gray T, Meller D. Amniotic membrane transplantation with or without limbal allografts for corneal surface reconstruction in patients with limbal stem cell deficiency. Arch Ophthalmol. 1998;116:431-41.
[224] Chen HJ, Pires RT, Tseng SC. Amniotic membrane transplantation for severe neurotrophic corneal ulcers. Br J Ophthalmol. 2000;84:826-33.

[225] Kim H, Son D, Choi TH, Jung S, Kwon S, Kim J, et al. Evaluation of an amniotic membrane-collagen dermal substitute in the management of full-thickness skin defects in a pig. Arch Plast Surg. 2013;40:11-8.
[226] Samandari MH, Yaghmaei M, Ejlali M, Moshref M, Saffar AS. Use of amnion as a graft material in vestibuloplasty: a preliminary report. Oral Surg Oral Med Oral Pathol Oral Radiol Endod. 2004;97:574-8.
[227] Fairbairn NG, Randolph MA, Redmond RW. The clinical applications of human amnion in plastic surgery. J Plast Reconstr Aesthet Surg. 2014;67:662-75.
[228] Willett NJ, Thote T, Lin AS, Moran S, Raji Y, Sridaran S, et al. Intra-articular injection of micronized dehydrated human amnion/chorion membrane attenuates osteoarthritis development. Arthritis Res Ther. 2014;16:R47.
[229] Taghiabadi E, Nasri S, Shafieyan S, Jalili Firoozinezhad S, Aghdami N. Fabrication and characterization of spongy denuded amniotic membrane based scaffold for tissue engineering. Cell J. 2015;16:476-87.
[230] Hortensius RA, Ebens JH, Harley BA. Immunomodulatory effects of amniotic membrane matrix incorporated into collagen scaffolds. J Biomed Mater Res A. 2016.
[231] Bentzen SM. Preventing or reducing late side effects of radiation therapy: radiobiology meets molecular pathology. Nat Rev Cancer. 2006;6:702-13.
[232] Gulotta LV, Rodeo SA. Growth factors for rotator cuff repair. Clin Sports Med. 2009;28:13-23.
[233] Molloy T, Wang Y, Murrell G. The roles of growth factors in tendon and ligament healing. Sports Med. 2003;33:381-94.
[234] Shen W, Chen X, Chen J, Yin Z, Heng BC, Chen W, et al. The effect of incorporation of exogenous stromal cell-derived factor-1 alpha within a knitted silk-collagen sponge scaffold on tendon regeneration. Biomaterials. 2010;31:7239-49.
[235] Alberti K, Davey RE, Onishi K, George S, Salchert K, Seib FP, et al. Functional immobilization of signaling proteins enables control of stem cell fate. Nat Methods. 2008;5:645-50.
[236] Klenkler BJ, Sheardown H. Characterization of EGF coupling to aminated silicone rubber surfaces. Biotechnol Bioeng. 2006;95:1158-66.
[237] Mann BK, Schmedlen RH, West JL. Tethered-TGF-beta increases extracellular matrix production of vascular smooth muscle cells. Biomaterials. 2001;22:439-44.
[238] Hanson JA, Chang CB, Graves SM, Li Z, Mason TG, Deming TJ. Nanoscale double emulsions stabilized by single-component block copolypeptides. Nature. 2008;455:85-8.
[239] Richardson TP, Peters MC, Ennett AB, Mooney DJ. Polymeric system for dual growth factor delivery. Nat Biotechnol. 2001;19:1029-34.
[240] Sohier J, Vlugt TJH, Cabrol N, Van Blitterswijk C, de Groot K, Bezemer JM. Dual release of proteins from porous polymeric scaffolds. J Control Release. 2006;111:95-106.
[241] Spillmann D, Lindahl U. Glycosaminoglycan protein interactions - a question of specificity. Curr Opin Struct Biol. 1994;4:677-82.
[242] Sakiyama-Elbert SE, Hubbell JA. Controlled release of nerve growth factor from a heparin-containing fibrin-based cell ingrowth matrix. J Control Release. 2000;69:149-58.
[243] Hudalla GA, Koepsel JT, Murphy WL. Surfaces that sequester serum-borne heparin amplify growth factor activity. Adv Mater. 2011;23:5415-8.

[244] Harley BA, Kim HD, Zaman MH, Yannas IV, Lauffenburger DA, Gibson LJ. Microarchitecture of three-dimensional scaffolds influences cell migration behavior via junction interactions. Biophys J. 2008;95:4013-24.
[245] Harley BA, Spilker MH, Wu JW, Asano K, Hsu HP, Spector M, et al. Optimal degradation rate for collagen chambers used for regeneration of peripheral nerves over long gaps. Cells Tissues Organs. 2004;176:153-65.
[246] Torres DS, Freyman TM, Yannas IV, Spector M. Tendon cell contraction of collagen-GAG matrices in vitro: effect of cross-linking. Biomaterials. 2000;21:1607-19.
[247] Ellis DL, Yannas IV. Recent advances in tissue synthesis in vivo by use of collagen-glycosaminoglycan copolymers. Biomaterials. 1996;17:291-9.
[248] Harley BA, Leung JH, Silva EC, Gibson LJ. Mechanical characterization of collagen-glycosaminoglycan scaffolds. Acta Biomater. 2007;3:463-74.
[249] James R, Kesturu G, Balian G, Chhabra AB. Tendon: biology, biomechanics, repair, growth factors, and evolving treatment options. J Hand Surg Am. 2008;33:102-12.
[250] Wang JH. Mechanobiology of tendon. J Biomech. 2006;39:1563-82.
[251] Caliari SR, Ramirez MA, Harley BAC. The development of collagen-GAG scaffold-membrane composites for tendon tissue engineering. Biomaterials. 2011;32:8990-8.
[252] Olde Damink LHH, Dijkstra PJ, Van Luyn MJA, Van Wachem PB, Nieuwenhuis P, Feijen J. Cross-linking of dermal sheep collagen using a water-soluble carbodiimide. Biomaterials. 1996;17:765-73.
[253] Kapoor A, Caporali EH, Kenis PJ, Stewart MC. Microtopographically patterned surfaces promote the alignment of tenocytes and extracellular collagen. Acta Biomater. 2010;6:2580-9.
[254] Pauly S, Klatte F, Strobel C, Schmidmaier G, Greiner S, Scheibel M, et al. Characterization of tendon cell cultures of the human rotator cuff. Eur Cell Mater. 2010;20:84-97.
[255] Park A, Hogan MV, Kesturu GS, James R, Balian G, Chhabra AB. Adipose-derived mesenchymal stem cells treated with growth differentiation factor-5 express tendon-specific markers. Tissue Eng Part A. 2010;16:2941-51.
[256] James R, Kumbar SG, Laurencin CT, Balian G, Chhabra AB. Tendon tissue engineering: adipose-derived stem cell and GDF-5 mediated regeneration using electrospun matrix systems. Biomedical Materials. 2011;6:025011.
[257] Costa MA, Wu C, Pham BV, Chong AK, Pham HM, Chang J. Tissue engineering of flexor tendons: optimization of tenocyte proliferation using growth factor supplementation. Tissue Eng. 2006;12:1937-43.
[258] Chamberlain LJ, Yannas IV, Hsu H-P, Strichartz G, Spector M. Collagen-GAG substrate enhances the quality of nerve regeneration through collagen tubes up to level of autograft. Exper Neurol. 1998;154:315-29.
[259] Schubert M. Chondroitin from chondroitin sulfate. In: Whistler R, BeMiller J, Wolfrom M, editors. Methods in carbohydrate chemistry: General polysaccharides. New York: Academic Press; 1965. p. 109-10.
[260] Farrell E, O'Brien FJ, Doyle P, Fischer J, Yannas I, Harley BA, et al. A collagen-glycosaminoglycan scaffold supports adult rat mesenchymal stem cell differentiation along osteogenic and chondrogenic routes. Tissue Eng. 2006;12:459-68.
[261] Hempel U, Hintze V, Moller S, Schnabelrauch M, Scharnweber D, Dieter P. Artificial extracellular matrices composed of collagen I and sulfated hyaluronan with adsorbed

transforming growth factor beta 1 promote collagen synthesis of human mesenchymal stromal cells. Acta Biomaterialia. 2012;8:659-66.
[262] Hacein-Bey-Abina S, von Kalle C, Schmidt M, Le Deist F, Wulffraat N, McIntyre E, et al. A serious adverse event after successful gene therapy for X-linked severe combined immunodeficiency. N Engl J Med. 2003;348:255-6.
[263] Somia N, Verma IM. Gene therapy: trials and tribulations. Nat Rev Genet. 2000;1:91-9.
[264] Luo D, Saltzman WM. Synthetic DNA delivery systems. Nat Biotechnol. 2000;18:33-7.
[265] Davis ME. Non-viral gene delivery systems. Curr Opin Biotechnol. 2002;13:128-31.
[266] Wu GY, Wu CH. Receptor-mediated gene delivery and expression in vivo. J Biol Chem. 1988;263:14621-4.
[267] Wagner E, Zenke M, Cotten M, Beug H, Birnstiel ML. Transferrin-polycation conjugates as carriers for DNA uptake into cells. Proc Natl Acad Sci U S A. 1990;87:3410-4.
[268] Pack DW, Hoffman AS, Pun S, Stayton PS. Design and development of polymers for gene delivery. Nat Rev Drug Discov. 2005;4:581-93.
[269] Curtin CM, Tierney EG, McSorley K, Cryan SA, Duffy GP, O'Brien FJ. Combinatorial Gene Therapy Accelerates Bone Regeneration: Non-Viral Dual Delivery of VEGF and BMP2 in a Collagen-Nanohydroxyapatite Scaffold. Adv Healthc Mater. 2014.
[270] Carrillo C, Sune JM, Perez-Lozano P, Garcia-Montoya E, Sarrate R, Fabregas A, et al. Chitosan nanoparticles as non-viral gene delivery systems: Determination of loading efficiency. Biomed Pharmacother. 2014.
[271] Boussif O, Lezoualc'h F, Zanta MA, Mergny MD, Scherman D, Demeneix B, et al. A versatile vector for gene and oligonucleotide transfer into cells in culture and in vivo: polyethylenimine. Proc Natl Acad Sci U S A. 1995;92:7297-301.
[272] Abdallah B, Hassan A, Benoist C, Goula D, Behr JP, Demeneix BA. A powerful nonviral vector for in vivo gene transfer into the adult mammalian brain: polyethylenimine. Hum Gene Ther. 1996;7:1947-54.
[273] Godbey WT, Wu KK, Mikos AG. Poly(ethylenimine) and its role in gene delivery. J Control Release. 1999;60:149-60.
[274] Caliari SR, Harley BAC. Structural and biochemical modification of a collagen scaffold to selectively enhance MSC tenogenic, chondrogenic, and osteogenic differentiation. Adv Healthc Mater. 2014.
[275] Caliari SR, Harley BAC. Collagen-GAG scaffold biophysical properties bias MSC lineage selection in the presence of mixed soluble signals. Tissue Eng A. 2014;20:2463-72.
[276] Tierney EG, McSorley K, Hastings CL, Cryan SA, O'Brien T, Murphy MJ, et al. High levels of ephrinB2 over-expression increases the osteogenic differentiation of human mesenchymal stem cells and promotes enhanced cell mediated mineralisation in a polyethyleneimine-ephrinB2 gene-activated matrix. J Control Release. 2013;165:173-82.
[277] Fischer D, Bieber T, Li Y, Elsasser HP, Kissel T. A novel non-viral vector for DNA delivery based on low molecular weight, branched polyethylenimine: effect of molecular weight on transfection efficiency and cytotoxicity. Pharm Res. 1999;16:1273-9.
[278] De la Riva B, Sanchez E, Hernandez A, Reyes R, Tamimi F, Lopez-Cabarcos E, et al. Local controlled release of VEGF and PDGF from a combined brushite-chitosan system enhances bone regeneration. J Control Release. 2010;143:45-52.
[279] Chen FM, Zhang M, Wu ZF. Toward delivery of multiple growth factors in tissue engineering. Biomaterials. 2010;31:6279-308.

[280] Capito RM, Spector M. Collagen scaffolds for nonviral IGF-1 gene delivery in articular cartilage tissue engineering. Gene Ther. 2007;14:721-32.
[281] Bonadio J, Smiley E, Patil P, Goldstein S. Localized, direct plasmid gene delivery in vivo: prolonged therapy results in reproducible tissue regeneration. Nat Med. 1999;5:753-9.
[282] Fang J, Zhu YY, Smiley E, Bonadio J, Rouleau JP, Goldstein SA, et al. Stimulation of new bone formation by direct transfer of osteogenic plasmid genes. Proc Natl Acad Sci U S A. 1996;93:5753-8.
[283] Hosseinkhani H, Hosseinkhani M, Gabrielson NP, Pack DW, Khademhosseini A, Kobayashi H. DNA nanoparticles encapsulated in 3D tissue-engineered scaffolds enhance osteogenic differentiation of mesenchymal stem cells. J Biomed Mater Res A. 2008;85:47-60.
[284] Weisgerber DW, Kelkhoff DO, Caliari SR, Harley BAC. The impact of discrete compartments of a multi-compartment collagen-GAG scaffold on overall construct biophysical properties. J Mech Behav Biomed Mater. 2013;28:26-36.
[285] Liu CF, Aschbacher-Smith L, Barthelery NJ, Dyment N, Butler D, Wylie C. Spatial and Temporal Expression of Molecular Markers and Cell Signals During Normal Development of the Mouse Patellar Tendon. Tissue Eng Part A. 2011.
[286] Schweitzer R, Zelzer E, Volk T. Connecting muscles to tendons: tendons and musculoskeletal development in flies and vertebrates. Development. 2010;137:2807-17.
[287] Watson SS, Riordan TJ, Pryce BA, Schweitzer R. Tendons and muscles of the mouse forelimb during embryonic development. Dev Dyn. 2009;238:693-700.
[288] Lin TW, Cardenas L, Soslowsky LJ. Biomechanics of tendon injury and repair. J Biomech. 2004;37:865-77.
[289] Price RD, Myers S, Leigh IM, Navsaria HA. The role of hyaluronic acid in wound healing: assessment of clinical evidence. Am J Clin Dermatol. 2005;6:393-402.
[290] Voigt J, Driver VR. Hyaluronic acid derivatives and their healing effect on burns, epithelial surgical wounds, and chronic wounds: a systematic review and meta-analysis of randomized controlled trials. Wound Repair Regen. 2012;20:317-31.
[291] Thomas SC, Jones LC, Hungerford DS. Hyaluronic acid and its effect on postoperative adhesions in the rabbit flexor tendon. A preliminary look. Clin Orthop Relat Res. 1986:281-9.
[292] Torres DS, Freyman TM, Yannas IV, Spector M. Tendon cell contraction of collagen-GAG matrices in vitro: effect of cross-linking. Biomaterials. 2000;21.
[293] Murphy GF, Orgill DP, Yannas IV. Partial dermal regeneration is induced by biodegradable collagen-glycosaminoglycan grafts. Lab Invest. 1990;62:305-13.
[294] Miki T, Marongiu F, Dorko K, Ellis EC, Strom SC. Isolation of amniotic epithelial stem cells. Curr Protoc Stem Cell Biol. 2010;Chapter 1:Unit 1E 3.
[295] Hopkinson A, Shanmuganathan VA, Gray T, Yeung AM, Lowe J, James DK, et al. Optimization of amniotic membrane (AM) denuding for tissue engineering. Tissue Eng Part C Methods. 2008;14:371-81.
[296] Samuel CS. Determination of collagen content, concentration, and sub-types in kidney tissue. Methods Mol Biol. 2009;466:223-35.
[297] Barbosa I, Garcia S, Barbier-Chassefiere V, Caruelle JP, Martelly I, Papy-Garcia D. Improved and simple micro assay for sulfated glycosaminoglycans quantification in biological extracts and its use in skin and muscle tissue studies. Glycobiology. 2003;13:647-53.
[298] Olde Damink LHH, Dijkstra PJ, Van Luyn MJA, Van Wachem PB, Nieuwenhuis P, Feijen J. Cross-linking of dermal sheep collagen using a water-soluble carbodiimide. Biomaterials. 1996;17.

[299] Krummel TM, Nelson JM, Diegelmann RF, Lindblad WJ, Salzberg AM, Greenfield LJ, et al. Fetal response to injury in the rabbit. J Pediatr Surg. 1987;22:640-4.
[300] Hu M, Sabelman EE, Cao Y, Chang J, Hentz VR. Three-dimensional hyaluronic acid grafts promote healing and reduce scar formation in skin incision wounds. J Biomed Mater Res B Appl Biomater. 2003;67:586-92.
[301] Mozdzen LC, Rodgers RC, Banks JM, Bailey RC, Harley BA. Increasing the strength and bioactivity of collagen scaffolds using customizable arrays of 3D-printed polymer fibers. Under review. 2015.
[302] Liu Y, Ramanath HS, Wang D-A. Tendon tissue engineering using scaffold enhancing strategies. Trends in Biotechnology. 2008;26:201-9.
[303] Mall NA, Tanaka MJ, Choi LS, Paletta GA, Jr. Factors affecting rotator cuff healing. J Bone Joint Surg Am. 2014;96:778-88.
[304] Derwin KA, Baker AR, Spragg RK, Leigh DR, Iannotti JP. Commercial extracellular matrix scaffolds for rotator cuff tendon repair. Biomechanical, biochemical, and cellular properties. J Bone Joint Surg Am. 2006;88:2665-72.
[305] Bond JL, Dopirak RM, Higgins J, Burns J, Snyder SJ. Arthroscopic replacement of massive, irreparable rotator cuff tears using a GraftJacket allograft: technique and preliminary results. Arthroscopy. 2008;24:403-9 e1.
[306] Wong I, Burns J, Snyder S. Arthroscopic GraftJacket repair of rotator cuff tears. J Shoulder Elbow Surg. 2010;19:104-9.
[307] Barber FA, Burns JP, Deutsch A, Labbe MR, Litchfield RB. A prospective, randomized evaluation of acellular human dermal matrix augmentation for arthroscopic rotator cuff repair. Arthroscopy. 2012;28:8-15.
[308] Lee DK. Achilles tendon repair with acellular tissue graft augmentation in neglected ruptures. J Foot Ankle Surg. 2007;46:451-5.
[309] Lee DK. A preliminary study on the effects of acellular tissue graft augmentation in acute Achilles tendon ruptures. J Foot Ankle Surg. 2008;47:8-12.
[310] Song L, Olsen RE, Spalazzi JP, Davisson T. Biomechanical evaluation of acellular collagen matrix augmented Achilles tendon repair in sheep. J Foot Ankle Surg. 2010;49:438-41.
[311] Tsuzaki M, Guyton G, Garrett W, Archambault JM, Herzog W, Almekinders L, et al. IL-1 beta induces COX2, MMP-1, -3 and -13, ADAMTS-4, IL-1 beta and IL-6 in human tendon cells. J Orthop Res. 2003;21:256-64.
[312] Yannas IV. Emerging rules for inducing organ regeneration. Biomaterials. 2013;34:321-30.
[313] Wolbank S, Hildner F, Redl H, van Griensven M, Gabriel C, Hennerbichler S. Impact of human amniotic membrane preparation on release of angiogenic factors. J Tissue Eng Regen Med. 2009;3:651-4.
[314] Carrillo-Galvez AB, Cobo M, Cuevas-Ocana S, Gutierrez-Guerrero A, Sanchez-Gilabert A, Bongarzone P, et al. Mesenchymal stromal cells express GARP/LRRC32 on their surface: effects on their biology and immunomodulatory capacity. Stem Cells. 2015;33:183-95.
[315] Pourgholaminejad A, Aghdami N, Baharvand H, Moazzeni SM. The effect of pro-inflammatory cytokines on immunophenotype, differentiation capacity and immunomodulatory functions of human mesenchymal stem cells. Cytokine. 2016;85:51-60.
[316] Uccelli A, Moretta L, Pistoia V. Mesenchymal stem cells in health and disease. Nat Rev Immunol. 2008;8:726-36.

[317] Ryan JM, Barry F, Murphy JM, Mahon BP. Interferon-gamma does not break, but promotes the immunosuppressive capacity of adult human mesenchymal stem cells. Clin Exp Immunol. 2007;149:353-63.
[318] Lacey DC, Simmons PJ, Graves SE, Hamilton JA. Proinflammatory cytokines inhibit osteogenic differentiation from stem cells: implications for bone repair during inflammation. Osteoarthr Cartilage. 2009;17:735-42.
[319] Ulivi V, Tasso R, Cancedda R, Descalzi F. Mesenchymal stem cell paracrine activity is modulated by platelet lysate: induction of an inflammatory response and secretion of factors maintaining macrophages in a proinflammatory phenotype. Stem Cells Dev. 2014;23:1858-69.
[320] Ding J, Ghali O, Lencel P, Broux O, Chauveau C, Devedjian JC, et al. TNF-alpha and IL-1beta inhibit RUNX2 and collagen expression but increase alkaline phosphatase activity and mineralization in human mesenchymal stem cells. Life Sci. 2009;84:499-504.
[321] Aktas E, Chamberlain CS, Saether EE, Duenwald-Kuehl SE, Kondratko-Mittnacht J, Stitgen M, et al. Immune modulation with primed mesenchymal stem cells delivered via biodegradable scaffold to repair an Achilles tendon segmental defect. J Orthop Res. 2016.
[322] Spiller KL, Anfang RR, Spiller KJ, Ng J, Nakazawa KR, Daulton JW, et al. The role of macrophage phenotype in vascularization of tissue engineering scaffolds. Biomaterials. 2014;35:4477-88.
[323] Landen NX, Li D, Stahle M. Transition from inflammation to proliferation: a critical step during wound healing. Cell Mol Life Sci. 2016.
[324] Godwin JW, Pinto AR, Rosenthal NA. Macrophages are required for adult salamander limb regeneration. Proc Natl Acad Sci U S A. 2013;110:9415-20.
[325] Li L, Yan B, Shi YQ, Zhang WQ, Wen ZL. Live imaging reveals differing roles of macrophages and neutrophils during zebrafish tail fin regeneration. J Biol Chem. 2012;287:25353-60.
[326] Witherel CE, Graney PL, Freytes DO, Weingarten MS, Spiller KL. Response of human macrophages to wound matrices in vitro. Wound Repair Regen. 2016;24:514-24.
[327] Weisgerber DW. Design, characterization, and reinforcement of mineralized collagen-glycosaminoglycan scaffolds for orthopedic wound repair. 2015.
[328] Ogle ME, Segar CE, Sridhar S, Botchwey EA. Monocytes and macrophages in tissue repair: Implications for immunoregenerative biomaterial design. Exp Biol Med (Maywood). 2016;241:1084-97.
[329] Kreider T, Anthony RM, Urban JF, Jr., Gause WC. Alternatively activated macrophages in helminth infections. Curr Opin Immunol. 2007;19:448-53.
[330] Edwards JP, Zhang X, Frauwirth KA, Mosser DM. Biochemical and functional characterization of three activated macrophage populations. J Leukoc Biol. 2006;80:1298-307.
[331] Mosser DM. The many faces of macrophage activation. J Leukoc Biol. 2003;73:209-12.
[332] Nawrocki-Raby B, Gilles C, Polette M, Martinella-Catusse C, Bonnet N, Puchelle E, et al. E-Cadherin mediates MMP down-regulation in highly invasive bronchial tumor cells. Am J Pathol. 2003;163:653-61.
[333] Goffin F, Munaut C, Frankenne F, Perrier D'Hauterive S, Beliard A, Fridman V, et al. Expression pattern of metalloproteinases and tissue inhibitors of matrix-metalloproteinases in cycling human endometrium. Biol Reprod. 2003;69:976-84.
[334] Lapthorne S, Pereira-Fantini PM, Fouhy F, Wilson G, Thomas SL, Dellios NL, et al. Gut microbial diversity is reduced and is associated with colonic inflammation in a piglet model of short bowel syndrome. Gut Microbes. 2013;4:212-21.

[335] Elgharably H, Ganesh K, Dickerson J, Khanna S, Abas M, Ghatak PD, et al. A modified collagen gel dressing promotes angiogenesis in a preclinical swine model of chronic ischemic wounds. Wound Repair Regen. 2014;22:720-9.
[336] Kyrova K, Stepanova H, Rychlik I, Faldyna M, Volf J. SPI-1 encoded genes of Salmonella Typhimurium influence differential polarization of porcine alveolar macrophages in vitro. BMC Vet Res. 2012;8:115.
[337] Miguel JC, Chen J, Van Alstine WG, Johnson RW. Expression of inflammatory cytokines and Toll-like receptors in the brain and respiratory tract of pigs infected with porcine reproductive and respiratory syndrome virus. Vet Immunol Immunopathol. 2010;135:314-9.
[338] Olde Damink LH, Dijkstra PJ, van Luyn MJ, van Wachem PB, Nieuwenhuis P, Feijen J. Cross-linking of dermal sheep collagen using a water-soluble carbodiimide. Biomaterials. 1996;17:765-73.
[339] Spiller KL, Wrona EA, Romero-Torres S, Pallotta I, Graney PL, Witherel CE, et al. Differential Gene Expression in Human, Murine, and Cell Line-derived Macrophages upon Polarization. Experimental Cell Research.
[340] Tierney CM, Jaasma MJ, O'Brien FJ. Osteoblast activity on collagen-GAG scaffolds is affected by collagen and GAG concentrations. J Biomed Mater Res A. 2009;91:92-101.
[341] Kim YJ, Sah RL, Doong JY, Grodzinsky AJ. Fluorometric assay of DNA in cartilage explants using Hoechst 33258. Anal Biochem. 1988;174:168-76.
[342] Duffy GP, McFadden TM, Byrne EM, Gill SL, Farrell E, O'Brien FJ. Towards in vitro vascularisation of collagen-GAG scaffolds. Eur Cells Mater. 2011;21:15-30.